ISBN 978-82-326-7150-2 (printed ver.)
ISBN 978-82-326-7149-6 (electronic ver.)
ISSN 1503-8181 (printed ver.)
ISSN 2703-8084 (electronic ver.)

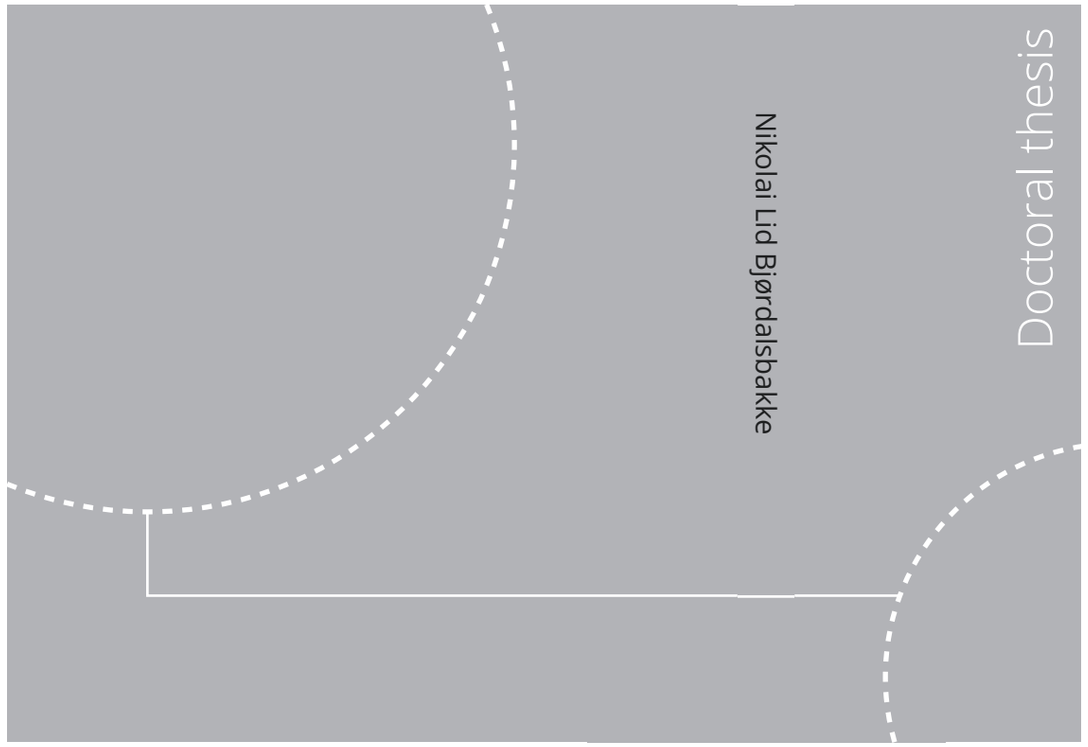

Doctoral theses at NTNU, 2023:225

Nikolai Lid Bjørdalsbakke

Robust Cardiovascular Models for Prediction of Hypertension Using Minimal Data Sets

Doctoral theses at NTNU, 2023:225

NTNU
Norwegian University of
Science and Technology
Thesis for the degree of
Philosophiae Doctor
Faculty of Engineering
Department of Structural Engineering

NTNU
Norwegian University of
Science and Technology

NTNU
Norwegian University of
Science and Technology

Nikolai Lid Bjørdalsbakke

Robust Cardiovascular Models for Prediction of Hypertension Using Minimal Data Sets

Thesis for the degree of Philosophiae Doctor

Trondheim, July 2023

Norwegian University of Science and Technology
Faculty of Engineering
Department of Structural Engineering

NTNU
Norwegian University of
Science and Technology

NTNU
Norwegian University of Science and Technology

Thesis for the degree of Philosophiae Doctor

Faculty of Engineering
Department of Structural Engineering

ISBN 978-82-326-7150-2 (printed ver.)
ISBN 978-82-326-7149-6 (electronic ver.)
ISSN 1503-8181 (printed ver.)
ISSN 2703-8084 (electronic ver.)

Doctoral theses at NTNU, 2023:225

PRINTED IN NORWAY
NO - 1598

NORDIC SWAN ECOLABEL
Printed matter
2041 0731

Printed by Skipnes Kommunikasjon AS

Preface

This thesis is submitted to the Norwegian University of Science and Technology (NTNU) for partial fulfillment of the requirements for the degree of philosophiae doctor (PhD). This doctoral work has been performed at the Department of Structural Engineering, NTNU, Trondheim from August 2018 through April 2023 under the supervision of Leif Rune Hellevik.

The funding in full is received from NTNU through the Digital Transformation initiative (1). The Digital Transformation initiative funded 9 projects consisting of approximately 48 PhD candidates. These projects were tasked with researching transformative technology and knowledge to take part in the digitalization of society. One of these 9 projects was the "My Medical Digital Twin" (MyMDT), under which this PhD project takes part (2). The MyMDT project aims to use knowledge, methods and technology from a wide range of disciplines to make a platform for personalized treatment of hypertension. This would be a step towards bringing hypertension treatment towards the realm of precision medicine.

The thesis is a collection of papers published in or submitted to international peer-reviewed journals. The thesis is organized in two parts. Part I is an introductory section that presents the themes and background of the thesis and part II includes the journal papers.

Abstract

As part of the My Medical Digital Twin (MyMDT) project, an effort to construct a cardiovascular model for use as a component in a digital twin for management of hypertension was undertaken. In this thesis we have developed and examined a simple cardiovascular model of the left-ventricle and systemic circulation. The model's ability to be personalized with a small data set and to be able to resolve and track changes over time in parameters was further analyzed.

A sedentary lifestyle is known to be a risk factor for developing high blood pressure (hypertension). Society is increasingly accommodating a sedentary lifestyle, and cardiovascular disease is a leading cause of death and disability worldwide. The aetiology of hypertension is complex and still not fully understood. A large majority of cases of hypertension are essensial hypertension, which have no identified cause and therefore it is challenging to prescribe an optimal course of treatment for the individual. Increased activity level, or exercise has been shown numerous times to effectively lower high blood pressure, but what individual factors will predict a blood pressure drop and of what magnitude is still uncertain. This response could be affected by individual properties, as well as type of exercise and exercise dose. To attempt to personalize treatment of hypertension, we proposed personalizing a cardiovascular model and interpreting the personalized mechanical parameters as indicators of lower-level hypertension phenotypes to learn about the impact of exercise as a therapy. Further, we investigated if we could use the parameter changes as a source of information to learn about the personalized impact of exercise as hypertension therapy.

To reach this goal we first constructed a three-chamber, closed-loop lumped para-

meter model of the left-ventricle and systemic circulation. To make the model more feasible in a clinical setting, local non-linear optimization techniques were applied for personalization of the model. Initially, we used synthetic data produced by the model itself with known parameter values for optimization and investigated the errors of the personalized parameters. By bounding the parameter space and sampling different initial parameter guesses we assessed the method's ability to recover the true parameters by optimization. Thus, we found that in the noiseless case all parameters could be recovered to high precision using aortic pressure and flow data. When applying noise, the errors were substantial, and a subset of the least sensitive parameters was deemed harder to accurately estimate than others.

For optimization to real data we applied blood pressure waveforms measured non-invasively both in the digital arteries, and carotid artery as proxies of the aortic waveform. In this process we also developed a heuristic for parameter estimation with local optimization and minimal data, based on the technique applied previously to synthetic data. We assessed the variability in personalized parameters introduced by the method compared to the variability over repeated measurements in the individual, and in the population. We found that the individual could in a majority of cases be resolved from the population and over repeated measurements.

Finally, we tested if we could explain the cause of estimated parameter changes by regression and correlation analysis. We could not prove any convincing explanatory relationship in parameter changes to $\mathrm{VO}_{2,\max}$. Neither could we disregard regression to the mean or day-to-day variability. However, some of the individual and unexplained parameter variability could be attributed to variation in hemodynamics measured in SV between different measurement days. We also found an open-loop version of the model to yield some parameters that were better explained by individual characteristics such as age, sex, body mass index and stroke volume in terms of variability. Additionally, the carotid pressure waveform recommended for optimization as it yielded more consistent parameter estimates with other estimation methods.

Acknowledgements

There are many people deserving of thanks as I most certainly never would have managed to complete the work in its current form in isolation. First and foremost I would like to thank my main supervisor, Professor Leif Rune Hellevik. I thank him for his guidance, for giving me the opportunities that have led me to this point, and for organizing the "My Medical Digital Twin" (MyMDT) project. Not to mention his efforts to keep our research group a tight-knit and positive one.

Next, I also thank my co-supervisors, Professor Ulrik Wisløff and Professor Frank Lindseth, whom I've collaborated with mainly through the MyMDT project. I am thankful to all the other members of the MyMDT project as well, Filip, Fredrik, Håvard, Karsten, Michail, Sampsa, and Torjus. It has been an excellent experience participating on such an exciting project together with you all. I would especially like to mention Emma Ingeström and master student Kjell-Arne Øyen, who organized the pilot study on exercise motivation from which the data has been crucial for my work. All of the other principal investigators have also given invaluable advice over the past years. Thank you, Ingelin, Kristian and Martin. Other excellent advisors to the project have been Rod and Stig William. Thank you for bringing both guidance, crucial pieces of advice, and a joyful atmosphere to our project and discussions.

I also need to thank all colleagues and administration at the Department of Structural Engineering for some great discussions, both work related and at social events. Thank you to all current and former members of our research group Andreas, Fredrik, Friederike, and Lucas for helping to build such a welcoming and competent community in our group. Their social presence has also been important to me, as

the global Covid-19 pandemic loomed over large parts of this thesis work. A special thanks to Dr. Jacob Sturdy who has provided excellent advice, support, editing and countless interesting discussions. His contribution has been invaluable.

List of Papers

Journal Papers

Paper 1: Parameter estimation for closed-loop lumped parameter models of the systemic circulation using synthetic data
N.L. Bjørdalsbakke, J. Sturdy, D.R. Hose, L.R. Hellevik

Published in *Mathematical Biosciences* (2022)

Paper 2: Monitoring Variability in Parameter Estimates for Lumped Parameter Models of the Systemic Circulation Using Longitudinal Hemodynamic Measurements
N.L. Bjørdalsbakke, J. Sturdy, E.M.L. Ingeström, L.R. Hellevik

Published in *BioMedical Engineering OnLine* (2023)

Paper 3: Examining Temporal Changes in Model Optimized Parameters Using Longitudinal Hemodynamic Measurements
N.L. Bjørdalsbakke, J. Sturdy, U. Wisløff, L.R. Hellevik

Submitted to *BioMedical Engineering OnLine* (2023)

Contents

Part I

Introductory Section

Nomenclature

0D - Zero dimensional
1D - One dimensional
2WK - Two-element Windkessel
3D - Three dimensional
3WK - Three-element Windkessel
4WK - Four-element Windkessel
ACE - Angiotensin-converting enzyme
CL - Closed-loop
CFD - Computational Fluid Dynamics
CP - Carotid artery pressure
CO - Cardiac output
CPET - Cardiopulmonary Exercise Test
CRF - Cardiorespiratory Fitness
CVD - Cardiovascular disease
CVS - Cardiovascular System
DALY - Disability-adjusted life years
DRAM - Delayed Rejection Adaption Metropolis
DT - Digital Twin
EDV - End-diastolic volume
EF - Ejection fraction
ESPVR - End-systolic pressure volume relationship FEM - Finite Element Model
FP - Finger artery pressure
FSI - Fluid Structure Interaction
HR - Heart Rate
$\mathrm{HR}_{\mathrm{max}}$ - Maximal Heart Rate
$\mathrm{HR}_{\mathrm{rest}}$ - Resting Heart Rate

HRR - Heart Rate Reserve
ICU - Intensive care unit
MCMC - Markov-chain Monte Carlo
MyMDT - My Medical Digital Twin
NTNU - Norwegian University of Science and Technology
NO - Nitrous oxide
ODE - Ordinary differential equation
OP - Open-loop
PP - Pulse Pressure
PT - Physical Twin
PV-loop - Pressure-volume-loop
PWV - Pulse wave velocity
SA - Sensitivity Analysis
SSRM - Stepwise Subset Reduction Method
SV - Stroke Volume
TRRA - Trust-region reflective algorithm
$\mathrm{VO2_{max}}$ - Maximal aerobic capacity, or maximal oxygen uptake
$\mathrm{VO2_{peak}}$ - Peak value of measured aerobic capacity

Symbols

β - Fixed-effect regression coefficient
γ - Random-effect regression coefficient
$\delta(...)$ - Model discrepancy
$\varepsilon(...)$ - Sample errors
$\boldsymbol{\theta}$ - Vector of model parameters.
θ_i - A particular parameter i in the parameter space.
C_{ao} - Total arterial compliance
$E_{\max}$ - Maximal left-ventricular elastance
E_{es} - End-systolic left-ventricular elastance
H - Hessian matrix
$J(...)$ - Objective function, or cost function used interchangeably.
L_{ao} - Total arterial inertance
$L_f g(x)$ - Lie derivative of function $g(x)$
r - Pearson correlation coefficient
R_{sys} - Total peripheral resistance
$S_{\mathrm{M},i}$ - Main Sobol index
$S_{\mathrm{T},i}$ - Total Sobol index
$\mathrm{TAS}_{\mathrm{M},i}$ - Variance weighted main Sobol index
$\mathrm{TAS}_{\mathrm{T},i}$ - Variance weighted total Sobol index
$\mathbf{u}(t)$ - Control input function
V_{d} - Virtual volume axis intercept for the end-systolic pressure volume relationship
$\mathbf{y}(...)$ - Vector of model outputs
$\mathbf{y}^m$ - Vector of measurements corresponding to model outputs
Z_{ao} - Characteristic aortic impedance

Chapter 1

Introduction

The thesis work has been performed at the Department of Structural Engineering under at the Norwegian University of Science and Technology (NTNU). The focus of the work has been to develop a primarily physics-based model of the cardiovascular system, suitable for being part of a Digital Twin under the "My Medical Digital Twin" (MyMDT) project. This would entail a cardiovascular model being capable of representing part of the physiological envelope, which in this case refers to describing individualized information about the hemodynamic state for the individual, and information relevant to the history and prediction of changes for this information. The digital twin (DT) holds great potential for future development within progressing the development of personalized precision medicine (3).

The fist notion in need of exploration is the DT concept. A DT can, in simple terms, be explained as a digital copy or representation of a physical system or other digital system. In this text a DT is referred to as the digital representation of an individual's cardiovascular system and state of arterial blood pressure and flow. Baricelli et al. have investigated the use of the concept across multiple disciplines, and extracted some common properties for DTs (4). The first of which being seamless and continuous data exchange between the physical twin (PT) and the DT. Communication and data exchange should also function between different DTs, and between DTs and domain experts, here relevant health care practitioners. Secondly, the DT needs proper ontologies for data comprehension and model formalization, which for example entails the alignment of model concepts to raw data. Thirdly, DT technology also expected to incorporate continually improving AI, and fourthly be self-adapting and self-parameterizing. Finally, the DT is ex-

pected to use descriptive and predictive techniques to make decisions relevant to its own destiny. As such the DT should be able to represent the current status of the physical twin, and other "what-if" scenarios. The cardiovascular models which have been utilised in this work could potentially play a part in realizing many of these properties. The work to be presented, however, focuses on the self-parameterization capabilities, representation and predictive capabilities of a MyMDT.

MyMDT has primarily targeted hypertension as the disease carries significant cost and loss of life to society. High blood pressure is the globally a leading risk factor for disability-adjusted life years (DALY) (5). The DALY is a measure of years of life lost to ill health, disability or premature death. Worldwide it is estimated that 32% of the adult population above 30 years are hypertensive per the European Society of Cardiology's definition of hypertension (6). Under this definition a persistent systolic blood pressure above 140 mmHg, and a diastolic blood pressure above 90 mmHg is diagnosed as hypertension (7). While 51% of men and 41% of women with hypertension are estimated to be undiagnosed, not all diagnosed individuals manage to control their blood pressure successfully. Only 23% of all women and 18% of all men who are estimated to have hypertension actually manage to control it and reduce it below the hypertension threshold. Further, high systolic blood pressure over 140 mmHg is estimated to contribute to the loss of 142 million years of DALY, and not to mention an estimated 7.8 millions deaths by various cardiovascular diseases per year (8). Therefore, by reducing the pervasiveness of hypertension in society, many lives and resources could be spared. Even reducing the general population's systolic blood pressure by 1 mmHg is thought to be sufficient for reducing incidence of cardiovascular disease considerably (9).

The MyMDT project is a collaboration between PhD candidates within a variety of disciplines, among them being biomedical engineering, statistics, machine learning, product and sensor development, exercise physiology and genetics. Aside from the papers appended in this thesis, Spitieris et al. have also performed work on developing bayesian model calibration of cardiovascular models (mainly applied to two- and three-element Windkessel models) and prepared three papers on the subject (10, 11, 12). Steffensen et al. have developed four different sensors based on a model of inductance to demonstrate their ability to measure pulse waves in vascular phantoms (13). However, work in all other fields of the project are progressing simultaneously and are expected to give results in the near future.

While mathematical models can take many forms, as pure statistical regression

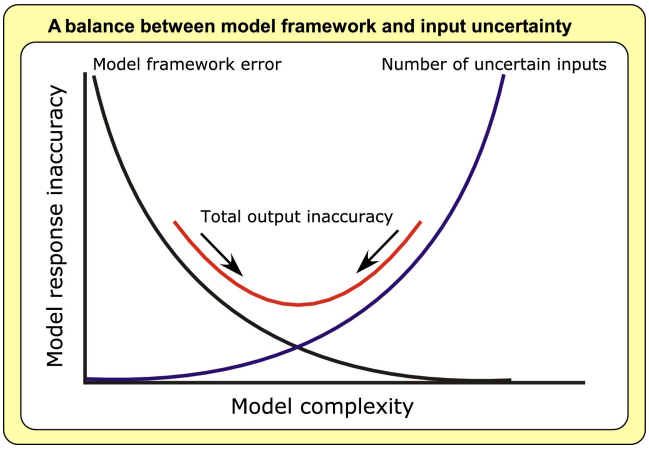

Figure 1.1: Model response inaccuracy versus model complexity: a balance between model framework error and the number of uncertain inputs. Reprinted with permission from (14).

based or neural networks, all the way to three dimensional fluid structure interaction models or even to molecular folding models, there is a huge span of models trying to capture and describe parts of reality at different scales. While in this work we mainly focus on models rooted in physics and mechanical systems, we also employ some statistical models to gain insight into measured and generated data. In the context of MyMDT where the DT needs to be robustly personalized we find the first principle guiding the work in this thesis. Huberts et al. discuss a road map for creating personalized cardiovascular models (14). They therein discuss the property of models where increased model complexity can cause the model to become more accurate, but also causes it to rely on more input parameters, which in turn are uncertain and increase model output uncertainty. We similarly assume there exists a minimum for optimal trade-off between model complexity and output uncertainty for a given application, as illustrated in Figure 1.1. Cardiovascular modeling also needs to provide outputs of the clinically relevant indices that are sufficiently precise to be used in practice for non-engineers and scientist (3). Another important concept in this context is also robustness, in normal mathematical use, a robust model is a model that is not majorly affected by outliers. The author would also like to interpret this concept as to be that a robust model in a DT for health care should be able to handle cases of missing or corrupted data from peripheral sensors performing intermittent or continuous personal data readings, by communication to the end user that predictions are based on partial data, or that no predictions can be made until all required data is acquired.

Naturally, the PhD project has focused on parsimonious lumped-parameter models. As a trade-off for highly detailed geometry or vasculature, the models should require less data for calibration, or more specifically personalization, and for faster simulations and personalization of models than higher dimensional and fidelity models allow. For a tool that is expected to be useful in a clinical setting, these are also important factors to consider. The project initially centered on finding a simple model, which easily could be personalized using a minimal set of data. Further the ambition was to develop exercise models to model the personalized physiological response to exercise to monitor and quantify the load on the cardiovascular system from individual and accumulated bouts of physical activity. Simultaneously, the ambition was to find a model for the long-term cardiovascular remodeling of the detected or planned pattern of physical activity. This added further requirements to the minimal model to be developed, as it needed to be sufficiently complex to be able to describe varying states of physical activity, and their loads on relevant vasculature.

Exercise was of chosen as a primary therapeutic target, and medication as a secondary. It is known that not all but many people with hypertension successfully can lower their blood pressure by engaging in more physical activity, as there are some non-responders. While the topic of which types of physical activity and the amount and intensity is still a controversial topic, this was chosen as a main target for implementation. Therefore, a model which could also describe bouts of physical activity with different intensities, durations and frequencies is important, not only to describe the different suggested therapies, but also possibly be a tool to learn more about the hypertension and hemodynamics in exercise. The lower level vascular phenotypes have also been investigated and shown to respond to exercise, however also here it is uncertain which populations will experience sustained change in these properties and for what physical activity stimuli.

To be able to predict the changes of parameters the changes must be sufficiently large to be detectable, and the variability or uncertainty in estimates for an individual set of measurements should be sufficiently low to be able to be able to resolve differences between parameters estimated under different conditions or time points. Whether parameter changes from a model required to change the hemodynamic state corresponds directly to the actual remodeling taking place in vivo has not been investigated for all models, and is not necessarily generally true. The data set used for personalization can also play a role in such a context. Studies by Gerringer et al. and by Audebert et al. investigate parameter developments during disease progression in animals (15, 16). Similarly, Colunga et al. performed lon-

gitudinal case studies for subjects post heart transplant which could exhibit signs of systemic and pulmonary hypertension (17), and was able to use this to interpret some observations to be complications during post intervention recovery. There are also studies in the physiology and epidemiology literature on the development of blood pressure, both long-term such as through initiatives such as the HUNT study (18), and short term randomized controlled trials, which assess the impact on cardiovascular parameters such as arterial resistance and stiffness (19, 20, 21) by a given stimuli or treatment. Such studies can inform how much the cardiovascular system can be expected to change over the course of a given treatment, and in such a context it can be investigated whether a model with a specified set of calibration data will reliably be able to resolve and detect such changes.

A plethora of different cardiovascular models exist already (22, 23, 24, 25, 26) of different scales, dimensionalities and complexities. In the context of MyMDT, some are more interesting than others and we here focus on lumped-parameter models, which have no spatial dimensions. A system developed by Conover et al. is a tool for evaluating the effects of different invasive treatments on the resting and higher intensity hemodynamics (27). This model is designed to focus on single ventricle physiologies such as Fontan and Norwood physiology patients and their predicted exercise capacity. What MyMDT aims for would be something similar for patients with a normal physiology, but also a system for tracking vascular remodelling long-term and incorporating the remodeling stimulus caused by exercise. To also build the exercise response model for the normal physiology, data from this cohort would also be necessary. Itu et al. have investigated personalization of an open-loop model focusing on the left ventricle and adjacent chambers using a very limited data set consisting of five measured values (28). Using these data, four parameters of the systemic circulation and left-ventricle are determined in order to properly characterize the left-ventricular pressure-volume loop (PV-loop). The question remains however if such a model is suitable for accurately capturing the adaptions to increased intensity and metabolic demand during physical activity, and whether it can capture parameter changes which are informative to systemic blood pressure changes and exercise stimulus. Works by the research group headed by Daniel Beard at the University of Michigan has worked on modeling of exercise and the understanding of the aetiology of hypertension (29, 30, 31). Recently, Jezek et al. have developed a model of the circulation which examines the effects of different postures on the hemodynamics in exercise. This is a step towards allowing the different activity types be encoded in the simulation of exercise, which perhaps could also be a component of simulating exercise as therapy or preventative action for hypertension. Gu et al. investigated how impairment of the baroreflex system can cause essential hypertension in rats (30), which is in line

with the ideas presented by Pettersen et al. (32). In summary, there are multiple ongoing efforts to study hypertension management using models as tools.

The aetiology of hypertension is not yet fully understood and still have many questions to be answered, and similarly from a mathematical modeling perspective there are still open questions with respect to a lot of what we already know about cardiovascular physiology and physics-based models. As investigated by for example Itu et al., models where the properties of large parts of the systemic vasculature can be described by few parameters do exist (28). However, one question which is not generally answered is what type of data and how much data is needed to sufficiently personalize such models and their parameters, or in other words make the model practically identifiable. We attempt to partially address this issue in the first appended paper (See chapter 6), where we attempt to solve the inverse problem of optimizing the model parameters using model outputs as the data to optimize for with and without noise (33). In this context, we also compared the use of waveform data to only single valued clinical indices to assess which gave the least errors in the parameter estimates. While for example Hann et al., deBournonVille et al., Pironet et al., and Marquis et al. focus on using measurements and information in several model compartments in order to successfully parameterize them (34, 35, 36, 37), it is also interesting to answer how well can personalized parameters be determined in contexts where very sparse data from even just a single model compartment are available. In a context such as MyMDT, where it would be beneficial if most measurements could be gathered from wearable, non-invasive sensors this is a crucial point, and leads to the pursuit of absolute minimal data sets. The first paper showed that all model parametrs could be estimated to high accuracy using only aortic pressure and flow waveforms in the noiseless case for synthetic data produced by the model itself. Application of 5% Gaussian noise to the data revealed that only the four most sensitive parameters could be reasonably well estimated using this combination of data. We decided to pursue using only this data set to assess the performance using real data, but since we also found that addition of information to the venous compartment improved most estimates, we continued while optimizing the model parameters to a prescribed level of mean venous pressure.

Gerringer et al., Marquis et al. among other estimate initial parameter guesses from the measurements before optimizing using a local optimization algorithm to find the best optimized parameter set (15, 35). Oppositely we take an approach where we sample multiple possible parameter combinations and try to find the optimal cost function minimum and accounting for some uncertainty in the resulting

minimum. By bounding the parameter space to a physiologically reasonable region, we thereby attempt to find the best minimum by exploration of this limited space and by used of the computational resources, rather than acquiring more data possibly adjacent to more model compartments.

A second question is whether the parameters can be estimated accurately enough to be able to meaningfully resolve possibly small changes that may explain changes in hemodynamics due to exercise stimuli or even just minor daily variations. A third question is whether a closed-loop or open-loop model formulation is best for detecting or quantifying the change in parameters, and if they are sufficient to model exercise induced changes both chronically long-term, and acutely short-term. The second appended paper investigates how much variability is introduced in parameters estimated from a single set of measurements with our developed estimation heuristic (See chapter 7). We compare this estimated variability to the variability over estimates made for the study population and to the variability of repeated estimates made at different time points in the same individuals. The third appended paper investigates (See chapter 8) what these changes are caused by. Both papers also compare results for the open-loop and closed-loop models.

In the coming chapters, the background of the project rooted in the physiology and pathophysiology of the cardiovascular system with focus on hypertension will be examined closer. Secondly, the models and some methods utilised in the papers will be described in the methods chapter, before thirdly a brief summary of the appended papers is presented. Finally, the conclusions drawn from the work is presented. The papers supporting these conclusions are appended at the very end.

Chapter 2

Background

2.1 The Cardiovascular System

The cardiovascular system transports oxygen, nutrients and hormonal signal carriers to all tissues of the human body (38). This system is illustrated in Figure 2.1 Through mainly the action of the heart and its two ventricles, blood is pumped from the left ventricles, through the systemic arteries, into the veins, before entering the right atrium and finally the right ventricle. The blood is again pumped from the right ventricle through the pulmonary arteries, and veins being oxygenated by the lungs before returning to the left ventricle through the left atrium. The inflow and outflow of each of the ventricles are affected by heart valves, which open and close depending on the pressure gradient across the valve. valve dynamics combined with the periodic contraction of the heart muscles (myocardium) causes pulsatile blood flow and pressure waves to propagate throughout the vasculature. The heart cycle is split into the systolic and diastolic phase. The cycle is usually taken to start at the ejection or systolic phase where the contraction of the left ventricle starts, and the atrioventricular valves close when the pressure of the ventricles exceed the pressures of the atria. All valves are closed as the ventricles continue to contract in the isovolumic contraction phase. When the left-ventricular pressure exceeds the aortic pressure, the aortic valve opens, and ejection starts. The ejection lasts until the ventricular pressure again is less than the aortic pressure and the ejection stops. The ventricle relaxes until the atrioventricular valve reopens and the ventricle is refilled. in the final phase of refilling, the atria contract in order to further increase ventricular filling. Both ventricles experience this heart cycle in parallel.

The vessels consist of the arteries transporting oxygenated blood throughout the cardiovascular system, while the veins transport deoxygenated blood towards the lungs. The large arteries are the most compliant and elastic arteries, which branch out into smaller arteries and eventually arterioles. These vessels are less elastic, but have thicker layers of smooth muscle which allows for better regulation of resistance, and most of the vascular resistance of the vascular tree is expressed in these vessels. From the arterioles spring the capillaries, which are the smallest blood vessels and allow exchange of gas and nutrients to organs. After the capillaries follow the venules, small veins and large central veins. The veins are more compliant than the arteries, and store most of the circulatory blood volume.

The structure of a single blood vessels themselves consist of mainly four sections. First is the lumen, or the open center of the vessel for blood flow to pass through. The vessel walls consist of the three layers of the tunica intima, tunica media and tunica externa. The layers of an artery are illustrated in Figure 2.2. The large and medium sized arteries follow this structure, while the smaller arteries, arterioles, deviate and omit most structural layers except the endothelium and muscular precapillary sphincters. The tunica externa is a layer of connective tissue, while the tunica media is mainly muscular tissue. The tunica interna consists partially of a layer of elastic lamina constructed by elastin. This layer lies outside a base membrane of glycoproteins, while the innermost layer bordering the lumen is the endothelium. The endothelium is part of the endocrine system and can emit endocrine agents. The endothelium can in this way control the vascular tone, by releasing endocrine signals which causes the tunica media to relax or contract. The lumen radii and distribution of tunica thicknesses alter the mechanical properties of the vessel and cause different vessels to behave differently with respect to resistance and compliance. the endothelium also plays a role in the transport of angiotensin and other hormonal signaling which is important in kidney function effects on blood volume regulation, and flow mediated dilatation of vessels.

2.2 Cardiovascular Disease and Hypertension

Hypertension is not primarily a disease, but rather a condition of persistently raised blood pressure. According to the European Society of Cardiology a hypertension diagnosis is usually given after brachial blood pressure is measured to be above 140 mmHg systolic and 90 mmHg diastolic. Here the blood pressure is given as systolic over diastolic (systolic/diastolic) in units of mmHg (7). Throughout the

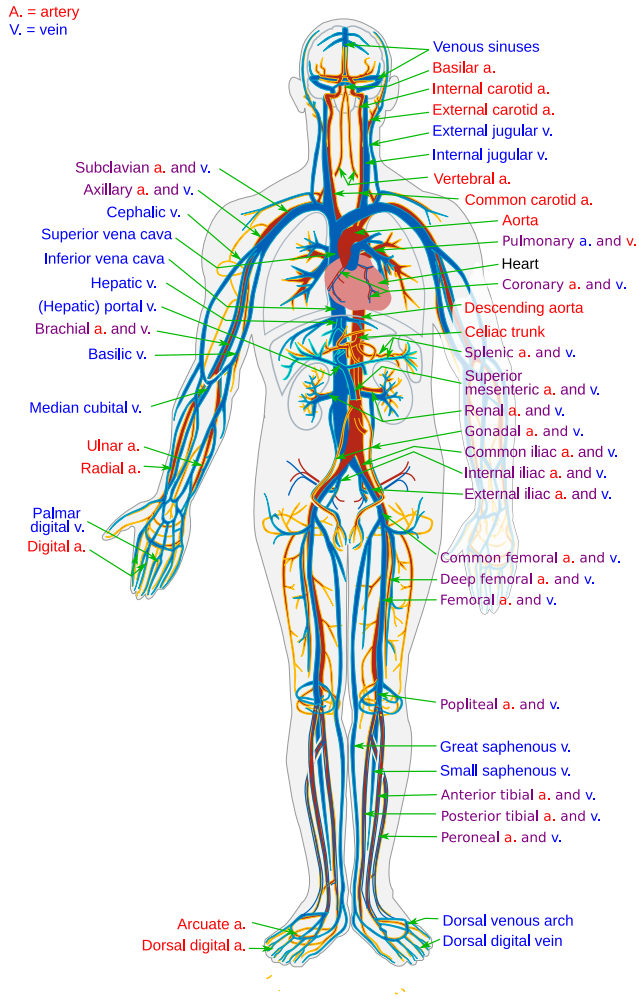

Figure 2.1: Illustration of the cardiovascular system with names of several large veins and arteries. The figure is created by Mariana Ruiz Villarreal (39). The figure is released to the Public Domain, and is used with permission.

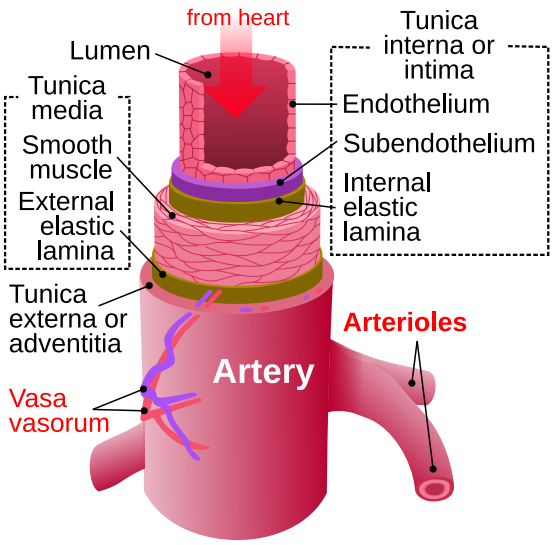

Figure 2.2: Illustration of the general arterial wall structure. The figure is created by user Kelvin13 on creative commons (40), and is under distributed under a CC BY-SA 3.0 license.

rest of the text blood pressure is given in these units, unless otherwise stated. To set a diagnosis multiple measurements are usually made and an average given as the final blood pressure value, since a single measurement can easily be affected by immediate factors such as mental stress or physical movements. The condition is usually split in two categories, primary or essential hypertension, in which the underlying cause is unknown, or secondary hypertension in which the cause can be attributed to a given cause. The large majority of hypertension cases are classified as essential hypertension (38). Secondary hypertension can be a result of conditions such as chronic renal disease, which affects the blood volume regulation through disturbances in urine secretion. Other causes are also identified; disturbances in neural regulation caused by high intracranial pressure or damage to the vasomotor center, elevated hormone levels, or other cardiovascular diseases such as complete heart block and aortic arteriosclerosis.

Mean arterial blood pressure is usually thought to be proportional to total peripheral resistance R_{sys} and cardiac output (CO),

$$\text{MAP} \approx \text{CO} \times R_{\text{sys}}. \tag{2.1}$$

Cardiac output is the volume of blood the left ventricle ejects per unit of time, usu-

ally measured in litres per minute (L/min), or millilitres per second (mL/s). The possible causes of secondary hypertension listed above contribute to increasing at least one of the two factors of the formula, but typically the resistance factor. The total blood volume can also be affected by one of these conditions, but this in turn affects the CO. Since most diagnosed cases are still essential hypertension, the aetiology of the disease is still not fully understood, but possible causes may still act by modifying these factors analogously to secondary hypertension. The disease is extremely complex as multiple regulatory systems affect blood pressure, and how these may transition into pathology and interact under lifestyle changes and aging is far from understood. A well-known model within the field is the Guyton model of hypertension where the complex control system of different regulatory systems is investigated. Although it in recent years has been criticized for a number of reasons, it still holds insight into several of the regulatory mechanisms which are known to affect blood pressure (41, 42). Beard refers to that the 1972 Guyton model recently has been shown to have poor agreement with the salt retention of the cardiovascular system and it is unknown why (31). This speaks to the continuing mystery surrounding the etiology of hypertension. Beard goes on to explain that the Guyton model is often used to argue the view that arterial pressure is determined uniquely by renal salt and fluid regulation, but that the revealed shortcomings may guide what should be further investigated. In recent years, research have partially by way of using physics-based models investigated whether dysfunction of the baroreflex system through stiffened vessel walls is sufficient to explain some cases of essential hypertension (32, 30, 43). This follows from work by for example Ursino et al. which earlier applied mathematical models to investigate the baroreflex system, perhaps not solely for hypertension research, but to gain insight into this regulatory mechanism (44). These, represent alternatives to views where the blood pressure influenced diuresis and natriuresis often is the mechanism investigated to explain essential hypertension (45). Or more broadly, views which consider that salt intake or other causes can provoke an overactive renin-aldosterone-angiotensin-system or overactive sympathetic neural signals. Models have also been applied in other ways than constructing detailed models which account for regulatory system interactions. Some such as Segers et al. also take a purely hemodynamic and descriptive view to study the disease (46). Segers et al. have applied simpler models to study the differences in parameter values for groups of patients with normotension or hypertension in combination with different cardiac remodelling patterns. Based on this they further studied which parameters contributed most to the elevated blood pressure in the latter category of groups.

The condition of hypertension itself causes direct pathological remodeling of the

cardiovascular system. The arterial walls remodel to adapt to changes in wall shear stress and azimuthal hoop stress (47). Increase in blood pressure causes the hoop stress to increase and induces the vessel wall to thicken in response. Therefore, in essential hypertension, resistance vessels experience inward euthropic remodeling. This means that vessel radii constrict, and wall thickness increases. During antihypertensive therapy, the vessels may experience outward euthropic remodeling, where vessel radius increases and the wall thickness decreases.

2.3 Treatment of Hypertension

Research indicates that the risk of developing cardiovascular disease (CVD) and Current treatment of hypertension is both habitual and pharmacological. The habitual treatment consists of lifestyle alterations which can include cessation of smoking, dietary changes such as lessened salt intake, or as change in physical activity levels.

There are 6 classes of medication which are typically used for treatment of hypertension; diuretics, sympathoadrenal system inhibitors, direct vasodilators, calcium channel blockers, angiotensin-converting enzyme (ACE) inhibitors, and angiotensin II-receptor antagonists. These target different mechanisms in vasoconstriction, blood volume regulation and cardiac output in order to lower one of the two main contributors in the equation (2.1) (38). According to the guidelines from the European Society of Cardiology/European Society of Hypertension, lifestyle intervention should be attempted first to lower blood pressure to under the hypertension threshold before prescribing pharmacological treatment (7). This applies unless there are factors such as elevated risk of other CVDs, demonstrated hypertension mediated organ damage or that the patient has hypertension grade 2 or higher. Hypertension diagnosis has three categories according to blood pressure level where grade 1 describes blood pressure levels of between 140/90 and 159/99, while grade 2 and up have blood pressure levels of 160/100 and upwards.

Lifestyle intervention can involve dietary changes, as mentioned, but we will here focus on the increase in physical activity level. The technological development in developed countries, especially, can encourage an increasingly sedentary lifestyle. This may lead an increasing part of the population to not engage in the amount of physical activity recommended to ensure a good quality of life and health. The WHO recommends that one should aim to engage in at least 150 minutes of moderately intense exercise or 75 minutes of high intensity exercise per week (48).

This is, however, general advice and not particularly well tailored to an individuals baseline level of activity or potential for improvement. There exist several studies which investigate the outcome of exercise on blood pressure levels in people with hypertension and normotension both with blood pressure and other descriptors of the cardiovascular system as outcomes/end-points (19, 20, 49, 21, 50). Additionally, these studies show that the effectiveness of the exercise intervention may be dependent upon type of exercise, duration and initial blood-pressure levels, as well as different cardiovascular dsieases and conditions. This further suggests that the blood pressure and phenotype response is highly dependent upon the individual. It is known that there are some individuals whose high blood pressure and hemodynamics may not respond to exercise intervention. However, exercise can be effective as therapy for those who do respond, since blood pressure has been observed over several studies to be reduced by -11 mmHg systolic on average for people with hypertension, and up to -25 mmHg in some cases (51).

2.4 The Cardiovascular System During Physical Activity

While the body always has a metabolic demand at rest in order to sustain life sustaining functions, this demand increases as energy expenditure rises with increasingly vigorous physical activity. The fraction of total blood flow to organs such as the kidneys, liver, and parts of the gastrointestinal tract is lessened, but are dramatically increased to the large muscle groups in order to satisfy the increased demand for energy. Under such conditions, the cardiac output can increase approximately fivefold at maximal intensity. The heart rate increases, as does stroke volume compared to baseline, partially due to increased venous return, but also due to increased contractility of the heart. In the vasculature several adaptions take place. The flow directed to the large muscle groups increases, while blood flow decreases for most other organs. The temperature of the body increases, and the thermoregulatory system also plays a part in adjusting flow to the surface of the skin in order to exchange excess heat to the surroundings. For the analysis in this work, we focus on the global adaptions as the models to be applied do not model the details of the different organs outside of vessels and cardiac chambers.

2.5 Exercise-induced Remodelling of the Cardiovascular System

As the hemodynamics and respiration changes during bouts of physical activity, the cardiovascular activity also remodels in response to this stimulus and experiences structural changes. The remodeling is dependent upon type of physical activity, but here we normally consider endurance or aerobic training, and not resistance training as the physical activity. After several weeks or more of endurance training the CO at rest will be almost unchanged, but the maximal CO during physical activity will be elevated. This is partially due to resting heart rate being lowered, while the SV is increased in both at rest and higher heart rates. The blood volume is also increased after exercise, which contributes to a larger end-diastolic volume (EDV) (52). The change in SV is also caused by structural changes in the myocardium (53). Similarly, systemic blood pressure is reduced by on average -3/-3 mmHg, but this will be -11/-8 mmHg for people with hypertension (51, 52).

It should be noted that there is also a group of non-responders to exercise in terms of improved cardiorespiratory fitness (CRF). There is currently no consensus on any explanation as to why this group does not respond or what characterises this group. One viewpoint is that non-responders simply need a higher amount of exercise in terms of duration per week and therefore the response is thought to be dose dependent. Montero et al. investigated this hypothesis in a study of healthy participants and found that non-response was eliminated by changing the exercise dose (54). However, if this holds true for people with hypertension, and whether this is also true with respect to drop in blood pressure levels is uncertain. While type of exercise and intensity and amount holds importance for blood pressure reduction, how this affects the magnitude of blood pressure reduction and in which type of individual is currently inconclusive. Individuals who do not experience blood pressure drops during night time have been observed to be non-responders in the past, and it has been proposed that causes can be both genetic or due to the specific pathophysiology of the individual cases (51).

In the coming subsections we look a little closer at a few parameters that are linked to exercise-induced remodeling. While more of the model parameters described in section 3.1.3 may respond to exercise, these are the ones of focus.

2.5.1 Total Peripheral Resistance

Total peripheral resistance (often interchangeably used with systemic vascular resistance) is a measure of how the collective geometric properties of the arterial tree

and the material properties of the blood cause blood pressure to change as blood ejected by the left ventricle passes through it. For a single blood vessel resistance to flow is influenced by the blood viscosity, radius and length of the vessel. For fully developed stationary flow through a tube, popularly known as Poiseulle flow, the resistance can be described as

$$R = \frac{8\eta l}{\pi r_i^4}. \tag{2.2}$$

Here, η is the dynamic viscosity of the blood, l is the vessel length and r_i is the internal radius of the vessel (47). From this formula we note that smaller radii cause higher resistance, and hence the smaller arteries typically contribute most to the resistance of the arterial tree. This relationship is only applicable in select parts of the circulation as it does not apply for pulsatile flow in distensible tubes as you would find in most parts of the circulation, but nevertheless gives an indication of how the resistance is related to the descriptors of a blood vessel.

However, the total peripheral resistance specifically refers to the resistance contribution from the entire arterial tree. Vessels diminish in diameter as the blood flows from the heart towards the capillaries, but they also bifurcate. Computing the total peripheral resistance could be achieved by adding the resistances in series, and adding the reciprocals of the parallel artery resistances. A simpler way to determine this quantity though is through the mean pressure drop across the relevant arteries and mean input flow as per Equation (2.1).

As stated, hypertension is a complex disease which is not yet fully understood, but some cases of exercise-induced lowered blood pressure is thought to partially be explained by remodelling of the blood vessels in participants whose blood pressure are responsive to exercise as treatment. Green et al. collects results showing how long-term exercise induced structural remodelling of the cardiovascular system can be mediated partially through the endothelial function (55). Increase in blood flow such as when the sympathetic neural system initiates increased heart rate during vigorous physical activity, cause changes in shear stress. The increased shear stress stimulates the endothelium which can then emit signaling substances such as nitrous oxide (NO), which becomes more abundant and affects muscle relaxation and contraction in the tunica media. This effect is acute as vigorous activity is ongoing. Long-term remodeling takes place as the vessel structure adapts to the new level of shear stress and reduces shear force to the previous set point by adjusting the diameter of the vessel. Note that other factors may affect vessel remodelling

and CO, an example of which being angiogenesis which causes more efficient oxygen uptake in muscles, reducing the need for increased blood flow. Additionally, increased angiogenesis and a larger number of vessels in the microvasculature may lower total peripheral resistance. Although, there are currently a number of possible hypotheses on how angiogenesis is stimulated during exercise. Additionally, functional changes of the renin-angiotensine-aldosterone system and sympathetic neural system may occur and further reduce the level of vasoconstriction at rest.

2.5.2 Arterial Compliance

Compliance is closely related to the concept of distensibility, but is also the reciprocal of the quantity known as elastance. Compliance is the ability of the blood vessels to accommodate an increased blood volume, and is usually defined as area or volume compliance. Area compliance is the rate of pressure change per change in area, typically the cross sectional blood vessel area, $C_{\mathrm{A}} = \frac{\Delta A}{\Delta P}$. Volume compliance on the other hand is useful for characterizing larger collections of vessels by defining it as the change of volume per change in pressure,

$$C_{\mathrm{V}} = \frac{\partial V}{\partial P} \approx \frac{\Delta V}{\Delta P}. \tag{2.3}$$

The vessel compliance relies both upon the structure and material properties of the vessel walls. Less muscular vessels such as the larger arteries are usually more compliant and express most of the compliant properties of the systemic vascular tree. Similarly to vascular resistance, the compliance of vessel segments can be aggregated into one compliance, but compliances must added for vessels in parallel, and the sum of reciprocal compliances can be used to add compliances in series.

The veins are also compliant and much more than the arteries. While the exact factor is probably personal, Hainsworth notes that it is approximately by a factor of 30 (56), and Rose et al. have shown that the factor is approximately 20 when measured in dogs (57).

Systemic arterial compliance has bee observed to be increased after exercise in both young healthy individuals and older individuals in various states of health (58, 59). In the exercise physiology literature, it is common to study the exercise effect on pulse wave velocity (PWV). Vessel compliance is known to be related to the structural and material properties of the vessel walls (47). PWV is the propagation speed of the pressure pulse wave travelling through the vessels, and is dependent

upon the wall properties. This relationship is modeled through the Bramwell-Hill and Moens-Korteweg equations

$$\mathrm{PWV} = \sqrt{\frac{hE_{\mathrm{inc}}}{2r_i\rho}} \tag{2.4}$$

and,

$$\mathrm{PWV} = \sqrt{\frac{A}{\rho C_{\mathrm{A}}}}. \tag{2.5}$$

Here, h is the vessel wall thickness, E_{inc} is the incremental elastic modulus of the vessel, ρ is the blood mass density, r_i the lumen radius, and A is the lumen area. Montero et al. and Ashor et al. have meta-analyzed multiple studies investigating the exercise effect on PWV. While Montero et al. found a decrease with intervention periods over 12 weeks, and when the decrease was supported by a decrease in blood pressure, it was not concluded that aerobic or resistance training could lower arterial stiffness. Ashor et al. on the other hand found significant decrease in PVW among prehypertensive and hypertensive study participants, although with a small sample of studies. Tanaka reports that studies using different types of aerobic exercise have found increased arterial compliance (60). Tanaka also explains that factors such as reduced elastin and increased collagen in vessels are thought to contribute to vascular stiffening with age. However, some evidence indicates that reduction in sympathetic vasoconstriction at rest can lead to increased compliance after exercise. What factors can explain increased compliance after exercise is not fully explored and is thought to be a combination of functional and mechanical factors. Many of the mechanisms are common to the ones that may adjust total perioheral resistance. Currently, only aerobic exercise has been shown to increase compliance, while resistance exercise may cause a decrease.

2.5.3 Maximal Left-Ventricular Elastance

The left-ventricle periodically contracts to increase pressure and cause blood flow to the systemic arteries. While the pressure and blood flow development is subject to interaction with other vessel compartments and a complex network of regulatory mechanisms, the myocardial muscle contraction itself may be characterized by contractility. While there is no single universal measure of contractility, it can be expressed in many ways. The ventricular ejection fraction (EF) is the proportion of the ejected blood per heart beat or stroke volume (SV) divided by the maximal volume of the ventricle which is the EDV. The EF characterizes contraction by

how much volume is displaced by the contractile motion, but is also dependent on the afterload which the ventricle ejects blood against, ie. the pressure of the systemic circulation when the heart is ejecting. The end-systolic elastance, which can be derived from the end-systolic pressure-volume relationship, is an example of a load-independent measure of the left-ventricular contractility.

The PV-loop, for which an illustration can be seen in Figure 2.3, shows the left-ventricular pressure and volume development throughout the heart-cycle. The elastance, the inverse of vascular compliance, can be defined as the change of pressure given a change in volume, $E = \frac{\Delta P}{\Delta V}$. A high elastance means that the ventricle accommodates less added blood volume. Therefore the maximal left-ventricular elastance, that is the maximal elastance slope in end-systole is often interpreted as a contractility measure. This slope is independent on ventricular load in normal physiological function, but requires multiple PV-loops under varying conditions, or additional information about the ventricular dead space volume to be determined. The dead-space volume (V_{d}) is here referred to as the ventricular volume at which the ventricular pressure would become zero. Suga et al. measured the ventricular pressure and volumes in dogs and computed the elastance curve as $E(t) = P(t)/(V(t) - V_{\mathrm{d}})$ (61). By varying the pre- and afterload of the heart, Suga et al. found that the maximal elastance value and time of maximal elastance was independent of the afterload, whenever the contractile (inotropic) state and heart rate of the heart was unaltered. The basic form of the curves were also found to be similar for all heart loads, rates and contractile states. They concluded that the maximal elastance and time of maximal elastance explicitly reflected ventricular contractility.

While contractility measures such as EF were found to improve after exercise in hypertensives by Molmen-Hansen et al. (50). However, this does not necessarily mean the end-systolic left-ventricular elastance increases after exercise. There is some evidence that this also would should increase after exercise, since end-systolic elastance has been found to increase after intensive exercise in rats. Additionally it has been showed that stiffening of the myocardium with age can also be expressed as increased elastance (62), and how these different mechanisms interact is uncertain.

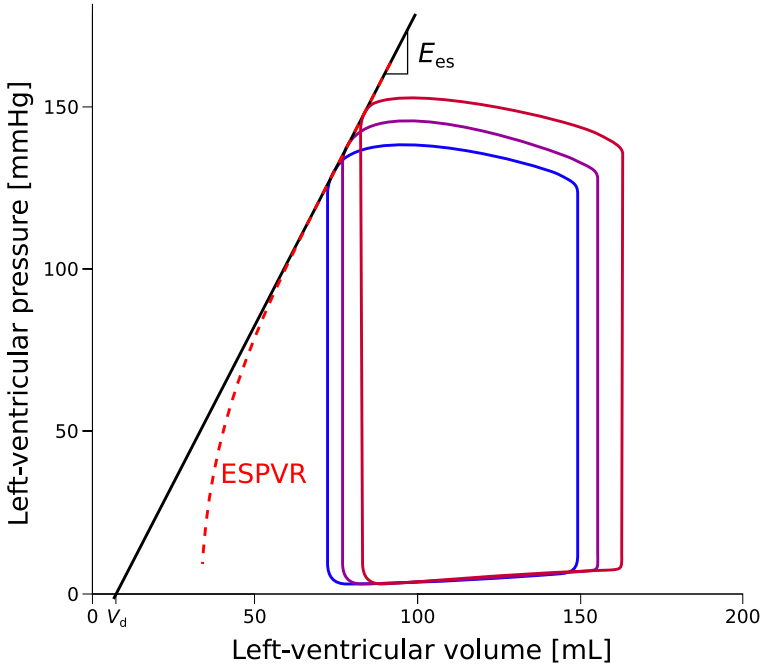

Figure 2.3: Depiction of three pressure-volume loops for the left-ventricle. The end-systolic pressure volume relationship (red) and the linear approximation (black) used to derive the end-systolic elastance (E_{es}). The linear approximation intercepts the volume axis at a virtual intercept volume V_{d}, which can be negative.

Chapter 3

Methods

3.1 Cardiovascular Models

This work is based on the principles of physics-based modelling of cardiovascular function and physiology. However these models exist in a wide range of complexities and model fidelities, which are suited for different types of problems and applications. This work applied only lumped-parameter models, which operate in the time domain, but has zero dimension in space and are therefore referred to as "0D-models" hereinafter.

3.1.1 Higher Dimensional Models

For problems where person specific geometry, a three dimensional description of blood flow, or spatial description of material properties and mechanics is needed, tools such as computational fluid dynamics (CFD), finite element models (FEM), and fluid-structure interaction (FSI) models are useful tools. These tools are highly detailed and can resolve complex geometries but are usually computationally costly, so they are often applied to investigate a select part of the cardiovascular model such a the aorta, or a other vessels (14, 63). This is a distributed parameter model in the sense that mechanical material parameters can vary with position in the 3D space (22).

Reducing the dimensionality we have 2D and 1D models, these are often applied to blood vessels and assuming axisymmetry for the 2D model, and further assumptions about the flow profile for the 1D case. These models are simpler and more efficient than 3D models, and give information about flow and pressure along the

vessel centerline or additionally along the radial line of the cross section for 2D models. These are also distributed models, as material parameters can vary along the spatial dimensions. Works such as by Mynard et al. use several 1D models to describe multiple connected vessels of the branching arterial tree (64).

3.1.2 0D-models

The lumped parameter models differ from the distributed parameter models in that the parameters characterize the behaviour of an entire volume compartment, and all pressure and flow is identical within this compartment. While the compartment has a fluid volume which is prone to change as a state variable, this volume is considered shapeless, hence zero spatial dimensions. These models are described by the same formalism as circuit theory and can be analyzed both in a time and frequency domain, and in this work we focus on the time-domain treatment.

The standard elements of a lumped parameter model are vascular resistance, compliance, and inertance elements. These are analogous to resistors, capacitors and inductors in circuit theory. Resistance and compliance have been described previously, but inertance is a property which takes into account the inertia of blood and relates the acceleration and deceleration of flow to the pressure drop over a vessel segment. The Ohm's law analogue describing pressure drop over a vessel segment in reality only describes mean flow (47). Single compartments are often organized as Windkessel models, which are reported to first be introduced by Otto Frank in 1899 (65). The most well-known variation of these consist of a resistance and compliance element and is known as the Two-element Windkessel (2WK). This model accounts for the total vessel resistance to flow. Otherwise, by adding another resistance element in series with the parallel compliance and resistance elements of the 2WK we find the Three-element Windkessel (3WK). And lastly by addition of an inertance element we have different variations of the Four-element Windkessel (4WK) depending on the placement of the inertance element. An illustration of some common model configurations can be seen in Figure 3.1. Segers et al. optimized these models to data from 2404 people and demonstrated differences in their resulting model outputs and parameters (23). The 4WK models were found to give better representations of the circuit input impedance and best goodness of fit figures. Still, the value of the inertance was highly dependent upon the model structure, and was often found to take unrealistic values. Although the 4WKs were most accurate in recreating the data, the paper concluded that which model was best for estimating parameters for the systemic arteries was still an open question. It was noted that the 4WK with the inertance in series often agreed well with parameter estimates from the 3WK. The 3WK was also the model which the Nelder-Mead method used the smallest amount of iterations to find an estimate for.

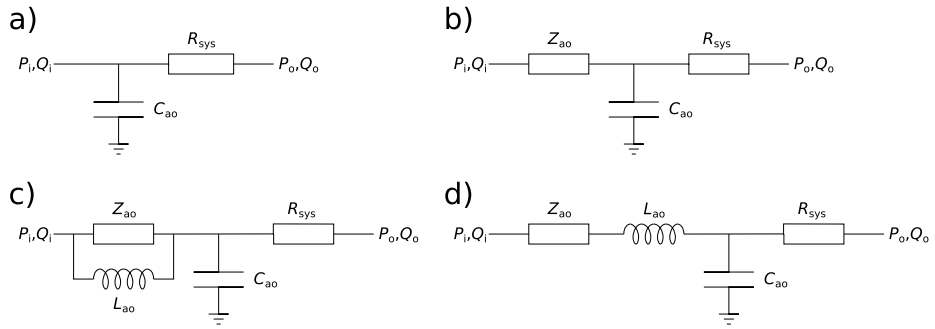

Figure 3.1: An illustration of some common and basic Windkessel models for the systemic circulation. a) The Two-element Windkessel model. b) The Three-element Windkessel model. c) The parallel Four-element Windkessel model. d) The series Four-element Windkessel model. The models are comprised of resistance (R_{sys}), compliance (C_{ao}), characteristic aortic impedance (Z_{ao}) and inertance elements (L_{ao}). Q_i and P_i are inflow and pressure, where subscript o indicates outflow and corresponding pressure.

Since the physical interpretability of estimates for L were uncertain and dependent on model configuration, and it is computationally simpler to find estimates for the Three-element Windkessel seems sufficiently detailed for describing a hypertension state in terms of arterial flow and pressure. However, using a 4WK could potentially adapt more subtle features in the waveforms and give more physiologically accurate parameter estimates.

3.1.3 The Three-Element Windkessel with the Varying-Elastance Model

The model used in this investigation is based on many previous similar models, among them models presented by Smith et al., Stergiopulos et al., and also Pironet et al. which use a very similar model (26, 24, 66, 37). We have used two models, one closed-loop version consisting of three compartments; the left ventricle, systemic arteries and systemic veins, where the venous return is directed into the mitral valve of the left-ventricle. The other model is practically identical to the open-loop model presented by Stergiopulos et al. (24). The model is formulated as a non-linear system of ordinary differential equations (ODEs) and are formulated as changes in compartment volume per unit time. The state variables of the system are stressed blood volume, pressure and flow.

The arteries are modeled as a 3WK where the aortic valve resistance is lumped with the characteristic aortic impedance, which acts as the first resistance element of the circuit. The venous compartment is modeled as a 2WK where the resistance element is lumped with the mitral valve resistance. Both ventricular valves are

modeled as unidirectional diodes, which close upon a negative pressure gradient in the direction of flow. Flow is allowed to go from the venous compartment into the ventricle, and from the ventricle into the arterial compartment. Flow can in theory go both ways between the arterial and venous compartment as there is no valve implemented here. The open-loop model formulation is exactly the same, except for the venous compartment which is set at a fixed venous pressure, and similarly, the left atria is fixed at a pressure, and both of these compartments are now infinitely accommodating blood volume at the given pressure. The closed-loop model has a constant blood volume.

The ventricle is modeled by the varying elastance model in the configuration as is presented by Stergiopulos et al. (24). This model is based on the concept of varying elastance by Suga et al. (61), which found that the ratio between pressure and volume in the ventricles were universal when corrected for heart rate and contractility state. The ventricle is modeled as having a pressure related to elastance and volume as $P_{\mathrm{lv}}(t) = E_{\mathrm{lv}}(t)V_{\mathrm{lv}(t)} + P_{\mathrm{th}}$, where P_{th} is the intrathoracic pressure. The elastance function $E_{\mathrm{lv}}(t)$ is a periodic function repeating the elastance shape which is parameterized to have a peak value at a given point of time in the heart cycle, and attain a maximum elastance value, and to never go below a minimum level. There are alternatives to the varying elastance models, such as the single fiber model as applied by Bovendeerd et al. (25) which gives a simplified description of the ventricular wall mechanics. Another alternative is the piecewise defined cosine function as used by Beard et al. (43). However, the varying elastance model is versatile and is directly based on global concepts such as elastance which are fairly closely related to clinical measurements which causes it to be simple to work with. The electromechanics of the myocardium are not described in detail in such a model formulation. The elastance function is identical for both the closed- and open-loop model configuration.

The current model assumes that there is no pressure and flow wave propagation and significant wave reflection in the vessels of the arterial system. the inertance effect of the vessels are also neglected such that the effects of flow acceleration are not accounted for in detail. The valve models assume there is no flow reversal at any point across the valves. The model also assumes that the flow from the systemic veins can adequately mimic the diastolic filling that the left-ventricle would normally receive from the pulmonary veins. The atrial effects on ventricular filling are also neglected as these are omitted from the model.

Lastly, it should be noted that assuming the model can be adequately personalized,

that the parameters can be viewed as representing to underlying lower level phenotypes leading to the hemodynamic signifiers of normo- or hypertension. However, these parameters do not by themselves reveal the pathways through which hypertension is hypothesized to manifest or develop without further analysis or some insight into the parts of parameter space characterizing a certain realization of a hypertension phenotype. To get the full understanding of hypertension development anyway, modeling of known blood pressure regulatory systems would also very likely be necessary. But the parameter combinations can likely in part play a role in further understanding of how the condition manifests, at least for an individual.

3.1.4 Structural Identifiability

Before even attempting to optimize model parameters or showing practical identifiability it can be beneficial to know that a mathematical model has a set of model parameters which can uniquely describe different states of the system under ideal conditions. By ideal conditions we here mean where the data for optimization is noiseless and is perfectly described by the model in the sense that there is no model discrepancy. First we define global structural identifiability as it is discussed by Miao et al. (67). If a model organized in a system of equations with a vector of model outputs $\mathbf{y}$ with a known valid control input $\mathbf{u}(t)$ and any two parameter vectors $\boldsymbol{\theta}_1$ and $\boldsymbol{\theta}_2$ satisfies that

$$\mathbf{y}(\mathbf{u}, \boldsymbol{\theta}_1, t) = \mathbf{y}(\mathbf{u}, \boldsymbol{\theta}_2, t), \text{if and only if } \boldsymbol{\theta}_1 = \boldsymbol{\theta}_2. \tag{3.1}$$

In the context of the model of focus for this work, we regardthe the control input $\mathbf{u}(t)$ as the input function $\tau(t)$ of the left-ventricular elastance function, which is periodic with the heart cycle period T [1]. However, this is a strict condition which is challenging to prove for the entire parameter space. This is essentially a one-to-one mapping of system input to output. Local structural identifiability is defined in the following way

$$\mathbf{y}(\mathbf{u}, \boldsymbol{\theta}_1, t) = \mathbf{y}(\mathbf{u}, \boldsymbol{\theta}_2, t), \text{if and only if } \boldsymbol{\theta}_1 = \boldsymbol{\theta}_2, \text{and } \boldsymbol{\theta}_1, \boldsymbol{\theta}_2 \in P^*. \tag{3.2}$$

P^* is in this context an open neighbourhood around a point $\boldsymbol{\theta}^*$. While structural identifiability can in some cases be shown analytically, it quickly becomes a complex task to do so as model complexity increases, and the model structure may

[1] $\tau(t) = t \mod T$, in this example.

cause additional challenges in achieving this. Many software tools have been proposed to solve this for application in chemistry, and biological systems. Castro et al. have compared many proposed techniques to solve this within the aforementioned disciplines (68). Their work points to tools such as DAISY and COMBOS, which apply algebraic techniques to systems of equations on a specific form, but this turned out not to be applicable to the model configuration outlined above. Castro et al. also suggest more computationally intensive methods which could treat systems on the form of our model.

Villaverde et al. developed the computational STRIKE-GOLDD tool, which implements a differential algebra method to show local structural identifiability (69). The method is based on the concept of observability, which will not be strictly defined here, but is analogous to identifiability. Observability assesses whether there are neighbouring states to a chosen initial system state which is indistinguishable from all states in a neighbourhood of the chosen state. If the initial state is distinguishable from the states in the neighborhood, then the state is locally observable. By state we here mean the combination of state variables describing the system, which for the model of section 3.1.3 can be compartment pressures or volumes. Further, the observability matrix is built by calculating the Lie derivative which is taken of the output function of the system with respect to the model state variables $\mathbf{x}$ and parameter vector $\boldsymbol{\theta}$. Note that what is in the rest of the text referred to as the model outputs $\mathbf{y}(..., t)$ are in many cases equivalent to the state variables $\mathbf{x}$ in this context. The vector of state parameters can be the compartment pressures or stressed blood volumes according to how the differential equations for the model are defined. The Lie derivatives are defined by

$$
\begin{aligned}
L_f g(x) &= \frac{\partial g(x)}{\partial \tilde{x}} f(x, u) \\
L_f^2 g(x) &= \frac{\partial L_f g(x)}{\partial \tilde{x}} f(x, u) \\
&... \\
L_f^i g(x) &= \frac{\partial L_f^{i-1} g(x)}{\partial \tilde{x}} f(x, u).
\end{aligned}
$$

Here $f(x, u)$ refers to the right hand side of the ODE for the relevant state parameter if arranged on the form $\frac{dx}{dt} = f(x(t), \mathbf{u}(t), \boldsymbol{\theta})$. Simultaneously $\tilde{x}$ can represent any state variable from $\mathbf{x}$ or input parameter from $\boldsymbol{\theta}$. However, for time varying inputs the Lie derivative is extended to

$$L_f^i g(x,u) = \frac{\partial L_f^{i-1} g(x,u)}{\partial \tilde{x}} f(x,u) + \sum_{j=0}^{j=i} \frac{\partial L_f^{i-1} g(x,u)}{\partial u^{(j)}} u^{(j+1)}. \tag{3.3}$$

The method works by constructing the observability matrix by performing the Lie derivatives over all state variables and model parameters for up to the "n+q"$^{\text{th}}$ first Lie derivatives and constructing a matrix based on this. The actual number of derivatives to be used can be less than this. The n is here the number of states, while q denotes the number of model parameters, while a superscript on the form (j) denotes j differentiations with respect to time. If the resulting matrix is full rank, the system is locally structurally identifiable. For more details, see Villaverde et al. (69, 70).

3.1.5 Practical Identifiability

Practical identifiability, in contrast to structural identifiability, also accounts for imperfections in data. As in the works of Brynjarsdóttir et al. (71), data measurements $y^m(t)$, can be expressed as the sum of model outputs, model discrepancy $\delta(t)$ and measurement noise $\varepsilon(t)$ as such

$$y^m(t) = y(\mathbf{u}(t), \boldsymbol{\theta}, t) + \delta(t) + \varepsilon(t). \tag{3.4}$$

In a realistic optimization scenario we are then given a set of data to optimize $\boldsymbol{\theta}$ for data which is on the form in equation (3.4). Errors in parameter estimates are then introduced jointly by the model discrepancy and measurement noise. The model parameters are practically identifiable if the model parameters can then be estimated to a sufficiently small error from the solution for different noise profiles and data samples characterizing the same measured state. The level of parameter error acceptable, should be predetermined, and how to practically evaluate this is a complex issue for nonlinear models since the true level of error can be unknown in application to real data. However, one can for example use methods to estimate reference values and apply profile-likelihood techniques such as Pironet et al. has done for a model similar to the one presented in this thesis (72). The level of accepted error is also problem specific and needs to be determined to be able to assess the practical identifiability (67).

It is important to note that the appended papers do not strictly demonstrate practical identifiability for the presented models. The papers of sections 6 and 7 are aimed towards answering how an estimation procedure based on multiple local optimizations with little prior information performs in estimating correct parameter

values given that it may terminate in other minima than the global minimum. Further, we aim to answer how this performs for model personalization and resolution for predicting and calculating personalized parameter changes (33, 73). This also refers to how the choice of local optimization with a small data set of synthetic or real data can fail to find the correct minimum for describing the physiologically correct state. It can also fail to find the global minimum of the objective function, regardless of if this truly is the most physiologically correct one or not. We examine the effect of varying the initial parameter estimate guesses in contrast to for example varying sampled noise profiles, or examining the statistical confidence intervals of the neighbourhood of an optimized estimate point.

3.2 Mathematical Optimization

In the following we assume the control input is always known, and unchanged, and does not affect the problem solution so we omit it in all subsequent mathematics. To personalize a cardiovascular model the problem of model optimization must be solved. We mean by this that we seek to find an estimate for optimized or personalized model parameters $\hat{\boldsymbol{\theta}}$ by solving the inverse problem

$$\hat{\boldsymbol{\theta}} = \min J(\boldsymbol{\theta}), \tag{3.5}$$

where $J(...)$ is a cost function, or objective function to be minimized. If the problem is successfully solved, the resulting parameter estimate $\hat{\boldsymbol{\theta}}$ is then the parameter set best describing the solution which satisfies the constraints implemented in the cost function. By inverse problem we here mean that we from data corresponding to model outputs, determine which model parameters (and optionally inputs) these are the product of given a mathematical model incorporating these parameters (and inputs). In this work we focus on a sum of least squares approach and formulation of the objective function, as opposed to for example a maximum likelihood approach.

We can separate between global and local optimization methods. Global optimization in this work refers to methods which search specifically for the objective function minimum with the lowest value if it exists, while local optimization methods search for any local minimum and do not search for the global minimum specifically. Global methods such as Monte Carlo methods, or differential evolution methods to mention some, can often be expensive computationally, and this makes these methods less feasible for optimization problems which ideally should

be solvable in a setting outside of academia or strictly research based activities, such as in the clinical setting.

We attempt to use local methods in this work, as they are less computationally costly. Well-known and popular methods which are often used within the field is the gradient descent method Levenberg-Marquard and direct search Nelder-Mead simplex method. Gradient descent methods operate by evaluating the gradient of the objective function in various ways and picks the steepest direction to look for a minimum. Direct search methods (represented by Nelder-Mead) on the other hand do typically not evaluate the objective function gradient.

3.2.1 Selected Previous Work in Parameter Estimation of Lumped-Parameter Models

Within the field of biomechanics, and biomedical engineering applied to lumped-parameter models specifically there has been different approaches to personalizing model parameters. Many different approaches have been proposed, while there is no apparent consensus on a generally best method for a wide range of models. Early works by for example Segers et al. use the Nelder-Mead simplex algorithm to estimate parameters from personalized data for different Windkessel models. Kind et al. take a different approach called Subspace Model Identification to optimizing Windkessel model parameters to data (74). By formulating the cardiovascular system equations as a matrix equation and solving by linear algebra methods and the MOESP algorithm they obtain parameter estimates for different noise profiles. The work concluded that the method was robust for the 3WK for different noise profiles on simulated data, but less convincing for the 4WK.

Moving on to systems models describing more compartments of the circulation we have for example the work by Colunga et al. and Marquis et al. (17, 35). The aforementioned authors treat more complex models where identifiable subsets of model parameters are first investigated, care is taken to find initial guesses for the personalizable parameters before optimizing using the Levenberg-Marquardt algorithm. They also verified their estimates by confidence intervals obtained by a global Markov-Chain Monte Carlo (MCMC) approach of the type known as the Delayed Rejection Adaption Metropolis (DRAM) algorithm. By application of sensitivity analysis they also reduce their parameter sets to identifiable sets based on sensitivity analysis. Pironet et al., and deBournonville et al. similarly find informed initial parameter guesses and optimize using a combination of a rapid proportional gain algorithm before refining the parameters using the Nelder-Mead simplex algorithm (36, 37). Hann et al. use a six compartment model similar to the

one used by Smith et al. and argue that standard non-linear local optimization is too liable to find other minima than the true global minimum and present a method where by examining the parameter changes and effects on model outputs iteratively approach a unique solution (34, 26). They have developed a computationally efficient iterative procedure for use in the intensive care unit (ICU) context, which gradually update parameter estimates such that the chosen model outputs were predicted to high accuracy when compared to data with noise. This procedure is envisioned for use with invasive data, and extracts information and time points from pressure and volume data to personalize 6 or more parameters per three chambers of the 6 chamber model. Their approach does not use the entire waveforms as they argue this lessens error by eliminating features that are not sufficiently accurately modeled by model discrepancy. A contrasting approach to this may be to take information from the entire waveform, and try to extract information from the local minima close to or surrounding the global minima as this may have useful information about the variability of the waveform and perhaps the parameters as well. Itu et al. take an approach to personalizing the pressure-volume loop by estimating relevant arterial and ventricular parameters using only 5 single valued indices from the arteries and left-ventricle (28). The dogleg trust-region method is used in combination with a fixed-point method to augment the next iterative step size in order to optimize the final three personalized parameters, while total peripheral resistance is estimated beforehand.

Moving up further in cardiovascular model complexity Pant et al. takes a different approach, where they use a Unscented Kalman-filtering approach to adapt the parameters of a Windkessel model. By starting with a 3D representation of the aorta, different subsections of the models are replaced by 3WK models, and Kalman-filtering is used to estimate parameters for the lumped-models for subsequent use in parameterizing a 3D model (75). Similarly, the method has been applied to a detailed model of the circulation including the pulmonary, systemic and pulmonary circulation in a single ventricle physiology, distinguishing between the upper and lower body circulation (76). The method demonstrates fast convergence to the experimentally measured value for the elements of 3WK models, and good recreation of model outputs. The method has also been tested with a single 3WK model using synthetic data and show similar good results. However, it is also shown that with poor initial choices for parameter values, the method may fail.

3.2.2 A Heuristic for Estimation Using Minimal Data

When optimizing the parameters of the model described in Section 3.1.3 to synthetic pressure and flow data with Gaussian noise, average parameter errors of 10% and upwards were found when performing multiple repetitions using a local op-

timization method (33). This suggests that there possibly are minima close to the global minimum which are almost as good as the best minimum. Daily variability in many of the hemodynamic states can be quite large. Throughout a 24 hour span of time, there is up to a 40 mmHg difference in systolic blood pressure for people with suspected hypertension (77). There are even differences between separate heart beats due to for example heart rate variability and respiratory effects. Therefore, we suggest that there is not necessarily one minimum which is a correct representation for the general hemodynamic state and parameters. Since, local optimization can find different minima which may still have similar cost function values to the best identified minimum, we take these minima into account to create an average parameter which takes some of the information from the other almost equally good minima. Although beat to beat variability can be alleviated by averaging data or other methods, this can be a supplement to such actions, since some uncertainty in the true minimum may arise from model and data discrepancy as well. As a remedy, we have developed an estimation heuristic which attempts to take into account information from minima close to what is deemed to be a reasonable minimum, if not the global minimum.

When averaging parameters for an unbounded parameter space during optimization we found that averaging the multiple minima could cause resulting estimates that did not yield a realistic hemodynamic state compared to the data. To ensure physiologically realistic parameter values we therefore opted for constraining the parameter space to physiologically relevant parameter values.

Further the procedure is organized in sequential steps; first an exploration of the parameter space to find a candidate for the global minimum is performed by sampling 30 initial parameter guesses from a uniform distribution within the parameter bounds. Secondly, 20 new initial parameter guesses are sampled around the previous initial guess yielding the best optimization minimum. This was done to partially explore the region close to the best minimum more closely, while still exploring other minima in the vicinity to continue the search for the best minimum. A uniform distribution with ranges of 10% above and below the previous values were taken to find the new estimates. The best remaining samples according to the objective function are then averaged to use information about the other best estimates found within this round. Let the vector of model parameters be $\boldsymbol{\theta}$, and θ_i is the i^{th} component of the vector. The optimization steps are as follows:

1. Apply the local optimization method to make 30 parameter estimates from 30 different sets of initial guesses.

2. Take the initial parameter guess which yields the lowest objective function value estimate and create a new uniform distribution centered on these parameter values.
3. Make 20 new initial guesses based on the best previous guess and produce 20 new vectors of estimates, we call this set of parameters $\mathbf{\Theta}_{\text{step2}}$.
4. Make a selection based on the best objective function values from Step 3, $\mathbf{\Theta}^k_{\text{filtered}}$, where k denotes the k^{th} filtered estimate.
5. Compute the final parameter estimate as the mean of the estimates from Step 3, such that $\hat{\theta}_{\text{mean},i} = \frac{1}{N_k}\sum_k \Theta^k_{\text{filtered},i}$. Here, N_k is the number of remaining estimated parameter vectors in $\mathbf{\Theta}_{\text{filtered}}$ after filtering.

A full description of the algorithm is given in appended paper of chapter 7. Colunga et al., and Marquis et al. take an approach to making more informed guesses about the initial values, and use local optimization methods with a 10% range around these predetermined initial guesses to ensure that the solution converges. However, they do not state whether they bound the allowed parameter space beyond allowing only positive valued estimates.

3.2.3 The Trust-Region Reflective Algorithm

For our approach we opted for the Trust-Region Reflective Algorithm (TRRA). This method is widely available as one of the optimization algorithms implemented in the popular Python library SciPy. This approach also supports use of bounds in contrast to standard SciPy implementations of for example the Levenberg-Marquardt algorithm. The algorithm is local and may therefore terminate in local minima, without further modification. The work described in this thesis focuses on using this algorithm to find candidates for global minima on a bounded parameter space.

The TRRA is a trust-region method. This means that to find the correct step and direction towards a minimum, the method approximates the objective function around the initial point by a second order Taylor series expansion, like a Levenberg-Marquardt algorithm would. If the step direction towards a minimum is $\boldsymbol{\theta}_s$, such that $\boldsymbol{\theta}_{k+1} = \boldsymbol{\theta}_k + \boldsymbol{\theta}_s$ then the objective function approximation can take the form

$$F_J(\boldsymbol{\theta}_k + \boldsymbol{\theta}_s) \approx J(\boldsymbol{\theta}_k) + \frac{\partial J}{\partial \boldsymbol{\theta}}(\boldsymbol{\theta}_k)^T \boldsymbol{\theta_s} + \frac{1}{2}\boldsymbol{\theta}_s^T \frac{\partial^2 J}{\partial \boldsymbol{\theta}^2}(\boldsymbol{\theta}_k)\boldsymbol{\theta}_s \tag{3.6}$$

$$\approx J(\boldsymbol{\theta}_k) + \nabla J(\boldsymbol{\theta})_k^T \boldsymbol{\theta}_s + \frac{1}{2}\boldsymbol{\theta}_s^T H_J(\boldsymbol{\theta}_k)\boldsymbol{\theta}_s. \tag{3.7}$$

This approximation is only trusted within the trust region Δ_k, which is updated for each iteration. The Hessian of the objective function H_J is approximated and amended by a term which accounts for the distance to the parameter constraint boundaries. An Newton step is found by using this Hessian approximation to find a candidate step within the trust region,

$$M(\boldsymbol{\theta}_k)\boldsymbol{\theta}_s = -D^{-1}(\boldsymbol{\theta}_k)\nabla\boldsymbol{\theta}_s. \tag{3.8}$$

Here, the $M(\boldsymbol{\theta}_k)$ matrix is the amended and approximated Hessian, and $D^{-1}(\boldsymbol{\theta}_k)$ is an inverse scaling matrix. The reflective part of the title refers to a method for reflecting the search step off the constraint boundary for the search, which is taken as a candidate for the step direction. The path to the boundary which is not reflected, as well as a step candidate solved strictly on the interior of the trust region which does not exceed any parameter constraints are also taken as candidate steps. The reflective step has been shown to increase the efficiency of the search in comparison to some other optimzation algorithms. We refer to the work by Branch et al. for further details (78).

3.3 Other Methods

3.3.1 Regression Models

To perform statistical analysis on data and estimated model parameters, linear regression has been applied in order to analyze the major influences of the parameter estimates. We apply linear regression models. The the dependent variable, which is taken to be stochastic Z, and p independent variables or predictors $X_1, X_2, ..., X_p$. By minimizing the sum of least squares, we can obtain a regression line for the best optimized line to the data on the form

$$\hat{z}_i = \beta_0 + \sum_{j=1}^{p} \beta_j x_{j,i} \tag{3.9}$$

Here, $\hat{z}_i$ denotes the regression model prediction for data point i, and β_j denotes the regression coefficients describing the contribution of each covariate and the y-axis intercept. The Pearson correlation r is a measure of how two variables move in relation to one another. The square of this is the coefficient of determination r^2 which can be defined as

$$r^2 = \frac{\sum_{i=1}^{n}(\hat{z}_i - \bar{z})}{\sum_{i=1}^{n}(z_i - \bar{z})}, \tag{3.10}$$

where $\bar{z}$ is the sample mean of the W variable, and z_i is data point number i. n here indicates the number of data points. The coefficient of determination indicates what percentage of the variability in the dependent variable is explained by the dependent variables. However, for multiple regression with multiple independent variables, the r^2 increases with every added independent variable. Therefore we define the adjusted r^2, which accounts for the number of covariates as the following

$$\text{Adj. } r^2 = 1 - (1 - r^2)\left(\frac{n-1}{n-p-1}\right), \tag{3.11}$$

where p indicates the number of independent variables. With these tools we can investigate what information adds to or subtracts from the explained variance and make conclusions on what influences the dependent variable.

The concept of linear regression models can be extended to allow interpretation of grouped hierarchical data, by allowing regression coefficients to vary with random components that can account for inter-group differences. This is a useful concept for analyzing repeated measurements among individuals which have different properties.

A generic model can be expressed as

$$\hat{z}_{i,k} = \beta_0 + \gamma_{0,k} + \sum_{j=1}^{p}(\beta_j x_{j,i,k} + \gamma_{j,k})x_{j,i,k}. \tag{3.12}$$

Here the β parameters express the fixed slopes and intercept of the fixed effects. The γ coefficients express the random effects attributable to groups or individuals. We assume that these are random and have a zero mean.

3.3.2 Sensitivity Analysis

Sensitivity analysis in short is a method to analyse how sensitive model outputs and predictions $y(\boldsymbol{\theta}, t)$ are to errors and uncertainties in model inputs $\boldsymbol{\theta}$, where θ_i is the i^{th} parameter of the vector. The output is represented by the stochastic variable Y for now, and the parameters are also regarded as stochastic with measurement

uncertainty and error. The notion of sensitivity analysis presented in this text is based on Sobol indices (79). The conditional expectation value of the output given a certain parameter is denoted as $\mathbb{E}[Y|\theta_i]$. Hence, we can express the first order, or main, Sobol sensitivity index as

$$S_{\mathrm{M},i}(Y) = \frac{\mathbb{V}[\mathbb{E}[Y|\theta_i]]}{\mathbb{V}[Y]}. \tag{3.13}$$

The variance of the variable Y is denoted as $\mathbb{V}[Y]$ in the above. This main Sobol index quantifies the contribution of only the parameter θ_i to the output Y and not any of the other parameters or any interaction effects with these parameters. One can compute the portion of the total variance of Y that is caused by the interaction between two or more parameters which would cause effects of higher order, but we do not apply these. The total sensitivity index of the model output Y is given by

$$S_{\mathrm{T},i}(Y) = 1 - \frac{\mathbb{V}[\mathbb{E}[Y|\theta_{-i}]]}{\mathbb{V}[Y]}, \tag{3.14}$$

which quantifies the total contribution of the parameter θ_i to the variance of output Y. The notation θ_{-i} signifies all parameters except parameter θ_i. The computation of these variables can be done in different ways, but this is not the focus of this thesis so we skip this here. Some popular methods to be mentioned are Monte Carlo methods and the polynomial chaos expansion.

The outputs of the model of Section 3.1.3 are time dependent and cyclical. Therefore, the different parameters may have non-uniform contributions to the output variance over the interesting time intervals, and the total variance itself may also vary with time. To account for this variability in time we use the variance weighted averages which are formulated as

$$TAS_{M,i} = \frac{\sum_k S_{\mathrm{M},i}(y(t_k))\mathbb{V}[y(t_k)]}{\sum_k \mathbb{V}[y(t_k)]}, \tag{3.15a}$$

$$TAS_{T,i} = \frac{\sum_k S_{\mathrm{T},i}(y(t_k))\mathbb{V}[y(t_k)]}{\sum_k \mathbb{V}[y(t_k)]}. \tag{3.15b}$$

From the quantities defined in eq. (3.15a) and (3.15b) we can make conclusions about which parameters are the most influential for specific model outputs. Addi-

tionally, we can pinpoint which parameters are less likely to be accurately estimated when the model parameters is optimized to data for which some parameters are barely influential. The parameters of low influence can then be candidates for parameters which should be fixed to measured values or known values from the population.

Chapter 4

Summary of Papers

4.1 Summary of Appended Papers

Paper 1: Parameter estimation for closed-loop lumped parameter models of the systemic circulation using synthetic data
N.L. Bjørdalsbakke, J. Sturdy, D.R. Hose, L.R. Hellevik
Published in *Mathematical Biosciences* (2022)

In this paper we investigated personalization of a closed-loop lumped parameter model of the systemic circulation and left ventricle using local optimization methods. Initially a sensitivity analysis of the model was performed where the parameters were ranked according to the influence on the aortic pressure waveform. Using synthetic data with and without noise, we attempted to make multiple initial guesses for the algorithm to find the best objective function minima and average the best cases within reasonable bounds for the parameter space. Since the data was synthetically produced by the model itself the true parameter values were known and the mean absolute percentage error could be calculated. Nine model parameters were chosen for optimization and were sequentially fixed at correct values according to the ascending order of sensitivity ranking to assess how parameter errors were impacted. We named this framework the stepwise subset reduction method (SSRM). The main results from this analysis was that using the waveforms of aortic pressure and flow gave superior estimates than using five standard clinical indices measured in the systemic arteries. The four most influential parameters could be estimated to an error less than approximately 10% when 5% Gaussian noise was applied to the synthetic waveforms. Additionally, results indicated that fixing the venous compliance parameter had a similar effect on estimated errors

as providing the venous pressure waveform for optimization. We concluded that among the least sensitive parameters, three were were particularly challenging to optimize when data was noisy, and these were venous compliance, minimal left-ventricular elastance, and mitral valve resistance.

Paper 2: Monitoring Variability in Parameter Estimates for Lumped Parameter Models of the Systemic Circulation Using Longitudinal Hemodynamic Measurements

N.L. Bjørdalsbakke, J. Sturdy, E.M.L. Ingeström, L.R. Hellevik
Published in *BioMedical Engineering OnLine* (2023)

Using data from a pilot randomized controlled trial on exercise motivation we attempted to personalize the model parameters for waveform data of flow and pressure recorded for each participant. In this analysis we used the same closed-loop cardiovascular model as in previous work, as well as an open-loop formulation almost identical to the one used by Stergiopulos et al. (24). An optimization heuristic based on doing multiple estimations with local optimization attempts, and then a second sweep for the best initial parameter guess was used to obtain personalized parameters. From the final 20 optimization attempts we picked the best sets of estimates and computed the interquartile range divided by the median parameter estimate to quantify the variability of estimates. This measure of variability was computed for each set of measurements, secondly across all three repeated days of measurement per individual, and thirdly across the entire set of measurements for the entire eligible study population. We computed these quantities for parameters optimized for both model formulations, as well as both pressure waveforms measured in the finger arteries, and the carotid artery. Both waveforms were taken as direct proxies to the central aortic waveform. We also compared model estimates to estimates made by conventional estimation methods, and found high correlation for estimates for total peripheral resistance, and medium to high correlation for aortic compliance estimates. We concluded that in a majority of cases the individual measurement variability was sufficiently low that it would be possible to distinguish parameter sets estimated at single measurements from the different measurements over multiple days, as well as from the entire study population.

Paper 3: Examining Temporal Changes in Model Optimized Parameters Using Longitudinal Hemodynamic Measurements

N.L. Bjørdalsbakke, J. Sturdy, E.M.L. Ingeström, L.R. Hellevik
Ready for submission (2023)

Using data from a pilot randomized controlled trial on exercise motivation we had previously personalized model parameters for waveform data of flow and pressure recorded for each participant. We had done so for both a closed- and open-loop model formulation. The analysis was also performed using both finger artery pressure and carotid pressure waveforms as proxies of central aortic pressure. For this investigation we focused on the total peripheral resistance, systemic arterial compliance, and maximal elastance of the left-ventricle. Parameter changes over the first half and the entire duration of the study intervention period were computed. From these data we wished to investigate whether changes were effects of regression to the mean, exercise stimuli, a poor personalization procedure, or stemmed from day-to-day hemodynamic variability. To do this we examined correlations between changes over different parts of the study period to changes computed by conventional estimates. Multiple linear regression models were built to assess whether measured $\mathrm{VO}_{2,\max}$ affected the predicted variables by explaining more variance. Case studies were also performed in order to assess if parameters changed as expected in response to exercise in the participants we most expected to change. We found that changes in total peripheral resistance and arterial compliance changes, correlated moderately or highly to with conventional estimates. For maximal left-ventricular elastance correlation could only be proven over the entire study period. Carotid pressure waveform based estimates peformed better than finger pressure based estimates. Regression analysis indicated that adding $\mathrm{VO}_{2,\max}$ would not add to the explained variability of the predicted variable any more than age, sex and body mass index. Stroke volume was found to explain more variance than $\mathrm{VO}_{2,\max}$. However, it could not be concluded that the predicted parameters could be attributed to something else than regression to a personal mean, day-to-day variability, or insufficiencies of the model personalization procedure.

4.2 Statement of Authorship

Paper 1

Nikolai Lid Bjørdalsbakke co-authored the code, and performed most of the analysis, except for the sensitivity analysis. He also wrote the major part of the manuscript, apart from the section focusing on sensitivity analysis.

Paper 2

Nikolai Lid Bjørdalsbakke co-authored the code, and performed all analysis. He also wrote the major part of the manuscript.

Paper 3

Nikolai Lid Bjørdalsbakke wrote all code, and performed all analysis. He also wrote the major part of the manuscript.

Chapter 5

Conclusions and Directions for Further Work

5.1 Conclusions

The work presented in the first paper produced evidence that using arterial waveforms rather than ordinary arterial derived clinical indices improved accuracy when estimating model parameters. This was achieved using a local estimation algorithm for synthetic data with and without noise and in absence model discrepancy (33). Without noise, the model parameters were estimated with less than 0.01% error. With added noise parameter errors increased but the four most sensitive parameters could be recovered to less than approximately 10% error. However, it was shown that the error could be reduced further by adding more data in the venous model compartment. From the same analysis it was found that among the least sensitive parameters, the venous compliance, minimal left-ventricular elastance, and mitral valve resistance were particularly challenging to estimate.

We further developed the estimation algorithm before application to real data collected in a clinical trial. Here, we found that the model estimates for arterial resistance and compliance exhibited moderate or high correlation with more conventional estimates made without application of cardiovascular systems models. This was true both when using finger arterial pressure (FP) and carotid arterial pressure (CP) waveforms as approximations of more central waveforms. We assessed the variability of parameter estimates in terms of inter-quartile range divided by

median parameter estimates. It was then shown that the parameter variability per set of measurements was smaller than the variability over estimates made for repeated measurements in the same individual, and for the variability over the study population. Estimates made for both an open- (OL) and closed-loop (CL) cardiovascular model, and both pressure waveforms, supported these results. This suggests that, in a majority of cases, we can resolve individuals from the population using parameter estimates, and to distinguish between measurement days. The results based on carotid pressure waveforms found marginally less personal variability for single measurements than the finger pressure based estimates. In terms of mean parameter values estimated for the population, the OL and CL models gave similar results with only minor deviations. In contrast, when using the FP waveform for estimating parameters, the arterial compliance was significantly different to estimates made with the CP waveform.

In the final part of the work we investigated the cause of parameter changes. Regression analysis revealed that change in fitness measured by $\mathrm{VO2}_{\max}$ could not explain more of the parameter variability than BMI, age, and sex. Using SV as a covariate was instead found to explain more of the parameter variability. We could not conclude that the cause of parameter change was not due to regression to the mean, week-to-week variability, or insufficiencies in the optimization algorithm. We found estimated parameter changes based on the CP waveform to be better correlated than the FP based estimates when compared to estimates made by more conventional estimation methods.

Based on the individual findings we can make some additional conclusions. On the application of an OL versus a CL model for the purposes of MyMDT there seems to be little difference in terms of personalization using the chosen algorithm. The OL has a minor advantage in better agreement with parameter changes made for other estimation methods, and therfore this could be preferred for estimation parameter changes. However, the CL model has more mechanisms and physically interpretable parameters than the OL model. In settings where venous return and the venous blood pool is of interest such as in states of exercise, these model concepts may still be interesting, although more effort to appropriately determine these parameters using a limited data set must be made.

In terms of FP versus CP, we observe that mean parameter values are generally similar except for the arterial compliance parameter. However, parameters derived from FP usually correlated less well with estimates made with more conventional estimation methods. This does not mean they are necessarily intrinsically poorer,

but when comparing parameter changes with changes from conventional methods, the correlations were either not statistically significant or they were lower than for estimated changes based on the CP waveform. Consequently, we recommend that use of the CP for parameter estimation, or there should be some transfer function applied to the FP especially to alleviate the effects of the heightened arterial compliance estimates. Despite the relative ease of FP collection it does not give as useful results as CP, seeing as arterial compliance can be a relevant parameter for explaining hypertension.

In partial agreement with works by Itu et al. and Hann et al. (28, 34), the 4 to 5 most sensitive parameters seem feasible to be determined at least in a synthetic data setting. For the same parameters under application of real data it seems challenging to reliably estimate parameter changes using measurements from a single model compartment with the chosen estimation method. Further, it seems challenging to reliably personalize other, less sensitive parameters even with waveform data.

Finally, we found that while the chosen parameter estimation heuristic was able to find appropriately personalized estimates to recreate the original data satisfactory, the tracking of parameter changes was more uncertain. Arterial resistance and compliance changes were at least moderately well estimated using the CP waveform. Changes for the maximal left-ventricular elastance parameter did not consistently show a non-zero correlation. Physical activity could not be shown to reliably explain changes in parameters either. Despite not being able to sufficiently describe the cause of changes, the model and estimation procedure seem able to partially track the changes reflected by the hemodynamic variability in measurements made weeks apart.

5.2 Future Work

There are many avenues in which this work could be advanced. Both from a primarily parameter estimation perspective, but also in the context of MyMDT.

First, we look at the parameter estimation work as discussed in the attached papers. The models treated in this work focus on models of the complete circulation, or the heart and arteries simultaneously. We tested their ability to be personalized with limited data in order to track parameter changes informed by exercise and other

factors. Analogously to work by Segers et al. (46), who used cardiovascular model parameters to separate different groups of patients with hypertension, we wished to separate different individuals based on parameters but also track their parameter changes. Studies who used similar models to track development of disease usually focused on the Windkessel in isolation, such as Gerringer et al. (15), or a single parameter in a much more extensive and complex model such as Audebert et al. (16). Since this work has tried to capture both cardiac and vascular changes, it could be interesting to compare the changes in optimized arterial parameters from the combined model with an isolated Windkessel model to investigate whether these changes are more informative about exercise remodeling.

Our final paper detailing an exploratory analysis on the monitoring of parameter changes (section 8), could benefit from a more thorough analysis on regression. Ordinary linear regression is applied in this work to investigate the effect of physical activity on the parameter development. Since the data is longitudinal, a linear mixed model is recommended for the analysis, but due to scarce data points, this caused data groups to become very small in terms of data points. Regardless of choice of model, the analysis would probably be improved by allowing collection of more data in a larger study group. But to add a predetermined exercise protocol to the trial could also prove to give a data set with a stronger signal for remodelling, as the change in cardiorespiratory fitness was often small in the analyzed data set, and activity levels between participants was very variable. Exploration of the effect on other personalized model parameters could also prove interesting, although some may be considered less clinically relevant. Reconducting the analysis where different smaller subsets of model parameters were personalized could also give some insight into whether the physical activity impact was most apparent in some of the other model parameters. The most easily accessible point of improvement however, could be to test another personalization method if one of the many suggested methods emerged as most reliable and was able to use only flow and pressure in a single compartment. There are several proposed methods, and as far as the author knows there are still no works comparing a selection of these methods in a structured way, which could have been a valuable addition within the field, since several groups are facing this problem simultaneously.

As results from the analysis on explanation of parameter changes in the paper of chapter 8 showed little correlation between the model estimated $E_{\max}$ and methods based on conventional equations, it could be beneficial to estimate a load-independent estimate from a different estimation method. This would give a better indication on whether this parameter is informed by real changes in the data.

Now, looking at the context of the MyMDT project there are several avenues to explore. Works by for example Fresiello et al., and Kung et al. (80, 81), have already demonstrated some more detailed exercise models, which combine the cardiovascular system with respiratory and gas exchange system models. Conover et al. demonstrated a system for partially personalizing a circulation model for Fontan and Norwood physiology patients which had capabilities of evaluating exercise capacity of the individual (27). For application in MyMDT, what is left unanswered is how this or a similar circulation and exercise model would be changed to reflect a normotensive and hypertensive patient group with a normal physiology. An unsolved problem is also how to adapt a model describing only the left-ventricle to describe exercise for an anatomically normal heart at different intensity levels. The right ventricle is recognized as being influential on the CO during physical activity. We refer to this form of exercise model describing the hemodynamic response during bouts of physical activity as the acute exercise model.

However, to be able to learn about and predict exercise-induced remodeling, an exercise model which incorporates the stimuli (increased pressure and flow) modeled by the acute exercise model to make chronic changes to the physiological envelope and thereby the resting hemodynamics can be valuable. The work in this thesis has been focused on the parameterization of a resting state to be modified by such a model and the acute exercise model. Herein, the chosen model and detectability of changes has been emphasized, to assess whether the parameterization scheme and parameter sensitivity to changes could be used to track changes reliably in a model predicting chronic changes in resting parameters. An unanswered question here is whether there is a difference in how the changes should be modeled due to whether it is resistance or endurance exercise, and even what intensity of endurance exercise, and how this would manifest. There has been observed a dependency in long-term hemodynamic and vascular remodeling responses to different exercise regimes (50, 60), and therefore this would have to guide informative for how the exercise remodelling modeling should operate. We refer to this type of model as the chronic exercise model. For the current work based in real data, the type of exercise has not been controlled and does not make distinction on the type of exercise. There are several avenues one may think about to get to a personalized chronic exercise model. First, one may use an initial period of training to calibrate the expected change and extrapolate based on this. Or one could calibrate using population data for different narrowly defined sub-populations, but this would likely require a high amount of studies with closely monitored and varied exercise dose, and the degree of personalization expressed could be questionable. Another

possibility is identifying genetic and personal characteristics, which are identified to be governing for the chronic response to exercise. This, of course, requires that some of these can be or have been identified, however this also requires more research to properly map. There are also avenues for using machine learning in such a context, where the space of possible informative factors are complex and if this could aid in finding a mapping of personal characteristics to the type of exercise response one would expect, but data requirements are perhaps even higher in this context.

Beyond predictive models of exercise remodeling given a planned exercise regime and physical activity stimuli, to be able to assess the benefit of exercise, one should also compare to expected cases where no exercise has been undertaken, ie. expected development with no change in lifestyle. Additionally, it would be beneficial to investigate the effect of different types of medication on lower level phenotypes encoded in cardiovascular models in order to assess the impact on blood pressure. This combination of functionality could potentially enable MyMDT to be a useful tool for clinicians.

So to summarize, what as a minimum remains from a MyMDT point of view is the

- A personalizable acute exercise model describing the acute response to physical activity.
- A personalizable chronic exercise model for cardiovascular exercise induced remodeling converting physical activity as stimuli into changes in the parameters of the cardiovascular model.
- Assessment of predicted change in resting blood pressure from various sources over different time scales to recommend a best course of hypertension management.
- All previous steps must be investigated for both prehypertensive and hypertensive subjects as potential users of the platform.

Aside from the work presented in this thesis, some work has gone into developing a quazi-personalized exercise model based on population data from Chantler et al. (82), as a starting point for the acute exercise model. This model builds adapted polynomial models for each application where a parameter value is prescribed at a given exercise intensity specified as heart rate reserve (HRR) according to the population averaged response. This is further personalized by using the ratio of the population resting value to the personalized resting value to scale the resulting curve, and thereby find a quazi-personalized model. HRR is defined as

$$\mathrm{HRR} = \frac{\mathrm{HR} - \mathrm{HR}_{\mathrm{rest}}}{\mathrm{HR}_{\mathrm{max}} - \mathrm{HR}_{\mathrm{rest}}}, \tag{5.1}$$

where $\mathrm{HR}_{\mathrm{max}}$ and $\mathrm{HR}_{\mathrm{rest}}$ are maximal and resting heart rate, respectively. The model has been further explored, developed and tested by Anne Øksnes Aal in her master's thesis (83).

Further, some work has gone into developing a prototype for the chronic exercise model as well. Based on the assumption that there will be a upper limit or saturation level for how well a parameter improves, we defined a simple metric based on integrating the cardiac power development simulated under physical activity at measured heart rate reserve levels. This would use a sigmoid function to prescribe how much a cardiovascular parameter would change after a set amount of time adhering to this exercise pattern. The sigmoid would ensure that a saturation level would be reached after a high dose of exercise. As a simple prototype these two models, were combined to illustrate a pipeline for how such a model could work. These are all initial developments of the summary points above, but require more development to see fruition.

Bibliography

[1] Norwegian University of Science and Technology. Digital Transformation; [Visited Sept 2022]. Webpage. Available from: https://www.ntnu.edu/digital-transformation.

[2] Norwegian University of Science and Technology. My Medical Digital Twin; [Visited Sept 2022]. Webpage. Available from: https://www.ntnu.no/cerg/mymdt.

[3] Hose DR, Lawford PV, Huberts W, Hellevik LR, Omholt SW, van de Vosse FN. Cardiovascular models for personalised medicine: Where now and where next? Medical Engineering & Physics. 2019;72:38–48. Available from: https://doi.org/10.1016/j.medengphy.2019.08.007.

[4] Barricelli BR, Casiraghi E, Fogli D. A Survey on Digital Twin: Definitions, Characteristics, Applications, and Design Implications. IEEE Access. 2019;7:167653–167671. Available from: https://doi.org/10.1109/ACCESS.2019.2953499.

[5] Forouzanfar MH, Afshin A, Alexander LT, Anderson HR, Bhutta ZA, Biryukov S, et al. Global, regional, and national comparative risk assessment of 79 behavioural, environmental and occupational, and metabolic risks or clusters of risks, 1990-2015: a systematic analysis for the Global Burden of Disease Study 2015. The Lancet. 2016 Oct;388(10053):1659–1724. Available from: https://doi.org/10.1016/S0140-6736(16)31679-8.

[6] Zhou B, Carrillo-Larco RM, Danaei G, Riley LM, Paciorek CJ, Stevens GA, et al. Worldwide trends in hypertension prevalence and progress in treatment and control from 1990 to 2019: a pooled analysis of 1201

population-representative studies with 104 million participants. The Lancet. 2021;398(10304):957–980. Available from: https://doi.org/10.1016/S0140-6736(21)01330-1.

[7] Williams B, Mancia G, Spiering W, Agabiti Rosei E, Azizi M, Burnier M, et al. 2018 ESC/ESH Guidelines for the management of arterial hypertension. European heart journal. 2018 Sep;39:3021–3104. Available from: https://doi.org/10.1093/eurheartj/ehy339.

[8] Forouzanfar MH, Liu P, Roth GA, Ng M, Biryukov S, Marczak L, et al. Global Burden of Hypertension and Systolic Blood Pressure of at Least 110 to 115 mm Hg, 1990-2015. JAMA. 2017 01;317(2):165–182. Available from: https://doi.org/10.1001/jama.2016.19043.

[9] Ettehad D, Emdin CA, Kiran A, Anderson SG, Callender T, Emberson J, et al. Blood pressure lowering for prevention of cardiovascular disease and death: a systematic review and meta-analysis. Lancet (London, England). 2016 Mar;387:957–967. Available from: https://doi.org/10.1016/S0140-6736(15)01225-8.

[10] Spitieris M, Steinsland I. Bayesian Calibration of Imperfect Computer Models using Physics-Informed Priors. arXiv; 2022. Available from: https://arxiv.org/abs/2201.06463.

[11] Spitieris M, Steinsland I, Ingestrom E. Bayesian calibration of Arterial Windkessel Model. arXiv; 2022. Available from: https://arxiv.org/abs/2201.06883.

[12] Spitieris M, Steinsland I. Learning Physics between Digital Twins with Low-Fidelity Models and Physics-Informed Gaussian Processes. arXiv; 2022. Available from: https://arxiv.org/abs/2206.08201.

[13] Steffensen TL, Auflem M, Vestad HN, Steinert M. Embedded Soft Inductive Sensors to Measure Arterial Expansion of Tubular Diameters in Vascular Phantoms. IEEE Sensors Journal. 2022;22(7):7240–7247.

[14] Huberts W, Heinen SGH, Zonnebeld N, van Den Heuvel DAF, de Vries JPPM, Tordoir JHM, et al. What is needed to make cardiovascular models suitable for clinical decision support? A viewpoint paper. Journal of Computational Science. 2018;24:68–84. Available from: https://doi.org/10.1016/j.jocs.2017.07.006.

[15] Gerringer JW, Wagner JC, Vélez-Rendón D, Valdez-Jasso D. Lumped-parameter models of the pulmonary vasculature during the progression of

pulmonary arterial hypertension. Physiological reports. 2018 Feb;6. Available from: https://doi.org/10.14814/phy2.13586.

[16] Audebert C, Peeters G, Segers P, Laleman W, Monbaliu D, Korf H, et al. Closed-Loop Lumped Parameter Modeling of Hemodynamics During Cirrhogenesis in Rats. IEEE Transactions on Biomedical Engineering. 2018;65(10):2311–2322. Available from: https://doi.org/10.1109/TBME.2018.2793948.

[17] Colunga AL, Kim KG, Woodall NP, Dardas TF, Gennari JH, Olufsen MS, et al. Deep phenotyping of cardiac function in heart transplant patients using cardiovascular system models. The Journal of Physiology. 2020;598(15):3203–3222. Available from: https://doi.org/10.1113/JP279393.

[18] Krokstad S, Langhammer A, Hveem K, Holmen T, Midthjell K, Stene T, et al. Cohort Profile: The HUNT Study, Norway. International Journal of Epidemiology. 2012 08;42(4):968–977. Available from: https://doi.org/10.1093/ije/dys095.

[19] Ashor AW, Lara J, Siervo M, Celis-Morales C, Mathers JC. Effects of exercise modalities on arterial stiffness and wave reflection: a systematic review and meta-analysis of randomized controlled trials. PloS one. 2014;9:e110034. Available from: https://doi.org/10.1371/journal.pone.0110034.

[20] Guimarães GV, Ciolac EG, Carvalho VO, D'Avila VM, Bortolotto LA, Bocchi EA. Effects of continuous vs. interval exercise training on blood pressure and arterial stiffness in treated hypertension. Hypertension research : Official Journal of the Japanese Society of Hypertension. 2010 Jun;33:627–32. Available from: https://doi.org/10.1038/hr.2010.42.

[21] Fagard RH, Cornelissen VA. Effect of exercise on blood pressure control in hypertensive patients [Review]. European Journal of Preventive Cardiology. 2007;14(1):12 – 17. Available from: https://doi.org/10.1097/HJR.0b013e3280128bbb.

[22] Shi Y, Lawford P, Hose R. Review of Zero-D and 1-D Models of Blood Flow in the Cardiovascular System. BioMedical Engineering OnLine. 2011 Apr;10(1):33. Available from: https://doi.org/10.1186/1475-925X-10-33.

[23] Segers P, Rietzschel ER, De Buyzere ML, Stergiopulos N, Westerhof N, Van Bortel LM, et al. Three- and four-element Windkessel models: assessment of their fitting performance in a large cohort of healthy middle-aged individuals. Proceedings of the Institution of Mechanical Engineers Part H, Journal of Engineering in Medicine. 2008 May;222:417–28. Available from: https://doi.org/10.1243/09544119JEIM287.

[24] Stergiopulos N, Meister JJ, Westerhof N. Determinants of stroke volume and systolic and diastolic aortic pressure. The American journal of physiology. 1996 Jun;270:H2050–9. Available from: https://doi.org/10.1152/ajpheart.1996.270.6.H2050.

[25] Bovendeerd PHM, Borsje P, Arts T, van De Vosse FN. Dependence of intramyocardial pressure and coronary flow on ventricular loading and contractility: a model study. Annals of biomedical engineering. 2006 Dec;34:1833–45. Available from: https://doi.org/10.1007/s10439-006-9189-2.

[26] Smith BW, Chase JG, Nokes RI, Shaw GM, Wake G. Minimal haemodynamic system model including ventricular interaction and valve dynamics. Medical Engineering & Physics. 2004;26(2):131 – 139. Available from: https://doi.org/10.1016/j.medengphy.2003.10.001.

[27] Conover T, Hlavacek AM, Migliavacca F, Kung E, Dorfman A, Figliola RS, et al. An interactive simulation tool for patient-specific clinical decision support in single-ventricle physiology. The Journal of Thoracic and Cardiovascular Surgery. 2018;155(2):712–721. Available from: https://doi.org/10.1016/j.jtcvs.2017.09.046.

[28] Itu L, Sharma P, Georgescu B, Kamen A, Suciu C, Comaniciu D. Model based non-invasive estimation of PV loop from echocardiography. Annual International Conference of the IEEE Engineering in Medicine and Biology Society IEEE Engineering in Medicine and Biology Society. 2014;2014:6774–7. Available from: https://doi.org/10.1109/EMBC.2014.6945183.

[29] Jezek F, Randall EB, Carlson BE, Beard DA. Systems analysis of the mechanisms governing the cardiovascular response to changes in posture and in peripheral demand during exercise. Journal of Molecular and Cellular Cardiology. 2022;163:33–55. Available from: https://doi.org/10.1016/j.yjmcc.2021.09.013.

[30] Gu F, Randall EB, Whitesall S, Converso-Baran K, Carlson BE, Fink GD, et al. Potential role of intermittent functioning of baroreflexes in the etiology of hypertension in spontaneously hypertensive rats. JCI Insight. 2020

10;5(19). Available from: https://doi.org/10.1172/jci.insight.139789.

[31] Beard DA. Assessing the Validity and Utility of the Guyton Model of Arterial Blood Pressure Control. Hypertension. 2018;72(6):1272–1273. Available from: https://doi.org/10.1161/HYPERTENSIONAHA.118.11998.

[32] Pettersen KH, Bugenhagen SM, Nauman J, Beard DA, Omholt SW. Arterial Stiffening Provides Sufficient Explanation for Primary Hypertension. PLOS Computational Biology. 2014 05;10(5):1–9. Available from: https://doi.org/10.1371/journal.pcbi.1003634.

[33] Bjørdalsbakke NL, Sturdy JT, Hose DR, Hellevik LR. Parameter estimation for closed-loop lumped parameter models of the systemic circulation using synthetic data. Mathematical Biosciences. 2022;343:108731. Available from: https://doi.org/10.1016/j.mbs.2021.108731.

[34] Hann CE, Chase JG, Desaive T, Froissart CB, Revie J, Stevenson D, et al. Unique parameter identification for cardiac diagnosis in critical care using minimal data sets. Computer Methods and Programs in Biomedicine. 2010;99(1):75 – 87. Available from: https://doi.org/10.1016/j.cmpb.2010.01.002.

[35] Marquis AD, Arnold A, Dean-Bernhoft C, Carlson BE, Olufsen MS. Practical identifiability and uncertainty quantification of a pulsatile cardiovascular model. Mathematical Biosciences. 2018;304:9 – 24. Available from: https://doi.org/10.1016/j.mbs.2018.07.001.

[36] de Bournonville S, Pironet A, Pretty C, Chase JG, Desaive T. Parameter estimation in a minimal model of cardio-pulmonary interactions. Mathematical Biosciences. 2019;313:81 – 94. Available from: https://doi.org/10.1016/j.mbs.2019.05.003.

[37] Pironet A, Dauby PC, Chase JG, Docherty PD, Revie JA, Desaive T. Structural identifiability analysis of a cardiovascular system model. Medical Engineering & Physics. 2016;38(5):433–441. Available from: https://www.sciencedirect.com/science/article/pii/S1350453316000497.

[38] Fox SI. Human physiology. New York: McGraw-Hill; 2013. 13th ed.

[39] Villarreal MR. Simplified Diagram of the Human Circulatory System in Anterior View; 2009. Wikimedia Commons. Available from: https://commons.wikimedia.org/wiki/File:Circulatory_System_en.svg.

[40] Username "Kelvin13" on Wikimedia Commons. Diagram of an Artery; 2013. https://commons.wikimedia.org/wiki/File:Artery.svg. Available from: https://commons.wikimedia.org/wiki/File:Artery.svg.

[41] Guyton AC, Coleman TG, Granger HJ. Circulation: Overall Regulation. Annual Review of Physiology. 1972;34(1):13–44. PMID: 4334846. Available from: https://doi.org/10.1146/annurev.ph.34.030172.000305.

[42] Guyton AC. The surprising kidney-fluid mechanism for pressure control–its infinite gain! Hypertension. 1990 Dec;16:725–30. Available from: https://doi.org/10.1161/01.hyp.16.6.725.

[43] Beard D, Pettersen K, Carlson B, Omholt S, Bugenhagen S. A computational analysis of the long-term regulation of arterial pressure. F1000Research. 2013;2(208). Available from: https://doi.org/10.12688/f1000research.2-208.v1.

[44] Ursino M. Interaction between carotid baroregulation and the pulsating heart: A mathematical model. American Journal of Physiology - Heart and Circulatory Physiology. 1998;275(5):H1733–H1747. Available from: https://doi.org/10.1152/ajpheart.1998.275.5.h1733.

[45] Beard DA, Mescam M. Mechanisms of pressure-diuresis and pressure-natriuresis in Dahl salt-resistant and Dahl salt-sensitive rats. BMC physiology. 2012 May;12:6. Available from: https://doi.org/10.1186/1472-6793-12-6.

[46] Segers P, Stergiopulos N, Westerhof N. Quantification of the Contribution of Cardiac and Arterial Remodeling to Hypertension. Hypertension. 2000;36(5):760–765. Available from: https://doi.org/10.1161/01.HYP.36.5.760.

[47] Westerhof N, Stergiopulos N, Noble MIM, Westerhof BE. Snapshots of Hemodynamics. 3rd ed. Springer International Publising, Springer Nature; 2010. Available from: https://link.springer.com/book/10.1007/978-1-4419-6363-5.

[48] World Health Organization. WHO Guidelines on Physical Activity and Sedentary Behaviour; 2020. [Visited: April 2023]. Available from: https://www.who.int/publications/i/item/9789240015128.

[49] Montero D, Roche E, Martinez-Rodriguez A. The impact of aerobic exercise training on arterial stiffness in pre- and hypertensive subjects: A

systematic review and meta-analysis. International Journal of Cardiology. 2014;173(3):361 – 368. Available from: http://www.sciencedirect.com/science/article/pii/S0167527314004999.

[50] Molmen-Hansen HE, Stolen T, Tjonna AE, Aamot IL, Ekeberg IS, Tyldum GA, et al. Aerobic interval training reduces blood pressure and improves myocardial function in hypertensive patients. European journal of preventive cardiology. 2012 Apr;19:151–60. Available from: https://doi.org/10.1177/1741826711400512.

[51] Wallace JP. Exercise in Hypertension. Sports Medicine. 2003 Jul;33(8):585–598. Available from: https://doi.org/10.2165/00007256-200333080-00004.

[52] Centers for Disease Control and Prevention. Physical Activity and Health: A Report of the Surgeon General: Chapter 3: Physiologic Responses and Long-Term Adaptions to Exercise; 1999. Visited: November 2022. Available from: https://www.cdc.gov/nccdphp/sgr/intro3.htm.

[53] Nystoriak MA, Bhatnagar A. Cardiovascular Effects and Benefits of Exercise. Frontiers in cardiovascular medicine. 2018;5:135. Available from: https://doi.org/10.3389/fcvm.2018.00135.

[54] Montero D, Lundby C. Refuting the myth of non-response to exercise training: 'non-responders' do respond to higher dose of training. The Journal of Physiology. 2017;595(11):3377–3387. Available from: https://doi.org/10.1113/JP273480.

[55] Green DJ, Hopman MTE, Padilla J, Laughlin MH, Thijssen DHJ. Vascular Adaptation to Exercise in Humans: Role of Hemodynamic Stimuli. Physiological reviews. 2017 Apr;97:495–528. Available from: https://doi.org/10.1152/physrev.00014.2016.

[56] Hainsworth R. The Importance of Vascular Capacitance in Cardiovascular Control. Physiology. 1990;5(6):250–254. Available from: https://doi.org/10.1152/physiologyonline.1990.5.6.250.

[57] Rose WC, Shoukas AA. Two-port analysis of systemic venous and arterial impedances. American Journal of Physiology-Heart and Circulatory Physiology. 1993;265(5):H1577–H1587. PMID: 8238570. Available from: https://doi.org/10.1152/ajpheart.1993.265.5.H1577.

[58] Cameron JD, Dart AM. Exercise training increases total systemic arterial compliance in humans. The American journal of physiology.

1994 Feb;266:H693–701. Available from: https://doi.org/10.1152/ajpheart.1994.266.2.H693.

[59] Cameron JD, Rajkumar C, Kingwell BA, Jennings GL, Dart AM. Higher systemic arterial compliance is associated with greater exercise time and lower blood pressure in a young older population. Journal of the American Geriatrics Society. 1999 Jun;47:653–6. Available from: https://doi.org/10.1111/j.1532-5415.1999.tb01585.x.

[60] Tanaka H. Antiaging Effects of Aerobic Exercise on Systemic Arteries. Hypertension. 2019;74(2):237–243. Available from: https://doi.org/10.1161/HYPERTENSIONAHA.119.13179.

[61] Suga H, Sagawa K, Shoukas AA. Load Independence of the Instantaneous Pressure-Volume Ratio of the Canine Left Ventricle and Effects of Epinephrine and Heart Rate on the Ratio. Circulation Research. 1973;32(3):314–322. Available from: https://doi.org/10.1161/01.RES.32.3.314.

[62] Redfield MM, Jacobsen SJ, Borlaug BA, Rodeheffer RJ, Kass DA. Age- and Gender-Related Ventricular-Vascular Stiffening. Circulation. 2005;112(15):2254–2262. Available from: https://doi.org/10.1161/CIRCULATIONAHA.105.541078.

[63] Sforza DM, Putman CM, Cebral JR. Computational fluid dynamics in brain aneurysms. International Journal for Numerical Methods in Biomedical Engineering. 2012;28(6-7):801–808. Available from: https://doi.org/10.1002/cnm.1481.

[64] Mynard JP, Smolich JJ. One-Dimensional Haemodynamic Modeling and Wave Dynamics in the Entire Adult Circulation. Annals of Biomedical Engineering. 2015 Jun;43(6):1443–1460. Available from: https://doi.org/10.1007/s10439-015-1313-8.

[65] Westerhof N, Lankhaar JW, Westerhof BE. The arterial Windkessel. Medical & Biological Engineering & Computing. 2009 Feb;47(2):131–141. Available from: https://doi.org/10.1007/s11517-008-0359-2.

[66] Pironet A, Dauby PC, Chase JG, Kamoi S, Janssen N, Morimont P, et al. Model-Based Stressed Blood Volume is an Index of Fluid Responsiveness. IFAC-PapersOnLine. 2015;48(20):291–296. 9th IFAC Symposium on Biological and Medical Systems BMS 2015. Available from: https://doi.org/10.1016/j.ifacol.2015.10.154.

[67] Miao H, Xia X, Perelson AS, Wu H. ON IDENTIFIABILITY OF NONLINEAR ODE MODELS AND APPLICATIONS IN VIRAL DYNAMICS. SIAM review Society for Industrial and Applied Mathematics. 2011 Jan;53:3–39. Available from: https://doi.org/10.1137/090757009.

[68] Castro M, de Boer RJ. Testing structural identifiability by a simple scaling method. PLOS Computational Biology. 2020 11;16(11):1–15. Available from: https://doi.org/10.1371/journal.pcbi.1008248.

[69] Villaverde AF, Barreiro A, Papachristodoulou A. Structural Identifiability of Dynamic Systems Biology Models. PLOS Computational Biology. 2016 10;12(10):1–22. Available from: https://doi.org/10.1371/journal.pcbi.1005153.

[70] Villaverde AF, Tsiantis N, Banga JR. Full observability and estimation of unknown inputs, states and parameters of nonlinear biological models. Journal of The Royal Society Interface. 2019;16(156):20190043. Available from: https://royalsocietypublishing.org/doi/abs/10.1098/rsif.2019.0043.

[71] Brynjarsdóttir J, O'Hagan A. Learning about physical parameters: the importance of model discrepancy. Inverse Problems. 2014 oct;30(11):114007. Available from: https://doi.org/10.1088/0266-5611/30/11/114007.

[72] Pironet A, Docherty PD, Dauby PC, Chase JG, Desaive T. Practical identifiability analysis of a minimal cardiovascular system model. Computer Methods and Programs in Biomedicine. 2019;171:53–65. Available from: https://www.sciencedirect.com/science/article/pii/S0169260715304570.

[73] Bjørdalsbakke NL, Sturdy J, Ingeström EML, Hellevik LR. Monitoring variability in parameter estimates for lumped parameter models of the systemic circulation using longitudinal hemodynamic measurements. BioMedical Engineering OnLine. 2023 Apr;22(1):34. Available from: https://doi.org/10.1186/s12938-023-01086-y.

[74] Kind T, Faes TJC, Lankhaar JW, Vonk-Noordegraaf A, Verhaegen M. Estimation of three- and four-element windkessel parameters using subspace model identification. IEEE transactions on bio-medical engineering. 2010 Jul;57:1531–8. Available from: https://doi.org/10.1109/TBME.2010.2041351.

[75] Pant S, Fabrèges B, Gerbeau J, Vignon-Clementel IE. A methodological paradigm for patient-specific multi-scale CFD simulations: from clinical measurements to parameter estimates for individual analysis. International Journal for Numerical Methods in Biomedical Engineering. 2014;30(12):1614 – 1648. Available from: https://doi.org/10.1002/cnm.2692.

[76] Pant S, Corsini C, Baker C, Hsia TY, Pennati G, Vignon-Clementel IE. Data assimilation and modelling of patient-specific single-ventricle physiology with and without valve regurgitation. Journal of Biomechanics. 2016;49(11):2162 – 2173. Selected Articles from the International Conference on CFD in Medicine and Biology (Albufeira, Portugal – August 30th - September 4th, 2015). Available from: https://doi.org/10.1016/j.jbiomech.2015.11.030.

[77] Littler WA, Honour AJ, Pugsley DJ, Sleight P. Continuous recording of direct arterial pressure in unrestricted patients. Its role in the diagnosis and management of high blood pressure. Circulation. 1975 Jun;51:1101–6. Available from: https://doi.org/10.1161/01.cir.51.6.1101.

[78] Branch MA, Coleman TF, Li Y. A Subspace, Interior, and Conjugate Gradient Method for Large-Scale Bound-Constrained Minimization Problems. SIAM Journal on Scientific Computing. 1999;21(1):1–23. Available from: https://doi.org/10.1137/S1064827595289108.

[79] Eck VG, Donders WP, Sturdy J, Feinberg J, Delhaas T, Hellevik LR, et al. A guide to uncertainty quantification and sensitivity analysis for cardiovascular applications. International journal for numerical methods in biomedical engineering. 2016 Aug;32. Available from: https://doi.org/10.1002/cnm.2755.

[80] Fresiello L, Meyns B, Di Molfetta A, Ferrari G. A Model of the Cardiorespiratory Response to Aerobic Exercise in Healthy and Heart Failure Conditions. Frontiers in Physiology. 2016;7. Available from: https://doi.org/10.3389/fphys.2016.00189.

[81] Kung E, Pennati G, Migliavacca F, Hsia TY, Figliola R, Marsden A, et al. A simulation protocol for exercise physiology in Fontan patients using a closed loop lumped-parameter model. Journal of biomechanical engineering. 2014 Aug;136:0810071–08100714. Available from: https://doi.org/10.1115/1.4027271.

[82] Chantler PD, Lakatta EG, Najjar SS. Arterial-ventricular coupling: mechanistic insights into cardiovascular performance at rest and during exercise. Journal of Applied Physiology. 2008;105(4):1342–1351. PMID: 18617626. Available from: https://doi.org/10.1152/japplphysiol.90600.2008.

[83] Øksnes Aal A. Development and Validation of a Hemodynamic Model for Varying Exercise Intensity [Master's Thesis]. Norwegian University of Science and Technology; 2022. Available from: https://hdl.handle.net/11250/3023718.

Part II

Research Papers

Chapter 6

Parameter Estimation for Closed-Loop Lumped Parameter Models of the Systemic Circulation Using Synthetic Data

The content of this chapter was published in *Mathematical Biosciences*, 2022.

Paper 1: Parameter estimation for closed-loop lumped parameter models of the systemic circulation using synthetic data

N.L. Bjørdalsbakke, J. Sturdy, D.R. Hose, L.R. Hellevik

Mathematical Biosciences 343 (2022) 108731

Contents lists available at ScienceDirect

Mathematical Biosciences

journal homepage: www.elsevier.com/locate/mbs

Original Research Article

Parameter estimation for closed-loop lumped parameter models of the systemic circulation using synthetic data

Nikolai L. Bjørdalsbakke [a,*], Jacob T. Sturdy [a], David R. Hose [b], Leif R. Hellevik [a]

[a] Department of Structural Engineering, Norwegian University of Science and Technology (NTNU), Richard Birkelandsvei 1a, Trondheim, 7491, Norway
[b] Department of Infection, Immunity and Cardiovascular Disease, University of Sheffield, Beech Hill Road, Sheffield, S10 2RX, United Kingdom

ARTICLE INFO

Keywords:
Lumped parameter models
Systemic circulation
Mathematical optimization
Parameter estimation
Sensitivity analysis

ABSTRACT

Physics-based models can be applied to describe mechanisms in both health and disease, which has the potential to accelerate the development of personalized medicine. The aim of this study was to investigate the feasibility of personalizing a model of systemic hemodynamics by estimating model parameters.

We investigated the feasibility of estimating model parameters for a closed-loop lumped parameter model of the left heart and systemic circulation using the step-wise subset reduction method. This proceeded by first investigating the structural identifiability of the model parameters. Secondly, we performed sensitivity analysis to determine which parameters were most influential on the most relevant model outputs. Finally, we constructed a sequence of progressively smaller subsets including parameters based on their ranking by model output influence. The model was then optimized to data for each set of parameters to evaluate how well the parameters could be estimated for each subset. The subsequent results allowed assessment of how different data sets, and noise affected the parameter estimates.

In the noiseless case, all parameters could be calibrated to less than 10^{-3}% error using time series data, while errors using clinical index data could reach over 100%. With 5% normally distributed noise the accuracy was limited to be within 10% error for the five most sensitive parameters, while the four least sensitive parameters were unreliably estimated for waveform data. The three least sensitive parameters were particularly challenging to estimate so these should be prioritized for measurement. Cost functions based on time series such as pressure waveforms, were found to give better parameter estimates than cost functions based on standard indices used in clinical assessment of the cardiovascular system, for example stroke volume (SV) and pulse pressure (PP). Averaged parameter estimate errors were reduced by several orders of magnitude by choosing waveforms for noiseless synthetic data. Also when measurement data were noisy, the parameter estimation procedure based on continuous waveforms was more accurate than that based on clinical indices. By application of the stepwise subset reduction method we demonstrated that by the addition of venous pressure to the cost function, or conversely fixing the systemic venous compliance parameter at an accurate value improved all parameter estimates, especially the diastolic filling parameters which have least influence on the aortic pressure.

1. Introduction

Mechanistic models have large potential within biomedical applications to possibly explain physiology and pathophysiology. Models which aim to describe physical systems are typically dependent upon model parameters to give an accurate description of reality. Parameters are primarily calibrated by using numerical optimization schemes and measured data. In biomedical applications it is desirable to predict a personalized response to a problem specific treatment or stimuli. Then using data measured for the present and previous states of an individual, predictions can be made about the future state of the personalized model, which has numerous applications in medicine. In the current literature there are many examples of cardiovascular models predicting different system states, medical intervention outcomes or disease [1–5]. Finding a model usable with minimal data from a typical clinical visit and low computational requirements is highly desirable to enable use of such models in the general health context. To investigate how well model parameters can be personalized in this context we approach the problem by using simple models.

* Corresponding author.
E-mail addresses: nikolai.l.bjordalsbakke@ntnu.no (N.L. Bjørdalsbakke), jacob.t.sturdy@ntnu.no (J.T. Sturdy), d.r.hose@sheffield.ac.uk (D.R. Hose), leif.r.hellevik@ntnu.no (L.R. Hellevik).

https://doi.org/10.1016/j.mbs.2021.108731
Received 28 May 2021; Received in revised form 7 September 2021; Accepted 8 October 2021
Available online 7 November 2021

In this manuscript we apply our analysis to a parsimonious model of the systemic circulation and the left ventricle to describe the cardiovascular state of an individual. The investigations are based on data types that should be available non-invasively and available outside extraordinary situations such as visits to the intensive care unit (ICU). Since changes in individuals correspond to changes in model parameters it is important to find reliable methods to accurately and reliably estimate these parameters, such that the models can be used to monitor changes in response to for example therapy.

A large body of work has been done on model personalization within medical applications, but much of the research has focused on complex models that draw from a large set of measurements to personalize the model, and animal studies are often conducted to collect intensive and invasive measurement sets [6,7]. Invasive data from human subjects has also been used as seen in work by Colunga et al. and Pant et al. [8–10]. For the individual providing such data it is less additional burden and risk if such measurements are non-invasive and limited to as few locations on the anatomy as possible. Model personalization of the cardiovascular system has been realized [8–12]. These studies often focus on the details of novel optimization approaches or the quality of outputs produced by the personalized models, while this manuscript focuses on the accuracy of the estimated parameters themselves. However, it remains a question just how much the available data set can be limited to successfully identify the necessary model parameters. The model must also be personalizable by the available data found within the context for model application, otherwise clinical application will likely be infeasible. The minimalistic model presented in this manuscript may provide a simple framework for monitoring changes in the systemic arterial and left heart hemodynamics.

Both model complexity and data modalities differ, while some studies use electronic data records from a large number of individuals, some efforts instead focus on intensive data from just a few individuals. Pant et al. [9,10], fit the parameters of a lumped parameter model using an Unscented Kalman Filter (UKF) approach. The technique was demonstrated to be able to reliably estimate parameters for a three element Windkessel (WK) using a single cycle noisy synthetic waveform data. In a clinical environment Pant et al. used MRI measurements, waveform data from catheters, and doppler ultrasound to estimate personalized parameters in two individuals. Meiburg et al. apply a similar approach using a UKF to estimate parameters in a different model of the systemic circulation using synthetic waveform data which yields promising results [11]. Hann et al. have developed a method for personalization where parameters are continuously re-estimated based on the forward model solution, which has been applied to both synthetic and real waveform data in combination with clinical indices measured in the ICU [12]. Colunga et al., Marquis et al. and de Bournonville et al. take an approach to personalizing closed-loop lumped parameter models using invasive data sets to compute good nominal values before model optimization [6–8]. This approach usually relies on measurements from multiple vessel compartments or population data, and thorough parameter identifiability analysis. Patient specific modeling would likely benefit from more accurate measurement techniques, which would improve estimated parameters and possibly improve predictions based on these estimates. However, not only improved accuracy but also novel measurement techniques that would make data acquisition easier and less burdensome for both the individual and society would make patient specific modeling feasible where it would earlier be stopped by lack of available data.

The question of how well and which personalized model parameters can be identified is also model specific. Hann et al. take a structured approach to reducing the available data sets, while reducing the model complexity in the process [12]. We take a different approach where the problem complexity is reduced by sequentially fixing parameters, but mainly examine the question of how well estimated parameters correspond to parameters that are known to describe a given set of data, which has not been investigated in many contexts. We refer to these known parameters as the "*true*" parameters, throughout this study. A method for assessing the accuracy of the estimated parameters with respect to the *true* parameters is introduced in this manuscript. Further, we investigate how different available data sets and cost functions affect the accuracy and precision of parameter estimates, using standard optimization methods. Guided by sensitivity analysis, we assess the impact of reducing the estimated parameter subset by a method which is applicable to any deterministic computer model with continuous output ranges and constant parameters. Effectively, a practical identifiability analysis of the model is performed under different scenarios. This investigation is motivated by the hypothesis that determination of accurate personalized model parameters is essential for predicting future states of the system, and for using models as potential diagnosis support systems.

In order to be able to evaluate the accuracy of parameter estimates we focus on synthetic data generated from the model, as the *true* value of parameters is in general impossible to know for real data situations. For this investigation we use synthetic data with and without noise to investigate the best possible cases for estimation of parameters while still approximating real data. We emphasize that we wish to assess how different choices of parameter subsets affect estimation of parameter values rather than to identify the model configuration which best emulates the data. Attempting to estimate the parameters for real data belongs to future work, but will shed more light on how model discrepancy influences the resulting parameter estimates.

2. Method

2.1. Model

The motivation of this work was to determine if hemodynamic measurements could be applied to estimate personal mechanical parameters characterizing an individual's cardiovascular system. In general the parameters are defined in terms of a mechanistic model of the cardiovascular system. While various anatomically and physiologically detailed models have been developed to describe the human cardiovascular system [13–15], in this study we implemented a closed-loop lumped parameter model of the systemic circulation and left ventricle as a realistic candidate for routine clinical application. In contrast to some more detailed models the model applied in this work is suitable to real-time simulation. Perhaps more significantly, reducing the number of parameters required to specify the model is expected to reduce the measurement burden required to personalize the model. More detailed models often require direct imposition of population average or nominal values for parameters which may limit their potential for personalization.

The lumped parameter model in this work is similar to that previously applied by Segers et al. [16], however, instead of assuming a constant filling pressure for the left ventricle, we included a venous compartment to represent the left ventricular filling pressure (See Fig. 1 for a graphical depiction of the model). This is a similar but simplified version of the approaches of Smith et al. [17] and Hann et al. [12]. Mathematically, the model consists of a system of differential equations that describe the time evolution of the state variables, which are the stressed volumes of the ventricle, arteries and veins. The pressures and flows are determined algebraically from the volumes.

$$\begin{aligned}
\frac{dV_{sa}}{dt} &= C_{sa}\frac{dP_{sa}}{dt} = Q_{lvao} - Q_{sys} \\
\frac{dV_{sv}}{dt} &= C_{sv}\frac{dP_{sv}}{dt} = Q_{sys} - Q_{svlv} \\
\frac{dV_{lv}}{dt} &= Q_{svlv} - Q_{lvao}
\end{aligned} \tag{1}$$

V_{sa}, V_{sv} and V_{lv} are the stressed blood volumes of the systemic arteries, systemic veins and left ventricle, respectively. C_{sa} and C_{sv} are the volume compliance values of the systemic arteries and veins, while P_{sa} and P_{sv} are the corresponding pressures of these compartments.

Q_{lvao} denotes the volume blood flow from the left ventricle to the systemic arteries, Q_{sys} is the flow between the systemic arteries and veins, and finally Q_{svlv} is the flow from the veins to the left ventricle. The left ventricular pressure is assumed to be a linear function of the volume of the left ventricle, $P_{lv} = E_{lv}(t)V_{lv}$, where $E_{lv}(t)$ is the elastance of the ventricle at time t. The elastance is modeled as a periodic function, which mimics the periodic contraction of the ventricle and the associated pressure gradient and ejection of blood into the arteries. The pressure in the arteries and veins are also modeled as linear functions of the corresponding volumes, $CP = V$, where C is the compliance of the respective compartment and describes aggregated stiffness of the arterial or venous walls. All equations describing the model are given in Appendix A.

The compartments and their connections are characterized by a set of mechanical parameters listed in Table 1 along with the symbols and selected reference values used in this study. Segers et al. report reference values for most of these parameters in both normotensive and hypertensive populations [18]. In this work we use the reference values for the normotensive population and manually adjusted the parameters not reported by Segers et al. The parameters originate from the mathematical description of each component. The lumped parameter approach represents the cardiovascular system as a set of compartments that contain a volume of blood at a particular pressure, and connections between these compartments which model the flow of blood between these compartments.

The flows between compartments are modeled as a linear function of the pressure difference between the compartments, $Q = \Delta P/R$, where R is a resistance and determines the mechanical energy required to sustain flow between compartments. The flows to and from the ventricle are slightly more complicated as the heart valves ensure these flows are always in the direction obeying the cardiac cycle. The valves are modeled as diodes such that the flow is linearly related to pressure for negative pressure gradients, and 0 otherwise. Note that flow from the venous compartment, representing the systemic veins, directly enters the left ventricle across the mitral valve, which conceptually assumes the systemic venous pressure is identical to the pulmonary venous pressure. We therefore assume the effects of atrial dynamics are negligible, as previous works also have [12,17], and that ventricular interaction effects are negligible.

The model presented in Fig. 1 produces very similar arterial hemodynamics as the referenced model by Smith et al. The latter is a four element WK (4WK) as the former is a three element WK (3WK). Studies show that this version of the 4WK can be better optimized to data than the 3WK, but introduces another personalizable parameter and often yields similar parameter values for aortic characteristic impedance and resistance when fitted to real data [19]. Vachiéry et al. highlight that pulmonary arterial hypertension is challenging to diagnose and that even this condition may not be reflected in the left heart or systemic circulation [20]. In exercise, the pulmonary circulation and right heart are recognized to be influential also on arterial hemodynamics through limitations on cardiac output [21,22]. The absence of the right heart and pulmonary circuit may then cause limited expressions of exercise hemodynamics and limit the applicability of the model, but confirmation of this statement requires further investigation beyond the scope of this manuscript. By redirecting the venous return directly into the left ventricle, the cardiac preload is modeled by the venous pressure and flow rather than fixing the preload and venous properties as in an open-loop model. By circumventing the pulmonary circulation and right heart we also omit many potentially personalizable parameters, which may further complicate the process of personalizing the model with limited data. If the model is sufficiently simple so that it can be run and personalized in real time it may be used to monitor changes in resting hemodynamics. As discussed by Huberts et al. model accuracy lessens as the model is simplified [23], so an important question to be answered in a different setting is whether a simplified model is able resolve small changes in hemodynamics caused by a chosen form of stimulus.

Table 1
The model parameters are listed with their corresponding symbols and reference values. For most parameters the reference values were reported by Segers et al. [18]. The remaining parameters have been manually tuned. We use these reference values as experimental estimates, and in our wording as the "*true*" parameters, to generate the data used for the parameter estimation procedure.

Symbol	Description	*True* values	Units
C_{ao}	Systemic arterial compliance	1.13	$\frac{mL}{mmHg}$
C_{sv}	Systemic venous compliance	11.0	$\frac{mL}{mmHg}$
E_{max}	Maximal left ventricular elastance	1.5	$\frac{mmHg}{mL}$
E_{min}	Minimal left ventricular elastance	0.03	$\frac{mmHg}{mL}$
R_{mv}	Mitral valve resistance	0.006	$\frac{mmHg\ s}{mL}$
R_{sys}	Systemic vascular resistance	1.11	$\frac{mmHg\ s}{mL}$
T	Heart period	0.85	s
t_{peak}	Time of peak ventricular elastance	0.3	s
V_{tot}	Total stressed blood volume	300	mL
Z_{ao}	Characteristic impedance of the aorta	0.033	$\frac{mmHg\ s}{mL}$

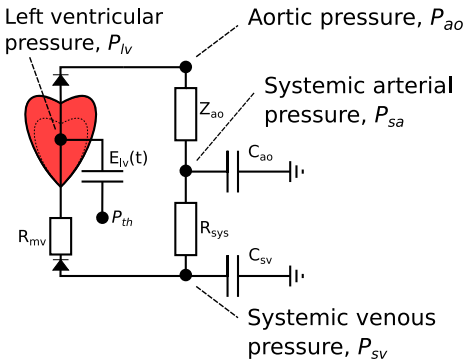

Fig. 1. The closed-loop, lumped parameter model of the systemic circulation and the left ventricle. The circuit equivalent formulation of the model is depicted, with the pressures of each compartment, as well as most of the mechanical parameters. The model describes three compartments: the left ventricular, arterial and venous compartments. P_{th} is the intrathoracic pressure, P_{lv} is the left ventricular pressure and $E_{lv}(t)$ indicates the left ventricular elastance function. For an explanation of the remaining parameters, see Table 1.

For the remainder of this article, it is convenient to treat the model variables, e.g. P_{ao}, Q_{ao} or P_{sv}, as functions of the parameters $\boldsymbol{\theta}$ and time, $y(t, \boldsymbol{\theta})$, where y denotes a particular variable. Thus the values at a particular time point are denoted $y(t_k, \boldsymbol{\theta})$. $\boldsymbol{\theta}$ denotes the vector of all model parameters. These functions are approximated numerically using SciPy's implementation of the 4th-order Runge–Kutta (RK4) method to integrate the differential equations [24]. The resulting system of equations may be stiff, and therefore we also tested solving the system with the backward differentiation formula (BDF), but it was found to be much more computationally expensive than RK4 while results were found to be comparable.

2.2. Data and measurements

A focus of this study was to determine how accurately and precisely specific model parameters could be estimated from various data sources. In order to quantify the performance of the estimation procedure, the true values of the parameters, $\boldsymbol{\theta}_{true}$, must be known. As this is

not possible for real clinical data, we simulated realistic measurement data based on the numerical solution of the model for particular parameter values such that the true values of the parameters are known. The data generated in this way stimulates continuous waveform data for pressure and flow in the aorta and large systemic veins of the cardiovascular system (Using the notation proposed previously, $P_{ao}(t_k, \boldsymbol{\theta}_{true})$, $Q_{ao}(t_k, \boldsymbol{\theta}_{true})$, and $P_{sv}(t_k, \boldsymbol{\theta}_{true})$. In addition, measurements of common clinical indices were simulated by computing these from the waveform data, e.g. $P_{sys} = \max_k P_{ao}(t_k, \boldsymbol{\theta}_{true})$. The time varying measurements and clinical indices are depicted in Fig. 2 and described in the following section. The model equations Appendix A were solved by the 4th order Runge–Kutta scheme. Model outputs were solved until they reached a steady periodic state, which was found to be reached by 10 heart cycles. We also tested the solution after more heart cycles but model outputs did not change and parameter estimates remained identical. In the following, we use the notation y_k^m to denote a measured value of the quantity y at time t_k if appropriate (y^m denotes a time independent measurement).

We expressed the time series simply as a list of continuous measurement points of pressure or flow. A series of 100 points per heart cycle were defined, corresponding in this example to a measurement frequency of approximately 117.6 Hz with the chosen heart rate. Pressure catheters or tonometry can be used to measure blood pressure waveforms [25], and doppler ultrasound is routinely applied to record flow velocity waveforms in the heart and aorta.

In clinical practice blood pressure is assessed by sphygmanometry of brachial systolic and diastolic blood pressure. These may be emulated as the maximum and minimum values of the simulated aortic pressure waveform, respectively. The model does not explicitly describe the brachial pressure, thus the simulated data may be thought of the best case where central aortic pressure is measured. Aortic pressure is typically comparable to brachial pressure (especially in healthy, young to middle aged individuals). The difference between systolic and diastolic pressures is the pulse pressure, which is also a common clinical measure often used to compute other hemodynamic quantities [26].

The stroke volume and maximal aortic flow are two additional measures commonly used in clinical practice. These may both be derived from ultrasound measurements of the flow velocity and diameter of the left ventricular outflow tract [27]. The peak value corresponds to maximal aortic flow, while the integral of the volumetric flow over a single cardiac cycle gives the volume of blood ejected by the ventricle, the stroke volume. Since the three volume compartments of the model (Section 2.1) do not represent any anatomical features these measurements are emulated from the flow across the aortic valve.

The model generated data may be represented as

$$y_k^m = y(t_k, \boldsymbol{\theta}_{true}) \tag{2}$$

where the superscript m emphasizes this is the measured value and subscript k denotes the time point, where relevant. For the case where y_k^m is a scalar extracted from a time series output the k index is without meaning.

Realistic clinical measurements will have some noise. In this analysis, we investigate both the ideal case of perfect measurements and the more realistic case of noisy measurements. Noisy measurements are simulated by adding randomly sampled perturbations to the model outputs

$$y_k^{noisy} = y(t_k, \boldsymbol{\theta}_{true}) \times \xi_k \tag{3}$$

where ξ_k are independently and identically distributed normal random variables with mean 1 and standard deviation 0.05. In reality, the noise may be biased at least in parts of the measured signal, but this may depend on the measurement technique or equipment. To keep the case most general and for simplicity we use normal distributed noise even though more sophisticated noise distributions can be constructed in theory.

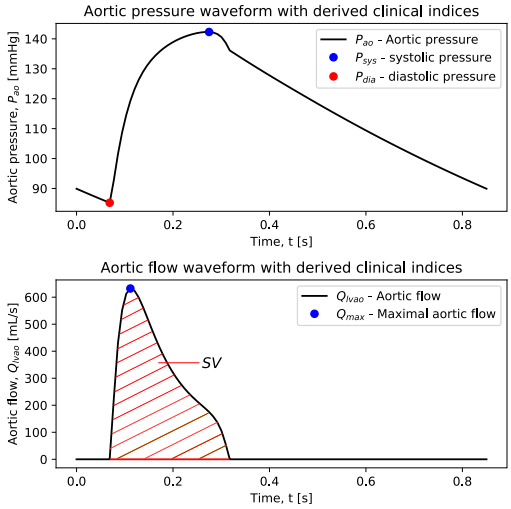

Fig. 2. Most of the data types and measurements are depicted, as well as their relations.

2.3. Structural identifiability analysis

Before investigating whether model parameters can be estimated in practice, a structural identifiability analysis will reveal if there is at all any possibility for estimating parameters from more realistic data. Structural identifiability only considers the model structure and data under perfect conditions.

Performing a global structural identifiability analysis means proving that a model formulation gives a unique model output for any given parameter vector $\boldsymbol{\theta}$. Alternatively, a model is globally structurally identifiable if for two distinct arbitrarily chosen vectors of parameters $\boldsymbol{\theta}_1$ and $\boldsymbol{\theta}_2$ from a parameter space Θ then $y(t_k, \boldsymbol{\theta}_1) = y(t_k, \boldsymbol{\theta}_2)$ holds if and only if $\boldsymbol{\theta}_1 = \boldsymbol{\theta}_2$ for all k [28,29]. A model is locally structurally identifiable if the condition $y(t_k, \boldsymbol{\theta}) \neq y(t_k, \boldsymbol{\theta}')$ is true for any $\boldsymbol{\theta}$ in an open interval around $\boldsymbol{\theta}'$ in the parameter space Θ. Therefore, for strictly local structural identifiability multiple but discretely different vectors of $\boldsymbol{\theta}$ can generate the same model outputs which causes additional concerns for practical parameter estimation, as there may be multiple parameter sets which recreates the output. However, it is not a given that the system has more than one solution within the domain for practical implementation. Practical identifiability analysis needs to be performed to assess this. Given that a model is locally identifiable, it can still be globally identifiable unless it is explicitly proven not to be.

Villaverde et al. have developed the STRIKE-GOLDD software package which determines the local structural identifiability of non-linear differential equation models by a method involving Lie derivatives [30]. We applied the MatLab implementation of STRIKE-GOLDD to our model with different data combinations to investigate identifiability. However, this software requires the right hand side of the system of ODEs to be infinitely differentiable functions with respect to both the state variables and parameters, and the valve models are not differentiable in this context. Therefore, we analyze the model in its ejection phase enforcing a closed mitral valve and open aortic valve using left ventricular pressure and aortic flow as the aortic pressure is equal to left ventricular pressure in the systolic ejection phase according to the model. For the diastolic phase, systemic arterial pressure is given while the valves are open and closed oppositely to the ejection phase. The dynamic driver function for the model which is the left ventricular elastance function is dependent upon a time signal which is periodic with the length of the heart cycle. The time signal controlling the elastance cycle is the time variable but defined as $u(t) = \tau = t \mod T$

and is treated as a known dynamic system input in this context. The full specification of the elastance function is given in Appendix A.

Pironet et al. perform a structural identifiability analysis by demonstrating that a unique solution for the parameter set can be found by using the information from perfectly observed model outputs [31]. The model examined by Pironet has a very similar formulation to our model, but includes more chambers, yet with a certain set of outputs the model was found to be globally structurally identifiable. Information from both the systolic and diastolic phases are used separately to identify parameters, as we have done using STRIKE-GOLDD. Parameters which are shown to be identifiable constant parameters are used to prove the identifiability of other parameters. Parameters identified during the model in the diastolic phase is used in identifying parameters in the ejection phase, and hence the reverse should also be valid. Some of the computations relevant to the identifiability analysis which required high amounts of memory were performed on the NTNU IDUN computing cluster [32].

2.4. Sensitivity analysis

Sensitivity analysis of the model quantities of interest can identify which parameters most influence the model's prediction of a quantity of interest. This method can subsequently be applied to identify which parameters may be estimated from given types of measurements, or conversely may be applied to identify which measurements are necessary to provide information about particular parameters [23,33,34]. We analyzed the sensitivity of the model outputs in terms of Sobol indices which are commonly used as a global measure of sensitivity [35]. Sobol indices quantify sensitivity as the proportion of variance of the model output attributable to variance of particular parameter values:

$$S_{M,i}(y) = \frac{\mathrm{Var}(\mathrm{E}(y|\theta_i))}{\mathrm{Var}(y)} \tag{4a}$$

$$S_{T,i}(y) = \frac{\mathrm{E}(\mathrm{Var}(y|\theta_{\sim i}))}{\mathrm{Var}(y)} \tag{4b}$$

where $S_{M,i}$ and $S_{T,i}$ denote respectively the main and total sensitivity to parameter θ_i, while y denotes the function sensitive to the parameters $\boldsymbol{\theta}$, or for this analysis a model output.

To interpret these indices, we note that a quantity of interest with high values of either index for given parameter suggests that measurement of that quantity may provide substantial information about that parameter. However, if $S_{M,i}$ is low but $S_{T,i}$ is large then parameter θ_i impacts the quantity of interest primarily through interactions with other parameters and consequently may substantially affect the quantity of interest. Unfortunately due to its interactivity it may remain challenging to estimate due to its dependence on the values of other parameters.

In general, parameter estimation becomes more challenging as more parameters are estimated. In addition, strong interactions between parameters may impede efficient numerical optimization. Prior works have employed a number of subset selection methods to reduce the number of parameters varied while fitting the model to data [36,37]. Most such methods are based on analysis of sensitivities and in general select subsets of parameters with high sensitivity to estimate, as the data will provide the most information about these. The complementary set of parameters with lower sensitivity is then fixed at nominal values, which is expected to have minimal impact on the fitting of the model to the data.

Sobol indices have a clear interpretation in terms of the behavior of individual variables, but the interpretation of the Sobol indices for many variables or for a time varying signal may not be as easily interpreted. For example simply averaging across variables or time will weight regions of low variance equally to those of high variance. To remedy this one may instead examine the variance weighted averages

$$TAS_{M,i}(y) = \frac{\sum_k S_{M,i}(y(t_k))\,\mathrm{Var}(y(t_k))}{\sum_k \mathrm{Var}(y(t_k))} \tag{5a}$$

$$TAS_{T,i}(y) = \frac{\sum_k S_{T,i}(y(t_k))\,\mathrm{Var}(y(t_k))}{\sum_k \mathrm{Var}(y(t_k))}. \tag{5b}$$

Here we abbreviate time-averaged as (TA). We computed the indices defined in (4) assuming all input parameters were independently and uniformly distributed over the range of 90% to 110% of their nominal values. The indices were estimated using a Monte-Carlo approach as proposed by Saltelli et al. with 2500 samples per parameter [35]. The weighted averages (5) were subsequently computed from these estimates of the Sobol indices [33,38].

2.5. Synthetic data generation and parameter estimation

For the purposes of fitting a model to data a typical approach is to assume the data, y_k^m, are simply a perturbation of the values predicted by the model for the true parameter values:

$$y_k^m = y(t_k, \boldsymbol{\theta}_{true}) + E_k. \tag{6}$$

Given the data and the model, the objective is then to determine the value of $\boldsymbol{\theta}$ that produces model predictions best matching the data, i.e. with minimal E_k. To quantify how well a given value of parameters matches the data, a cost function must be defined, for example

$$J(\boldsymbol{\theta}) = \sum_k (y(t_k, \boldsymbol{\theta}) - y_k^m)^2. \tag{7}$$

To estimate the parameters a minimization problem is solved

$$\hat{\boldsymbol{\theta}} = \arg\min J(\boldsymbol{\theta}) \tag{8}$$

which corresponds with ordinary least squares regression. The minimization problem is typically solved using a numerical optimization method, and the Trust Region Reflective algorithm (TRRA) was chosen for this study due to accepting parameter bounds, and is available through SciPy [24]. The constraint applied to the cost functions used in this investigation are given in higher detail in Appendix B.

Four cost functions were considered in this work, corresponding to three sets of clinical measurements. The first corresponds with fitting the model to standard clinical measurements

$$\begin{aligned} J(\boldsymbol{\theta}) = &\left(\frac{P_{sys}(\boldsymbol{\theta}) - P_{sys}^m}{K_{psys}}\right)^2 \\ &+ \left(\frac{P_{dia}(\boldsymbol{\theta}) - P_{dia}^m}{K_{pdia}}\right)^2 \\ &+ \left(\frac{PP(\boldsymbol{\theta}) - PP^m}{K_{pp}}\right)^2 \\ &+ \left(\frac{SV(\boldsymbol{\theta}) - SV^m}{K_{SV}}\right)^2 \\ &+ \left(\frac{Q_{max}(\boldsymbol{\theta}) - Q_{max}^m}{K_{qmax}}\right)^2. \end{aligned} \tag{9}$$

The K_j are scaling factors, where subscript j indicates a type of measurement the parameter normalizes. These were used to ensure that all quantities contributing to the cost function were weighted approximately equally. See Appendix B for the values used in our computations.

The second cost function corresponds to making use of continuous pressure and flow waveform data which is not typically measured in the clinic:

$$\begin{aligned} J(\boldsymbol{\theta}) = &\sum_k^N \left(\frac{P_{ao,k}(\boldsymbol{\theta}) - P_{ao,k}^m}{K_p}\right)^2 \\ &+ \sum_k^N \left(\frac{Q_{ao,k}(\boldsymbol{\theta}) - Q_{ao,k}^m}{K_q}\right)^2 \end{aligned} \tag{10}$$

where k indicates the sample time points of the measurements for a total N points per measurement type.

The third cost function requires measurement of the venous systolic and diastolic pressure values:

$$\begin{aligned} J(\boldsymbol{\theta}) = &\left(\frac{P_{sys}(\boldsymbol{\theta}) - P^m_{sys}}{K_{psys}}\right)^2 \\ &+ \left(\frac{P_{dia}(\boldsymbol{\theta}) - P^m_{dia}}{K_{pdia}}\right)^2 \\ &+ \left(\frac{PP(\boldsymbol{\theta}) - PP^m}{K_{pp}}\right)^2 \\ &+ \left(\frac{SV(\boldsymbol{\theta}) - SV^m}{K_{SV}}\right)^2 \\ &+ \left(\frac{Q_{max}(\boldsymbol{\theta}) - Q^m_{max}}{K_{qmax}}\right)^2 \\ &+ \left(\frac{P_{sv,sys}(\boldsymbol{\theta}) - P^m_{sv,sys}}{K_{psvsys}}\right)^2 \\ &+ \left(\frac{P_{sv,dia}(\boldsymbol{\theta}) - P^m_{sv,dia}}{K_{psvdia}}\right)^2. \end{aligned} \tag{11}$$

The fourth cost function requires measurement of the venous pressure wave form in addition to the aortic pressure and flow:

$$\begin{aligned} J(\boldsymbol{\theta}) = &\sum_k^N \left(\frac{P_{ao,k}(\boldsymbol{\theta}) - P^m_{ao,k}}{K_p}\right)^2 \\ &+ \sum_k^N \left(\frac{Q_{ao,k}(\boldsymbol{\theta}) - Q^m_{ao,k}}{K_q}\right)^2 \\ &+ \sum_k^N \left(\frac{P_{sv,k}(\boldsymbol{\theta}) - P^m_{sv,k}}{K_{psv}}\right)^2. \end{aligned} \tag{12}$$

As many optimization methods such as the Quasi-Newton method used in this analysis may be attracted to local minima, we attempted to mitigate this by performing the numerical optimization with several initial parameter values randomly sampled according to the formula

$$\theta_{sampled,i} = \theta_{ref,i}(1 + \delta_i), \tag{13}$$

where δ_i are stochastic values drawn independently from a normal distribution with a zero mean and standard deviation of 0.3. $\boldsymbol{\theta}_{ref}$ was a set of reference parameters used to sample initial guesses arbitrarily chosen within a physiologically realistic combination of parameters. They are not equal to $\boldsymbol{\theta}_{true}$, as to not center the distribution of the sampled parameters at the desired cost function minimum. See Appendix B for the list of reference values.

2.6. Quantities of interest

The main goal of fitting the model to personal data is to accurately estimate $\boldsymbol{\theta}_{true}$, thus the measure of error for this is $\hat{\boldsymbol{\theta}} - \boldsymbol{\theta}_{true}$, where $\hat{\boldsymbol{\theta}}$ is the estimated parameter vector. $\boldsymbol{\theta}_{true}$ are the synthetic reference parameters, listed in Table 1. We evaluated how well local optimization algorithms could calibrate the lumped parameter model by recovering the "true" parameters when we used no prior knowledge about the parameters aside from what was considered approximately physiologically realistic ranges for the parameters. We generated the data sets used in this study with the "true" parameter values, $\boldsymbol{\theta}_{true}$, set to the values reported by Segers et al. for normotensive individuals [18]. The remaining parameters of the parameter vector which are not reported by Segers et al. were chosen by manual tuning and their values are reported in Table 1. Thus, the true parameters, $\boldsymbol{\theta}_{true}$, are mostly chosen to be values used in the literature.

Specifically, to recover these parameters we optimized the model outputs according to the measurements in Section 2.2. Table 2 lists the relevant quantities, and Fig. 2 depicts them.

Table 2
The model waveform outputs are listed along with any derived quantities that are or serve as approximations to clinical indices. Abbreviations are also specified.

Model outputs/measurements	Derived clinical index
Aortic pressure waveform, P_{ao}	– Aortic systolic and diastolic pressures, P_{sys} and P_{dia} – Pulse Pressure, PP
Aortic flow waveform, Q_{ao}	– Maximal aortic flow, $Q_{ao,max}$ – Stroke Volume, SV
Systemic venous pressure waveform, P_{sv}	– Venous systolic and diastolic averaged pressures, $P_{sv,sys}$ and $P_{sv,dia}$

2.7. The stepwise subset reduction method

Based on the total Sobol indices in (4), and (5) we ranked parameters with respect to aortic pressure, and devised an approach to investigate how adding additional less sensitive parameters to the fitting procedure affects parameter estimation. We named the method the stepwise subset reduction method (SSRM).

The purpose of parameter estimation based on the model presented here is to develop a method for identifying personal characteristics from clinically measured data. In this context, the personal characteristics are the parameter values $\boldsymbol{\theta}_{true}$; however, simultaneous estimation of all parameter values may be challenging, particularly when measurements are noisy. We thus sought to investigate how this approach performed for various subsets of parameters in order to determine if any less influential model parameters should be fixed in order to improve the robustness of this approach. For similar models, calibration of stable parameters with low variability have been demonstrated [6,12].

For each cost function and data set (to be described later), we performed the numerical optimization procedure outlined in the previous section for each subset of parameters (described in the following section) for $N_s = 50$ sets of $\boldsymbol{\theta}_{sampled}$ as initial guesses for the parameters. For each set of initial guesses, the cost function at the termination of the optimization procedure was recorded. Subsequently the minimum cost function observed in the subset was identified, and only the cases where the cost function was less than 125% of the minimum observed cost function were retained for evaluation of the subset.

The subsets of parameters were defined as follows. At maximum all nine parameters (see Table 1) were estimated at once as described in the previous paragraph. After fitting all nine model parameters we repeated this step eight times, while fixing one additional parameter at its true value according to $\boldsymbol{\theta}_{true}$ in ascending order of sensitivity per repetition. In practice this means that the subset selection was reduced by one additional parameter at each iteration. See Table 3 for the full sequence of subsets in the SSRM. All nine parameters are estimated N_s times, then the eight most sensitive parameters are estimated N_s times, and so on until only the most sensitive parameter is estimated. From here on this method is referred to as the stepwise subset reduction method (SSRM).

The SSRM was then performed for ten different estimation scenarios. First, for standard clinical indices as specified in Eq. (9) with (III) and without noise (I). Subsequently, for aortic flow and pressure waveforms (10) with (IV) and without noise (II). Another four scenarios (V–VIII) were all based on noisy waveform data (3). Two approaches (V and VI) included venous information as per Eqs. (11) and (12), respectively. Two additional scenarios focused on the impact of fixing either t_{peak} (VII) or C_{sv} (VIII) at their true values by applying the SSRM for estimating the remaining parameters based on noisy aortic data (11).

The motivation for the investigations with fixed t_{peak} (VII) or C_{sv} (VIII) was the observation that by inclusion or removal of certain parameters in the estimated subset, the estimation error of the remaining parameters changed by an order of magnitude. The addition of more data from the venous compartment was motivated by the observation

Table 3
A table representing the sequence of model parameter subsets as estimated by the SSRM.

The sequence of subsets in SSRM	Subset parameters
#1	V_{tot}, E_{max}, C_{ao}, R_{sys}, t_{peak}, C_{sv}, E_{min}, Z_{ao}, and R_{mv}
#2	V_{tot}, E_{max}, C_{ao}, R_{sys}, t_{peak}, C_{sv}, E_{min}, and Z_{ao}
#3	V_{tot}, E_{max}, C_{ao}, R_{sys}, t_{peak}, C_{sv}, and E_{min}
#4	V_{tot}, E_{max}, C_{ao}, R_{sys}, t_{peak}, and C_{sv}
#5	V_{tot}, E_{max}, C_{ao}, R_{sys}, and t_{peak}
#6	V_{tot}, E_{max}, C_{ao}, and R_{sys}
#7	V_{tot}, E_{max}, and C_{ao}
#8	V_{tot}, and E_{max}
#9	V_{tot}

that many of the least sensitive and hardest to estimate parameters relate to ventricular filling, which in turn is largely determined by venous pressure.

As stated, the SSRM was conducted by fixing the model parameters that were not in the subset at their true values. To investigate the effect on parameter estimates by fixing the parameters at wrong values, we repeated the SSRM with the cost function in Eq. (10) but fixed the parameters at 30% above their true value (X), and the effect on parameter estimates was observed.

In the previous estimation cases (I)–(VIII) and (X), the same sampled values of noise, ξ_k, were used in all optimization runs. To assess the general impact of noise, we estimated parameters from N_s cases of normally distributed noise (3) applied to the data in Eq. (10) (IX). For each sample of ξ_k, we estimated parameters from only one initial parameter guess. The sampling values in Table B.6 from Appendix B were used as initial guesses in this exercise, which were confirmed to estimate all parameters to negligible error without noise.

The performance of the parameter estimation procedure was evaluated for each subset and cost function by calculating the mean absolute percentage error (MAPE) between estimated and true parameter values

$$MAPE_i = \frac{1}{N_s}\sum_{j=1}^{N_s}\left|\frac{\hat{\theta}_{i,j} - \theta_{true,i}}{\theta_{true,i}}\right| \cdot 100\%. \tag{14}$$

i indicates the ith parameter of the vector $\boldsymbol{\theta}$, while j indicates estimate number out of N_s estimates. The mean percentage error (MPE) is defined nearly identically, but without the modulus operation. The standard deviation of the MAPE measurements was computed as

$$\begin{aligned} APE_i\ STD &= \mathrm{Std}\left(\left|\frac{\hat{\theta}_i - \theta_{true,i}}{\theta_{true,i}}\right| \cdot 100\%\right) \\ &= \sqrt{\frac{1}{N_s}\sum_{j=1}^{N_s}\left(APE_{i,j} - MAPE_i\right)^2} \end{aligned} \tag{15}$$

The workflow for calculating parameter estimation error for a selected cost function and number of fixed parameters is illustrated in Fig. 3. For each such configuration the non-linear optimization was repeated $N_s = 50$ times with a new initial parameter value $\boldsymbol{\theta}_{sampled}$ from Eq. (13) for each run. The features of all the applied cost functions are organized in Section 2.8.

2.8. Summary

Parameter sensitivity was quantified by estimating variance weighted averages and total Sobol indices as per Eqs. (4) and (5b), respectively. Based on the sensitivities to the timeseries output for the aortic pressure, we ranked the model parameters. To assess the impact of adding parameters of varying sensitivity to the estimation procedure we developed the SSRM (stepwise subset reduction method). The SSRM was applied by ranking model parameters by sensitivity, then estimating all model parameters in the first "step", and then reducing the estimated subset by the least sensitive parameter for the second "step" and making new parameter estimates. The subset reduction continues stepwise until only the most sensitive parameter is estimated. The SSRM was repeated in 10 estimation scenarios:

- I For a cost function using clinical indices
- II For a cost function using waveform data
- III For a cost function using clinical indices with noise
- IV For a cost function using waveform data with noise
- V For a cost function using clinical indices with noise including systolic and diastolic venous pressure
- VI For a cost function using waveform data with noise including the venous pressure waveform.
- VII For a cost function using waveforms with noise where the t_{peak} is always fixed at its *true* value.
- VIII For a cost function using waveforms with noise where the C_{sv} is always fixed at its *true* value.
- IX For a cost function using waveforms where noise is varied N_s times for each step in the SSRM.
- X For a cost function using waveforms where parameters are fixed at 30% above their true value as they are left out of the estimated parameter subset.

After these steps were completed we computed and examined the MAPE and MPE for the estimated parameters compared to the *true* parameters to assess accuracy, precision and bias.

3. Results

3.1. Structural identifiability analysis

Local structural identifiability was analyzed using the STRIKE-GOLDD software. The measured aortic pressure is defined as $P_{ao} = \max P_{lv}, P_{sa}$ in our model, which means that during ejection the aortic pressure is equal to the left ventricular pressure, but is equal to the systemic arterial pressure in diastole. When given aortic flow and left ventricular pressure during ejection all model parameters were found to be locally structurally identifiable except R_{mv} as it was eliminated from the model description by closing the mitral valve. The filling phase model was analyzed using only systemic arterial pressure as aortic flow is zero at this point in the heart cycle. The parameters R_{sys}, C_{ao}, Z_{ao}, and C_{sv} were taken as parameters known to be structurally identifiable upon the second analysis and the rest of the parameters were also found to be locally structurally identifiable in this analysis given waveform data.

3.2. Sensitivity analysis

The sensitivity analysis yielded a parameter ranking based on the sensitivity of the parameters to model outputs. Table 5 shows the ranking according to Sobol indices (4b) for systolic and diastolic pressure and variance weighted sensitivity (5b) to dynamic output signals. Table 4 displays the parameter sensitivities, which for dynamic signals are the total variance weighted average from Eq. (5b) over a heart cycle and for the clinical indices are the total Sobol indices from Eq. (4b).

3.3. Parameter estimation

Computation of the MAPE for all $N_s = 50$ model evaluations yielded substantial errors in some estimated parameters for most cost functions. The exception was the noiseless case with the cost function in Eq. (10) (II) where all parameters were estimated to an error of order of magnitude 10^{-3} percent or less, see Fig. 4. The bar graphs presented from Figs. 4–13 present the parameter MAPE or MPE with standard deviations for all parameter subsets in the SSRM, cases I–X. The bars corresponding to n parameters are the errors of the estimates

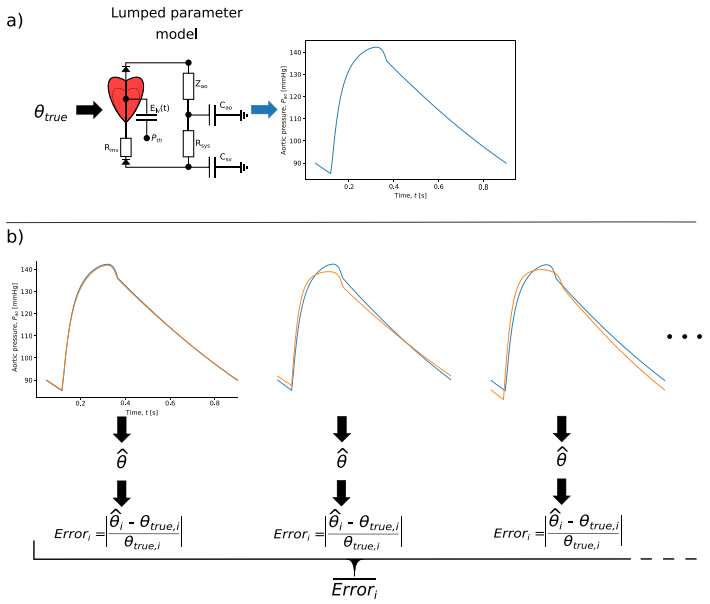

Fig. 3. An illustration of SSRM for one chosen cost function is described. (a) A "true" parameter set (θ_{true}) is defined and used to generate corresponding model output, which is illustrated by an aortic pressure curve in this example. In (b) multiple sampled $\theta_{sampled}$ initial parameter values are used to estimate N_s parameter sets $\hat{\theta}$. The pipeline is repeated nine or eight times as the parameter subset selection is reduced by one parameter for each repetition. For this manuscript the entire SSRM is repeated in ten different estimation scenarios. The errors are computed elementwise for each of the parameters in the parameter vector.

Table 4
Sensitivity values for the parameters to different model outputs. The values given for the time averaged outputs are the total variance weighted averages, see (5), and the derived clinical indices are given as the total Sobol indices (4).

Model output	$TAS_{T,i}(P_{ao})$	$TAS_{T,i}(V_{lv})$	$TAS_{T,i}(Q_{lvao})$	P_{sys}	P_{dia}
V_{tot}	$6.8 \cdot 10^{-1}$	$6.3 \cdot 10^{-1}$	$1.2 \cdot 10^{-1}$	$7.1 \cdot 10^{-1}$	$6.6 \cdot 10^{-1}$
E_{max}	$1.1 \cdot 10^{-1}$	$6.4 \cdot 10^{-2}$	$1.0 \cdot 10^{-1}$	$9.9 \cdot 10^{-2}$	$1.1 \cdot 10^{-1}$
C_{ao}	$8.3 \cdot 10^{-2}$	$1.0 \cdot 10^{-1}$	$4.7 \cdot 10^{-2}$	$1.5 \cdot 10^{-1}$	$3.7 \cdot 10^{-3}$
R_{sys}	$6.5 \cdot 10^{-2}$	$1.7 \cdot 10^{-2}$	$1.8 \cdot 10^{-1}$	$1.5 \cdot 10^{-2}$	$2.1 \cdot 10^{-1}$
t_{peak}	$3.6 \cdot 10^{-2}$	$1.6 \cdot 10^{-1}$	$5.7 \cdot 10^{-1}$	$8.3 \cdot 10^{-3}$	$3.8 \cdot 10^{-3}$
C_{sv}	$2.4 \cdot 10^{-2}$	$2.1 \cdot 10^{-2}$	$4.0 \cdot 10^{-3}$	$2.4 \cdot 10^{-2}$	$2.3 \cdot 10^{-2}$
E_{min}	$1.3 \cdot 10^{-2}$	$1.6 \cdot 10^{-2}$	$4.3 \cdot 10^{-3}$	$1.6 \cdot 10^{-2}$	$8.1 \cdot 10^{-3}$
Z_{ao}	$3.0 \cdot 10^{-4}$	$4.0 \cdot 10^{-5}$	$1.0 \cdot 10^{-2}$	$2.0 \cdot 10^{-4}$	$3.9 \cdot 10^{-5}$
R_{mv}	$2.0 \cdot 10^{-4}$	$1.7 \cdot 10^{-3}$	$2.0 \cdot 10^{-4}$	$3.0 \cdot 10^{-4}$	$3.8 \cdot 10^{-5}$

Table 5
Based on the sensitivity values calculated and presented in Table 4, the following rankings of how sensitive the chosen outputs are to each respective parameter have been compiled. The parameters at the 1st position are the most influential parameters to the model output they are listed under.

Model output	$TAS_{T,i}(P_{ao})$	$TAS_{T,i}(V_{lv})$	$TAS_{T,i}(Q_{lvao})$	P_{sys}	P_{dia}
1st	V_{tot}	V_{tot}	t_{peak}	V_{tot}	V_{tot}
2nd	E_{max}	t_{peak}	R_{sys}	C_{ao}	R_{sys}
3rd	C_{ao}	C_{ao}	V_{tot}	E_{max}	E_{max}
4th	R_{sys}	E_{max}	E_{max}	C_{sv}	C_{sv}
5th	t_{peak}	C_{sv}	C_{ao}	E_{min}	E_{min}
6th	C_{sv}	R_{sys}	Z_{ao}	R_{sys}	t_{peak}
7th	E_{min}	E_{min}	E_{min}	t_{peak}	C_{ao}
8th	Z_{ao}	R_{mv}	C_{sv}	R_{mv}	Z_{ao}
9th	R_{mv}	Z_{ao}	R_{mv}	Z_{ao}	R_{mv}

for the n most sensitive parameters while the rest of the less sensitive parameters are fixed at their *true* values. Consequently, the figures allow the reader to assess how increasing or decreasing the number of estimated parameters affect the parameter estimation error.

For the cost functions using clinical indices (I), all errors were considerably larger when compared to the waveform based error estimates (II). For the subsequent plots only the parameter estimates with the smallest cost functions, which were here defined to be less than 125% of the smallest achieved cost function value, are included. Limiting the selection of estimates to the best cost functions is common practice when performing repeated estimates. This filtering improved the clinical index based estimates for the subsets containing up to four of the most sensitive parameters when all other parameters were fixed at their true value, and made these comparable to the waveform estimates, see Fig. 5. Small improvements were seen for most subsets on the left hand side of the figure, but for subsets with more than five parameters, there was no clear trend that the parameter estimates improved.

All parameters of our model were estimated with good accuracy when noise was omitted for the cost function in Eq. (10). For clinical indices only the estimates of the four most sensitive parameters were reasonably accurate. The maximal MAPE for the waveform parameter estimates was on the order of 10^{-3}%, while for clinical indices this was order 10^{2}%, as shown in Fig. 5.

Fig. 6 shows little noticeable bias for parameter estimates based on waveform data, though the estimates of C_{sv} and R_{mv} have minor negative and positive bias, respectively. The estimates based on clinical indices are all biased to a noticeable degree with especially large positive biases for $E_{max}, C_{ao}, C_{sv}, E_{min}$ and Z_{ao}.

For the cost function in Eq. (9), when more than four parameters were estimated, the accuracy was reduced and the worst cases yielded an average error of over 100% for some of the least sensitive parameters. Estimates for the four least sensitive parameters in the model: C_{sv}, E_{min}, Z_{ao}, and R_{mv}, generally displayed larger errors, emphasizing that these parameters were challenging to estimate.

Fig. 7 shows the results of the SSRM for the same cost functions as in Fig. 5, but with noise (III and IV). The noise reduced the accuracy of estimates, especially for the waveform cost function.

Including either venous indices or waveform data as in cost functions (11) (V) and (12) (VI) improved estimates for at least the seven

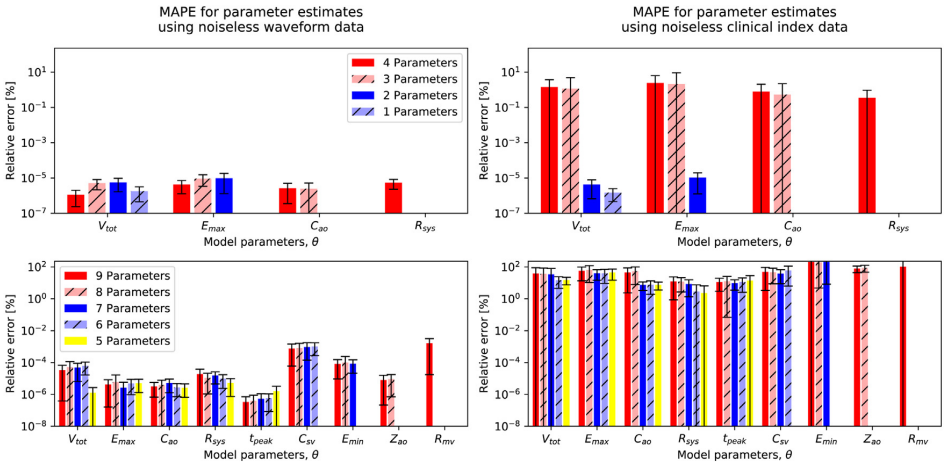

Fig. 4. The plots display a comparison of the MAPE for the parameter estimates using cost functions (10) (left) and (9) (right). These results correspond to scenarios (II) and (I). All N_s estimates are presented in this graph. The bottom row of figures illustrate how the estimates change when you estimate all nine parameters at once and gradually fix one by one parameter at their "true" or correct values. The top row illustrates the same procedure when the five least sensitive parameters are always fixed. The number of parameters indicates how many parameters are estimated while the rest are fixed.

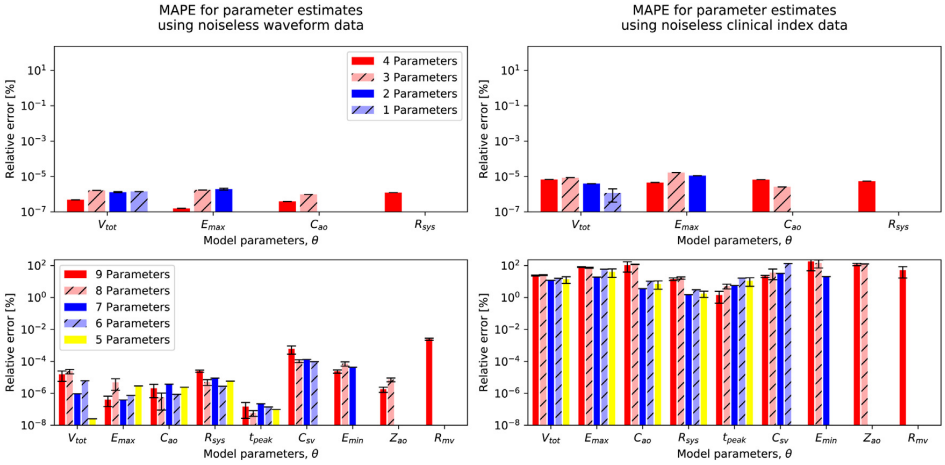

Fig. 5. The plots display a comparison of the MAPE for the parameter estimates using cost functions (10) (left) and (9) (right). These results correspond to scenarios (II) and (I). Only the estimates with a cost function value below 125% of the smallest cost function found for each parameter subset were included. The bottom row of figures illustrate how the estimates change when you estimate all nine parameters at once and gradually fix one by one parameter at their "true" or correct value. The top row illustrates the same procedure when the five least sensitive parameters are always fixed. The number of parameters indicates how many parameters are estimated while the rest are fixed.

most sensitive parameters as seen in Fig. 8. The estimates of E_{min} and C_{sv}, which largely determine ventricular filling in the model, improved noticeably for both cost functions. However, the cost function based on clinical indices still resulted in estimates with substantially larger errors in the majority of cases.

Figs. 9 displays the results found when t_{peak} was fixed at its correct value and the subset selection method was performed only on the remaining parameters (VII). A comparison of Fig. 9 and the left panel of Fig. 7 reveals that the errors of the parameter estimates were not substantially affected by fixing t_{peak}. The same analysis was conducted for C_{sv} (VIII), but in this case all estimates were improved when estimating five or more parameters (compare Fig. 10 and the left panel of Fig. 7). Most errors were reduced by an order of magnitude, with the exceptions of E_{min} and R_{mv} for which the improvements were between 14.9% and 88.4%.

One estimation case was performed where the noise added to the data was varied for each estimation rather than the initial parameter guesses (IX), see Figs. 11 and 13. Some negative biases were observed for R_{sys} and C_{sv}, while the least sensitive parameter R_{mv} exhibited a large positive bias.

Fig. 12 shows the results of applying the SSRM to cost function (10), but where fixed parameters were set at 30% above their true value (X). Estimated errors were shown to increase as more parameters were left out of the estimated subsets.

4. Discussion

We sought to evaluate the potential for estimation of personal cardiovascular parameters for a lumped parameter model that may serve as the basis for predicting long-term changes of the resting systemic hemodynamics in an individual. In order to know that it is theoretically

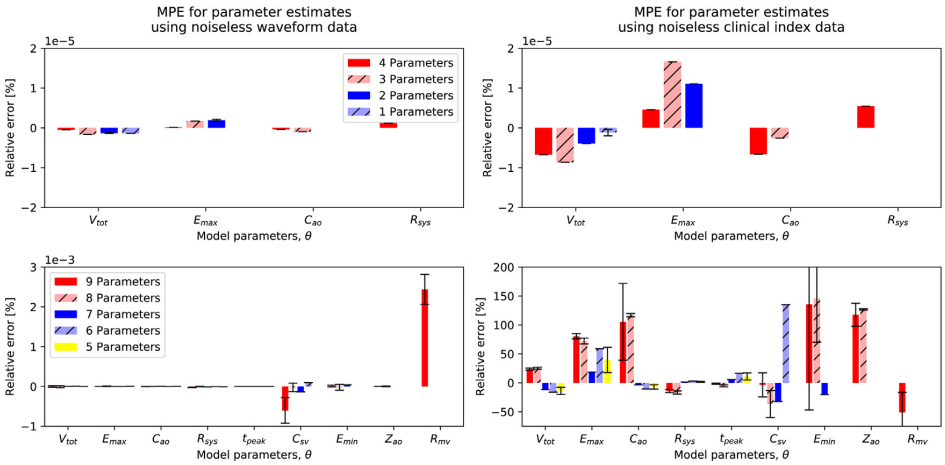

Fig. 6. The plots display a comparison of the MPE for the parameter estimates using cost functions (10) (left) and (9) (right). These results correspond to scenarios (II) and (I). Only the estimates with a cost function value below 125% of the smallest cost function found for each parameter subset were included. The MPE metric gives an indication of whether estimates are biased toward being higher or lower than the true value. The bottom row of figures illustrate how the estimates change when you estimate all nine parameters at once and gradually fix one by one parameter at their "true" or correct value. The top row illustrates the same procedure when the five least sensitive parameters are always fixed. The number of parameters indicates how many parameters are estimated while the rest are fixed.

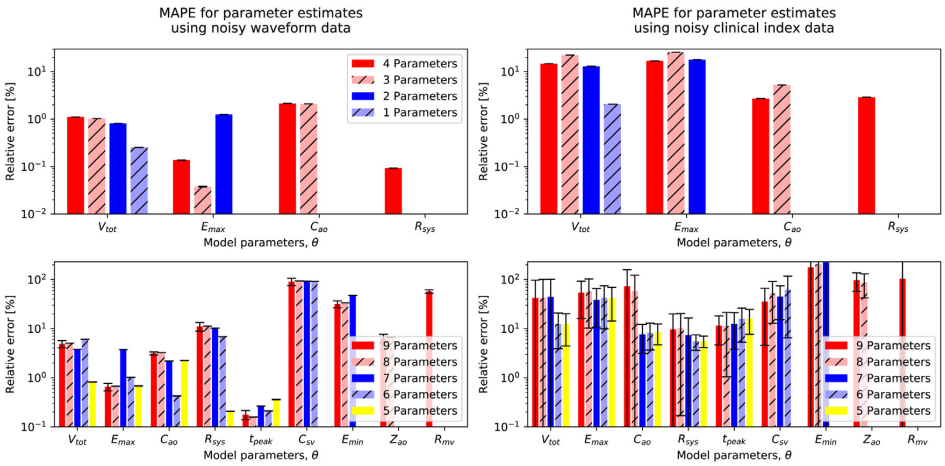

Fig. 7. The plots display a comparison of the MAPE for the parameter estimates using cost functions (10) (left) and (9) (right) where 5% normally distributed noise is added to the signals to which the model is fitted. These results correspond to scenarios (IV) and (III). Only the estimates with a cost function value below 125% of the smallest cost function found for each parameter subset were included. The bottom row of figures illustrate how the estimates change when you estimate all nine parameters at once and gradually fix one by one parameter at their "true" or correct value. The top row illustrates the same procedure when the five least sensitive parameters are always fixed. The number of parameters indicates how many parameters are estimated while the rest are fixed.

possible to recover the model parameters at all we first performed a structural identifiability analysis. The model was found to be locally structurally identifiable, hence demonstrating that it is possible to find at least one identifiable parameter vector for a given model output. As the possibility of estimating the model parameters depends on the data available, we compared an approach using only commonly measured clinical quantities to more data rich approaches using waveform data describing pressures and flows. Both types of data sets were synthetically generated from simulations of a computer model. In addition, we expected that attempting to estimate all parameters in the model simultaneously might inhibit the quality of the parameter estimates, so we applied the SSRM to investigate the benefits of fixing some of the parameters to generic values, while estimating the remaining parameters. This performance of the parameter estimation was evaluated by the SSRM for ten distinct combinations of measurement data and constraints.

The results indicate that it is possible to estimate the most influential parameters to the aortic pressure output signal within an accuracy of 10^{-5}% using both cost functions (9) and (10), if the rest of the parameters are set at their correct value. Introducing noise on the other hand, worsens the accuracy for all parameters as seen in Fig. 7, yet the time series results are still most reliable despite the added noise. These results are also only achieved in one model realization, so how well this result generalizes to other models is yet uncertain.

Gill et al. analyzed the appropriate step sizes for numerical differentiation of functions with numerical errors and showed that the step size should be larger than the square root of the expected relative error [39]. As the model is solved by a Runge–Kutta numerical

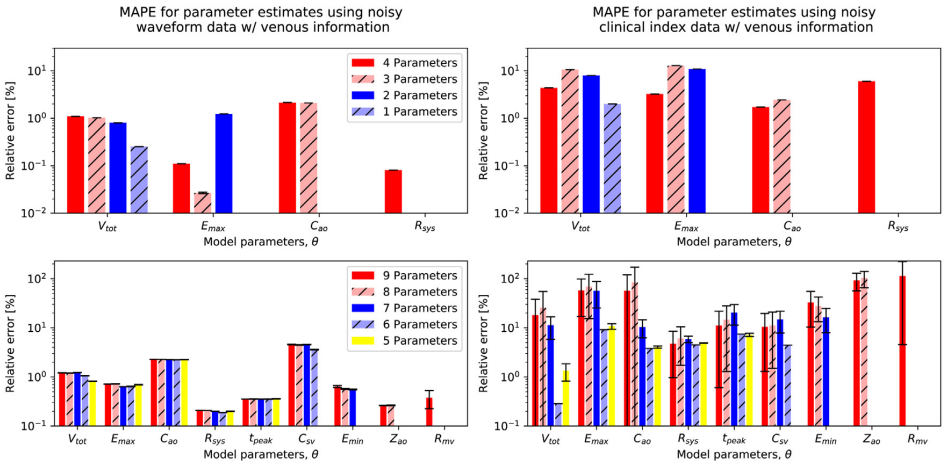

Fig. 8. The plots display the results of parameter the MAPE for the parameter estimates using cost function (10) (left) and (9) (right) for noisy data with added terms containing information from the systemic venous pressure waveform. These results correspond to scenarios (VI) and (V). Only the estimates with a cost function value below 125% of the smallest cost function found for each parameter subset were included. The bottom row of figures illustrate how the estimates change when you estimate all nine parameters at once and gradually fix one by one parameter at their "true" or correct value. The top row illustrates the same procedure when the five least sensitive parameters are always fixed. The number of parameters indicates how many parameters are estimated while the rest are fixed.

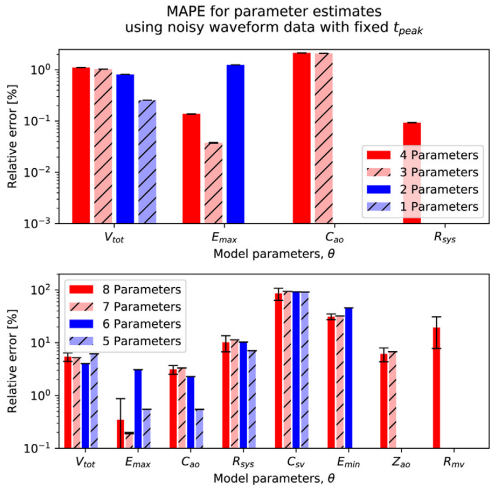

Fig. 9. The plots display the MAPE for the parameter estimates using cost function (10) with noise, while always keeping parameter t_{peak} fixed at its true value. These results correspond to scenario (VII). Only the estimates with a cost function value below 125% of the smallest cost function found for each parameter subset were included. The bottom row of figures illustrate how the estimates change when you estimate all nine parameters at once and gradually fix one by one parameter at their "true" or correct value. The top row illustrates the same procedure when the five least sensitive parameters are always fixed. The number of parameters indicates how many parameters are estimated while the rest are fixed.

integration procedure with relative error tolerance set to 10^{-9}, the minimum step-size for numerical differentiation of the model output is $10^{-4.5}$. Consequently, it should not be expected to estimate parameters to greater accuracy than this when using a numerical gradient based optimization method. The results show the parameters are estimated to the expected accuracy, well below any physically significant error level.

The addition of noise reduced accuracy in the parameter estimates based on waveform data, see the left hand side of Fig. 7. The four previously well estimated parameters became biased when the model was fitted to clinical indices, although still with high precision when a subset of four or fewer parameters were estimated, as seen on the right hand side of Fig. 7. When five or more parameters were estimated, the noise did result in poorer estimates compared to the noiseless case shown on the right hand side of Fig. 5. By further inspection, it emerged that the waveform data estimates were more accurate than for clinical indices when using noisy data in terms of average error, especially when estimating only the most sensitive parameters.

Inclusion of venous information in both cost function classes proved beneficial, especially for estimates concerning parameters important pertaining to the filling phase of the heart, in this case C_{sv} and E_{min}. This was not unexpected as more data in a compartment which is the source of inflow for the heart should provide more information to these parameters.

Fig. 7 shows that the average errors decreased substantially after C_{sv} was removed from the estimated subset. C_{sv} was the first parameter to appear with errors on the scale of 10^2 when added to the estimated subset. The results of fixing C_{sv} for all estimated subsets, can be seen in Fig. 10. A substantial improvement in most estimation errors was observed. Similarly to adding venous information to the cost functions, estimation of the ventricular filling parameters improved, but also estimation of some more sensitive parameters, indicating that this parameter has a larger influence on the estimates of other parameters. Therefore, making accurate estimates for the central systemic venous compliance C_{sv} can be an alternative to inconvenient pressure measurements in the central veins.

An interesting observation can be made from Fig. 8 for the waveform data parameter estimates: As soon as 5 or more parameters are selected in the estimated subset, the estimation error for all parameters are practically constant and unperturbed by estimation of additional parameters. This signifies that the deviation from true parameters is sufficiently small, which according to the figure is 10% or less, such that the estimation error in the least sensitive parameters does not influence the other estimates in any way. It appears that the same minimum is found in the cost function regardless of the additional lesser sensitive parameters, and this must then mean the noise level in the data limits more accurate optimization with respect to parameters. For the large majority of parameters the error is well below 5% which was the specified noise amplitude. Consequentially, if the venous

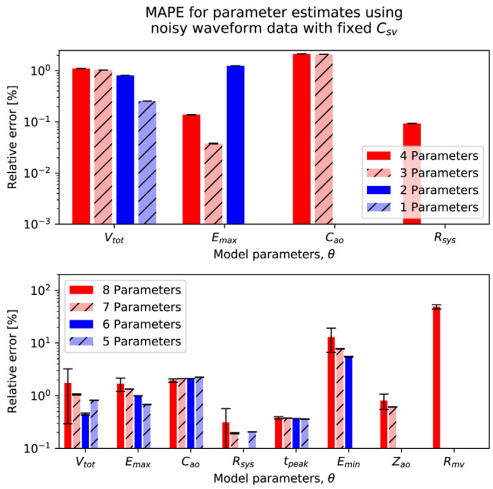

Fig. 10. The plots display the MAPE for parameter estimates using cost function (10) with noise, while always keeping parameter C_{sv} fixed at its true value. These results correspond to scenario (VIII). Only the estimates with a cost function value below 125% of the smallest cost function found for each parameter subset were included. The bottom row of figures illustrate how the estimates change when you estimate all nine parameters at once and gradually fix one by one parameter at their "true" or correct value. The top row illustrates the same procedure when the five least sensitive parameters are always fixed. The number of parameters indicates how many parameters are estimated while the rest are fixed.

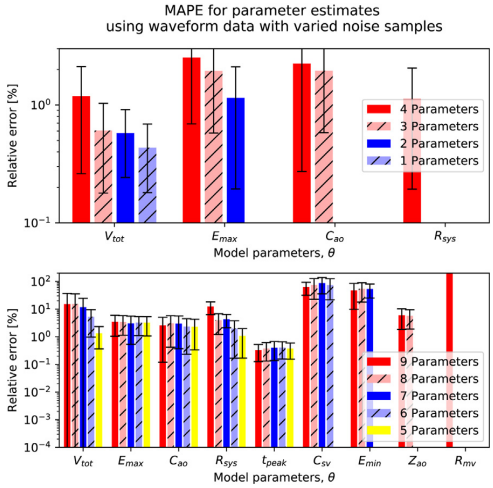

Fig. 11. The plots display the MAPE for parameter estimates using cost function (10) with $N_s = 50$ different noise cases, but the same initial parameter guess for each case. These results correspond to scenario (IX). Only the estimates with a cost function value below 125% of the smallest cost function found for each parameter subset were included. The bottom row of figures illustrate how the estimates change when you estimate all nine parameters at once and gradually fix one by one parameter at their "true" or correct value. The top row illustrates the same procedure when the five least sensitive parameters are always fixed. The number of parameters indicates how many parameters are estimated while the rest are fixed.

pressure waveform is available, all parameters should be obtainable to within 10% accuracy based on the noise sample used. Compared to Fig. 12 where parameters are fixed at 30% above their true value, but without noise and venous data we find errors of approximately 10% for most estimates when less than 7 parameters are estimated, but some errors approach 100% as progressively fewer parameters are estimated. Therefore, the estimation procedure seems more sensitive to poor estimates for fixed parameters than to noise in the data. This is even the case when the three least sensitive parameters are fixed at their wrong values.

In Fig. 13 we observe that for most parameters, the estimation error is averaged out and shows little or no bias for most parameters over a larger number of noisy samples as one might expect for Gaussian noise. The four least sensitive parameters do show some bias which emphasizes that estimates of these cannot be trusted in general. In Fig. 11 presenting MAPE, the errors are maximally 15.4% for the five most sensitive parameters, and up to 88.1% for the next three most sensitive parameters, and even over 10^3% for R_{mv}. Therefore, noise can have a large impact on a single cycle of data. However the estimate error variance is for the most part quite low, so based on this it appears that it is not the details of the different noise samples which mainly dictate the estimation error, but rather the presence of normally distributed noise of the given magnitude.

From our investigation it was also demonstrated that fixing parameters at wrong values will substantially affect estimates. We observed that the estimation error fell in a range of 0.1%–100% for all parameters as seen in Fig. 7. Adding 30% to the fixed parameter values was then determined to be a suitable level for comparison on average. Fig. 12 shows that the estimation errors then fell in the range of 10^{-6}%–50% for most parameters in the model, regardless of which estimated subset was considered. When all 9 parameters are estimated, none are fixed at erroneous values. As more parameters were fixed, the estimation error also grew rapidly. This was true even for a noiseless case, implying that parameters set at wrong values may strongly influence the other parameter estimates. To be able to personalize, or calibrate this model means that the three or four least sensitive parameters should be estimated or measured to high accuracy, before the chosen least squares optimization methods can estimate the rest to good accuracy, unless venous pressure data are available. Some of the three least sensitive parameters can be estimated from pressure, flow and/or volume measurements, but most often require measurements in or around the left ventricle [40,41], which is costly and burdensome for an individual. In the case of E_{min} one may perhaps estimate this from the end-diastolic pressure–volume relationship but there are not any examples of this being demonstrated, that are known by the authors.

The SSRM was performed in the sequence prescribed by the parameter sensitivity ranking according to the aortic pressure time series in Table 5, because this is among the most easily observed outputs to predict and is therefore also used to constrain the cost function either as a time series or as extrema values. The optimization approach presented relies solely on the local Quasi-Newton optimization method TRRA, as opposed to more computationally expensive global optimization methods such as for instance Markov Chain Monte Carlo methods, or genetic algorithms [12]. Partial motivation for this work is to develop methods where computational time is another parameter to be minimized and is the reason why computationally cheaper algorithms are preferred in this investigation. Other notions of sensitivity could have been chosen to rank the parameters, but the total variance weighted averaged Sobol indices were chosen in this instance. For the notions of sensitivity tested the least sensitive three parameters were often the same. On the other hand there were some variations among the more sensitive parameters, but there were no dominating patterns.

Only for a limited subset of the most sensitive parameters is the local optimization by TRRA robust for parameter estimation given that all other parameters are fixed at their true values. Robust means here that the results are practically independent of the initial parameter values, and that the estimates are made to low error. The four least sensitive parameters C_{sv}, E_{min}, Z_{ao} and R_{mv} could not be reliably estimated in all cases as they were estimated with large errors. The conclusion must be that the inclusion of these parameters makes the cost function very flat

around the true minimum in parameter space and causes difficulties for the numerical optimization method. Conclusions based on the estimates of these parameters can therefore not be trusted in a majority of cases. Counter intuitively, the second least influential parameter Z_{ao} could for cost functions using waveforms often be better estimated compared to the other three least influential parameters. This may be explained by limited resolution in the sensitivity analysis. For parameters of sensitivities below 0.1 it is challenging to make an accurate ranking, and hence Z_{ao} might actually be more influential than the other three parameters since they were all estimated to similar low values.

The data used in this analysis is purely synthetic, which in contrast to real data exhibit no model discrepancy, and has no structured noise or hidden bias. Still, in this perfect case it is not always possible to fit the model to its own output data using the applied methods given randomly sampled initial parameter guesses. This lends credence to the methods presented by Colunga et al. and de Bournonville et al. which emphasize that using good nominal values used as initial values for the optimization problem is necessary for accurate parameter estimation [7,8]. To make the estimation scenario more realistic we applied Gaussian noise to the output signals from the model. The standard clinical method of measuring blood pressure is to measure the systolic and diastolic blood pressure by cuff plethysmography and the measurement uncertainty is widely regarded to be ± 5 mmHg. Using 100 mmHg as a reference scale for blood pressure and adding noise from a normal distribution with 5% standard deviation the error should be comparable and even introduce larger deviations at some points, making this a realistic measurement error. During measurement of blood flow velocity a slight misalignment of only $2\,\mathrm{deg}$ between measurement probe and direction of blood flow may introduce large errors, so as a general rule of thumb for Doppler velocity uncertainty is $\pm 10\%$. As we have observed when comparing the results from using noiseless to noisy data the results are majorly affected by adding 5% normally distributed noise, and we hypothesize that knowing personalized parameters accurately is essential to make personalized predictions about an individual. However, it would also be beneficial if measurements could be made more readily available and less burdensome to the patient such that more data can be collected and make it easier to perform analysis for an individual at all, rather than be limited by not having any data to attempt this.

This study can be described as a practical identifiability study where we attempted to personalize a model to a given set of data under both ideal and noiseless conditions. The structural identifiability was demonstrated and supported by the demonstration of practically recovering the *true* parameters in the noiseless case using waveforms. The other scenarios investigated in this paper showed that the model was not practically identifiable by the given set of measurements with noise. By application of the STRIKE-GOLDD software tool we showed that the model was locally structurally identifiable using aortic pressure and flow waveforms. Local structural identifiability implies that there may be an infinite set of solutions to the problem, yet we seem to find the correct cost function minimum in the noiseless case using waveforms which may support that there is only one solution in the chosen domain of valid parameters.

The estimation results were chosen by picking the estimates with the best cost function values, and therefore the limit was set at a cost function value 125% higher than the lowest cost function value. Controlling the cost function by picking the best results are common practice in optimization problems. The result, however, is that in some cases depending on the variation in the results all results are included if all estimates yield an equally good cost function value and the operation means nothing is done. In other cases the limit may be too strict and only a few of the results are used in the final average. This also means that the standard deviation bars are calculated based on little data and may be uncertain.

In most of the results we observed uneven improvement in estimates as the subset size of estimated parameters decreased. Some of the uneven variation may be explained by the addition of noise and finite points of the waveform data. The minimum which the optimization algorithm finds for noisy data may not correspond exactly to the

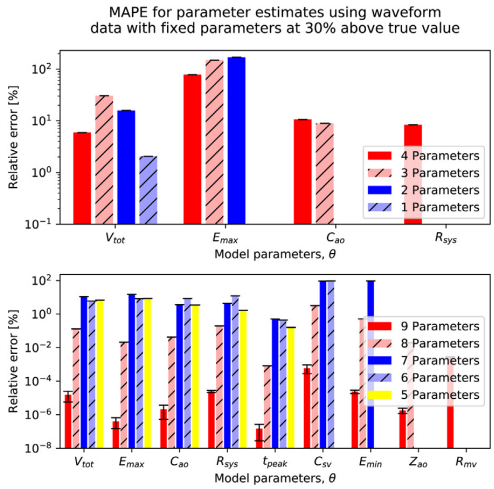

Fig. 12. The plots display model fits using cost function (10), but where fixed parameters are fixed at 30% above their true value. These results correspond to scenario (X). Only the estimates with a cost function value below 125% of the smallest cost function found for each parameter subset were included. The bottom row of figures illustrate how the estimates change when you estimate all nine parameters at once and gradually fix one by one parameter at their "true" or correct value. The top row illustrates the same procedure when the five least sensitive parameters are always fixed. The number of parameters indicates how many parameters are estimated while the rest are fixed.

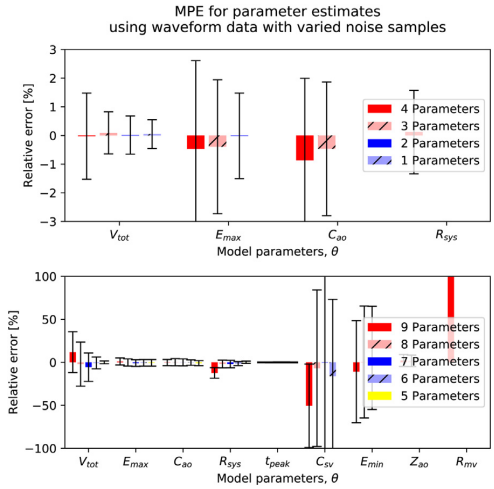

Fig. 13. The plots display the MPE for parameter estimates using cost function (10) with N_s different noise cases, but the same initial parameter guess for each case. Only the estimates with a cost function value below 125% of the smallest cost function found for each parameter subset were included. The MPE metric gives an indication of whether estimates are biased toward being higher or lower than the true value. The bottom row of figures illustrate how the estimates change when you estimate all nine parameters at once and gradually fix one by one parameter at their "true" or correct value. The top row illustrates the same procedure when the five least sensitive parameters are always fixed. The number of parameters indicates how many parameters are estimated while the rest are fixed.

solution defined by $\boldsymbol{\theta}_{\mathbf{true}}$. Therefore, as different parameter subsets are optimized for the perturbed optimal solution the estimates may unevenly approach more accurate estimates as the metric used can compare a cost function minimum which differs slightly from the minimum defined by the noiseless waveforms.

The results of our study are somewhat in contrast to prior works on parameter estimation and subset selection for *cardiovascular* models [36,42] which propose that fixing insensitive and some strongly correlated parameters may improve parameter estimates and model fits. Some of these methodologies have been tested primarily on fitting models to experimental or clinical data, and have not been evaluated on synthetic data sets where the *true* values of model parameters can be directly known. Many such studies argue that parameter estimates show good convergence to the estimated values (e.g. Pant et al. [10]) and some have employed statistical approaches to quantify uncertainty and variability of the parameter estimates such as Colunga et al. and Marquis et al. [6,8]. These studies have estimated lower uncertainties in parameter estimates than have been found in our synthetic approach, but use more sophisticated optimization methods. While the models, measurements, and parameter estimation methods differ in numerous ways, the patterns in these results may well be a general feature of lumped parameter circulatory models.

5. Conclusion

We have applied the stepwise subset reduction method (SSRM) to a closed-loop lumped parameter model in order to investigate how well this model can be calibrated using limited, in this case synthetic, data. Consequentially we have demonstrated a framework for assessing the accuracy and precision of parameter estimation for different subsets of model parameters. We first performed a structural identifiability analysis which revealed the model to be structurally identifiable with waveform data from the aorta. The local optimization methods applied in this analysis were sensitive to initial parameter guesses, and we investigated the effect on the precision and accuracy of estimated parameters. We demonstrated, that using waveform data as opposed to scalar clinical indices improves the accuracy of parameter estimates, and the waveform data cost functions are far more robust in terms of providing the best estimates despite the introduction of normally distributed noise to the data. Standard local optimization methods can be used for model calibration of the five most sensitive parameters in the presented simple-lumped parameter model of the systemic circulation and left ventricle. The most sensitive parameters are generally recovered with errors less than 10% given that the other parameters are fixed at correct values, and noise is normally distributed at 5%. We also showed that when parameters were fixed at 30% above their true value, estimation error can be comparable to the error introduced by noise even if only the three least sensitive parameters are fixed at erroneous values. The four least sensitive parameters could not be generally reliably estimated by this method without more information, and no conclusions should be based on estimates of these parameters. The three least sensitive parameters especially should be considered for measurements. The addition of venous information to the cost function further improved parameter estimates, and after analysis by the SSRM the central venous compliance of the systemic circulation was found to be a positive influence on the less sensitive parameter estimates if it could be measured and fixed at an accurate value.

Declaration of competing interest

The authors declare that they have no known competing financial interests or personal relationships that could have appeared to influence the work reported in this paper.

Acknowledgments

Some of the computations were performed on resources provided by the NTNU IDUN/EPIC computing cluster [32].

Appendix A. Model equations

The model is comprised as a system of nonlinear ODEs describing the volume state variable of the three model compartments. The dynamic elastance function of the heart contributes a source term to the system of ODEs.

$$\begin{aligned}\frac{dV_{sa}}{dt} &= C_{sa}\frac{dP_{sa}}{dt} = Q_{lvao} - Q_{sys}\\ \frac{dV_{sv}}{dt} &= C_{sv}\frac{dP_{sv}}{dt} = Q_{sys} - Q_{svlv}\\ \frac{dV_{lv}}{dt} &= Q_{svlv} - Q_{lvao}\end{aligned} \tag{A.1}$$

V_{sa}, V_{sv} and V_{lv} are the stressed blood volumes of the systemic arteries, systemic veins and left ventricle respectively. C_{sa} and C_{sv} are the compliance values of the systemic arteries and veins, while P_{sa} and P_{sv} are the corresponding pressures of these compartments. Q_{lvao} denotes the volume blood flow from the left ventricle to the systemic arteries, Q_{sys} is the flow between the systemic arteries and veins, and finally Q_{svlv} is the flow from the veins to the left ventricle. The two remaining state variables, pressure and flow, are mainly modeled by linear relationships as expressed below

$$\begin{aligned}V_{sa} &= C_{sa}P_{sa}\\ V_{sv} &= C_{sv}P_{sv}\\ P_{lv} &= E_{lv}(t)V_{lv} + P_{th}(t)\\ E_{lv}(t) &= (E_{\max} - E_{\min})e(t) + E_{\min}\\ P_{ao} &= \max[P_{sa}, P_{lv}]\\ Q_{lvao} &= I(P_{lv} > P_{sa})\frac{P_{lv} - P_{sa}}{Z_{ao}}\\ Q_{svlv} &= I(P_{sv} > P_{lv})\frac{P_{sv} - P_{lv}}{R_{mv}}\\ Q_{sys} &= \frac{P_{sa} - P_{sv}}{R_{sys}}.\end{aligned} \tag{A.2}$$

P_{ao} indicates aortic pressure, while P_{lv} denotes left ventricular pressure. Z_{ao} is the characteristic aortic impedance while R_{sys} and R_{mv} are total systemic vascular and mitral valve resistances. The indicator function $I(x)$ has the value 1 when the argument x is true and 0 when x is false. The activation function $e(\tau)$ is defined as

$$e(\tau) = \alpha \times \frac{(\tau/a_1)^{n_1}}{1 + (\tau/a_1)^{n_1}} \times \frac{1}{1 + (\tau/a_2)^{n_2}} \tag{A.3}$$

where τ is position in the cardiac cycle between the end of the last diastolic period and the end of the next diastolic period $\tau = 1$. The parameters a_1 and n_1 determine the shape of contraction and a_2 and n_2 determine the shape of relaxation of the elastance curve and the timing of peak elastance. The choice of values for these parameters are identical to those of Stergiopulos et al. [13]. We wrote the parameter values for a_1 and a_2 in terms of the ratio of $\frac{t_{peak}}{T}$, and set $\alpha = 1.672$, to ensure normalization of the curve. t_{peak} describes the time of peak ventricular elastance, and therefore determines when the left ventricular elastance $E_{lv}(t)$ reaches E_{max}. The intrathoracic pressure function P_{th} describes the external pressure effects on the ventricular muscle aside from pressure gradients inside the blood vessels and is here modeled as a constant of $P_{th}(t) = -4$ mmHg. Otherwise the parameters are as defined by Table 1.

The V_{tot} parameter describes total stressed volume and is enforced by setting initial compartment volumes and pressures such that the total stressed volume equals the parameter value. The model was demonstrated to conserve the volume and hence the total blood volume will not change. The initial volumes and pressures are set according to the equations

$$\begin{aligned}V_{ao,0} &= C_{ao}P_{ao,0}, \text{and}\\ P_{sv,0} &= \frac{V_{tot} - V_{ao,0} - V_{lv,0}}{C_{sv}}\end{aligned} \tag{A.4}$$

Table B.6
All model parameters that are assigned to be personalizable are listed along with their upper and lower bounds as chosen for this study. The sampling value is the mean value of the normal distribution from which initial parameter guesses are sampled.

Parameter	Upper bounds	Lower bounds	Sampling value	Units
C_{ao}	10.0	0.5	1.0	$\frac{mL}{mmHg}$
C_{sv}	30.0	0.5	10.0	$\frac{mL}{mmHg}$
E_{max}	5.0	0.9	2.0	$\frac{mmHg}{mL}$
E_{min}	1.0	0.0	0.06	$\frac{mmHg}{mL}$
R_{mv}	0.1	0.0	0.003	$\frac{mmHg\ s}{mL}$
R_{sys}	3.0	0.5	1.0	$\frac{mmHg\ s}{mL}$
T	0.85	0.85	0.85	s
t_{peak}	0.75	0.05	0.32	–
V_{tot}	2000.	50.	250.	mL
Z_{ao}	1.0	0.0	0.1	$\frac{mmHg\ s}{mL}$

Table B.7
The scaling factors K which are used to balance and approximately normalize the terms in the specified cost functions. Subscripts: p — Aortic pressure waveform, q — Aortic flow, PP — pulse pressure, psys — Systolic aortic pressure, pdia — Diastolic aortic pressure, psvsys — Systolic averaged venous pressure, psvdia — Diastolic averaged venous pressure, psv — Averaged venous pressure waveform, SV — stroke volume, and qmax — maximal aortic flow.

Symbol	Value	Unit
K_p	100.0	mmHg
K_q	500.0	$\frac{mL}{s}$
K_{PP}	40.0	mmHg
K_{psys}	120.0	mmHg
K_{pdia}	80.0	mmHg
K_{psvsys}	20.0	mmHg
K_{psvdia}	20.0	mmHg
K_{psv}	20.0	mmHg
K_{SV}	100.0	mL
K_{qmax}	500.0	mL

where the initial aortic pressure is set to $P_{ao,0} = 100$ mmHg, and initial left ventricular volume is set to $V_{lv,0} = 100$ mL. The initial venous pressure is denoted by $P_{sv,0}$.

Appendix B. Algorithm specification

The algorithm applied for computations within this study was chosen to be the Trust Reflective Region Algorithm as implemented in SciPy version 1.4.1 [24].

The function scipy.optimize.least_squares() function is applied given the arguments listed below and a initial parameter guess. The reference parameters for the initial parameter guesses are listed in Table 1 and are sampled as vectors with normally distributed noise with a standard deviation of 30% as per Eq. (13). Each parameter is assigned its own random perturbation, except T which is always fixed. The parameters are also assigned upper and lower bounds, which are set to the values given in Table B.6. The initial parameter guesses are limited to fall within these bounds.

Scaling factors used to balance the different components in the cost functions as specified in Section 2 are listed in Table B.7.

Otherwise some function specific parameters for the accuracy of the method are set as $xtol = 2.3 \cdot 10^{-16}$, $ftol = 2.3 \cdot 10^{-16}$, $gtol = 2.3 \cdot 10^{-16}$ and $diff\_step = 1. \cdot 10^{-3}$.

For sampling noise applied to time series signal according to formula (3) the numpy seed, np.random.seed() function was initialized at the value 87654321. The seed was set at 112233, for sampling initial parameter guesses, $\theta_{sampled}$, as prescribed by formula (13).

References

[1] P.D. Morris, D. Ryan, A.C. Morton, R. Lycett, P.V. Lawford, D.R. Hose, J.P. Gunn, Virtual fractional flow reserve from coronary angiography: modeling the significance of coronary lesions: results from the VIRTU-1 (VIRTUal Fractional Flow Reserve From Coronary Angiography) study, JACC. Cardiovasc. Intervent. 6 (2013) 149–157.

[2] E. Kung, G. Pennati, F. Migliavacca, T.-Y. Hsia, R. Figliola, A. Marsden, A. Giardini, A simulation protocol for exercise physiology in Fontan patients using a closed loop lumped-parameter model, J. Biomech. Eng. 136 (2014) 0810071–08100714.

[3] L. Fresiello, B. Meyns, A. Di Molfetta, G. Ferrari, A model of the cardiorespiratory response to aerobic exercise in healthy and heart failure conditions, Front. Physiol. 7 (2016).

[4] A. Di Molfetta, A. Amodeo, M.G. Gagliardi, M.G. Trivella, L. Fresiello, S. Filippelli, A. Toscano, G. Ferrari, Hemodynamic effects of ventricular assist device implantation on Norwood, Glenn, and Fontan Circulation: A Simulation Study, Artif. Organs 40 (2016) 34–42.

[5] H. Ho, H.B. Yu, A. Bartlett, P. Hunter, An in silico pipeline for subject-specific hemodynamics analysis in liver surgery planning, Comput. Methods Biomech. Biomed. Eng. 23 (4) (2020) 138–142, PMID: 31928213.

[6] A.D. Marquis, A. Arnold, C. Dean-Bernhoft, B.E. Carlson, M.S. Olufsen, Practical identifiability and uncertainty quantification of a pulsatile cardiovascular model, Math. Biosci. 304 (2018) 9–24.

[7] S. de Bournonville, A. Pironet, C. Pretty, J.G. Chase, T. Desaive, Parameter estimation in a minimal model of cardio-pulmonary interactions, Math. Biosci. 313 (2019) 81–94.

[8] A.L. Colunga, K.G. Kim, N.P. Woodall, T.F. Dardas, J.H. Gennari, M.S. Olufsen, B.E. Carlson, Deep phenotyping of cardiac function in heart transplant patients using cardiovascular system models, J. Physiol. 598 (15) (2020) 3203–3222.

[9] S. Pant, B. Fabrèges, J.-F. Gerbeau, I.E. Vignon-Clementel, A methodological paradigm for patient-specific multi-scale CFD simulations: from clinical measurements to parameter estimates for individual analysis, Int. J. Numer. Methods Biomed. Eng. 30 (12) (2014) 1614–1648.

[10] S. Pant, C. Corsini, C. Baker, T.-Y. Hsia, G. Pennati, I.E. Vignon-Clementel, Data assimilation and modelling of patient-specific single-ventricle physiology with and without valve regurgitation, J. Biomech. 49 (11) (2016) 2162–2173, Selected Articles from the International Conference on CFD in Medicine and Biology (Albufeira, Portugal – August 30th - September 4th, 2015).

[11] R. Meiburg, W. Huberts, M.C.M. Rutten, F.N. van de Vosse, Uncertainty in model-based treatment decision support: Applied to aortic valve stenosis, Int. J. Numer. Methods Biomed. Eng. 36 (10) (2020) e3388.

[12] C. Hann, J. Chase, T. Desaive, C. Froissart, J. Revie, D. Stevenson, B. Lambermont, A. Ghuysen, P. Kolh, G. Shaw, Unique parameter identification for cardiac diagnosis in critical care using minimal data sets, Comput. Methods Programs Biomed. 99 (1) (2010) 75–87.

[13] N. Stergiopulos, J.J. Meister, N. Westerhof, Determinants of stroke volume and systolic and diastolic aortic pressure, Am. J. Physiol. 270 (1996) H2050–9.

[14] Y. Shi, P. Lawford, R. Hose, Review of zero-D and 1-D models of blood flow in the cardiovascular system, BioMed. Eng. OnLine 10 (1) (2011) 33.

[15] J.P. Mynard, J.J. Smolich, One-dimensional haemodynamic modeling and wave dynamics in the entire adult circulation, Ann. Biomed. Eng. 43 (6) (2015) 1443–1460.

[16] P. Segers, N. Stergiopulos, P. Verdonck, R. Verhoeven, Assessment of distributed arterial network models, Med. Biol. Eng. Comput. 35 (6) (1997) 729–736.

[17] B.W. Smith, J. Chase, R.I. Nokes, G.M. Shaw, G. Wake, Minimal haemodynamic system model including ventricular interaction and valve dynamics, Med. Eng. Phys. 26 (2) (2004) 131–139.

[18] P. Segers, N. Stergiopulos, N. Westerhof, Quantification of the contribution of cardiac and arterial remodeling to hypertension, Hypertension 36 (5) (2000) 760–765.

[19] P. Segers, E.R. Rietzschel, M.L. De Buyzere, N. Stergiopulos, N. Westerhof, L.M. Van Bortel, T. Gillebert, P.R. Verdonck, Three- and four-element windkessel models: assessment of their fitting performance in a large cohort of healthy middle-aged individuals., Proc. Inst. Mech. Eng. H 222 (2008) 417–428.

[20] J.-L. Vachiéry, S. Gaine, Challenges in the diagnosis and treatment of pulmonary arterial hypertension, Eur. Respir. Rev. 21 (126) (2012) 313–320.

[21] A. La Gerche, D.J. Rakhit, G. Claessen, Exercise and the right ventricle: a potential Achilles' heel, Cardiovasc. Res. 113 (12) (2017) 1499–1508.

[22] T.D. Miller, N.S. Anavekar, Right ventricle and exercise capacity, Circulation: Cardiovasc. Imaging 9 (11) (2016) e005703.

[23] W. Huberts, S.G. Heinen, N. Zonnebeld, D.A. van Den Heuvel, J.-P.P. de Vries, J.H. Tordoir, D.R. Hose, T. Delhaas, F.N. van de Vosse, What is needed to make cardiovascular models suitable for clinical decision support? A viewpoint paper, J. Comput. Sci. 24 (2018) 68–84.

[24] P. Virtanen, R. Gommers, T.E. Oliphant, M. Haberland, T. Reddy, D. Cournapeau, E. Burovski, P. Peterson, W. Weckesser, J. Bright, S.J. van der Walt, M. Brett, J. Wilson, K. Jarrod Millman, N. Mayorov, A.R.J. Nelson, E. Jones, R. Kern, E. Larson, C. Carey, İ. Polat, Y. Feng, E.W. Moore, J. Vand erPlas, D. Laxalde, J. Perktold, R. Cimrman, I. Henriksen, E.A. Quintero, C.R. Harris, A.M.

Archibald, A.H. Ribeiro, F. Pedregosa, P. van Mulbregt, S... Contributors, SciPy 1.0: FUndamental algorithms for scientific computing in Python, Nature Methods (2020).
[25] H. Miyashita, Clinical assessment of central blood pressure, Curr. Hypertens. Rev. 8 (2012) 80–90.
[26] J. Lee, J. Sohn, J. Park, S. Yang, S. Lee, H.C. Kim, Novel blood pressure and pulse pressure estimation based on pulse transit time and stroke volume approximation, Biomed. Eng. Online 17 (2018) 81.
[27] C.W.L. Chin, H.J. Khaw, E. Luo, S. Tan, A.C. White, D.E. Newby, M.R. Dweck, Echocardiography underestimates stroke volume and aortic valve area: implications for patients with small-area low-gradient aortic stenosis, Can. J. Cardiol. 30 (2014) 1064–1072.
[28] H. Miao, X. Xia, A.S. Perelson, H. Wu, On identifiability of nonlinear ode models and applications in viral dynamics, SIAM Rev. Soc. Ind. Appl. Math. 53 (2011) 3–39.
[29] L. Ljung, T. Glad, On global identifiability for arbitrary model parametrizations, Automatica 30 (2) (1994) 265–276.
[30] A.F. Villaverde, A. Barreiro, A. Papachristodoulou, Structural identifiability of dynamic systems biology models, PLoS Comput. Biol. 12 (10) (2016) 1–22.
[31] A. Pironet, P.C. Dauby, J.G. Chase, P.D. Docherty, J.A. Revie, T. Desaive, Structural identifiability analysis of a cardiovascular system model, Med. Eng. Phys. 38 (5) (2016) 433–441.
[32] M. Själander, M. Jahre, G. Tufte, N. Reissmann, EPIC: An energy-efficient, high-performance GPGPU computing research infrastructure, 2019.
[33] V.G. Eck, W.P. Donders, J. Sturdy, J. Feinberg, T. Delhaas, L.R. Hellevik, W. Huberts, A guide to uncertainty quantification and sensitivity analysis for cardiovascular applications, Int. J. Numer. Methods Biomed. Eng. 32 (8) (2016) e02755.
[34] W.P. Donders, W. Huberts, F.N. Vosse, T. Delhaas, Personalization of models with many model parameters: an efficient sensitivity analysis approach, Int. J. Numer. Methods Biomed. Eng. 31 (10) (2015).
[35] A. Saltelli, P. Annoni, How to avoid a perfunctory sensitivity analysis, Environ. Model. Softw. 25 (12) (2010) 1508–1517.
[36] M.S. Olufsen, J.T. Ottesen, A practical approach to parameter estimation applied to model predicting heart rate regulation, J. Math. Biol. 67 (1) (2013) 39–68.
[37] C.H. Olsen, J.T. Ottesen, R.C. Smith, M.S. Olufsen, Parameter subset selection techniques for problems in mathematical biology, Biol. Cybernet. 113 (1) (2019) 121–138.
[38] A. Alexanderian, P.A. Gremaud, R.C. Smith, Variance-based sensitivity analysis for time-dependent processes, Reliab. Eng. Syst. Saf. 196 (2020) 106722.
[39] P.E. Gill, W. Murray, M.A. Saunders, M.H. Wright, Computing forward-difference intervals for numerical optimization, SIAM J. Sci. Stat. Comput. 4 (2) (1983) 310–321.
[40] H.S. Roshdy, A.M. Meshrif, I.I. El-Dosouky, Value of the mitral valve resistance in evaluation of symptomatic patients with mild and moderate mitral stenosis–a dobutamine stress echocardiographic study., Echocardiography (Mount Kisco, N.Y.) 31 (2014) 347–352.
[41] R. Kelly, D. Fitchett, Noninvasive determination of aortic input impedance and external left ventricular power output: A validation and repeatability study of a new technique, J. Am. Coll. Cardiol. 20 (4) (1992) 952–963.
[42] A. Cintrón-Arias, H.T. Banks, A. Capaldi, A.L. Lloyd, A sensitivity matrix based methodology for inverse problem formulation, J. Inverse Ill-Posed Probl. 17 (6) (2009) 545–564.

Chapter 7

Monitoring Variability in Parameter Estimates for Lumped Parameter Models of the Systemic Circulation Using Longitudinal Hemodynamic Measurements

The content of this chapter was published in *BioMedical Engineering OnLine*, 2023.

Paper 2: Monitoring Variability in Parameter Estimates for Lumped Parameter Models of the Systemic Circulation Using Longitudinal Hemodynamic Measurements

N.L. Bjørdalsbakke, J. Sturdy, E.M.L. Ingeström, L.R. Hellevik

Bjørdalsbakke *et al.*
BioMedical Engineering OnLine (2023) 22:34
https://doi.org/10.1186/s12938-023-01086-y

BioMedical Engineering OnLine

RESEARCH Open Access

Monitoring variability in parameter estimates for lumped parameter models of the systemic circulation using longitudinal hemodynamic measurements

Nikolai L. Bjørdalsbakke[1*], Jacob Sturdy[1], Emma M. L. Ingeström[2] and Leif R. Hellevik[1]

*Correspondence:
nikolai.l.bjordalsbakke@ntnu.no

[1] Department of Structural Engineering, Norwegian University of Science and Technology (NTNU), Richard Birkelandsvei 1a, Trondheim, Norway
[2] Department of Circulation and Medical Imaging, Norwegian University of Science and Technology (NTNU), Prinsesse Kristinas gt. 3, Trondheim, Norway

Abstract

Background: Physics-based cardiovascular models are only recently being considered for disease diagnosis or prognosis in clinical settings. These models depend on parameters representing the physical and physiological properties of the modeled system. Personalizing these parameters may give insight into the specific state of the individual and etiology of disease. We applied a relatively fast model optimization scheme based on common local optimization methods to two model formulations of the left ventricle and systemic circulation. One closed-loop model and one open-loop model were applied. Intermittently collected hemodynamic data from an exercise motivation study were used to personalize these models for data from 25 participants. The hemodynamic data were collected for each participant at the start, middle and end of the trial. We constructed two data sets for the participants, both consisting of systolic and diastolic brachial pressure, stroke volume, and left-ventricular outflow tract velocity traces paired with either the finger arterial pressure waveform or the carotid pressure waveform.

Results: We examined the feasibility of separating parameter estimates for the individual from population estimates by assessing the variability of estimates using the interquartile range. We found that the estimated parameter values were similar for the two model formulations, but that the systemic arterial compliance was significantly different ($p < 10^{-6}$) depending on choice of pressure waveform. The estimates of systemic arterial compliance were on average higher when using the finger artery pressure waveform as compared to the carotid waveform.

Conclusions: We found that for the majority of participants, the variability of parameter estimates for a given participant on any measurement day was lower than the variability both across all measurement days combined for one participant, and for the population. This indicates that it is possible to identify individuals from the population, and that we can distinguish different measurement days for the individual participant by parameter values using the presented optimization method.

Keywords: Cardiovascular modeling, Model personalization, Lumped-parameter models, Parameter variability

Background

Cardiovascular disease is a leading cause of loss of quality of life and premature death worldwide [1]. Although much of the pathophysiology is known, cardiovascular disease typically progresses over several years before detectable, and then often severe, symptoms emerge. Furthermore, subsequent prediction of the cardiovascular response and determining the benefits of early intervention remain challenging. Computational modeling has been proposed, by several engineers and researchers, to improve early detection and treatment of cardiovascular disease [2–4]. These models parallel similar applications in engineering. However, one of the main issues in medical applications is the estimation of model parameter values representing an individual patient (model personalization) [4].

Previous research has shown promising results for personalizing cardiovascular models [5–12] or predicting intervention effects in settings of localized cardiovascular disease and critical care [13, 14]. In this work, we investigated the application of such models as a tool for monitoring of the left ventricle and systemic circulation in apparently healthy adults at risk of developing cardiovascular disease. The parameters of hemodynamic models represent mechanical properties of the heart and blood vessels, such as contractility, compliance, and resistance, and their estimation can be seen as low-level phenotyping. Longitudinal monitoring of subtle changes in individual hemodynamics may provide means for early detection of novel risk factors and cardiovascular disease progression, which may otherwise be ignored or undetected. Furthermore, hemodynamic modeling may be used to predict changes to a given stimuli to determine the best course of treatment.

Various approaches for personalizing cardiovascular models have been demonstrated [5–12]. We focused on an approach for improving screening of apparently healthy adults at risk of cardiovascular disease in clinical practice. In this context, we identified three main factors influencing the choice of model and personalization method. First, we considered the cardiovascular physiology of interest which was defined by targeted model outputs such as central blood pressure, ventricular and aortic blood flow. Second, the objective of widespread hemodynamic monitoring limits the feasibility of acquiring detailed anatomical data on vascular networks, and thus, we considered which data may be available in a realistic clinical setting. We focused on models and personalization methods that can be accomplished from widely available non-invasive clinical measurements, such as echocardiography and continuous blood pressure monitoring. Third, we considered model performance in terms of precision, accuracy, and predictive power. A main consideration was that increased model complexity may give a better representation of underlying mechanisms, but requires more data to constrain the additional parameters [3, 15]. Another consideration, of relevance to clinical practice, was the computational complexity and time cost of evaluating more sophisticated models. Indeed, increased model complexity becomes particularly problematic in the personalization process as computational demands for estimation of personalized parameters can increase. Additionally, a more complex model with more personalizable parameters increases uncertainty in model outputs [3]. We investigated two effectively minimal models of the cardiovascular system consisting of lumped parameter representations of the left ventricle and the systemic circulation in a closed- and open-loop,

respectively. In summary, the minimal approach in this work was motivated by the cardiovascular physiology of interest, the limited clinical data, and the long-term goal of enabling personalized predictions in clinical practice without a large additional burden to the patient and healthcare provider.

In this work, we developed a computationally efficient approach to personalize two minimal models based on numerical optimization to adapt the model outputs to measured data. Our approach is presented as a computationally cheaper method compared to more complex global methods. Simultaneously, we used an ensemble of estimates to account for uncertainty in the initial parameter estimates. We evaluated this modeling and personalization approach with available data from 25 individuals, with initially low physical activity levels, participating in a pilot study investigating the effects of physical activity self-monitoring on blood pressure. The participants were given advice on how much physical activity they should aim to engage in over the course of 12 weeks while monitoring their activity by wrist-worn heart rate sensors. Clinical measurements of blood pressure, volume, and flows were acquired at the beginning, middle, and end of the intervention period to detect potentially non-linear parameter changes. This study, similarly to the work of [16], investigates the change of parameters throughout an intervention period, which could give more insight into progression of disease or therapy. However, Audebert et al. focus on a parameter in response to disease progression in rats, while we monitor exercise as hypertension therapy in humans.

Our primary objective was to find personalization methods which could reliably estimate model parameter values specific for each participant and measurement day. Our evaluation of the parameter estimates used the relative variability of individual parameter estimates in comparison to the variation of parameter estimates for all participants. To this end, we express variability as the interquartile parameter range normalized by the median and refer to it as the interquartile range (IQR). Furthermore, we evaluated the consistency in parameter estimates from the closed- and open-loop models and using various pressure waveforms. The model output of primary interest was the central aortic pressure wave for monitoring of medical conditions such as hypertension. In summary, this study investigates the feasibility of using lumped parameter models with different data to detect personalized changes in model parameters after 6 to 12 weeks of exercise.

Method

In this work, we used data on brachial arterial pressure, finger arterial pressure, pulse wave velocity (PWV), and volumetric flow in the left-ventricular outflow tract (LVOT) before and after 6 and 12 weeks of physical activity.

Study design, setting, and participants

Personal Activity Intelligence (PAI) is a personalized and relative metric of exercise frequency, duration, and intensity based on heart rate monitoring and an accumulated score of $\geq$ 100 PAI/week is associated with higher cardiorespiratory fitness and lower cardiovascular mortality [17, 18]. We used data from a pilot randomized controlled trial to assess whether a 12-week intervention with PAI monitors increase physical activity and reduce 24-h ambulatory blood pressure in adults with elevated blood pressure [19].

A secondary aim of the trial was to collect data for computational models describing cardiovascular remodeling of physical activity. The data provided varied opportunities for personalizing models, and this work outlines our approach for model personalization. The trial was approved by Regional Committee on Medical and Health Research Ethics of Norway (Identifier: 2019/1084) and preregistered on clinicaltrials.org (Identifier: NCT 04151537).

Data collection

All hemodynamic measurements were collected at pre- (baseline), mid- (6 weeks), and post-intervention (12 weeks), denoted 1, 2, and 3 as superscripts in the formulations, respectively.

Physical activity monitoring

To assess physical activity level at baseline and during the whole 12-week intervention period, all participants were provided a wrist-worn heart rate monitor without a display (LYNK2). The monitor automatically processed raw heart rate data to an aggregated weekly PAI score. The baseline period lasted one initial week directly before the intervention period. Twenty-six initially inactive participants (< 50 PAI/week based on self-reported physical activity) with elevated blood pressure (systolic $\geq$ 130 mmHg and/or diastolic $\geq$ 80 mmHg) were randomized 1:1 to an active intervention or passive control. Participants in the active intervention were provided with a mobile application for self-monitoring of PAI score and were instructed to obtain and maintain $\geq$ 100 PAI/week. Participants in the passive control were recommended to follow the World Health Organization's physical activity guidelines of 150 min of moderate intensity or 75 min of vigorous intensity activity or any combination thereof per week [20].

Blood pressure recordings

Brachial and finger pressure were measured with non-invasive cuff-based devices. Brachial pressure measurement yielded momentaneous measurements of systolic and diastolic blood pressures, while the finger pressure measurements provided continuous waveforms.

Brachial pressure was recorded in two ways. First, brachial pressure was assessed in the sitting position with an automatic blood pressure monitor (TangoM2, SunTech Medical Inc) at the test station, which is from this point on referred to as office blood pressure. Second, brachial pressure was measured with a 24-h ambulatory blood pressure monitor (Oscar 2 model 250, SunTech Medical Inc), which is abbreviated to ABPM. We used the average systolic and diastolic blood pressure during waking hours in the data analyses.

Finger arterial pressure was measured in the left lateral recumbent position using Finometer PRO (FinaPres) for 4 of the participants and Non-Invasive Blood Pressure Nano (FinaPres) for the remaining participants. We synchronized all finger artery recordings with LVOT flow obtained with echocardiography.

Echocardiography

All participants underwent three full echocardiographic assessments (Vivid E95, VingMed). Velocity flow trace in the LVOT and stroke volume (SV) from the left ventricle were the considered most relevant measurements. Traces of LVOT flow was synchronized with finger pressure for at least three heart cycles. The first cycle was assumed to be less prone to noise and extracted as the sample cycle. We converted the velocity trace as the volumetric flow in units of milliliters per second (mL/s) to be compatible with the model formulation. Stroke volume was computed from 4D measurement of the left ventricle which was automatically segmented to determine SV and averaged over multiple heart cycles using EchoPAC (GE Healthcare). Stroke volume was used to rescale the LVOT flow cycle integral such that the cycle sample corresponded to the volume measured in 4D, which we have assumed to be a more accurate and stable measure of the SV as it was automatically averaged over multiple heart cycles.

Applanation tonometry

Pulse wave velocity was acquired by applanation tonometry (SphygmoCor CvMS v9, AtCor Medica). The PWV was estimated by monitoring the carotid and femoral pressure waves and computing the time of pulse propagation from the ventricle to the two points. Uncalibrated pressure cycles are reported as an image with marker points for each QRS complex. We extracted carotid pressure waveforms from the tonometry traces. The cyclic waveform data points were digitized using WebPlotDigitizer [21]. We used carotid and finger pressure waveform data for our model optimizations as continuous blood pressure data have been shown to give better estimates than using momentaneous measurements using synthetic data [22].

Data preprocessing

The data preprocessing described in this section and the data analyses described in the subsequent sections were executed in Python (Version 3.9).

Finger pressure

Arterial finger pressure was synchronized to the LVOT flow signal to the precision of the closest heart beat for all three aortic flow measurement locations. The flow data were interpolated to match the time points of the pressure recording to ensure the same frequency and enable applying a standard numeric solver to the paired data. The pressure cycle was rescaled to match ambulatory blood pressure to use the finger pressure waveform as a proxy of more central waveforms.

Tonometry traces

The tonometry traces were of varying quality and we assessed all cycles manually before determining which to include in the analyses. The waveforms were assessed visually and discarded if they were obviously distorted, lacked any signs of the dicrotic notch plateau, or did not represent complete heart cycles. The remaining cycles, each representing a heartbeat, were normalized to a uniform scale, averaged, and subsequently scaled to match ambulatory blood pressure. The cycle lengths were averaged to estimate the heart rate, and the final pressure cycle was standardized to this heart rate.

Pressure and flow waveform alignment

None of the collected pressure and flow waveforms were collected at the same sampling rate which was required by the chosen estimation algorithm. Matching time points ensures equal weighting of the two waveform signals due to number of contributing residuals in an optimization context. When pairing flow and the finger pressure signals, the heart cycle was determined by identifying the distance between start of upstroke for the first flow cycle and to the next start of upstroke. These time points were then used to extract a corresponding pressure cycle from the continuous pressure recording. The flow signal was linearly interpolated to match the time points of the finger pressure. For the carotid waveforms, the data with the largest mean interpoint distance in time had their measurement points rearranged to be evenly distributed over the corresponding heart cycle. Afterwards, both pressure and flow signals were interpolated to the new uniformly distanced time points. The number of total data points for the flow and carotid pressure waveforms were often comparable and therefore the number of total discretized points were not changed considerably in most cases due to interpolation. All pressure measurements were linearly rescaled so that the maximum and minimum of the waveform matched the ambulatory blood pressure systolic and diastolic values. However, in a single set of measurements the ambulatory blood pressure was missing and office blood pressure was used instead.

In both cases, the flow cycle length in time was rescaled to have the same heart rate as the pressure sample, and to have the same SV as recorded in 4D echocardiography mode. In cases where 4D SV were missing, we used the SV calculated by EchoPac from the LVOT flow. All pressure and flow cycles were aligned to start at systolic upstroke.

Models

In this work, we applied two models of the left ventricle and systemic circulation. One closed-loop model in which the venous pressure and volume was estimated as a model prediction and one open-loop model which assumed fixed venous pressure and left atrial pressure. The parameters chosen for personalization in our models are shown in Table 1.

Closed-loop model

The simplified closed-loop model used for personalization has been presented by Bjørdalsbakke et al. [22], and is based on similar models by Segers, Smith and Stergiopulos et al. [2, 23–26]. An illustration of our version of the model is provided in Fig. 1.

The closed-loop model is described by a system of differential equations characterizing the behavior of the stressed volumes of the ventricle, arteries, and veins. All flows were computed as the pressure gradient across resistances between the model compartments. Each separate compartment was modeled using a linear relationship between pressure and volume. See "Model equations" section for the full mathematical model description.

Open-loop model

The open-loop model formulation is identical to the closed-loop model, except that the venous compartment is removed. This means the venous compliance parameter

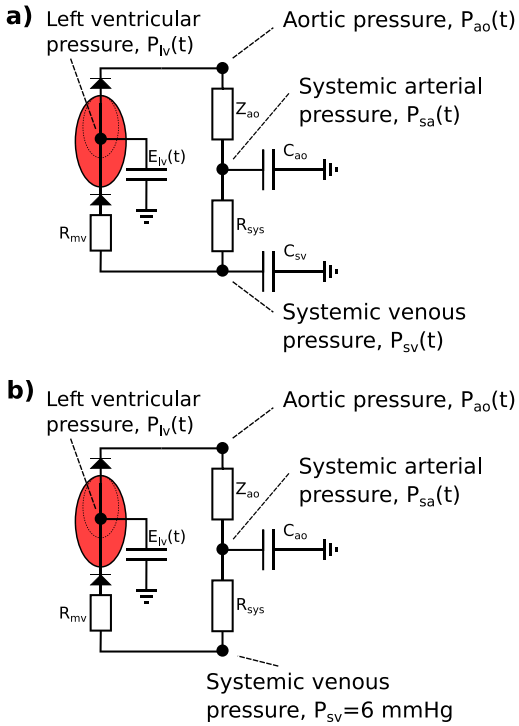

Fig. 1 **a** The closed-loop, lumped parameter model of the left ventricle, systemic arteries, and veins. **b** The open-loop lumped parameter model of the left ventricle and systemic arteries. The circuit equivalent formulation of the models are depicted with the pressures and most of the mechanical parameters used to describe the systemic circulation. The venous compartment is volumeless and only partially described in the open-loop model. Adapted from Bjørdalsbakke et al. [22], and used under CC-BY 4.0

is replaced by a fixed venous pressure value, which in turn means that the total stressed blood volume parameter fluctuates. The model is identical to the one used by Stergiopulos et al. [24], but we set the constant venous pressure to $P_{sv} = 6.0$ mmHg, which is a value within the range of a normal central venous pressure (CVP) [27, 28]. See Fig. 1 for an illustration of the model. Additional details of the mathematical description can be found in "Model equations" section.

Model output

The model outputs such as pressure and flow are denoted as $y(t, \boldsymbol{\theta})$ to emphasize that each output varies with time t and the parameter vector $\boldsymbol{\theta}$. From these model predictions, estimates of clinical measurements can be derived. The model predictions were computed numerically using SciPy's implementation of the 4th-order Runge–Kutta (RK4) method to integrate the differential equations [29]. The model was solved for 10 heart cycles, and the tenth cycle was taken as the model prediction.

Table 1 The closed-loop model parameters are listed with their corresponding symbols and units. The same parameters are used to describe the open-loop model except for C_{sv} and V_{tot}

Symbol	Description	Unit
C_{ao}	Systemic arterial compliance	$\frac{\text{mL}}{\text{mmHg}}$
C_{sv}	Systemic venous compliance	$\frac{\text{mL}}{\text{mmHg}}$
E_{max}	Maximal left ventricular elastance	$\frac{\text{mmHg}}{\text{mL}}$
E_{min}	Minimal left ventricular elastance	$\frac{\text{mmHg}}{\text{mL}}$
R_{mv}	Mitral valve resistance	$\frac{\text{mmHg s}}{\text{mL}}$
R_{sys}	Total peripheral resistance	$\frac{\text{mmHg s}}{\text{mL}}$
T	Heart period	s
t_{peak}	Time of peak ventricular elastance	s
V_{tot}	Total stressed blood volume	mL
Z_{ao}	Characteristic impedance of the aorta	$\frac{\text{mmHg s}}{\text{mL}}$

Parameter estimation

The inference method for the parameters was based on a local optimization method, similar to the work outlined in [22]. We preferred a local optimization method as it is most feasible to apply to routine screening in clinical practice as global methods often demand higher computational costs. The SciPy implementation of the Trust-Region Reflective Algorithm (TRRA) was chosen as it supports the use of bounds for different parameters [29], which can constrain the parameter space to more physiologically realistic parameters.

Both models take a vector of parameters $\boldsymbol{\theta}$ and generate outputs $y(t_k, \boldsymbol{\theta})$ at time point k. A real measurement at the same time point can be described as being composed by this model output and other terms of the form

$$y_k^m = y(t_k, \boldsymbol{\theta}) + E_k, \tag{1}$$

where E_k is a measurement error or noise. However, to infer the parameters which reproduce a measured set of data, a problem on the form

$$\hat{\boldsymbol{\theta}} = \arg\min J(\boldsymbol{\theta}) \tag{2}$$

must be solved. Here, J is a cost function which characterizes the optimization problem. In this work, we focused on non-linear least squares optimization.

The TRRA is dependent upon a set of initial parameter guesses $\boldsymbol{\theta}$ where the ith component of the vector is θ_i. We found personalized parameter estimation by applying the TRRA in a five-step procedure. In short, the procedure can be described as follows:

1 Use the TRRA to make 30 parameter estimates from 30 different sets of initial guesses.
2 Take the initial parameter guess which yields the lowest cost function value estimate and create a new uniform distribution centered on these parameter values.
3 Make 20 new initial guesses based on the best previous guess and produce 20 new sets of estimates, we call this set of parameters $\boldsymbol{\Theta}_{\text{step2}}$.

4 Make a selection based on the best cost function values from Step 3, $\boldsymbol{\Theta}^{p,d,k}_{\text{filtered}}$, where k denotes the kth filtered estimate, and p refers to participant, while d represents pre-, mid-, and post-intervention measurement days encoded as 1, 2, and 3.
5 Compute the final parameter estimate as the mean of the estimates from Step 3, such that $\hat{\theta}^{p,d}_{\text{mean},i} = \frac{1}{N_k}\sum_k \Theta^{p,d,k}_{\text{filtered},i}$. N_k is the number of remaining estimated parameter vectors in $\boldsymbol{\Theta}^{p,d}_{\text{filtered}}$ after filtering.

To find the best parameter estimates, guesses for each component of the parameter vector were sampled from a uniform distribution with a lower bound $\theta_{\text{lower},i}$ and upper bound $\theta_{\text{upper},i}$. Consequently, we sampled the initial parameter guesses in Step 1 as

$$\theta_i = U(\theta_{\text{lower},i}, \theta_{\text{upper},i}), \tag{3}$$

where $U(a, b)$ is a continuous uniform distribution, with upper and lower bound a and b. Thirty sets of initial parameters sets were sampled and used to optimize the cost function $J(\boldsymbol{\theta})$. In Step 2, the initial parameter guess resulting in the optimization with the smallest cost function value was taken as a new reference set $\boldsymbol{\theta}_{\min}$ to sample 20 more guesses, in Step 3, from a uniform distribution with limits 10% below and above the components of the reference parameter set as in

$$\theta_i = U(0.9\theta_{\min,i}, 1.1\theta_{\min,i}). \tag{4}$$

This procedure resulted in multiple sets of estimated parameters $\hat{\boldsymbol{\theta}}$ which in Step 4 were filtered by only accepting the results with a cost function value smaller than or equal to the mean value of the 20 optimized parameter sets from Step 3. Lastly, in Step 5, the mean of the selected parameter sets were taken as the final parameter estimate for participant p on measurement day d, $\hat{\boldsymbol{\theta}}^{p,d}_{\text{mean}}$.

The cost function was designed to adapt the model to the pressure and flow waveforms, SV, and ambulatory blood pressure. If we let P^m_k denote the measured pressure and $P_{\text{ao,k}}$ denotes the model output aortic pressure at time point k, while Q^m_k and Q_k denote the aortic flow, then the cost function can be expressed as

$$\begin{aligned} J(\boldsymbol{\theta}) \quad &= \sum_i^N \left(\frac{P^m_i - P_{\text{ao},i}}{K_{\text{p}}}\right)^2 + \sum_i^N \left(\frac{Q^m_{\text{ao},i} - Q_{\text{ao},i}}{K_{\text{q}}}\right)^2 \\ &+ \frac{7.5^2N^2}{40^2}\left[\left(\frac{P^m_{\text{sys}} - P_{\text{sys}}}{K_{\text{p,sys}}}\right)^2 + \left(\frac{P^m_{\text{dia}} - P_{\text{dia}}}{K_{\text{p,dia}}}\right)^2\right] \\ &+ \frac{7.5^2N^2}{40^2}\left[\left(\frac{\text{SV}^m - \text{SV}}{K_{\text{SV}}}\right)^2 + \frac{1}{9}\left(\frac{6.0 - \text{MVP}}{K_{\text{MVP}}}\right)^2\right]. \end{aligned} \tag{5}$$

Here, N is the number of time points in the waveform sample, P_{sys} and P_{dia} are the systolic and diastolic values of the pressure waveform, SV^m is the SV corresponding to the area under the flow waveform, and the m superscript denotes a real measurement. SV as determined by the model is the SV calculated as the maximal change of volume in the left ventricle throughout the final heart cycle. The final term constrained the mean venous pressure (MVP) computed by the model to approximately 6 mmHg, which is a value within the range of a normal central venous pressure (CVP) [27, 28]. The model only models the P_{sv} which is the averaged pressure of all veins and is not actually tied to a vein in particular. We calculate the mean value of the pulsatile P_{sv} signal to create

the mean venous pressure indice MVP. We thereafter approximate the MVP indice to be equal to the CVP as this influences ventricular filling, and the is the model concept most closely related to CVP. All constants K are scaling constants with a magnitude similar to a reference level for the different measurement types. For further details, settings, and bounds for the optimization routine, see Optimization algorithm details. The cost function was identical for both models, except for the final venous pressure term, which was not applicable to the open-loop model. The weights $\frac{7.5^2N^2}{40^2}$ and $\frac{2.5^2N^2}{40^2}$ were manually tuned to assign more weight to the pressure extrema values and clinical indices as these are particularly important in clinical settings, and perhaps also more likely to express cardiovascular remodeling. The number 40 was chosen as a reference scale since the number of data points in the carotid waveform and LVOT flow signals were usually close to this number before interpolation.

Previous optimization of parameters for the closed-loop model using aortic pressure and flow shows that $E_{\text{min}}, R_{\text{mv}}$ and Z_{ao} are among the most challenging parameters to estimate in synthetic data produced by the model itself with Gaussian noise [22]. These three parameters were found to be least sensitive to aortic pressure when applying a sensitivity analysis to the model. In the parameter optimization routine used, these parameters were therefore not prioritized for attempted personalization. The remaining parameters in Table 1 were chosen for estimation, except for T which was estimated directly from the waveform cycle lengths. Despite the low sensitivity value, Z_{ao} was included for optimization since initial attempts at optimizing the model to real data indicated that this improved the model's ability to recreate the pressure waveform during systole. For the open-loop model, the same parameters were personalized as for the closed-loop model, except for V_{tot} and C_{sv}. The mitral valve resistance was fixed to be $R_{mv} = 0.02\frac{\text{mmHg s}}{\text{mL}}$. E_{min} was fixed to 0.055 or 0.06 depending on whether or not the systolic pressure was below 140 mmHg, see Optimization algorithm details for further details.

All model output waveforms incorporated in the cost function were aligned with pressure and flow data by enforcing that the model outputs always started at beginning of systole. No single parameter determines the start of systole in the model, so this was done by translating the waveforms in time until they started at the correct value.

Post-processing of parameter estimates

All computed parameters were normalized by body surface area (BSA) computed as

$$\text{BSA} = \sqrt{\frac{\text{Height} \cdot \text{Weight}}{3600}}. \tag{6}$$

All participants had height and weight measured at pre-intervention, while weight was also measured at mid- and post-intervention and BSA updated accordingly. All parameter estimates, except for t_{peak}, have been BSA indexed as a normalization to account for variations in body size for parameters, which may be assumed to be body size dependent.

Due to noisy or missing data or missing synchronization data, we could not compute parameters for all study participants. Thus, we defined two data sets, both included the LVOT flow trace converted to volumetric flow, the ambulatory blood pressure values and stroke volume. The first data set included the finger pressure waveform scaled by ambulatory blood pressure and synchronized with the LVOT flow cycle, while the second data set included the averaged carotid pressure waveform scaled by ambulatory blood pressure paired with the LVOT flow cycle.

The data sets based on finger pressure had 50 eligible measurements across all participants and measurement days, while the carotid pressure had eligible 62 measurements. For finger pressure, 9 participants could be identified at all three measurement days, whereas 14 participants were identified for carotid pressure. Seven of these participants had eligible measurements for both pressures. The total number of unique study participants in the data set was 25 when counting all data sets where all three measurement days were not present. For all eligible participants, and for both models, we estimated $E_{\max}$, R_{sys}, C_{ao}, t_{peak}, Z_{ao}. For the closed-loop model, C_{sv} and V_{tot} were also estimated.

The variability within estimates for each individual participant and the population as a whole were assessed by computing the interquartile range and dividing by the median value. In this manuscript, we refer to this as the interquartile ratio (IQR):

$$\text{IQR} = \frac{\theta_{i,75\%} - \theta_{i,25\%}}{\hat{\theta}_{i,\text{median}}}, \tag{7}$$

where the 25% and 75% subscripts refer to the corresponding percentiles. The means for the parameters over all participants and all measurement days were computed to also assess if there were differences in estimates between model formulations and pressure waveforms.

We used IQR to assess estimate variability in three different contexts. First, we investigated the variability in estimates for single participants on any measurement day, for which we calculated the IQR based on the set of estimates $\boldsymbol{\Theta}_{\text{filtered}}$ yielded from a single set of raw data, i.e., a given participant on a given measurement day. The median IQR for these estimates was found, and the first and third quartiles were interpreted as a measure of variability in the IQR for each participant on any measurement day. We computed the IQR for all eligible participants whether they had 1, 2 or 3 available measurement days. We refer to this as the "Single day IQR".

Second, the variation across an individual over all measurement days d was assessed for each individual p. The three estimated sets $\boldsymbol{\Theta}_{\text{filtered}}$ resulting in parameter estimates $\hat{\boldsymbol{\theta}}^{p,1}_{\text{mean}}$, $\hat{\boldsymbol{\theta}}^{p,2}_{\text{mean}}$, and $\hat{\boldsymbol{\theta}}^{p,3}_{\text{mean}}$ for each participant p were combined to make one common set of parameters $\boldsymbol{\Theta}^{p}_{\text{all days}}$ containing the best optimized parameter estimates across all measurement days for each individual. Only participants whose parameters could be estimated for all 3 days were included. For each participant, the IQR was computed based on the set $\boldsymbol{\Theta}^{p}_{\text{all days}}$, and afterwards the median IQR and first and third quartiles were determined. We named this quantity the "Multiple day IQR".

Third, we computed the final parameter estimates $\hat{\boldsymbol{\theta}}^{p,d}_{\text{mean}}$ for all participants on all measurements days and subsequently collected these in a set for which we computed the IQR value. This IQR value was interpreted as the variability in parameters across the

population and across all measurement days. All participants were included, and this IQR measure is referred to as the "Population IQR". This quantity is not presented with standard deviations as it is a single value characterizing the study population. All three IQR analyses were repeated for both models and the data sets with pressure waveform measured in either the carotid artery or finger artery.

Other methods for estimating model parameters

The arterial parameter estimates from the personalization could be compared to estimates made with more traditional methods to estimate these. Arterial compliance can be estimated by

$$\tilde{C}_{\mathrm{ao}} \approx \frac{\mathrm{SV}^{\mathrm{m}}}{\mathrm{PP}^{\mathrm{m}}}, \tag{8}$$

where PP is the brachial artery pulse pressure as a proxy for more central pressure. Similarly, the vascular resistance can be estimated by

$$\tilde{R}_{sys} \approx \frac{\mathrm{MAP}^{\mathrm{m}}}{\mathrm{CO}^{\mathrm{m}}}, \tag{9}$$

where CO is cardiac output and MAP is mean arterial pressure calculated as the mean of the pressure waveform scaled with brachial pressure.

Quality of waveform optimizations

To assess whether the estimated model parameters could recreate the waveforms and, especially, the other indices included in the cost function accurately, we examined the unscaled residuals between model predictions and data. Instead of listing each residual for every participant and measurement day, we assessed the mean absolute value of residuals on each measurement day for both data sets and model formulations separately. The model outputs used to compute the residuals are the outputs based on the final parameter set based on the averaged parameters from the best optimization sets, $\hat{\theta}^{p,d}_{\mathrm{mean},i}$.

Summary

From a pilot randomized controlled trial on self-monitoring of physical activity, blood pressure and echocardiography data for initially inactive adults were available. We implemented a closed- and open-loop model of the left ventricle and systemic circulation in Python, and optimized these using local methods to paired data of pressure and flow waveforms, including SV. Pressure waveforms collected by non-invasive finger pressure measurement and carotid applanation tonometry were paired with aortic flow data and applied to parameter estimations for the trial participants. We computed the variability in estimates for each individual and the population as whole using our definition of the IQR and assessed how well the parameters of participants and possible parameter changes could be resolved from the population.

Results

The results in this section are based on analysis of parameter estimates for individuals over multiple measurement days (model personalization). We computed estimates for both a closed- and an open-loop model, but added an additional dimension in doing so for two different data sets including either the carotid or finger pressure waveforms.

Parameter estimate variability in individuals compared to the population

The IQR as defined by equation (7) was calculated for the variation in estimates for the population given either the finger pressure or carotid pressure waveform. Similarly, the IQR scores for all individuals across all measurement days were expressed by the median IQR and variation presented as the first and third quartiles. The IQR values were calculated for both the closed- and open-loop models and the results are shown in Figs. 2 and 3, respectively. Figures 2–5 display the IQR for several model parameters and outputs. The IQR is unitless, but otherwise the units used are the same as in Table 1 for model parameters, only BSA indexed, and hence divided by m^2 unless otherwise noted. Only t_{peak} is not BSA indexed.

The IQR was computed for different model outputs which are shown in Figs. 4, 5, for the closed- and open-loop models, respectively. All pressures P_{sys}, P_{dia}, PP (pulse

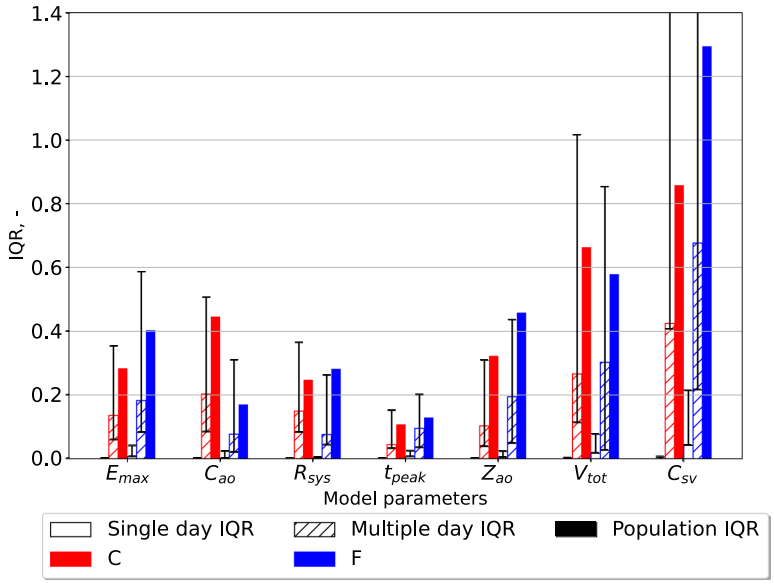

Fig. 2 The interquartile ratio (IQR) computed for the parameters of the closed-loop model. The "Single day IQR" which is based on the median IQR values for the estimates for single individuals on any measurement day are included. The whiskers indicate first and third quartiles. The variation in individuals over all measurement days are displayed as "Multiple day IQR". The final parameter estimates for all individuals in the different data sets yield the "Population IQR". "F" indicates the data set with finger pressure waveform, and "C" indicates the data set with the carotid pressure waveform. The IQR refers to the difference between the upper and lower quartiles divided by the mean parameter value. E_{max} is the maximal left-ventricular elastance, C_{ao} is the systemic arterial compliance, R_{sys} is the total peripheral resistance, t_{peak} is the time of maximal ventricular elastance, Z_{ao} is the characteristic aortic impedance, V_{tot} is the total stressed blood volume, and C_{sv} is the systemic venous compliance

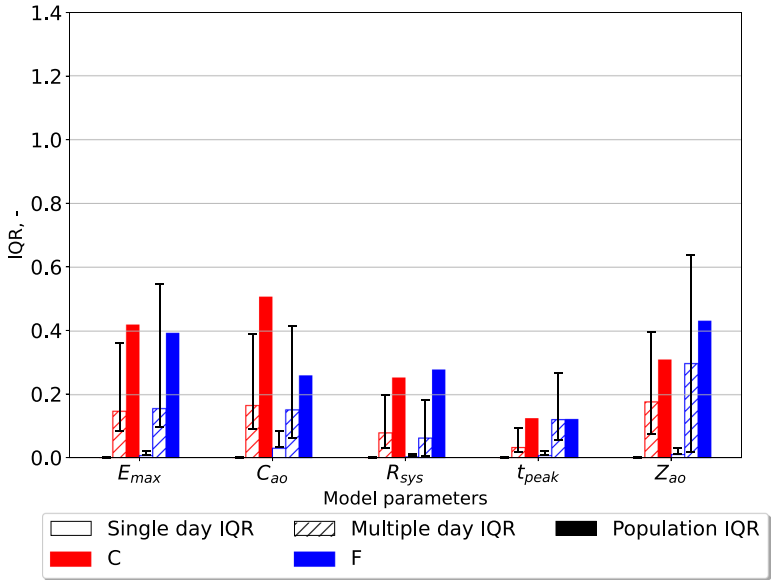

Fig. 3 The interquartile ratio (IQR) computed for the parameters of the open-loop model. The "Single day IQR" which is based on the median IQR values for the estimates for single individuals on any measurement day are included. The whiskers indicate first and third quartiles. The variation in individual participants over all measurement days are displayed as "Multiple day IQR". Final parameter estimates for all individuals in the different data sets yield the "Population IQR". "F" indicates the data set with finger pressure waveform, and "C" indicates the data set with the carotid pressure waveform. The IQR refers to the difference between the upper and lower quartiles divided by the mean parameter value. $E_{\max}$ is the maximal left-ventricular elastance, C_{ao} is the systemic arterial compliance, R_{sys} is the total peripheral resistance, t_{peak} is the time of maximal ventricular elastance, and Z_{ao} is the characteristic aortic impedance

pressure), MAP (mean arterial pressure) and MVP (mean venous pressure) are measured in units of mmHg. Stroke volume SV is given in mL, while stroke work SW is expressed in mmHg·mL.

Parameter estimates compared between different data sources

The mean parameter values scaled by BSA were compared for the different pressure waveforms (finger and carotid) and for the closed- and open-loop models. The results are displayed as mean values with standard deviations in Fig. 6. There are minor differences between the estimate averages, especially between model formulations. The open-loop models have on average a marginally lower $E_{\max}$ than the closed-loop model. The estimate differences are larger between the different waveforms, where for example the C_{ao} estimates are on average higher for the finger pressure waveform than the carotid pressure waveform.

Figure 6 contains the results from the complete case analysis of both models and pressure waveforms. We also picked the 47 paired samples where both pressure waveforms were available for the same participant and compared the means in Table 2. The function ttest() from the Pingouin Python library version 0.5.1 was used to perform a paired sample t-test and compute the mean difference and 95% confidence interval between

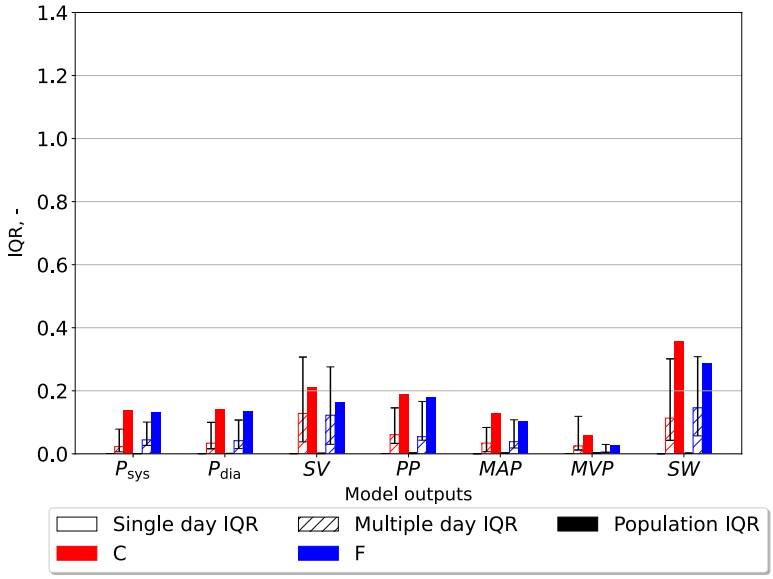

Fig. 4 The interquartile ratio (IQR) computed for model outputs generated by the closed-loop models, each model instance optimized for one individual. The "Single day IQR" is based on the median IQR values for the model outputs from the variation in parameter estimates for single individuals on any measurement day. The whiskers indicate first and third quartiles. The variation in the best optimized sets of model outputs from individuals over all measurement days are displayed as "Multiple day IQR". The model outputs based on the final parameter estimates for all individuals in the different data sets yield the "Population IQR". "F" indicates the data set with finger pressure waveform, and "C" indicates the data set with the carotid pressure waveform. The IQR refers to the difference between the upper and lower quartiles divided by the mean parameter value. P_{sys} is the systolic aortic pressure, P_{dia} is the diastolic aortic pressure, SV is the stroke volume indexed by body surface, PP is the aortic pulse pressure, MAP is the mean arterial pressure, MVP is the mean venous pressure, and SW is the left-ventricular stroke work

finger and carotid pressure [30]. The difference between sample means was found to be statistically significant for both models, see Table 2. The paired sample differences for arterial compliance C_{ao} were computed and the 5th, 25th, 50th, 75th and 95th percentiles were presented to give an indication of the distribution of differences not being extremely asymmetrical. For the closed-loop model these percentiles were −0.005, 0.233, 0.430, 0.575, and 0.771, respectively, while for the open-loop model they were 0.035, 0.186, 0.380, 0.538, and 0.709 in units mL / (mmHg·m^2). The paired samples mean C_{ao} estimates were 1.275 and 0.876 for the closed-loop model with the finger pressure waveforms and carotid pressure waveforms, respectively. Similarly, for the open-loop model the finger pressure-based sample mean was 1.221, while the carotid pressure-based sample mean was 0.860. Paired t-tests for other parameters can be seen in the supplementary materials.

Comparison of arterial parameter estimates to other estimation methods

To assess the credibility of arterial parameter estimates, we compared model estimates to more conventional estimation techniques for C_{ao} and R_{sys} as expressed by equations

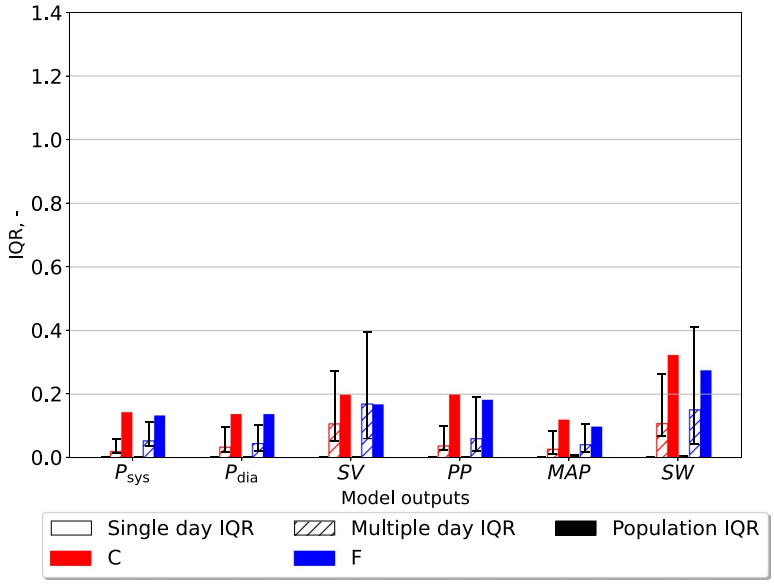

Fig. 5 The interquartile ratio (IQR) computed for model outputs generated by the open-loop models, each model instance optimized for one individual. The "Single day IQR" is based on the median IQR values for the model outputs from the variation in parameter estimates for single individuals on any measurement day. The whiskers indicate upper and lower quartiles. The variation in the best optimized sets of model outputs from individuals over all measurement days are displayed as "Multiple day IQR". The model outputs based on the final parameter estimates for all individuals in the different data sets are used to compute bars labeled as the "Population IQR". "F" indicates the data set with finger pressure waveform, and "C" indicates the data set with the carotid pressure waveform. The IQR refers to the difference between the upper and lower quartiles divided by the mean parameter value. P_{sys} is the systolic aortic pressure, P_{dia} is the diastolic aortic pressure, SV is the stroke volume indexed by body surface, PP is the aortic pulse pressure, MAP is the mean arterial pressure, and SW is the left-ventricular stroke work

(8) and (9), respectively. Figs. 7–8 show the results for the parameter comparisons in scatter plots for the closed- and open-loop models, respectively. The Pearson correlation coefficient (r) was calculated for all comparisons as shown in Table 3. The correlation coefficient and confidence intervals were found by the corr() function in the Pingouin Python library. Estimates for R_{sys} had a high degree of correlation to the other estimation method, while C_{ao} showed a moderate amount of correlation. While both models yielded similar results, the measurement location for the pressure waveform does affect the results for C_{ao} reducing the correlation.

Quality of optimization results

Closed-loop model

The quality of model optimization was assessed by the unweighted percentage errors of the measurements in the cost function (equation (5)). The results are shown in Table 4, for estimates based on the carotid and finger pressure waveforms for all measurement days separately and collectively. The upper and lower quartiles for the percentage errors along the data points of the pressure and flow waveforms were computed, and the median values for these quartiles across all participants at different choices of

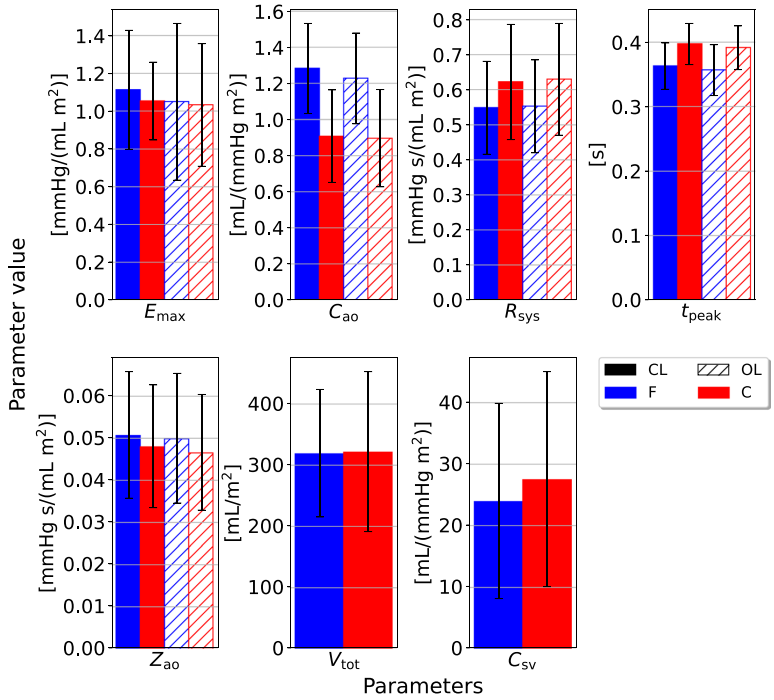

Fig. 6 The mean parameter estimates, and standard deviations, for all individuals in the different data sets. These results originate from estimates made for the closed-loop ("CL") and open-loop ("OL") models, respectively. "F" indicates the finger pressure waveform, and "C" indicates the data set with the carotid pressure waveform. The y-axis represents model parameters and units listed in Table 1 as BSA indexed values, with the exception of t_{peak} which is given in units seconds, s. E_{max} is the maximal left-ventricular elastance, C_{ao} is the systemic arterial compliance, R_{sys} is the total peripheral resistance, t_{peak} is the time of maximal ventricular elastance, Z_{ao} is the characteristic aortic impedance, V_{tot} is the total stressed blood volume, and C_{sv} is the systemic venous compliance

measurement days are given in the table. Typical examples of the quality of waveform fits can be found in Figs. 9 and 10. The worst optimized samples according to cost function value can be found in Figs. 11 and 12.

Open-loop model

The quality of model optimization were assessed by the unweighted residuals of the clinical indices in the cost function (equation [5)] in Table 5, for estimates based on the carotid and finger pressure waveforms for all measurement days separately and collectively. Waveform percentage error quartiles and their median value across all participants are given in the table, equivalently as for the closed-loop model. Typical examples of the quality of waveform fits can be found in Figs. 13 and 14. The worst optimized samples according to cost function value can be found in Figs. 15 and 16.

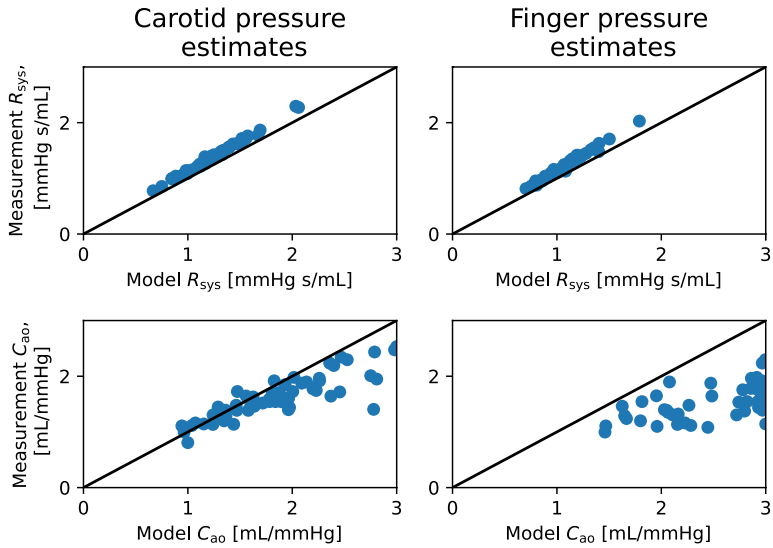

Fig. 7 The scatter plots of closed-loop model parameter estimates for total peripheral resistance R_{sys} (top panels) and arterial compliance C_{ao} (bottom panels), compared to estimates from conventional methods, using the data sets with the carotid (left panels) and the finger pressure (right panels) waveforms. Model estimates are on the x-axes, while conventional estimates are on the y-axes

Table 2 Mean arterial compliance C_{ao} parameter values averaged over different samples of measurements for both model formulations and choice of data set. The *p*-value and 95% confidence interval (CI 95%) are obtained by a two-tailed t-test for paired data comparing the mean parameter values using the finger and carotid pressure waveforms, respectively, within the same model

Model	Samples	Mean C_{ao} w/ finger pressure [mL/(mmHg·m^2)]	Mean C_{ao} w/ carotid pressure [mL/(mmHg·m^2)]	95% CI for mean difference [mL/(mmHg·m^2)]	*p*-value
Closed-loop	Mixed	1.28	0.91	–	–
Closed-loop	Paired	1.28	0.88	[0.33, 0.47]	$p < 1.0e-14$
Open-loop	Mixed	1.23	0.90	–	–
Open-loop	Paired	1.22	0.86	[0.29, 0.43]	$p < 1.0e-13$

Discussion

The variation in parameter estimates for individuals were consistently smaller than the variability in the same parameters for the whole study population, as shown in Figs. 2 and 3. Consequently, this study shows that it is possible to estimate the model parameters for individuals and separate them from parameters of other individuals in the population for the presented estimation heuristic.

The estimates for C_{sv}, and V_{tot} were subject to the most variability in the population regardless of using the pressure waveform from the carotid or finger artery for the closed-loop model. However, for the open-loop model E_{max}, C_{ao}, and Z_{ao} were the most

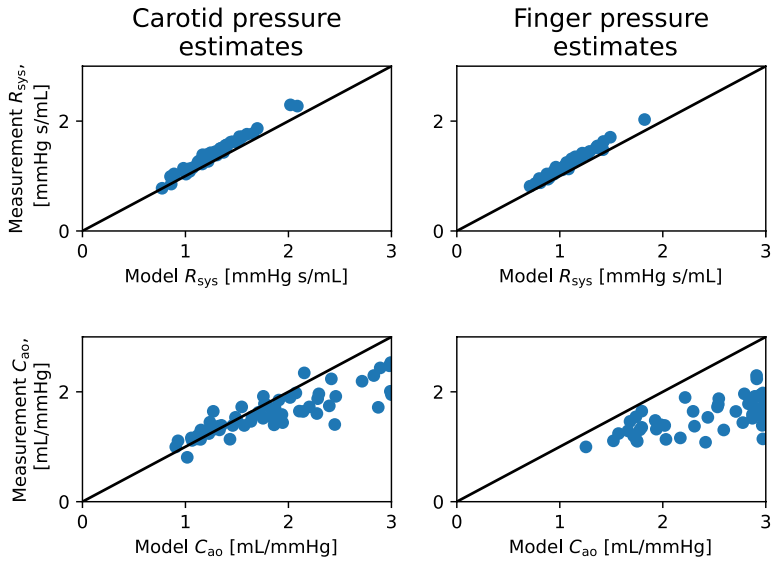

Fig. 8 The scatter plots of open-loop model parameter estimates for total peripheral resistance R_{sys} (top panels) and arterial compliance C_{ao} (bottom panels), compared to estimates from conventional methods, using the data sets with the carotid (left panels) and the finger pressure (right panels) waveforms. Model estimates are on the x-axes, while conventional estimates are on the y-axes

Table 3 Correlation coefficients for parameters estimated by the local optimization approach compared to estimates from more conventional methods. Hence, the correlations are found between C_{ao} and $\tilde{C}_{ao}$ for arterial compliance, while R_{sys} versus $\tilde{R}_{sys}$ yield the correlation for peripheral resistance. The *p*-value and 95% confidence interval (95% CI) was obtained by a two-tailed t-test

Parameter	Model	Pressure waveform	Correlation coefficient, *r*	p-value	95% CI
R_{sys}	Closed-loop	Finger	0.990	$p < 1.0e-41$	[0.98, 0.99]
R_{sys}	Closed-loop	Carotid	0.994	$p < 1.0e-59$	[0.99, 1.00]
R_{sys}	Open-loop	Finger	0.987	$p < 1.0e-39$	[0.98, 0.99]
R_{sys}	Open-loop	Carotid	0.988	$p < 1.0e-50$	[0.98, 0.99]
C_{ao}	Closed-loop	Finger	0.601	$p < 1.0e-5$	[0.39, 0.75]
C_{ao}	Closed-loop	Carotid	0.864	$p < 1.0e-18$	[0.78, 0.92]
C_{ao}	Open-loop	Finger	0.647	$p < 1.0e-6$	[0.45, 0.78]
C_{ao}	Open-loop	Carotid	0.852	$p < 1.0e-17$	[0.76,0.91]

The scatter plots of these variables can be seen in Figs. 7 and 8

variable parameters, but the variability was similar in all three parameters. This study indicates that the estimates using the carotid pressure waveform are more or equally stable for the individual than using the finger pressure waveform, as seen in Figs. 2 and 3. This same pattern is not as apparent in the open-loop model, which may be due to either the parameter space having fewer dimensions or the altered model structure itself. Figures 4 and 5 show that the estimates for the individual had low variation, which was far smaller compared to the population IQR. This suggests that high variability in some model parameters, such as venous compliance, does not affect model outputs

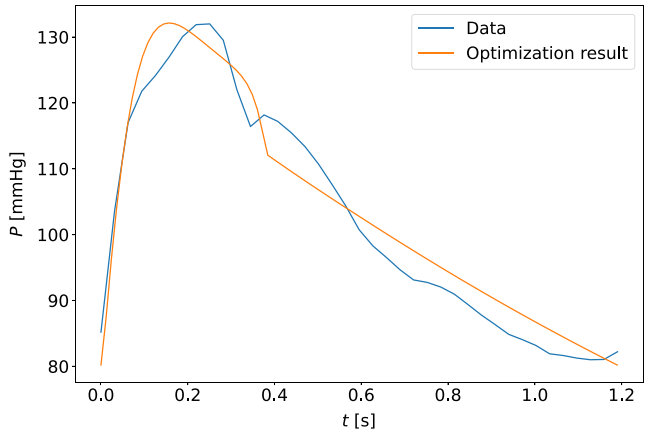

Fig. 9 The model-optimized pressure curve based on the mean of the best parameter estimates for the individual is shown with the raw data to which it is optimized for a participant. The model predictions are based on the final averaged parameter estimate for each participant. This is an example of a typical waveform fit for the closed-loop model and the carotid pressure waveform

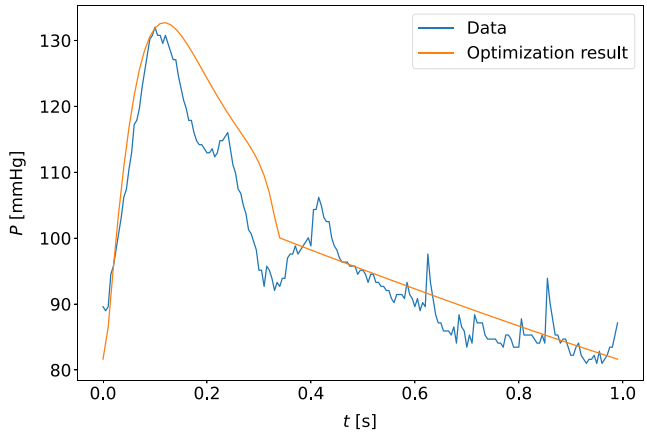

Fig. 10 The model-optimized pressure curve based on the mean of the best parameter estimates for the individual is shown with the raw data to which it is optimized for a participant. This is an example of a typical waveform fit for the closed-loop model and the finger pressure waveform

substantially. IQRs calculated for the closed-loop model using carotid pressure exhibits very little variability for the individual, indicating that in a majority of cases there is a well-defined local or global minimum which the optimization algorithm chooses. For the same results using finger pressure, there is a higher level of variability, which indicates that a single minimum is harder to obtain in this case.

Examination of results presented in Figs. 2 and 3 shows that the majority of multiple day IQRs were smaller than the population IQR. The only case this was not true was for t_{peak} in the open-loop model using the finger pressure waveform. This parameter is heart rate dependent which changes from beat-to-beat, hence it is not surprising that this

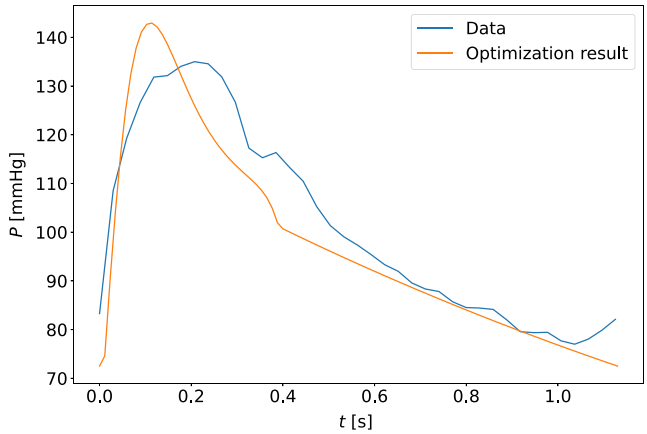

Fig. 11 The model-optimized pressure curve based on the mean of the best parameter estimates for the individual is shown with the raw data to which it is optimized for a participant. The sample shown is for the measurement sample with the highest cost function value when compared to other participants and measurement days. This is a waveform adapted to the closed-loop model with the carotid pressure waveform

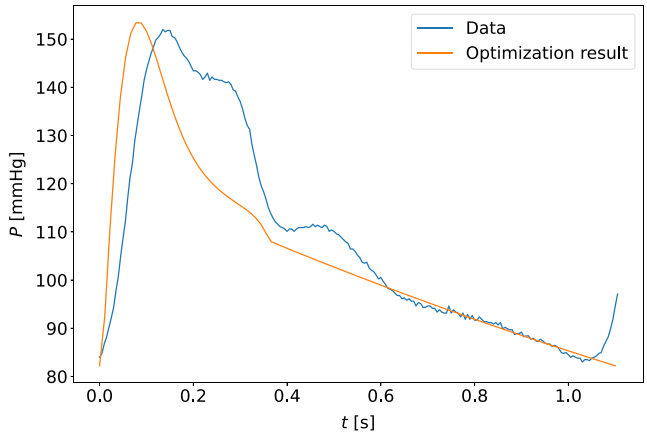

Fig. 12 The model-optimized pressure curve based on the mean of the best parameter estimates for the individual is shown with the raw data to which it is optimized for a participant. The sample shown is for the measurement sample with the highest cost function value when compared to other participants and measurement days. This is a waveform adapted to the closed-loop model with the finger pressure waveform

parameter could experience variation over all measurement days similar to the population IQR. The t_{peak} is related to the heart rate of the signal as the length of systole varies with heart rate. Although measurements were performed in a state of rest, it is not guaranteed that everyone had reached their true resting heart rate on each measurement day. For the other parameters, we saw that due to the variability in the multiple-day IQR the standard deviations show that this variability will grow beyond the value of the population IQR for some participants. This means that we potentially could calculate rather large changes from one measurement day to the next. Whether this is realistic remains

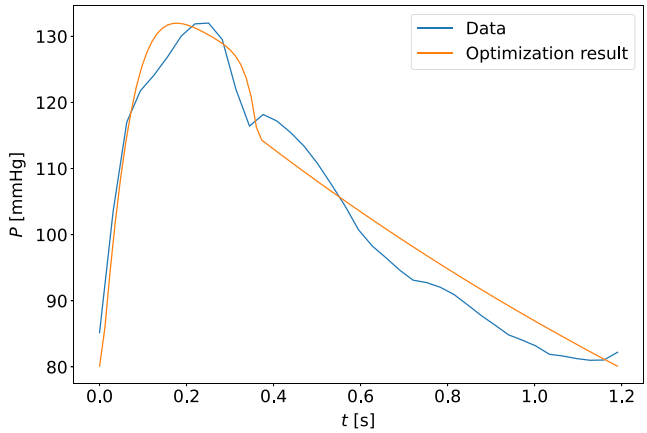

Fig. 13 The model-optimized pressure curve based on the mean of the best parameter estimates for the individual is shown with the raw data to which it is optimized for a participant. This is an example of a typical waveform fit for the open-loop model and the carotid pressure waveform

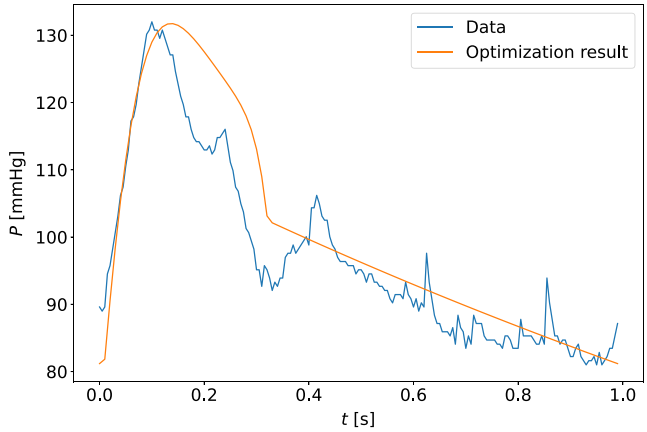

Fig. 14 The model-optimized pressure curve based on the mean of the best parameter estimates for the individual is shown with the raw data to which it is optimized for a participant. This is an example of a typical waveform fit for the open-loop model and the finger pressure waveform

to be examined, but it can be hypothesized that physical activity induced changes in model parameters larger than the population IQR are unrealistic during a 12-week clinical trial. This would be unrealistic for most of the parameters, aside from t_{peak}. However, the variation in single-day IQR is far lower compared to the multiple-day IQR, in most cases. Exceptions can be noted for C_{ao}, V_{tot}, and Z_{ao} based on finger pressure where the first and third quartiles overlap for the multi-day and the single-day IQR. This indicates that the single and multi-day IQR may be equally high in some participants, and that changes in these parameters may not in many cases be trusted to be changes caused by the data, and may be artifacts of the numerical uncertainties of the estimation method.

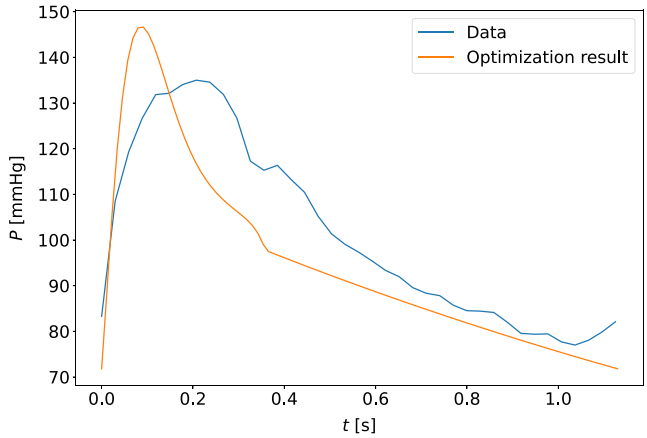

Fig. 15 The model-optimized pressure curve based on the mean of the best parameter estimates for the individual is shown with the raw data to which it is optimized for a participant. The sample shown is for the measurement sample with the highest cost function value when compared to other participants and measurement days. This is a waveform adapted to the open-loop model with the carotid pressure waveform

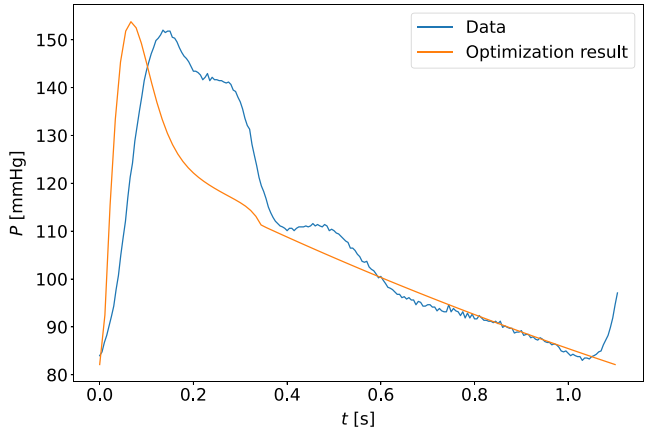

Fig. 16 The model-optimized pressure curve based on the mean of the best parameter estimates for the individual is shown with the raw data to which it is optimized for a participant. The sample shown is for the measurement sample with the highest cost function value when compared to other participants and measurement days. This is a waveform adapted to the open-loop model with the finger pressure waveform

This would especially be a challenge for detecting small changes in the individual compared to the variation over the population.

The individual estimates were computed as the mean of the estimates with a cost function value lower than the mean of the final 20 parameter estimate sets, see Sect. Parameter estimation. This allowed the amount of samples used in the computation of the mean parameter estimates to vary. Furthermore, there is a possibility that choosing only the best fitted parameter estimate provides better results in some cases. The averaging over different solutions was chosen to account for sensitivity of the exact location of the cost

function minimum due to noise and model structure insufficiency. If, for example, noise causes multiple smaller minima, or a displacement of the local minimum compared to the unperturbed cost function minimum, having multiple estimates in this region and averaging them may mitigate these noise effects. However, using the averaging procedure without bounds for the problem sometimes introduced much higher variability in the resulting solutions, and the averaging would yield parameter values which would not recreate the data well. In contrast, with bounds, we found that the averaged parameters provide acceptable solutions as seen in the table and figures of Sect. Quality of optimization results. The estimates for systolic and diastolic pressures are more accurate for the finger pressure-based estimates since they were more heavily weighted due to more data points since the finger pressure was sampled at a higher frequency than the carotid pressure. We cannot be certain that the algorithm has found the global minimum using this procedure, but it is also a possibility that the global minimum does not correspond the most physiologically accurate combination of parameters. The averaging of solutions around a local minimum gives some information about solutions that are almost as good as the local minimum itself and may be just as physiologically viable. Should the local minimum not be the global minimum, then it is still a minimum which provides a good description of the data as observed in Tables 4 and 5.

In Fig. 6, it is demonstrated that the mean estimates from for the two models only showed small differences based on choice of pressure waveform. A notable exception was found for C_{ao}, for which the finger pressure-based estimates were statistically significantly higher in both model formulations. This may be explained by the finger pressure waveform having a flatter slope during diastole. The t_{peak} was another notable exception, which was estimated with a small difference between waveforms. As previously noted, the corresponding heart rates of the two waveforms could be different. This could potentially contribute to some variation in estimates. The paired sample t-tests between other combinations of model formulations and pressure waveforms are shown in the supplementary materials. The finger pressure was not transformed into a more central pressure

Table 4 Percentage errors between measurements and model outputs optimized using the closed-loop model with carotid pressure waveforms. These residual statistics are computed across all individuals, i.e. they are not grouped by individual, but by measurement day. The mean and standard deviations of the absolute residuals are given. P_{sys} is the systolic aortic pressure, P_{dia} is the diastolic aortic pressure, and SV is the stroke volume, and MVP is the mean venous pressure. pWF_x, and qWF_x indicates the median value across all measurements for the x^{th} percentile percentage error of the waveform residuals for a single measurement (pWF_x for pressure and qWF_x for flow)

Pressure	Meas. day	P_{sys} [%]	P_{dia} [%]	SV [%]	MVP [%]	$\mathrm{pWF}_{75\%}$ [%]	$\mathrm{pWF}_{25\%}$ [%]	$\mathrm{qWF}_{75\%}$ [%]
Carotid	All	1.62 ± 1.71	1.38 ± 1.36	2.32 ± 2.38	6.71 ± 9.13	5.03	1.65	26.63
Carotid	1	1.82 ± 1.6	1.4 ± 1.34	2.4 ± 2.06	6.04 ± 7.74	4.94	1.71	22.69
Carotid	2	1.95 ± 2.09	1.63 ± 1.69	2.92 ± 2.81	8.7 ± 9.96	5.32	1.61	30.68
Carotid	3	0.84 ± 0.9	1.0 ± 0.69	1.34 ± 1.88	4.8 ± 9.76	4.52	1.56	25.52
Finger	All	0.61 ± 0.79	0.72 ± 0.91	1.29 ± 1.54	3.4 ± 4.21	5.52	1.48	25.28
Finger	1	0.61 ± 0.72	0.74 ± 0.95	1.39 ± 1.63	4.15 ± 5.22	5.3	1.46	18.7
Finger	2	0.72 ± 1.01	0.83 ± 1.1	1.67 ± 1.82	3.74 ± 3.96	5.65	1.4	30.3
Finger	3	0.47 ± 0.54	0.56 ± 0.6	0.72 ± 0.85	2.15 ± 3.03	5.74	1.79	22.64

Table 5 Percentage errors between measurements and model outputs optimized using the open-loop model with carotid pressure waveforms. These residual statistics are computed across all individuals, i.e. they are not grouped by individual, but by measurement day. The mean and standard deviations of the absolute residuals are given. P_{sys} is the systolic aortic pressure, P_{dia} is the diastolic aortic pressure, and SV is the stroke volume. pWF_x, and qWF_x indicates the median value across all measurements for the x^{th} percentile percentage error of the waveform residuals for a single measurement (pWF_x for pressure and qWF_x for flow)

Measurement	Meas. day [%]	P_{sys} [%]	P_{dia} [%]	SV [%]	$pWF_{75\%}$ [%]	$pWF_{25\%}$ [%]	$qWF_{75\%}$ [%]
Carotid	All	0.99 ± 1.3	1.07 ± 0.87	2.82 ± 4.27	4.64	1.38	31.24
Carotid	1	1.03 ± 1.13	1.04 ± 0.6	2.47 ± 3.54	4.27	1.42	30.62
Carotid	2	1.13 ± 1.62	1.25 ± 1.16	3.37 ± 4.75	5.14	1.15	34.05
Carotid	3	0.71 ± 1.04	0.86 ± 0.69	2.51 ± 4.67	4.66	1.72	29.65
Finger	All	0.56 ± 1.12	0.65 ± 1.33	1.44 ± 2.29	5.73	1.57	27.0
Finger	1	0.79 ± 1.3	0.88 ± 1.54	1.95 ± 2.55	5.86	1.68	31.9
Finger	2	0.65 ± 1.35	0.68 ± 1.62	1.73 ± 2.74	5.42	1.47	30.99
Finger	3	0.21 ± 0.13	0.35 ± 0.38	0.52 ± 0.67	5.46	1.78	23.68

by a transfer function, as it was seen as interesting to compare the distal measurement to the carotid waveform which is a more proximal measurement. A question for future work is to answer whether the change in the compliance estimated using the two pressure signals, will change similarly given the same stimulus.

There are no other very large differences in mean parameter estimates between the two models. Therefore, the venous compartment in the closed-loop formulation does not seem to affect the other model estimates to a large extent. Also, it seems like the effect of adjusting the total stressed blood volume can be counteracted by appropriately tuning the venous compliance. Hence, there seems to be little gain of adding these compartments from a parameter estimation perspective.

Two models were applied in this study. Although the closed-loop model may give more insight into the physiology, ventricular filling and fluid distributions of different states and individuals, some parameters could have interacted and caused difficulty in reaching the correct minimum for the cost function in the parameter space. For example, multiple parameters which were all influential on the ventricular filling properties in the model could have caused optimization challenges when adapting all of them to tune the filling properties according to the optimization data set which contained both noise and model discrepancy. One or both of the models may be practically unidentifiable for the data used in this analysis, which could result from such parameter interactions. Specifically, the high variability of stressed volume and venous compliance in the closed-loop model may be the result of such a situation as a higher blood volume would increase the pressure of the closed-loop system, while an increased compliance would accommodate the increased volume and counteract the pressure increase. Similarly, previous work found that the aortic impedance parameter was among the least influential parameters of the aortic pressure waveform [22]. Insensitivity can lead to practical unidentifiability and thus variability in estimates of Z_{ao} may only reflect this and not any meaningful changes in the hemodynamic state. For the remaining parameters, we have focused on comparing the variability in individual estimates to those of the whole group

(Figs. 2, 3) and further compared estimated values to clinical indices to further investigate the consistency of the estimates (Figs. 7, 8). A more formal practical identifiability analysis would be beneficial, but would require a good characterization of the expected variability in measurements and model discrepancy, and this would require same-day repeated measurements of individuals to characterize measurement variation. Further, a required level of precision must be specified for each parameter value. The multiple day IQR found in this study can be interpreted as a conservative estimate of the precision achievable as the repeated measurements included are expected to correspond to changed parameter values in many cases as the measurements are over 12 weeks while increasing physical activity.

The estimated parameter combinations were not assessed in terms of how credible they are to be found in real individuals aside from being bounded by values taken from the literature. By estimating R_{sys} as MAP/CO and C_{ao} as SV/PP, we found high positive correlation between these estimates and the model-predicted resistance. However, this was not the case for C_{ao}, as seen in Figs. 7, 8 where the correlation was lower but still moderately high. The Pearson correlation coefficients are shown in Table 3, and indicate high correlation for R_{sys} in all cases, even if the conventional method estimates are not used for sampling initial parameter guesses for the model optimization.

We focused on using single heart beat cycles of data. The data comprised either synchronized waveforms as for the finger pressure waveform and LVOT flow, or as a single averaged waveform as for pairing the carotid waveform with the LVOT flow data. Colebank et al. and Marquis et al. used an approach where optimization is performed for multiple consecutive cycles at the same anatomical locations which is a convincing approach for accounting for beat-to-beat variations [6, 7], but this requires a large amount of continuous waveform data. We did not do any analysis on the impact of using more than one cycle of data, but previous examinations show that one cycle should be sufficient under ideal conditions for synthetic data [22].

By scaling the waveforms by ABPM systolic and diastolic values, some of the daily variability of measurements should be accounted for. While the waveform shape itself was subject to noise, it may also have been subjected to other perturbations and daily variability through changes in, for example, respiration patterns and heart rate. These effects should be partially accounted for in the averaged carotid waveform. The finger pressure waveforms did not benefit from the same effect as they were not averaged, but were on the other hand synchronized to the simultaneously recorded flow cycles.

Even though the model captures the approximated aortic pressure values reasonably well, this is a highly simplified model of the cardiovascular system with some limitations. Firstly, the model is geometryless, which means that it ignores all personalizable traits relying on spatial geometry more specific than a global compartment of vessels. Despite this, we still observe that the model is able to capture total peripheral resistance, extreme pressures and stroke volumes relatively well, at least when compared to conventional estimation methods for the parameters and the raw data used in the cost function. Secondly, the model neglects the inertance of the vessels and combined with its 0-dimensional nature it therefore ignores potential reversal of blood flow and reflected wave propagation. This makes the model unable to fully describe some features of central pressure waveforms, such as the dicrotic and anacrotic notch. Thirdly, other relevant

physiological functions which affect and regulate the cardiovascular system, such as neural, respiratory, renal, metabolism, and gas exchange have been neglected. Any diseases which are not detectable by changes in the systemic hemodynamics and the left ventricle will not be detectable by this model. The parameter ranges that bound the optimization should allow for some types of heart disease and both normal and hypertensive ranges of blood pressure. Any disease or condition which is described by a combination of parameters which needs to exceed one or more of these ranges may not be possible to detect by this personalization algorithm. For the case of monitoring hypertension and possibly related heart remodeling and disease such as heart failure, the model may be able to capture this combined remodeling. However, this has not been investigated by the authors and is beyond the scope of this paper. The ejection fraction (EF) of the model is not necessarily realistic as the ventricular volume intercept is set to a volume of 0. Consequently, if heart failure is to be detected it would likely be more reliably detected by other measures than EF, such as cardiac output or contractility. Lastly, as the inertance is neglected and valve resistances are not explicitly personalized, this model will not account for cardiac valve diseases or leakage.

Some of the synchronized finger pressure waveforms were subject to a high level of noise, while still retaining some characteristic waveform features. This was a drawback for the optimization as it made it more difficult to detect changes and probably contributed to increased variability in estimates. Despite this, we observed similar mean estimates for most model parameters using both finger and carotid waveforms. The only major difference was found in C_{ao} which can be partially be explained by the flatter diastolic slope of the finger pressure waveforms. The finger pressure waveform does experience pressure amplification and distortion of the waveform compared to more central pressures such as the carotid pressure waveform. Therefore, we may have expected to see some differences in the mean parameters as well. In Eq. 5, the clinical indices get additional weighting to increase their priority in the optimization scheme. If the weights were removed the optimization procedure would be able to recreate the waveforms even closer, but also allow larger discrepancies in the remaining terms of the cost function. This could in turn have caused even larger discrepancies between results from the different choices of pressure waveform, but for this investigation we chose a balance between adaption to waveform or more clinically relevant measures such as systolic and diastolic pressures.

Conclusion

Model personalization was performed for blood pressure and echocardiography data collected from 25 participants in an physical activity motivational study were used for model optimization.

Mean parameter estimates were practically equivalent across both model formulations and for both choices of waveforms, except for a few cases. The C_{ao} parameter was found to have a higher value on average when estimated using the finger pressure waveform as compared to the carotid waveform, regardless of model choice. For both models, the estimates for arterial resistance and compliance were found to correlate at least moderately well ($r > 0.60$) with other conventional estimation methods (Additional files 1, 2).

Changes in pressure and flow waveforms, as well as SV are reproduced reasonably well by both models for the estimated parameters. Using the closed-loop model did not prove to aid the ability to resolve single participants' parameter estimates from the model population compared to the open-loop model. This supports using the open-loop model formulation for further efforts in personalizing the ventricle and arterial compartments of a lumped parameter model.

Resolving parameter changes for individuals and distinguishing these changes from the population seems feasible given the IQR values, assuming the real changes are sufficiently large to not be lost in the personal estimation variability. Questions for further research are whether or not these changes are realistic or a product of noise, insufficient data, or uncertainty introduced in the estimation procedure. Whether the data are sufficient to detect cardiovascular remodeling given the recorded exercise stimulus remains to be investigated.

Appendix

Model equations

Closed-loop model

This subsection is largely a repetition of details described in [22]. The closed-loop model comprised a system of non-linear ordinary differential equations (ODEs) describing the volume state variable of the three model compartments. The dynamic elastance function of the heart contributes a source term to the system of ODEs:

$$\begin{aligned}
\frac{dV_{sa}}{dt} &= C_{sa}\frac{dP_{sa}}{dt} = Q_{lvao} - Q_{sys} \\
\frac{dV_{sv}}{dt} &= C_{sv}\frac{dP_{sv}}{dt} = Q_{sys} - Q_{svlv} \\
\frac{dV_{lv}}{dt} &= Q_{svlv} - Q_{lvao}.
\end{aligned} \tag{10}$$

The two remaining state variables, pressure and flow, are mainly modeled by linear relationships as expressed below:

$$\begin{aligned}
V_{sa} &= C_{sa}P_{sa} \\
V_{sv} &= C_{sv}P_{sv} \\
P_{lv} &= E(t)V_{lv} + P_{th}(t) \\
E(t) &= (E_{\max} - E_{\min})e(t) + E_{\min} \\
P_{ao} &= \max\left[P_{sa}, P_{lv}\right] \\
Q_{lvao} &= I(P_{lv} > P_{sa})\frac{P_{lv} - P_{sa}}{Z_{ao}} \\
Q_{svlv} &= I(P_{sv} > P_{lv})\frac{P_{sv} - P_{lv}}{R_{mv}} \\
Q_{sys} &= \frac{P_{ao} - P_{sv}}{R_{sys}}.
\end{aligned} \tag{11}$$

The indicator function $I(x)$ has the value 1 when the argument x is true and 0 when x is false. The activation function $e(\tau)$ is defined as:

$$e(\tau) = \alpha \times \frac{(\tau/a_1)^{n_1}}{1+(\tau/a_1)^{n_1}} \times \frac{1}{1+(\tau/a_2)^{n_2}}, \tag{12}$$

where τ is position in the cardiac cycle between the end of the last diastolic period and the end of the next diastolic period $\tau = 1$. The parameters a_1 and n_1 determine the shape of contraction and a_2 and n_2 determine the shape of relaxation of the elastance curve and the timing of peak elastance. The choice of values for these parameters are identical to those of Stergiopulos et al [24]. We wrote the parameter values for a_1 and a_2 in terms of the ratio of $\frac{t_{peak}}{T}$, and set $\alpha = 1.672$, to ensure normalization of the curve. t_{peak} describes the time of peak ventricular elastance, and therefore determines when the left-ventricular elastance $E(t)$ reaches E_{max}. The intrathoracic pressure function P_{th} describes the external pressure effects on the ventricular muscle aside from pressure gradients inside the blood vessels and is here modeled as a constant of $P_{th}(t) = -4$ mmHg. Otherwise, the parameters are defined as in Table 1.

The V_{tot} parameter describes total stressed volume and is enforced by setting initial compartment volumes and pressures such that the total stressed volume equals the parameter value. The model was demonstrated to conserve the volume and hence the total blood volume will not change. The initial volumes are set according to the equations:

$$\begin{aligned} V_{ao,0} &= C_{ao}\, P_{ao,0}, \text{ and} \\ P_{sv,0} &= \frac{V_{tot}-V_{ao,0}-V_{lv,0}}{C_{sv}}, \end{aligned} \tag{13}$$

where the initial aortic pressure is set to $P_{ao,0} = 100$ mmHg, and initial left-ventricular volume is set to $V_{lv,0} = 100$ mL. The initial venous pressure is denoted by $P_{sv,0}$.

Open-loop model

The open-loop model describes two compartments, the left ventricle and arteries. The heart compartment is identical to the one described for the closed-loop model. The state equations describing the model are as follows:

$$\begin{aligned} \frac{dV_{sa}}{dt} &= C_{sa}\frac{dP_{sa}}{dt} = Q_{lvao} - Q_{sys} \\ \frac{dV_{lv}}{dt} &= Q_{svlv} - Q_{lvao}. \end{aligned} \tag{14}$$

The state variables pressure, flow and volume are mainly modeled by linear relationships as seen here:

$$
\begin{aligned}
V_{sa} &= C_{sa}P_{sa} \\
P_{lv} &= E(t)V_{lv} + P_{th}(t) \\
E(t) &= (E_{\max} - E_{\min})e(t) + E_{\min} \\
P_{ao} &= \max\left[P_{sa}, P_{lv}\right] \\
Q_{lvao} &= I(P_{lv} > P_{sa})\frac{P_{lv} - P_{sa}}{Z_{ao}} \\
Q_{svlv} &= I(P_{sv} > P_{lv})\frac{P_{sv} - P_{lv}}{R_{mv}} \\
Q_{sys} &= \frac{P_{ao} - P_{sv}}{R_{sys}},
\end{aligned}
\tag{15}
$$

where $e(t)$ is as defined in Equation (12), while $P_{\text{sv}} = 6.0$ mmHg is now a fixed quantity. Now the initial volumes are set as

$$
\begin{aligned}
V_{ao,0} &= C_{ao}\, P_{ao,0}, \text{ and} \\
V_{lv,0} &= 100 \text{ mL},
\end{aligned}
\tag{16}
$$

where the initial aortic pressure is set to $P_{ao,0} = 100$ mmHg.

Optimization algorithm details

The Trust Region Reflective Algorithm (TRRA) as implemented in SciPy version 1.7.1 was applied for the parameter optimization procedure [29]. In particular, the implementation of the algorithm as expressed through the function scipy.optimize.least_squares() was used. We executed this function given the arguments below and a list of initial parameter guesses as sampled from Eq. (3). The function specific parameters passed to the TRRA to set the accuracy of the method were set to $xtol = 2.3 \cdot 10^{-16}, ftol = 2.3 \cdot 10^{-16}, gtol = 2.3 \cdot 10^{-16}$ and $diff\_step = 1.0 \cdot 10^{-3}$.

The uniform distributions from which the first 30 initial parameter guesses are sampled were bounded by the upper and lower bounds presented in 6. For the next 20 initial parameter guesses the sampling was made from the uniform distribution with bounds expressed as (4). In Eq. (4), $\theta_{min,i}$ refers to the initial parameter guess form the first 30 guesses which optimized the solution with the minimal cost function value from that

Table 6 All model parameters that were assigned to be personalizable are listed along with their upper and lower bounds. The bounds determine the uniform distributions from which the initial parameter guesses are sampled

Parameter	Upper bounds	Lower bounds	Units
C_{ao}	3.0	0.148	$\frac{\text{mL}}{\text{mmHg}}$
C_{sv}	90.0	1.48	$\frac{\text{mL}}{\text{mmHg}}$
E_{max}	$\frac{10.48}{\text{BSA}}$	0.5	$\frac{\text{mmHg}}{\text{mL}}$
R_{sys}	2.963	$\frac{0.917}{\text{BSA}}$	$\frac{\text{mmHg s}}{\text{mL}}$
t_{peak}	$\min(0.442, T)$	$\min(0.15, 0.9T)$	s
V_{tot}	1503.	150.	mL
Z_{ao}	0.2	0.001	$\frac{\text{mmHg s}}{\text{mL}}$

first set of guesses. The same bounds were upper and lower limits for parameters in both sampling distributions.

All parameters from Table 1 were sampled, except T which was always set to the heart beat period of the given waveform, as well as E_{min} and R_{mv} which were fixed to predetermined values. Mitral valve resistance should be a small resistance according to Stergiopulos et al. [24], which we fixed it to 0.02 mmHg s/mL. The value of E_{min} was set according to apparent phenotype based on blood pressure. Segers et al. estimated values for minimal left-ventricular elastances as 0.03 mmHg/mL for normotensive people [12], while we calculated the same parameter to be 0.034 when taken as the weighted average over all hypertensive groups presented in their study. This value caused difficulties in estimating the left-ventricular elastance by constantly estimating it to the lowest bound for all participants. Therefore the value of 0.06 mmHg/mL as used by Stergiopulos was used instead, but separation was made according to if the systolic blood pressure was above or below 140 mmHg as was similar to the case for the estimates by Segers et al. [12]. For systolic blood pressure below 140 mmHg, $E_{\text{min}} = 0.055$ mmHg/mL was opted for, while we used for values above $E_{\text{min}} = 0.06$ mmHg/mL.

The bounds in Table 6 were set based on many different sources in literature. The study from Vardoulis et al. simulated a wide range of total arterial compliances [31], and we used a similar range for our concept of arterial compliance, but it was slightly widened as finger pressure estimates tend to have a low diastolic slope, which might indicate a high compliance. Central venous compliance is often estimated to be 30 times the value of arterial compliance [32, 33], and therefore, we used estimates of the venous compliance 10–30 times the arterial compliance values to make the widest range possible. For E_{max} we used the body surface area (BSA) indexed results from a study by Bombardini et al. which estimated end-systolic elastances for patients in both disease and health to estimate a wide range to use as bounds for sampled elastances [34]. For R_{sys}, Chantler et al. estimated vascular resistance in groups men and women with normo- or hypertension [35]. We considered all four groups, the group with the lowest mean value minus two standard deviations was taken as the lowest bound, and the group with the highest mean was used in the opposite direction to determine the highest bound. t_{peak} was bounded using results from studies by Weissler et al. and Mertens et al., which both measured systolic timing properties of the heart [36, 37]. Their measurements of the QS_2 period of the heart ejection time determined by electromechanical considerations were taken as and indication of how large the allowed range for t_{peak} should be, and hence the bounds were determined by a technique similar to how it was done for R_{sys}. The lower bound was lowered further as to accommodate an even wider range. The total stressed blood volume bounds were estimated by taking the measurements of total blood volume from a paper by Feldschuh et al. and applying a formula as demonstrated by Colunga et al. to estimate the total blood volume [5, 38]. This was done by taking the total blood volume value and estimating the total stressed volume fraction by this formula:

$$V_{\text{tot}} \approx \text{TBV} \cdot (0.13 \cdot 0.27 + 0.64 \cdot 0.18 + 0.035 \cdot 0.5), \tag{17}$$

where the total stressed blood volume V_{tot} is computed by assuming what fraction of the total blood volume (TBV) can be found in the left ventricle, systemic arteries, and systemic veins, and what fractions of these volumes are assumed to be stressed. The mean

Table 7 The scaling factors *K*, which are used to balance and approximately normalize the terms in the specified cost functions. *MVP* - mean venous pressure, *p* - aortic pressure waveform, *pdia* - diastolic brachial pressure, *psys* - systolic brachial pressure, *q* - aortic flow, and *SV* - stroke volume

Symbol	Value	Unit
K_{MVP}	5.0	mmHg
K_p	100.0	mmHg
K_{pdia}	80.0	mmHg
K_{psys}	120.0	mmHg
K_q	500.0	$\frac{mL}{s}$
K_{SV}	100.0	mL

blood volumes, of the study groups examined by Feldschuh et al. [38], with the highest and lowest mean values were adjusted by adding or subtracting 3–4 times the standard deviations to find the widest possible range based on these data. Two standard deviations gave volumes which were larger than what was expected to give reasonable results with our model. Finally, the bounds for Z_{ao} were based on the values reported by Segers et al. [12], but we allowed a range 33 times wider as this was a small parameter compared to the other arterial parameters. The upper range was set to ensure that it likely would be smaller than the total peripheral resistance. The resulting parameter range also corresponds reasonably well with the range found by Segers et al. when optimizing the parameter to multiple data sets for a three-element Windkessel model [39].

The scaling factors used to balance the different terms in the cost functions in (5) are listed in Table 7. The initialization for the random seed using the numpy.random.seed() function from the NumPy libary [40], was set to be 112233 for sampling initial parameter guesses from the distributions defined by (3) and (4).

Supplementary Information

The online version contains supplementary material available at https://doi.org/10.1186/s12938-023-01086-y.

Additional file 1. Table S1. Two-tailed t-tests for parameter means using different models and pressure waveforms. Parameter values averaged over different samples of measurements for both model formulations and choices of data sets. Standard deviations are presented in parentheses. The p-value and 95% confidence interval (CI95%) are obtained by a two-tailed t-test for paired data comparing the mean parameter values using the finger and carotid pressure for the same model formulation, or using the same pressure waveform but different model formulations. "Group" indicates which combination of model and pressure waveform is used to generate the data for the group. "CL" indicates the closed-loop model, and "OL" signifies the open-loop model. "-C" indicates the carotid pressure waveform, and "-F" indicates the finger pressure waveform. The parameters included in the analysis are systemic arterial compliance (Cao), total peripheral resistance (Rsys), time of peak elastance in the left ventricle (tpeak), characteristic aortic impedance (Zao), and maximal left-ventricular elastance (Emax).

Additional file 2: Table S1. Two-tailed t-tests for parameter means using different models and pressure waveforms. Parameter values averaged over different samples of measurements for both model formulations and choices of data sets. Standard deviations are presented in parentheses. The p-value and 95% confidence interval (CI95%) are obtained by a two-tailed t-test for paired data comparing the mean parameter values using the finger and carotid pressure for the same model formulation, or using the same pressure waveform but different model formulations. "Group" indicates which combination of model and pressure waveform is used to generate the data for the group. "CL" indicates the closed-loop model, and "OL" signifies the open-loop model. "-C" indicates the carotid pressure waveform, and "-F" indicates the finger pressure waveform. The parameters included in the analysis are systemic arterial compliance (Cao), total peripheral resistance (Rsys), time of peak elastance in the left ventricle (tpeak), characteristic aortic impedance (Zao), and maximal left-ventricular elastance (Emax).

Acknowledgements
We would like to thank master student Kjell-Arne Øyen and University College Teacher Hans Olav Nilsen for preforming the measurements from the clinical trial from which the data used in this study are collected.

Author contributions
NB wrote the main manuscript text. JS, and EI contributed to and edited the main manuscript. NB performed all analysis and created all figures with advice from all other authors. NB and JS performed the data preprocessing for analysis and cooperated on writing the code for analysis. LH supervised the work. All authors reviewed the manuscript. All authors read and approved the final manuscript.

Funding
Open access funding provided by Norwegian University of Science and Technology. The study is funded in full by the hosting institution, the Norwegian University of Science and Technology (NTNU), through the Digital Transformation Initiative.

Availability of data and materials
The data sets and code used and/or analyzed during the current study can be provided by the corresponding author upon reasonable request.

Declarations

Ethics approval and consent to participate
The study from which the data obtained was approved by Regional Committee on Medical and Health Research Ethics of Norway (Identifier: 2019/1084) and preregistered on clinicaltrials.org (Identifier: NCT 04151537). Written informed consent was obtained from all participants.

Consent for publication
Not applicable.

Competing interests
The authors have no competing interests to declare.

Received: 16 August 2022 Accepted: 23 February 2023
Published online: 13 April 2023

References

1. Forouzanfar MH, Afshin A, Alexander LT, Anderson HR, Bhutta ZA, Biryukov S, et al. Global, regional, and national comparative risk assessment of 79 behavioural, environmental and occupational, and metabolic risks or clusters of risks, 1990–2015: a systematic analysis for the global burden of disease study 2015. Lancet. 2016;388(10053):1659–724. https://doi.org/10.1016/S0140-6736(16)31679-8.
2. Shi Y, Lawford P, Hose R. Review of zero-D and 1-D models of blood flow in the cardiovascular system. Biomed Eng Online. 2011;10(1):33. https://doi.org/10.1186/1475-925X-10-33.
3. Huberts W, Heinen SGH, Zonnebeld N, van Den Heuvel DAF, de Vries JPPM, Tordoir JHM, et al. What is needed to make cardiovascular models suitable for clinical decision support? A viewpoint paper. J Comput Sci. 2018;24:68–84. https://doi.org/10.1016/j.jocs.2017.07.006.
4. Hose DR, Lawford PV, Huberts W, Hellevik LR, Omholt SW, van de Vosse FN. Cardiovascular models for personalised medicine: Where now and where next? Med Eng Phys. 2019;72:38–48. https://doi.org/10.1016/j.medengphy.2019.08.007.
5. Colunga AL, Kim KG, Woodall NP, Dardas TF, Gennari JH, Olufsen MS, et al. Deep phenotyping of cardiac function in heart transplant patients using cardiovascular system models. J Physiol. 2020;598(15):3203–22. https://doi.org/10.1113/JP279393.
6. Marquis AD, Arnold A, Dean-Bernhoft C, Carlson BE, Olufsen MS. Practical identifiability and uncertainty quantification of a pulsatile cardiovascular model. Math Biosci. 2018;304:9–24. https://doi.org/10.1016/j.mbs.2018.07.001.
7. Colebank MJ, Colunga AL, King M, Schell C, Sheldon M, Kharbat M, et al. Parameter inference in a computational model of hemodynamics in pulmonary hypertension. arXiv. 2021. https://doi.org/10.48550/arXiv.2101.06266.
8. Pant S, Fabrèges B, Gerbeau J, Vignon-Clementel IE. A methodological paradigm for patient-specific multi-scale CFD simulations: from clinical measurements to parameter estimates for individual analysis. Int J Num Method Biomed Eng. 2014;30(12):1614–48. https://doi.org/10.1002/cnm.2692.
9. Pant S, Corsini C, Baker C, Hsia TY, Pennati G, Vignon-Clementel IE. Data assimilation and modelling of patient-specific single-ventricle physiology with and without valve regurgitation. J Biomech. 2016;49(11):2162–73. https://doi.org/10.1016/j.jbiomech.2015.11.030.

10. Hann CE, Chase JG, Desaive T, Froissart CB, Revie J, Stevenson D, et al. Unique parameter identification for cardiac diagnosis in critical care using minimal data sets. Comput Method Progr Biomed. 2010;99(1):75–87. https://doi.org/10.1016/j.cmpb.2010.01.002.
11. Kind T, Faes TJC, Lankhaar JW, Vonk-Noordegraaf A, Verhaegen M. Estimation of three- and four-element windkessel parameters using subspace model identification. IEEE Trans Biomed Eng. 2010;57:1531–8. https://doi.org/10.1109/TBME.2010.2041351.
12. Segers P, Stergiopulos N, Westerhof N. Quantification of the contribution of cardiac and arterial remodeling to hypertension. Hypertension. 2000;36(5):760–5. https://doi.org/10.1161/01.HYP.36.5.760.
13. Meiburg R, Huberts W, Rutten MCM, van de Vosse FN. Uncertainty in model-based treatment decision support: applied to aortic valve stenosis. Int J Num Method Biomed Eng. 2020;36(10): e3388. https://doi.org/10.1002/cnm.3388.
14. Conover T, Hlavacek AM, Migliavacca F, Kung E, Dorfman A, Figliola RS, et al. An interactive simulation tool for patient-specific clinical decision support in single-ventricle physiology. J Thorac Cardiovasc Surg. 2018;155(2):712–21. https://doi.org/10.1016/j.jtcvs.2017.09.046.
15. Eck VG, Donders WP, Sturdy J, Feinberg J, Delhaas T, Hellevik LR, et al. A guide to uncertainty quantification and sensitivity analysis for cardiovascular applications. Int J Numer Method Biomed Eng. 2016. https://doi.org/10.1002/cnm.2755.
16. Audebert C, Peeters G, Segers P, Laleman W, Monbaliu D, Korf H, et al. Closed-loop lumped parameter modeling of hemodynamics during cirrhogenesis in rats. IEEE Trans Biomed Eng. 2018;65(10):2311–22. https://doi.org/10.1109/TBME.2018.2793948.
17. Nes BM, Gutvik CR, Lavie CJ, Nauman J, Wisløff U. Personalized activity intelligence (PAI) for prevention of cardiovascular disease and promotion of physical activity. Am J Med. 2017;130:328–36. https://doi.org/10.1016/j.amjmed.2016.09.031.
18. Nauman J, Nes BM, Zisko N, Revdal A, Myers J, Kaminsky LA, et al. Personal activity intelligence (PAI): a new standard in activity tracking for obtaining a healthy cardiorespiratory fitness level and low cardiovascular risk. Progr Cardiovasc Dis. 2019;62(2):179–85. https://doi.org/10.1016/j.pcad.2019.02.006.
19. Øyen KA. The effect of Personal Activity Intelligence (PAI) on ambulatory blood pressure in adults with elevated blood pressure: a 12-week pilot randomized controlled trial [Master's thesis]. Norwegian University of Science and Technology; 2020. https://hdl.handle.net/11250/2782710.
20. Organization GWH. WHO Guidelines on physical activity and sedentary behaviour; 2020. https://www.who.int/publications/i/item/9789240015128 (Visited May 2022).
21. Rohatgi A. Webplotdigitizer: Version 4.5; 2021. https://automeris.io/WebPlotDigitizer.
22. Bjordalsbakke NL, Sturdy JT, Hose DR, Hellevik LR. Parameter estimation for closed-loop lumped parameter models of the systemic circulation using synthetic data. Math Biosci. 2022;343: 108731. https://doi.org/10.1016/j.mbs.2021.108731.
23. Smith BW, Chase JG, Nokes RI, Shaw GM, Wake G. Minimal haemodynamic system model including ventricular interaction and valve dynamics. Med Eng Phys. 2004;26(2):131–9. https://doi.org/10.1016/j.medengphy.2003.10.001.
24. Stergiopulos N, Meister JJ, Westerhof N. Determinants of stroke volume and systolic and diastolic aortic pressure. Am J Physiol. 1996;270:H2050-9. https://doi.org/10.1152/ajpheart.1996.270.6.H2050.
25. Segers P, Stergiopulos N, Verdonck P, Verhoeven R. Assessment of distributed arterial network models. Med Biol Eng Comput. 1997;35(6):729–36. https://doi.org/10.1007/BF02510985.
26. Pironet A, Dauby PC, Chase JG, Kamoi S, Janssen N, Morimont P, et al. Model-based stressed blood volume is an index of fluid responsiveness. IFAC-PapersOnLine. 2015;48(20):291–6. https://doi.org/10.1016/j.ifacol.2015.10.154.
27. Tansey EA, Montgomery LEA, Quinn JG, Roe SM, Johnson CD. Understanding basic vein physiology and venous blood pressure through simple physical assessments. Adv Physiol Educ. 2019;43:423–9. https://doi.org/10.1152/advan.00182.2018.
28. Debrunner F, Bühler F. "Normal central venous pressure," significance of reference point and normal range. British Med J. 1969;3:148–50. https://doi.org/10.1136/bmj.3.5663.148.
29. Virtanen P, Gommers R, Oliphant TE, Haberland M, Reddy T, Cournapeau D, et al. SciPy 10: fundamental algorithms for scientific computing in python. Nat Method. 2020;17:261–272. https://doi.org/10.1038/s41592-019-0686-2.
30. Vallat R. Pingouin: statistics in python. J Open Source Softw. 2018;3(31):1026. https://doi.org/10.21105/joss.01026.
31. Vardoulis O, Papaioannou TG, Stergiopulos N. On the estimation of total arterial compliance from aortic pulse wave velocity. Ann Biomed Eng. 2012;40:2619–26. https://doi.org/10.1007/s10439-012-0600-x.
32. Hainsworth R. The importance of vascular capacitance in cardiovascular control. Physiology. 1990;5(6):250–4. https://doi.org/10.1152/physiologyonline.1990.5.6.250.
33. Rose WC, Shoukas AA. Two-port analysis of systemic venous and arterial impedances. Am J Physiol Heart Circ Physiol. 1993;265(5):H1577–87. https://doi.org/10.1152/ajpheart.1993.265.5.H1577.
34. Bombardini T, Mulieri LA, Salvadori S, Costantino MF, Scali MC, Marzilli M, et al. Pressure-volume Relationship in the Stress-echocardiography Laboratory: Does (Left Ventricular End-diastolic) Size Matter? Revista Espanola de Cardiologia. 2017;70(2):96–104. https://doi.org/10.1016/j.recesp.2016.04.038.
35. Chantler PD, Lakatta EG, Najjar SS. Arterial-ventricular coupling: mechanistic insights into cardiovascular performance at rest and during exercise. J Appl Physiol. 2008;105(4):1342–51. https://doi.org/10.1152/japplphysiol.90600.2008.
36. Mertens HM, Mannebach H, Trieb G, Gleichmann U. Influence of heart rate on systolic time intervals: effects of atrial pacing versus dynamic exercise. Clin Cardiol. 1981;4:22–7. https://doi.org/10.1002/clc.4960040106.
37. Weissler AM, Harris WS, Schoenfeld CD. Systolic time intervals in heart failure in man. Circulation. 1968;37(2):149–59. https://doi.org/10.1161/01.CIR.37.2.149.
38. Feldschuh J, Enson Y. Prediction of the normal blood volume. Relation of blood volume to body habitus. Circulation. 1977;56:605–12. https://doi.org/10.1161/01.cir.56.4.605.

39. Segers P, Rietzschel ER, De Buyzere ML, Stergiopulos N, Westerhof N, Van Bortel LM, et al. Three- and four-element Windkessel models: assessment of their fitting performance in a large cohort of healthy middle-aged individuals. Proc Inst Mech Eng. 2008;222:417–28. https://doi.org/10.1243/09544119JEIM287.
40. Harris CR, Millman KJ, van der Walt SJ, Gommers R, Virtanen P, Cournapeau D, et al. Array programming with NumPy. Nature. 2020;585(7825):357–62. https://doi.org/10.1038/s41586-020-2649-2.

Publisher's Note

Chapter 8

Examining Temporal Changes in Model Optimized Parameters Using Longitudinal Hemodynamic Measurements

The content of this chapter has been submitted to Biomedical Engineering OnLine, 2023.

Paper 3: Examining Temporal Changes in Model Optimized Parameters Using Longitudinal Hemodynamic Measurements

N.L. Bjørdalsbakke, J. Sturdy, U. Wisløff, L.R. Hellevik

Examining Temporal Changes in Model Optimized Parameters Using Longitudinal Hemodynamic Measurements

Nikolai L. Bjørdalsbakke[a], Jacob T. Sturdy[a], Ulrik Wisløff[b], Leif R. Hellevik[a]

[a] *Department of Structural Engineering, Norwegian University of Science and Technology (NTNU), Richard Birkelandsvei 1a, Trondheim, 7491, Norway*

[b] *Cardiac Exercise Research Group at the Department of Circulation and Medical Imaging, Norwegian University of Science and Technology (NTNU), Prinsesse Kristinas gt. 3, Trondheim, 7491, Norway*

Abstract

Background:

Clinical trials have repeatedly detected beneficial changes in blood pressure after physical activity and uncovered changes in lower level phenotypes (such as stiffened or high resistance blood vessels). These phenotypes can be characterized by parameters describing the mechanical properties of the circulatory system. These parameters may be incorporated in and contextualized by physics-based cardiovascular models of the circulation, which in combination can become tools for monitoring cardiovascular disease progression and management in the future. In this manuscript we specifically target hypertension. The main aim of the study was to identify patterns in the data that could potentially explain the estimated parameter changes. This includes investigating whether the parameters can be used to track the effect of physical activity on high blood pressure.

Method:

Closed-loop and open-loop models of the left ventricle and systemic circulation were previously optimized to data from a pilot study with a 12 week exercise intervention period. Basal characteristics and hemodynamic data such as blood pressure in the carotid, brachial and finger arteries, as well as left-ventricular outflow tract flow traces were collected in the trial. Model parameters estimated for measurements made on separate days during the trial were used to compute parameter changes for total peripheral resistance, systemic arterial compliance, and maximal left-ventricular elastance. We compared the changes in these cardiovascular model based estimates to changes from more conventional estimates made without the use of physics-based models by correlation analysis. Additionally, ordinary linear regression and linear mixed effects models were applied to determine the most informative measurements for the selected parameters. We applied maximal aerobic capacity (measured by $VO_{2,max}$) data to examine if exercise had any impact on parameters through regression analysis and case studies.

Results and conclusion:

Parameter changes in arterial parameters estimated using the cardiovascular models correlated moderately well with conventional estimates. Estimates based on carotid pressure waveforms as proved to give higher correlations than those for finger arterial pressure. Parameter changes over the 12-week study duration were of similar magnitude when compared to short term changes after a bout of intensive exercise in the same parameters. The short term changes were computed from measurements made immediately before and 24h after a cardiopulmonary exercise test. Regression analysis indicated that changes in $VO_{2,max}$ did not account for any substantial amount of variability in total peripheral resistance, systemic arterial compliance, or maximal left-ventricular elastance. On the contrary, changes in stroke volume contributed to far more explained variability.

1. Introduction

Cardiovascular disease is a leading cause of loss of quality of life and premature death worldwide [1]. Disease progression is usually slow, and it may take years before detectable symptoms appear. Although it is possible to monitor biological and behavioral risk factors at regular clinical visits, these measures may not provide sufficient insight into the underlying mechanisms contributing to the disease. In the case of essential hypertension, a persistently elevated blood pressure without an identifiable medical cause, we envision that monitoring the underlying hemodynamics may improve early detection and intervention in primary prevention of cardiovascular disease [2]. By hemodynamics we refer to for example measurements of blood pressure and flow, such as systolic and diastolic

brachial pressure, and cardiac output (CO). Furthermore, we believe that this can in part be achieved by application of personalized physics-based cardiovascular models.

Physics-based cardiovascular models have already been applied to predict the outcome of specific interventions [3, 4, 5, 6]. Some of these studies focused on interventions which can be made rapidly by invasive procedures or medical treatments with changes expected to take effect almost immediately. Other studies focused directly on the post-intervention hemodynamics rather than the change in parameters themselves. In such contexts the parameter change can be prescribed according to what is altered during an invasive procedure or treatment and its development is not necessarily considered an interesting outcome in itself. Some examples such as work by Audebert et al. and by Gerringer et al. focused on a specific parameter during disease progression [7, 8]. Personalized cardiovascular models which predict the development of parameters given different stimuli can be valuable clinical tools and provide more detailed information about response to treatment beyond the measurable hemodynamics alone. For example, models could potentially give more insight into disease aetiology than conventional parameter estimates alone, by providing continuous updates about lower level phenotypes normally not easily measurable. For this to be useful, parameter estimates and their changes must be reliable and interpretable in a clinical context. By conventional estimates, we refer to estimates made by methods that are algebraic in nature and not dependent upon models of the cardiovascular system. Here, we focus on parameters estimated for two lumped-parameter models and compare the results to their conventional estimates of similar parameters from the same hemodynamic measurements.

In this work, we treat the mechanical model parameters as the quantities of interest and use these as proxies for observing changes in low-level phenotypes in the progression of cardiovascular disease, such as arterial stiffening, change in vascular tone and altered cardiac hemodynamics. Regular physical activity is recommended in prevention and management of hypertension [9]. However, the effect depends on the duration, frequency, and intensity of exercise. Our hypothesis is that cardiovascular remodeling can be sufficiently represented by mechanical parameters which reflect the exercise-induced changes in hemodynamics.

Changes in habitual exercise have been observed to produce changes throughout the cardiovascular systems. A meta-analysis by Fagard et al. concluded that aerobic exercise lowers blood pressure and systemic vascular resistance in a mixed population with both normal and high blood pressure [10]. Molmen-Hansen et al. observed a significant reduction of total peripheral resistance in patients with hypertension undergoing aerobic interval training [11]. Ashor et al. compared studies with exercise interventions lasting between 8-26 weeks in a meta-review and reported reduced arterial stiffness estimated via pulse wave velocity (PWV) in individuals with high normal blood-pressure and hypertension after aerobic exercise [12]. In contrast, Montero et al. found reduced arterial stiffness in adults with high normal blood pressure and hypertension only in studies with an exercise intervention longer than 12 weeks or where the change could be associated with a large reduction in systolic blood pressure [13]. PWV is not equivalent to the arterial compliance parameters often used in lumped parameter models, but is related to the structural and material properties influencing arterial compliance. Changes in PWV thus imply that exercise can affect arterial wall properties. The resting ventricular function is also affected by exercise. Molmen-Hansen also found changes in multiple markers related to ventricular contractility after aerobic interval training, such as ejection fraction (EF) and peak velocity of the tricuspid valve annulus in systole [11]. By study of rats after periods of training and detraining, Oláh et al. observed increase in the end-systolic left-ventricular elastance after 12 weeks of exercise [14]. Hence, we expect that vascular properties can change as an effect of regular physical activity.

An exercise motivation trial conducted at the Norwegian University of Science and Technology in 2019-2020 monitored the hemodynamics of participants three times during the 12-week intervention period. The trial was originally designed to examine the effect of using Personal Activity Intelligence (PAI) score as an exercise motivator and its effect on blood pressure. PAI score is the output of a mathematical model considering an individual's heart rate history to compute an easily understandable personalized metric of physical activity [15, 16]. Using data from this trial, Bjørdalsbakke et al. personalized two simple cardiovascular models of the systemic circulation and analyzed the variability in parameter estimates due to personalization method as well as variation in the population [17]. The chosen personalization method was an ensemble method based on local non-linear optimization producing multiple parameter estimates to find an averaged solution after filtering out the worst estimates. Consequently, the choice of method introduced some variability to the parameter estimates themselves. Whether changes in parameters were primarily caused by the optimization procedure, the exercise intervention, or simply day-to-day variation in hemodynamics remained undetermined. Hence, the parameter changes during the intervention period and their explanation are the main focus of this manuscript. The analysis was undertaken by focusing on the arterial parameters of total peripheral resistance, systemic arterial compliance, as well as maximal left-ventricular elastance. Additionally, we investigate if there are differences between model formulations in estimation of parameter changes, and if the pressure waveform applied as a substitute for aortic hemodynamic measurements is important in this regard.

2. Method

2.1. Study Design, Setting, and Participants

The data originated from a pilot randomized controlled trial for exercise motivation. The study participants were randomly split into two groups. One group was asked to achieve a score of of over a 100 weekly PAI points by using a mobile application reading data from their wrist worn heart-rate sensor. The second group was instructed to follow the World Health Organization's general recommendations for physical activity [18]. A total of 26 adults (13 females), 45-65 years of age, met the inclusion criteria at screening: prehypertensive or hypertensive, currently physically inactive (self-reported < 50 PAI per week), not using antihypertensive medication and no history of cardiovascular disease. Hypertensive is here defined as having a systolic and diastolic blood pressure of $\geq 140/90$ mmHg, while prehypertensive is defined as values above $\geq 130/80$ mmHg. One participant dropped out due to becoming unable to perform exercise for a longer period during the trial period. The the study period lasted for 12 weeks, and hemodynamic measurements were made at the beginning, after 6 weeks and at the end. We refer to these as measurement days 1, 2, and 3. Parts of the trial have previously been described by Øyen, and Bjørdalsbakke et al. [19, 20]. The characteristics of the study population can be found in Table 1.

	n = 25	
Height	174.3±8.9	cm
Weight	85.9±14.2	kg
BSA	2.0±0.2	m^2
BMI	28.2±3.6	kg/m^2
Age	55.9±3.9	years
Sex M/F	13/12	-
SBP	138.5±12.6	mmHg
DBP	87.3±8.7	mmHg
$VO_{2,max}$	36.4±6.8	mL/(kg min)
24h ABPM awake SBP	141.0±13.5	mmHg
24h ABPM awake DBP	85.4±9.1	mmHg
SV (4D)	85.5±20.0	mL
SV LVOT	79.7±20.2	mL

Table 1: Baseline characteristics of the study population. SBP and DBP signifies systolic and diastolic office blood pressure measurement. BSA: body surface area, BMI: body mass index, ABPM: ambulatory blood pressure monitoring, SV: stroke volume, LVOT: left-ventricular outflow tract. 4D refers to 3D measurement averaged over time.

2.2. Data Collection

Varied hemodynamic data was recorded during the course of the study in the form of blood pressure, aortic flow, and pulse wave velocity. The cardiorespiratory fitness (CRF) was also measured as $VO_{2,max}$ through a cardiopulmonary exercise test (CPET) at measurement days 1 and 3 of the study period. Additionally, the activity levels throughout the study period was monitored using wrist worn heart rate monitors. Waveform data preprocessing has been described previously by Bjørdalsbakke et al. [17].

2.2.1. Physical Activity Monitoring

Physical activity monitoring was made by wearable wrist-worn heart rate monitors (LYNK2). The collected heart rate data were aggregated into daily PAI scores representing the physical activity level over the past week. The study group which asked to achieve a 100 weekly PAI were able to see their PAI scores during the study intervention, while the other group asked to follow the current recommendations were not able to monitor their PAI score.

2.2.2. Cardiopulmonary Exercise Test

A cardiopulmonary exercise test (CPET) was conducted for participants on measurement days 1 and 3. The test was performed using a treadmill (Woodway PPS 55) with Metalyzer II (Cortex).

Participants warmed up for 15 minutes at approximately 70% of estimated maximal heart rate. After warm-up workload was increased by 0.5-1 km/h and/or 1-2% inclination per minute until volitional exhaustion or $VO_{2,max}$ criteria were met. $VO_{2,max}$ was defined as a plateau in VO_2 despite increase in workload and respiratory exchange ratio >1.05. 22 of initially 26 participants reached this requirement, and therefore when $VO_{2,max}$ is referred in this text, we actually mean $VO_{2,peak}$ in some cases.

2.2.3. Blood Pressure Recordings

Ambulatory blood pressure monitoring (ABPM) of brachial artery blood pressure over 24 hours was measured using Oscar 2 model 250 (SunTech Medical Inc). Conventional office blood pressure (OBP), which is also a brachial artery measurement, was measured using a TangoM2 automatic blood pressure monitor (SunTech Medical Inc). The full pressure waveform was also measured non-invasively in the carotid artery, and finger arteries.

Office blood pressure was recorded in both arms upon screening, and the arm with the highest blood pressure was chosen for all subsequent measurements on all measurement days. Three measurements were taken, with 1.5 minute rest between each measurement. Participants were seated throughout the procedure. OBP measurements were taken for all measurements days. For 24h ABPM, measurements were taken at 30 minute intervals

at night, and 20 minute intervals by day. ABPM was performed for all measurement days.

Digital artery pressure waveforms in the finger were acquired by a Finometer PRO system (FinaPres) for 4 participants, while the remaining participants were measured by a Non-Invasive Blood Pressure Nano system (FinaPres). We refer to this type of measurement as finger pressure in the following. Participants were placed in the left lateral recumbent position during recordings, and measurements were made in the right hand. Measurements could be made in the index, middle or ring finger depending on where a clear signal was found. The pressure waveforms were subsequently calibrated to brachial blood pressure values obtained by ABPM during participants' waking hours.

We measured synchronized flow and finger pressure before performing the CPET test at both measurement day 1 and 3. Then the next day, and within 24 hours of conducting the CPET, the measurements were repeated for a subset of the participants. On these extra measurement days OBP and 24h ABPM was also measured. These measurements only exist for finger pressure waveform data, not for the carotid wavefom.

A SphygmoCor (CvMS v9, AtCor Medica) system traced the pressure waveform of the carotid artery by applanation tonometry, while also estimating the carotid-femoral pulse wave-velocity. We also calibrated these to ABPM measurements.

2.2.4. Echocardiography

An echocardiographic examination was performed on all measurement days. In particular the left-ventricular outflow tract flow (LVOT) flow trace was synchronized to finger pressure recordings during measurement. 4D recordings of stroke volume (SV) were also acquired.

Taking the traced carotid artery waveforms, we paired them with the same aortic flow waveforms which the finger pressure waveforms were synchronized to.

2.3. Inclusion Criteria

2.3.1. Inclusion Criteria for Correlation and Regression Analysis

The requirement for inclusion was having blood pressure measurements, LVOT flow and at least one type of pressure waveforms, as well as body mass data for all three measurement days. As a consequence, all drop-outs are excluded. Further, $VO_{2,max}$ estimates should exist for both measurement day 1 and 3. Height data was also required at measurement day 1.

For blood pressure, awake measurements from 24h ABPM measurements, or alternatively OBP measurements where ABPM data was missing were required. For blood pressure waveforms, either finger pressure waveforms or carotid pressure waveforms were acceptable. Finger pressure also required synchronization data to LVOT flow in the raw data files. In terms of SV data, 4D SV was preferred, but SV derived from LVOT flows was sufficient if the former was missing.

Due to drop outs, missing data, or missing synchronization data we selected 55 eligible sets of measurements for synchronised finger pressure and LVOT flow. Among these measurements 9 participants were identified with complete records. Similarly, for the data sets with carotid pressure, 14 eligible participants had complete records. The characteristics for the selected groups using differing pressure waveforms are found in Appendix A.

These inclusion criteria applies for all subsequent analyses as well.

2.3.2. Inclusion Criteria for Analysis of CPET Induced Change

The CPET induces changes in hemodynamics, and bouts of exercise have been observed to impact hemodynamics and specifically blood pressure for up to 24 hours afterwards [21]. This analysis was made to compare the change observed over longer periods to the change after one bout of strenuous exercise, or to daily variability if exercise effects have attenuated after 24 hours. This would indicate whether the model would see any difference or resolve this change similarly.

Inclusion criteria for the sub-analysis on changes after the CPET we require the same blood pressure and echocardiography measurements as described in previous sections on the days immediately following measurement day 1 and 3. By also requiring complete records for flow and finger pressure alignment, this left 4 participants out of the 9 identified in the previous paragraph. Consequently, these 4 participants had complete pressure and flow measurements within 24 hours after CPETs conducted at the beginning and end of the intervention (day 1 and 3).

2.3.3. Inclusion Criteria for Individual Participant Case Analysis

In this sub-analysis, we included the participants expected to have exercise-induced cardiovascular remodelling based on the measured cardiorespiratory fitness. Individual cardiovascular response to physical activity over both the short- and long-term is likely dependent upon properties in the individual which also causes challenges in predicting which type and amount of exercise is sufficient to

expect measurable cardiovascular remodeling.

To investigate the parameter changes of those we expected to be most likely to experience cardiovascular remodelling, we selected participants based on change in $VO_{2,max}$. We set the inclusion criteria to be that the participants should fall in the upper quartile of measured changes in $VO_{2,max}$. This left 4 participants.

2.4. Models

The models used have been presented in detail previously by Bjørdalsbakke et al. [20, 17]. The closed-loop model is based on previous models by Smith et al., Segers et al., and Bovendeerd et al. [22, 23, 24]. The open-loop model is equivalent to the model presented by Stergiopulos et al. [25]. The models are depicted in Figure 1, and the model parameters which are chosen for personalization are given in Table 2. Both models are investigated in this paper since they describe mainly the same hemodynamics with exception of the venous compartment and ventricular filling. They also have varying amounts of potentially personalizable, which may interact during optimization and cause different parameter estimates between models.

Symbol	Description	Unit
C_{ao}	Systemic arterial compliance	$\frac{\text{mL}}{\text{mmHg}}$
C_{sv}	Systemic venous compliance	$\frac{\text{mL}}{\text{mmHg}}$
E_{max}	Maximal left ventricular elastance	$\frac{\text{mmHg}}{\text{mL}}$
E_{min}	Minimal left ventricular elastance	$\frac{\text{mmHg}}{\text{mL}}$
R_{mv}	Mitral valve resistance	$\frac{\text{mmHg s}}{\text{mL}}$
R_{sys}	Total peripheral resistance	$\frac{\text{mmHg s}}{\text{mL}}$
T	Heart period	s
t_{peak}	Time of peak ventricular elastance	s
V_{tot}	Total stressed blood volume	mL
Z_{ao}	Characteristic impedance of the aorta	$\frac{\text{mmHg s}}{\text{mL}}$

Table 2: The closed-loop model parameters are listed with their corresponding symbols and units. The same parameters are used to describe the open-loop model except for C_{sv} and V_{tot}. Taken from Bjørdalsbakke et al. [17] under a CC-BY-4.0 license.

2.4.1. Model Output and Parameter Estimation

The models were formulated as a set of differential equations where a 4^{th} order Runge-Kutta scheme imple-

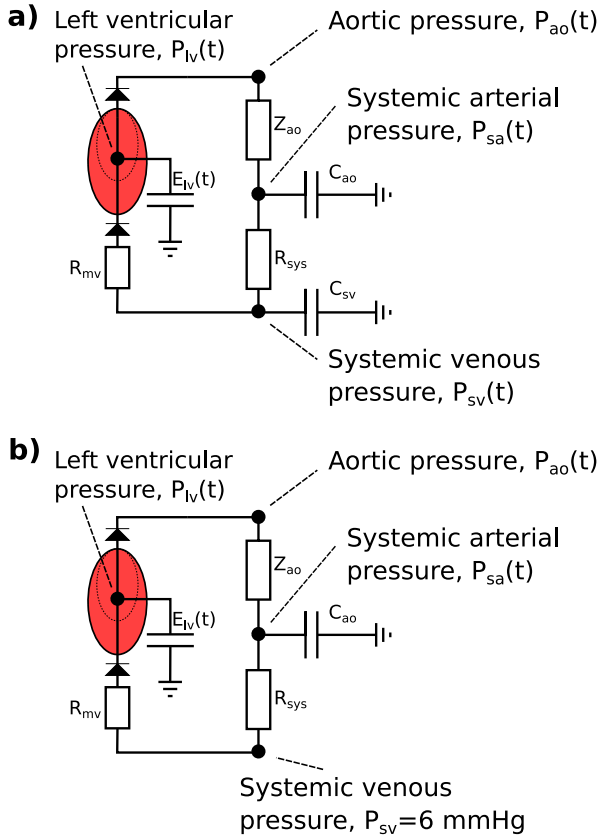

Figure 1: a) The closed-loop, lumped parameter model of the left ventricle, systemic arteries, and veins. b) The open-loop lumped parameter model of the left ventricle and systemic arteries. The circuit equivalent formulation of the models are depicted with the pressures and most of the mechanical parameters used to describe the systemic circulation. The venous compartment is volumeless and only partially described in the open-loop model. Pressures P, denote pressures in different parts of the cardiovascular system. Subscripts are as indicated by the figure text. E_{lv} indicates the left-ventricular elastance function. Z_{ao}: characteristic aortic impedance, C_{ao}: systemic arterial compliance, R_{sys}: total peripheral resistance, R_{mv}: mitral valve resistance. Taken from Bjørdalsbakke et al. [17] under a CC-BY-4.0 License.

mented in SciPy [26]. Model outputs are denoted as time-dependent signals $y(t, \boldsymbol{\theta})$, where $\boldsymbol{\theta}$ is a vector of mechanical model parameters.

Parameters are estimated by an ensemble of local optimizations, where the aortic flow and pressure waveforms with additional weight for systolic and diastolic values are included in the cost function. Hence, the parameter estimates have some inherent variability stemming from the optimization method, in addition to the intra-individual variability over time. The variability for parameters estimated for a single participant at a given point in time was found in previous work to be smaller than for the inter-personal parameter variability for the study population, and smaller than the intra-individual variability over all measurement days in a majority of cases. Further details on implementation, optimization and waveform processing can be found in Bjørdalsbakke et al. [17]. The parameters were normalized by body surface area (BSA), defined as $\mathrm{BSA} = \sqrt{\frac{\mathrm{height} \cdot \mathrm{weight}}{3600}}$ [27]. BSA has units of m^2. This is to account for interindividual variation in parameters that are known or can be assumed to be dependent upon such factors.

2.5. Parameter and Statistical Analysis

In addition to the parameter estimates optimized to the model itself, we computed estimates based on conventional estimation methods for C_{ao} and R_{sys} by the formulas

$$C_{\mathrm{ao}}^{m} = \frac{\mathrm{PP}}{\mathrm{SV}}, \tag{1}$$

and

$$R_{\mathrm{sys}}^{m} = \frac{\mathrm{MAP}}{\mathrm{CO}}. \tag{2}$$

For these equations PP denotes pulse pressure, SV is stroke volume, CO is cardiac output, and MAP is the mean arterial pressure as computed by averaging the carotid or finger pressure waveform calibrated by brachial blood pressure. Here, PP is defined as the difference between systolic and diastolic brachial blood pressure.

The end-systolic pressure-volume relation (ESPVR) is often approximated to be linear [28]. Estimation methods based on single heart beats using ventricular data have been proposed [29, 30]. However, we do not use ventricular volumes in this investigation, so therefore we use another simpler method to estimate the maximal left-ventricular elastance by neglecting the volume axis intercept for the ESPVR ($\mathrm{V_d}$) as follows

$$E_{max}^{m} \approx \frac{\mathrm{ESP}}{\mathrm{ESV}} \approx \frac{P_{\mathrm{br,sys}}}{\mathrm{ESV}}. \tag{3}$$

Here, ESP denotes left-ventricular end-systolic pressure, ESV is the left-ventricular end-systolic volume, and $P_{\mathrm{br,sys}}$ is the brachial systolic pressure. This estimate carries some additional uncertainty due to this measure being load dependent [28]. This means that the elastance estimated in this way changes with changed afterload of the heart, while the slope of the end-systolic pressure-volume relation in the normal operating range is normally load independent.

Equations (1), (2), and (3) allowed us to compute the changes in these parameters for comparison to changes estimated using model optimized parameters. Estimates made by these equations will be referred to as "conventional estimates".

2.5.1. Regression Analysis

Ordinary Linear Regression analysis as implemented in the Python library "statsmodels" [31], and correlation analysis performed through by the "Pingouin" Python library were the main employed statistical tools for this exploratory analysis.

Ross et al. have suggested research designs and statistical methods to model exercise response variability to changes in CRF for different study designs [32]. For our analysis we instead include CRF as a predictor to explain changes in model parameters. Ross et al. recommend using linear mixed effect models for trials with repeated measurements over time, but without a control groups. We consequently look at the personalized parameters where the parameter for an individual i is given as

$$\theta_i = \mu + \alpha_i + \varepsilon_i. \tag{4}$$

Further, μ indicates the population average parameter, including both the intercept, and common regressor coefficients estimated for the population. Simultaneously, α_i is the personal deviation from the average, which includes permanent effects such as sex, and transient effects such as age and lifestyle (diet, activity level, etc.), and we only allowed personal deviations in the model intercept for our analysis. ε_i indicates all sources of random error, which includes measurement errors, and error from the estimation procedure, but also short term day-to-day variation. Although the model structure for the dynamic cardiovascular model may be simple, the behaviour of state variables and model parameters may be complex and depend on data quality, noise, and the model structure itself. However, we are interested to see whether the data holds patterns which may be linked to how the parameters are influenced by fitness level, as they change over the study period. In order to understand some of these relationships better we apply ordinary linear regression and linear mixed modeling in the context of equation (4). Ordinary regression is also applied to investigate the explanatory variables of the direct change in parameters. Our models are built in various configurations using age, sex, BMI, SV, $\mathrm{VO_{2,max}}$,

and changes in the last three. The letters A-D indicate different models with different choices of the listed regressors used to predict the chosen parameter value or change. A is the baseline model (including age, sex, and BMI), B includes $VO_{2,max}$, C includes SV, and D includes all listed predictors.

To investigate regression to the mean, we tested whether the value on the last measurement day of an individual's parameters highly correlated to the deviation of the individual's average value ($\theta_{\text{pers,avg}}$) from the population average parameter value over all measurement days (θ_{pop}). The individual average was computed using only the first two measurement days. A high adjusted r^2 would indicate how much variance is explained in the final parameter value by the personal average variability, and indicate a clustering about a personal mean. The clinical trial was uncontrolled in terms of parameter changes and non-exercising participants. Therefore, we needed to test whether it was likely that calculated changes were due to extreme observations of random effects, or if they were influenced by the exercise stimulus or other causes. Additionally, the change of the parameter value between measurement day 1 and 3 was tested by whether it would correlate highly to the difference between the initial parameter value and the population value. In this case a high negative correlation would indicate regression to the population mean. We refer to these two investigations of regression to the mean as the "regression to the mean analyses".

Next, for the second part of the regression analysis focusing on other covariates than parameter values, we investigated whether the level of or change in CRF could explain variability in the parameters and parameter changes. This was assessed by comparing unexplained (estimated residual variance) and explained variance (adjusted r^2) for regression models. We designed models for determining either the parameter change over all 12 weeks, or the parameter development over all 12 weeks including individual variation. We would then assess whether any added parameters contributed to explaining more of the observed variability. For prediction of changes, the changes from day 1 to 3 were analysed for the parameters $E_{\max}$, C_{ao}, and R_{sys}. The change between measurement day j and i is denoted as $\Delta_{i,j}$. For all regression models the dependent variables are Z-score standardized. The regressors for the linear mixed effects models are grand mean centered for the standardization.

3. Results

3.1. Comparison of Estimated Parameter Changes

For ease of readability, most of the closed-loop model results are presented in Appendix B. We calculated the parameter changes between all measurement days. Changes for parameters estimated using either carotid or finger pressure waveforms were then compared to the conventional estimates computed by equations (1) - (3). Tables 3 and B.13 show summary statistics for the parameter changes between any of the three measurement days. The mean absolute changes computed by conventional estimates are larger than for the model estimates except for C_{ao} regardless of model or data, and for $E_{\max}$ for the open-loop model using finger pressure waveforms. C_{ao} exhibits the largest difference between means by a factor of approximately 2.

Parameter	Waveform	Estimation method	Maximal abs. change	Minimal abs. change	Maximal change	Minimal change	Mean change	Mean abs. change	Units
R_{sys}	C	Model	0.208	0.001	0.208	-0.165	-0.008	0.074	$\frac{\text{mmHg}\cdot\text{s}}{\text{mL}}$
C_{ao}	C	Model	0.583	0.002	0.583	-0.518	0.058	0.206	$\frac{\text{mL}}{\text{mmHg}}$
$E_{\max}$	C	Model	0.497	0.006	0.429	-0.497	-0.043	0.177	$\frac{\text{mmHg}}{\text{mL}}$
R_{sys}	C	Conv.	0.213	0.000	0.213	-0.203	-0.011	0.091	$\frac{\text{mmHg}\cdot\text{s}}{\text{mL}}$
C_{ao}	C	Conv.	0.324	0.001	0.265	-0.324	0.016	0.122	$\frac{\text{mL}}{\text{mmHg}}$
$E_{\max}$	C	Conv.	0.793	0.004	0.504	-0.793	-0.074	0.188	$\frac{\text{mmHg}}{\text{mL}}$
R_{sys}	F	Model	0.151	0.002	0.151	-0.142	-0.011	0.045	$\frac{\text{mmHg}\cdot\text{s}}{\text{mL}}$
C_{ao}	F	Model	0.740	0.000	0.740	-0.425	0.094	0.192	$\frac{\text{mL}}{\text{mmHg}}$
$E_{\max}$	F	Model	1.444	0.006	1.444	-1.058	0.043	0.270	$\frac{\text{mmHg}}{\text{mL}}$
R_{sys}	F	Conv.	0.163	0.002	0.157	-0.163	-0.019	0.055	$\frac{\text{mmHg}\cdot\text{s}}{\text{mL}}$
C_{ao}	F	Conv.	0.243	0.001	0.243	-0.113	0.065	0.098	$\frac{\text{mL}}{\text{mmHg}}$
$E_{\max}$	F	Conv.	0.793	0.019	0.161	-0.793	-0.175	0.207	$\frac{\text{mmHg}}{\text{mL}}$

Table 3: Maximal, minimal, average and average absolute changes for total peripheral resistance (R_{sys}), systemic arterial compliance (C_{ao}), and maximal left-ventricular elastance ($E_{\max}$). Results are given for parameter changes produced by open-loop model optimization and by computation using conventional techniques, based on both carotid (C) and finger (F) pressure waveforms. Maximal and minimal changes are given unsigned, and can be any changes between the first, second and third measurement days. The carotid measurements describe 14 participants with carotid pressure measurements, while the finger pressure includes 9 participants with synchronized flow and pressure.

Tables 4 and B.14 show the Pearson correlation (r) between parameter changes estimated by model parameter optimization, and conventional estimates. The tables describe the correlation for changes in parameters R_{sys}, C_{ao}, and $E_{\max}$ using both choice of pressure waveforms and models. Changes in R_{sys} are highly correlated in all scenarios. C_{ao} is mainly moderately to highly correlated for carotid pressure, but we cannot find significant correlation when using finger pressure. $E_{\max}$ has no significant correlation except for moderate negative correlation for carotid pressure for the change from measurement day 1 to 3, and for all changes collected when using the closed-loop model.

Figure 2 shows examples of the correlations between parameter changes of different parts for the study period and compares results for both models, as well as the different choice of pressure waveforms. Firstly, the correlations for the closed- and open-loop models are very similar in all cases. Secondly, we observe that the correlations are mainly consistent between model estimates and conventional estimates by equations (2) - (3), except for $E_{\max}$ where the equation based conventional estimates often exhibit the opposite behaviour to the model estimates. There is also a pattern revealing that changes over the first half of the study period and over second half of the exercise period are often correlated to a low or moderate degree

Parameter	Wave-form	Temporal change (meas. days)	r	p value	CI95%
R_{sys}	C	1-2	0.992	$< 10^{-3}$	[0.97, 1.00]
R_{sys}	C	1-3	0.988	$< 10^{-310}$	[0.96, 1.00]
R_{sys}	C	2-3	0.973	$< 10^{-3}$	[0.91, 0.99]
R_{sys}	C	All	0.986	$< 10^{-3}$	[0.97,0.99]
C_{ao}	C	1-2	0.649	0.012	[0.18, 0.88]
C_{ao}	C	1-3	0.672	0.009	[0.22, 0.89]
C_{ao}	C	2-3	0.496	0.071	[-0.05, 0.81]
C_{ao}	C	All	0.618	$< 10^{-3}$	[0.39, 0.78]
E_{max}	C	1-2	-0.385	0.194	[-0.77, 0.21]
E_{max}	C	1-3	-0.579	0.038	[-0.86, -0.04]
E_{max}	C	2-3	-0.012	0.967	[-0.54, 0.52]
E_{max}	C	All	-0.267	0.096	[-0.53, 0.05]
R_{sys}	F	1-2	0.951	$< 10^{-3}$	[0.78, 0.99]
R_{sys}	F	1-3	0.990	$< 10^{-3}$	[0.96, 1.00]
R_{sys}	F	2-3	0.992	$< 10^{-3}$	[0.96, 1.00]
R_{sys}	F	All	0.984	$< 10^{-3}$	[0.96, 0.99]
C_{ao}	F	1-2	-0.105	0.789	[-0.72, 0.60]
C_{ao}	F	1-3	0.233	0.547	[-0.51, 0.78]
C_{ao}	F	2-3	0.369	0.329	[-0.39, 0.83]
C_{ao}	F	All	0.181	0.365	[-0.21, 0.53]
E_{max}	F	1-2	-0.206	0.625	[-0.80, 0.58]
E_{max}	F	1-3	-0.126	0.767	[-0.76, 0.64]
E_{max}	F	2-3	-0.466	0.206	[-0.86, 0.29]
E_{max}	F	All	-0.356	0.081	[-0.66, 0.05]

Table 4: Correlation statistics for parameter changes from total peripheral resistance (R_{sys}), systemic arterial compliance (C_{ao}), and maximal left-ventricular elastance (E_{max}). Results are given for correlations between parameter changes produced by open-loop model optimization and by computation using conventional equations, based on both carotid (C) and finger (F) pressure waveforms.

and with a negative sign.

3.2. Longitudinal and Post Exercise Parameter Variability

To assess whether changes monitored after 12 weeks were different to the day to day variability and short-term transient exercise effects of the hemodynamics, we computed the parameter changes between measurements made before the CPET and the day after. This was only possible for the finger pressure waveforms, since only these were monitored before and after the CPET. The average parameter changes are presented in tables 5 and B.15. The average change from measurements made before the CPET to measurements made after the CPET are typically on the same order of magnitude as the change after 12 weeks. There are some notable exceptions especially for conventional parameter estimates for left-ventricular elastance and arterial compliance where changes over 12 weeks are two to four times larger than the average changes computed directly before and after the CPET test. Comparing to tables 3 and B.13 we see that the range of computed CPET changes are similar to these changes that are computed over longer periods and over all participants. Also according to this comparison the average short term changes connected to a single CPET are very similar to the average change for any of the longer term changes for most parameters. The longer term changes for participants are usually higher for C_{ao}. It should also be noted that for the changes following a single CPET session compared to the change over all 12 weeks, the sign changes for R_{sys}.

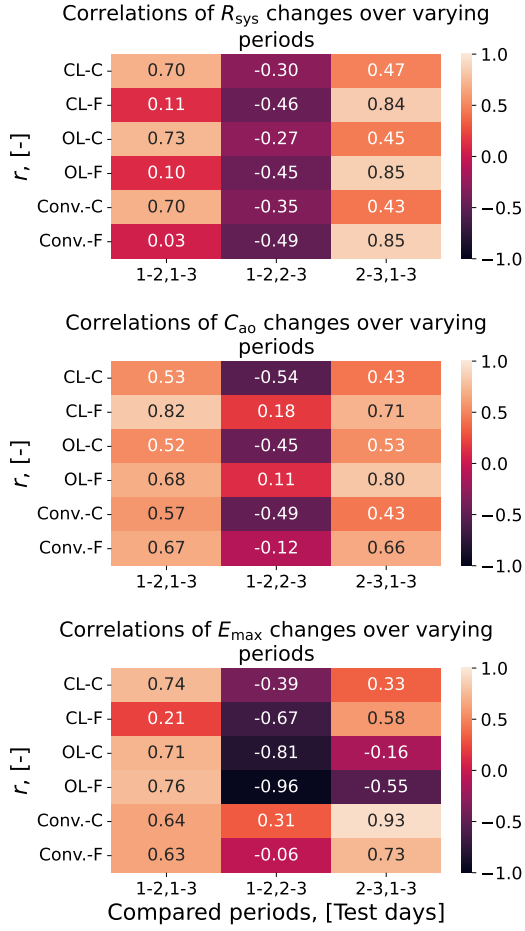

Figure 2: Correlations between parameter changes over the first half, second half and the entire study period for the closed-loop and open-loop models. "F" indicates finger pressure waveform, while "C" indicates carotid waveform. From top to bottom panel: R_{sys}, C_{ao}, E_{max}. The "Conventional" (Conv.) estimate correlations are based on the the data with the carotid waveform. The Conv. estimates of R_{sys} are slightly different for each of the waveforms as the mean pressure is estimated from the calibrated waveform.

Parameter	Estimation change	Temporal change	Mean abs. change	Mean change
R_{sys}	Model	CPET week 0	0.043(0.040)	0.020(0.060)
R_{sys}	Model	CPET week 12	0.059(0.022)	0.030(0.060)
R_{sys}	Model	Pre CPET week 0-12	0.050(0.061)	-0.042(0.069)
R_{sys}	Conv.	CPET week 0	0.052(0.043)	0.016(0.072)
R_{sys}	Conv.	CPET week 12	0.064(0.022)	0.035(0.066)
R_{sys}	Conv.	Pre CPET week 0-12	0.055(0.066)	-0.053(0.068)
C_{ao}	Model	CPET week 0	0.076(0.083)	0.076(0.083)
C_{ao}	Model	CPET week 12	0.254(0.349)	-0.190(0.400)
C_{ao}	Model	Pre CPET week 0-12	0.327(0.359)	0.327(0.359)
C_{ao}	Conv.	CPET week 0	0.072(0.071)	0.068(0.076)
C_{ao}	Conv.	CPET week 12	0.031(0.024)	-0.003(0.044)
C_{ao}	Conv.	Pre CPET week 0-12	0.127(0.069)	0.127(0.069)
E_{max}	Model	CPET week 0	0.141(0.073)	0.037(0.173)
E_{max}	Model	CPET week 12	0.254(0.217)	-0.030(0.364)
E_{max}	Model	Pre CPET week 0-12	0.102(0.081)	0.097(0.90)
E_{max}	Conv.	CPET week 0	0.082(0.090)	-0.082(0.090)
E_{max}	Conv.	CPET week 12	0.070(0.040)	0.070(0.040)
E_{max}	Conv.	Pre CPET week 0-12	0.281(0.078)	-0.281(0.078)

Table 5: Average and average absolute parameter changes over different periods throughout the study period, describing the parameter change from measurements made before a CPET and the day after. Pre CPET denotes parameter changes calculated between the first and final measurement day based on measurements made prior to the CPET. Results are given for parameter changes produced by open-loop model optimization and by computation using conventional techniques, based on the finger pressure waveforms.

3.3. Case Study

Based on the observation that the parameter changes based on finger pressure lack clear correlation to the conventional estimate changes in many instances, we drop these in the case and regression analyses onwards. Four participants who fulfilled the selection criteria as outlined in 2.3.3 have their parameters throughout the study period shown in Figures C.3 - C.4 in the appendix Appendix C. The plots also show the pairwise relationships between the variables incorporated in the regression analysis.

3.4. Regression Analysis

The results for the first two regression analyses to investigate regression to the mean are shown in tables 6 and B.16. These results indicate that the final parameter values are generally moderately to highly positively correlated with the difference of personal and population averages. The resistance and ventricular elastance parameters on the final parameter day are moderately to highly correlated for either model, while compliance is approximately moderately correlated. For the correlation of the parameter change to the difference between the initial parameter value and the population mean, the trend shows that regression coefficients are negative, and with apparently low to moderate values of correlation. The adjusted r^2 is highest in R_{sys} and this would also suggest a higher level of regression to the mean compared to the other parameters.

For the second part of the regression analysis, we built ordinary and linear mixed regression models for prediction of parameter values or changes based on age, BMI, and gender. We also considered the scatter plots of model

DV:	$R_{\text{sys},3}$	$C_{\text{ao},3}$	$E_{\text{max},3}$	$\Delta_{1,3}R_{\text{sys}}$	$\Delta_{1,3}C_{\text{ao}}$	$\Delta_{1,3}E_{\text{max}}$
Intercept	0.598*	0.969*	0.985*	-0.012	0.088	-0.064
$R_{\text{sys,avg}}$-$R_{\text{sys,pop}}$	0.101*					
$C_{\text{ao,avg}}$-$C_{\text{ao,pop}}$		0.166*				
$E_{\text{max,avg}}$-$E_{\text{max,pop}}$			0.307*			
$R_{\text{sys,1}}$-$R_{\text{sys,pop}}$				-0.056*		
$C_{\text{ao,1}}$-$C_{\text{ao,pop}}$					-0.111	
$E_{\text{max,1}}$-$E_{\text{max,pop}}$						-0.045
Adj. r^2	0.673	0.337	0.867	0.250	0.129	0.001
N	14	14	14	14	14	14
F-statistic	27.72	7.616	85.62	5.330	2.925	1.014
F-test p-value	0.000*	0.017*	0.000*	0.040*	0.113	0.334

Table 6: Ordinary linear regression models based on the difference between the individual average parameter values over the two first measurement days (subscript: avg) and the population average (subscript: pop). The model parameters are optimized for the open-loop model using the carotid pressure waveform. Indices, 1-3 indicate measurement day. DV: dependent variable.

parameters versus the measurements to investigate possible variable relationships. The scatter plots are shown in Figures C.4 and C.3.

Linear mixed effects regression models are shown in tables 7 and 8. In the majority of cases, addition of SV to the baseline model caused the highest level of explained variance, as indicated by the unexplained variance measure (residual variance). Adding solely CRF (C) to the baseline model (A) did not improve the level of explained variance when compared to any of the models incorporating SV (B and D). For resistance, the the various models performed similarly in terms of residual variance, and the coefficients for sex, BMI, SV were consistently significant across both models with sex being the most influential. For arterial compliance only SV was a consistent explanatory factor across models with Sex being the most influential. Finally, for ventricular elastance, sex and SV explained the larges amount of variation. While $\text{VO}_{2,\text{max}}$ was sometimes significant for C_{ao} in model C the regression coefficient typically changed sign and/or magnitude in model D for all parameters. Patterns in estimated coefficients and unexplained variance are generally similar between both the closed- and open-loop model. An exception of note is that the models for ventricular elastance displays a higher group variance and higher values for the significant coefficients for the open-loop derived parameters.

R_{sys}:	A	B	C	D
Intercept	0.655*	0.635*	0.626*	0.649*
Age	-0.016	-0.011	-0.022	-0.005
Sex	-0.143*	-0.097*	-0.077	-0.129*
BMI	-0.098*	-0.093*	-0.118*	-0.085*
SV		-0.076*		-0.069*
$VO_{2,\max}$			-0.035	0.023
Unex. Var.	0.005	0.002	0.006	0.003
N	42	42	28	28
Groups	14	14	14	14
Group size	3	3	2	2
Group variance	0.002	0.003	0.002	0.002
C_{ao}:	A	B	C	D
Intercept	0.973*	1.021*	1.127*	1.055*
Age	0.016	0.006	0.103	0.047
Sex	-0.013	-0.124*	-0.424*	-0.237
BMI	0.054	0.048	0.234*	0.120
SV		0.187*		0.218*
$VO_{2,\max}$			0.306*	0.107
Unex. Var.	0.035	0.023	0.028	0.008
N	42	42	28	28
Groups	14	14	14	14
Group size	3	3	2	2
Group variance	0.033	0.005	0.030	0.017
$E_{\max}$:	A	B	C	D
Intercept	0.955*	0.977*	0.930*	0.905*
Age	0.021	0.015	0.004	-0.018
Sex	0.173*	0.121	0.178	0.246*
BMI	-0.064	-0.074*	-0.074	-0.124*
SV		0.087*		0.102*
$VO_{2,\max}$			-0.014	-0.092
Unex. Var.	0.014	0.013	0.015	0.016
N	42	42	28	28
Groups	14	14	14	14
Group size	3	3	2	2
Group variance	0.019	0.009	0.022	0.008

Table 7: Linear mixed regression models for the model parameters for total peripheral resistance, systemic arterial compliance, and maximal left-ventricular elastance. The models parameter are estimated for closed-loop model using carotid pressure waveform data. "Unex. Var." is short for unexplained variance, while N is the number of observations. The regression coefficients are normalized. Asterisks indicate significant coefficients with a p-value less than 0.05.

R_{sys}:	A	B	C	D
Intercept	0.660*	0.643*	0.640*	0.656*
Age	-0.010	-0.006	-0.011	0.003
Sex	-0.134*	-0.094*	-0.089	-0.134*
BMI	-0.096*	-0.092*	-0.110*	-0.081*
SV		-0.067*		-0.061*
$VO_{2,\max}$			-0.020	0.030
Scale	0.004	0.002	0.005	0.003
N	42	42	28	28
Groups	14	14	14	14
Group size	3	3	2	2
Group variance	0.002	0.003	0.001	0.002
C_{ao}:	A	B	C	D
Intercept	0.937*	0.988*	1.065*	0.985*
Age	0.014	0.003	0.074	0.013
Sex	0.045	-0.074	-0.313	-0.107
BMI	0.069	0.062	0.225*	0.103
SV		0.199*		0.224*
$VO_{2,\max}$			0.243	0.028
Scale	0.034	0.022	0.036	0.013
N	42	42	28	28
Groups	14	14	14	14
Group size	3	3	2	2
Group variance	0.043	0.009	0.033	0.019
$E_{\max}$:	A	B	C	D
Intercept	0.835*	0.890*	0.947*	0.873*
Age	0.036	0.023	0.057	-0.002
Sex	0.443*	0.315*	0.167	0.359*
BMI	-0.012	-0.032	0.096	-0.034
SV		0.215*		0.214*
$VO_{2,\max}$			0.168	-0.033
Scale	0.024	0.010	0.015	0.011
N	42	42	28	28
Groups	14	14	14	14
Group size	3	3	2	2
Group variance	0.056	0.010	0.080	0.014

Table 8: Linear mixed regression models for the model parameters for total peripheral resistance, systemic arterial compliance, and maximal left-ventricular elastance. The models parameter are estimated for open-loop model using carotid pressure waveform data. "Unex. Var." is short for unexplained variance, while N is the number of observations. The regression coefficients are normalized. Asterisks indicate significant coefficients with a p-value less than 0.05.

The ordinary linear regression models for parameter changes are shown in tables 9 and 10 indicate that trends are similar in terms of patterns of by the adjusted r^2 across cardiovascular models. Further, SV is the most prominent explanatory variable, and model B typically has the highest amount of explained variance. An exception of note is that the change in ventricular elastance has a higher degree of explained variance for the open-loop model compared to the closed-loop formulation.

For R_{sys}, increases in CRF and SV correlated with negative change in $(\Delta_{1,3}R_{\text{sys}})$, while increased BMI exhibited the opposite pattern. Change in arterial compliance increases with increased SV, and so does ventricular elastance in both cardiovascular model formulations. Change in maximal ventricular elastance is explained by increases in SV, but also by age for the open-loop model, which is not shown to affect this parameter when compared to the linear mixed effects models.

$\Delta_{1,3}R_{\text{sys}}$:	A	B	C	D
Intercept	-0.001	-0.004	0.004	0.005
Age	-0.058	-0.021	-0.053	-0.020
Sex	-0.028	-0.020	-0.039	-0.020
$\Delta_{1,3}$BMI	0.009	0.006	-0.004	0.006
$\Delta_{1,3}$SV		-0.081*		-0.082*
$\Delta_{1,3}\text{VO2}_{\text{max}}$			-0.035	0.013
Adj. r^2	0.073	0.615	0.100	0.567
N	14	14	14	14
F-statistic	1.343	6.192	1.361	4.405
F-test p-value	0.315	0.011*	0.321	0.032*
$\Delta_{1,3}C_{\text{ao}}$:	A	B	C	D
Intercept	0.053	0.062	0.038	0.060
Age	0.082	-0.024	0.066	-0.023
Sex	-0.008	-0.013	0.044	-0.008
$\Delta_{1,3}$BMI	-0.004	-0.007	0.038	0.012
$\Delta_{1,3}$SV		0.225*		0.218*
$\Delta_{1,3}\text{VO2}_{\text{max}}$			0.111	0.015
Adj. r^2	-0.157	0.683	-0.027	0.647
N	14	14	14	14
F-statistic	0.414	8.997	0.9156	5.775
F-test p-value	0.747	0.005*	0.495	0.015*
$\Delta_{1,3}E_{\text{max}}$:	A	B	C	D
Intercept	-0.103	-0.102	-0.099	-0.096
Age	0.026	0.020	0.030	0.017
Sex	0.143	0.142	0.136	0.128
$\Delta_{1,3}$BMI	0.042	0.043	0.033	0.030
$\Delta_{1,3}$SV		0.015		0.033
$\Delta_{1,3}\text{VO2}_{\text{max}}$			-0.024	-0.038
Adj. r^2	0.189	0.108	0.124	0.055
N	14	14	14	14
F-statistic	2.009	1.393	1.461	1.153
F-test p-value	0.177	0.311	0.292	0.408

Table 9: Ordinary linear regression models for the model parameters for total peripheral resistance, systemic arterial compliance, and maximal left-ventricular elastance. The models parameter are estimated for closed-loop model using carotid pressure waveform data. "Adj. r^2" is the adjusted r^2, while N is the number of observations. The regression coefficients are normalized. Asterisks indicate significant coefficients with a p-value less than 0.05.

$\Delta_{1,3}R_{\text{sys}}$:	A	B	C	D
Intercept	0.002	-0.001	0.006	-0.002
Age	-0.053	-0.018	-0.049	-0.017
Sex	-0.032	-0.026	-0.042	-0.024
$\Delta_{1,3}$BMI	0.012	0.008	0.001	0.010
$\Delta_{1,3}$SV		-0.075*		-0.078*
$\Delta_{1,3}\text{VO2}_{\text{max}}$			-0.029	-0.006
Adj. r^2	0.061	0.588	0.055	0.540
N	14	14	14	14
F-statistic	1.280	5.638	1.189	4.058
F-test p-value	0.334	0.015*	0.379	0.039*
$\Delta_{1,3}C_{\text{ao}}$:	A	B	C	D
Intercept	0.069	0.077	0.061	0.082
Age	0.128	0.040	0.112	0.038
Sex	0.043	0.025	0.062	0.014
$\Delta_{1,3}$BMI	-0.021	-0.012	0.000	-0.023
$\Delta_{1,3}$SV		0.187*		0.202*
$\Delta_{1,3}\text{VO2}_{\text{max}}$			0.058	-0.031
Adj. r^2	0.020	0.548	-0.022	0.509
N	14	14	14	14
F-statistic	1.090	4.943	0.931	3.694
F-test p-value	0.398	0.022*	0.448	¡0.050*
$\Delta_{1,3}E_{\text{max}}$:	A	B	C	D
Intercept	-0.049	-0.045	-0.053	-0.041
Age	0.139*	0.089*	0.135*	0.087*
Sex	-0.035	-0.045	-0.026	-0.054
$\Delta_{1,3}$BMI	-0.052	-0.047*	-0.042	-0.056*
$\Delta_{1,3}$SV		0.106*		0.118*
$\Delta_{1,3}\text{VO2}_{\text{max}}$			0.026	-0.026
Adj. r^2	0.432	0.856	0.402	0.867
N	14	14	14	14
F-statistic	4.294	20.38	3.182	23.16
F-test p-value	0.034*	0.000*	0.069	0.000*

Table 10: Ordinary linear regression models for the model parameters for total peripheral resistance, systemic arterial compliance, and maximal left-ventricular elastance. The models parameter are estimated for open-loop model using carotid pressure waveform data. "Adj. r^2" is the adjusted r^2, while N is the number of observations. The regression coefficients are normalized. Asterisks indicate significant coefficients with a p-value less than 0.05.

4. Discussion

Total peripheral resistance has been reported to decrease after bouts of physical activity both in the short and long term [33, 11]. The size of this decrease is also dependent upon the baseline blood pressure, type of physical activity, and individual properties. As a consequence the trend of marginally lowered systemic resistance seen in these results on average (see tables 3, B.13, 5, and B.15) is in agreement with previous findings. A trend of resistance is also observed in several of the participants chosen for the case analysis.

By comparing the computed changes between measurement days and comparing to the changes pre- to post-CPET, there did not seem to be any clear signal of sustained exercise-induced remodeling in parameters over the 12 weeks which was consistently different than the transient short-term post CPET effects. This may have been due to insufficient data, insufficient physical activity or lack of response to exercise in these individuals, as only one of the four participants with CPET measurements met the criteria for and is included in the case study. One cannot rule out that there are possible non-responders to exercise in this study sample either.

Comparing the correlation of parameter changes between different parts of the study period (Figure 2), we note that the changes in the first half of the study period tend towards a negative and low correlation with the changes of the second half usually. Although these corre-

lations are not necessarily significant, this is a normally recognized as a pattern which may indicate that the parameter values regress to a personal mean. This would mean that the changes may be extreme observations by chance, and not necessarily caused by the study intervention. Additionally, the correlation patterns are more similar between parameters changes estimated using the same pressure waveforms than when using the same cardiovascular model with different pressure waveforms. This suggests that the pattern of changes are more dependent upon measurement modality than the cardiovascular models themselves. Further, this would be a sign of no or little effect of exercise on the parameter changes. The cardiovascular model based changes for resistance and compliance seem to correlate reasonably well with the data from conventional estimates (See tables 4 and B.14). This suggests that changes in parameter estimates made for the cardiovascular models are informed by changes in the data and are not purely results of uncertainty or poor performance by the estimation method. Even though the change in hemodynamics may not be convincingly informed by exercise, the fact that the pattern of changes in many cases agree based on different estimation approaches supports that both methods produce similar week-to-week variations as expressed by the data. Ventricular elastance on the other hand does not show the same behaviour in all cases, and often has a negative relationship. The results also indicate that the carotid pressure waveform more often produces estimates higher correlated with the conventional parameter change estimates. The correlation patterns identified here are similar for both cardiovascular model formulations.

For the closed-loop model and case analysis we found the following: Total peripheral resistance decreased compared to baseline in two out of four participants. The arterial compliance parameter increased in four out of four participants. Maximal ventricular elastance increased in one out of four participants. Only estimates for one participant saw all of the listed changes simultaneously, which indicates that these parameters saw changes expected to lower blood pressure or improve cardiac function. For the open-loop model, the case analysis gives the following observation: Total peripheral resistance decreased compared to baseline in two out of four participants, while maximal ventricular elastance increased. Arterial compliance increased in four out of four participants. The parameters in two participants saw all of the listed changes simultaneously. Hence, the open loop-model seems to express a pattern of consistent remodeling in more participants than the closed-loop model, although this is very limited data and possibly only marginal differences.

The regression analysis was subject to scarce data, and regression coefficients were rarely significant, such that these results cannot not reliably prove any influence and the trial study was not designed for this. However, the models may instead give an indication of whether physical activity or fitness did influence parameter estimates and if trends support what is expected from the literature. Therefore, we try to interpret the trend from non-significant coefficients as well.

In tables 6 and B.16, the difference of the personal mean and population mean exhibits medium to high adjusted r^2 for most parameters on the final measurement day. This means that the more extreme the final value is, the more extreme the personal average is likely to be. For the relationship between parameter change and the population mean subtracted from the initial parameter value, low to medium values of adjusted r^2 were observed. For the closed-loop model the arterial compliance exhibited the highest r^2 value, but the peripheral resistance was similarly highest in the open-loop model. These two parameters could therefore be more likely to be expected to regress to the population mean for their respective models than the other parameters. As observed in 2 a pattern of regression to a personal mean is also observed. Combined, these two observations suggest that some of the changes are caused by chance. These results and the observed correlation between estimation methods could both at least partially be explained by day-to-day variability in individuals fluctuating about a personal mean.

For the linear mixed models we observed that trends revealed in parameters for R_{sys}, practically all covariates have a negative coefficient. This negative relationship is consistent with prior studies and physiological understanding of how improved fitness and vascular remodelling result in increased cardiac output through improved conduit function of the vasculature. They would be expected to be negative as increased SV, BMI and $\text{VO}_{2,\text{max}}$ is expected to decrease the resistance value due to for example increased cardiac output, and improved fitness. For C_{ao} there are mainly positive coefficients with the exception of sex. This is in agreement with the expected effect of increased SV (while maintaining blood pressure) and $\text{VO}_{2,\text{max}}$. For increased age and BMI, vessels are expected to stiffen, but the age range of included participants may be insufficient to detect this. Finally, for E_{max}, we find negative coefficients for BMI and $\text{VO}_{2,\text{max}}$. A full understanding of the relationship between BMI and ventricular contractility has not been established from prior works. Manoliu et al. estimated end-systolic elastance and found that contractility slowly increased with BMI in middle-aged subjects [34], but other studies suggest that obesity decreases with other load-independent contractility indices in people with hypertension [35]. Fernandes-Silva et al. observed increased end-systolic elastance with increased BMI in the elderly also when adjusting for age [36]. Similarly, some findings have indicated contractility to increase in terms of EF after exercise [11], so we would expect to find positive coefficients for $\text{VO}_{2,\text{max}}$ if increased fitness has an effect. While different notions for cardiac contractility are used

to describe human hearts and can be contradictory, Oláh et al. observed increased resting end-systolic elastance in rats after 12 weeks of exercise [14]. Positive coefficients for SV seem reasonable as increased contractility could lead to a higher SV by ejecting more blood per heart beat by for example an increased EF.

Increases in SV and $VO_{2,max}$ tend to correspond with decreased$\Delta_{1,3}R_{sys}$. It decreases when the change in SV and $VO_{2,max}$ is positive, which is what is expected physiologically. On the other hand, the change of resistance seems to weakly increase with BMI. Change in arterial compliance increases with increased SV, and so does ventricular elastance in both cardiovascular model formulations. Ventricular elastance change is explained mainly by SV, and age, but is also an exception in that it has a significantly higher level of explained variance for the open-loop model parameters compared to the closed-loop formulation parameters.

It should also be noted that a weak signal for remodeling may be caused by low activity levels as only eight out of initially twenty-six participants increased their average weekly PAI from less than 50 PAI to over 100 PAI over the course of the study period. Previous studies have shown that reaching a 100 PAI weekly reduces risk of cardiovascular disease and extends lifespan as compared to those who do not reach this target [15, 16]. We would therefore expect the individuals that achieved this to be more likely to experience remodeling. However, $VO_{2,max}$ is the more well established measure in the context of improved fitness, and by extension cardiorespiratory remodeling, and therefore preferred in the case analysis. All parameters for both cardiovascular models seem to be best explained by the addition of SV as an explanatory variable, and therefore suggests that the model parameters captures the hemodynamic changes from day to day or week to week, as opposed to any influence of physical activity in this study.

Results from Bjørdalsbakke et al. indicate that the closed-loop model does not have any advantage compared to the open-loop model in terms of resolving parameter changes [17]. Results from the current study suggest that the open-loop model is better suited for detecting parameter changes. This is evidenced by higher correlations between parameters optimized to the model with conventional estimates, but also in that maximal left-ventricular elastance changes can be explained with higher confidence using the open-loop framework. Therefore, analogously to results by Itu et al. [37] an open-loop model with only the adjacent vasculature could be sufficient to determine a selection of highly influential mechanical parameters, describing the pressure-volume loop and global arterial hemodynamics. However, Itu et al. did not explore if this was sufficient to monitor a system in different states of exercise or under cardiovascular disease, which remains unknown and is likely problem dependent.

The comparison of the two cardiovascular models yields information about whether different model complexities impact what information is reflected by the parameter estimates given the chosen estimation method. The closed-loop formulation is partially described by a stressed blood volume parameter, which the open-loop does not as its total blood volume can vary during each heart cycle. Total stressed blood volume is highly influential on blood pressure levels, but can add complexity to personalization procedures as this parameter affects the state variables of all model compartments and can possibly interact with several other parameters simultaneously. Therefore, we investigated whether the personalization of each model variant by a given personalization procedure captured the same parameter dependencies or whether one of the models was better suited to track parameter changes which were expected to come from for example exercise stimulus, or other explainable causes. From the first regression analysis, it seems that both models yield parameters that may to some degree regress towards a population mean, but mainly C_{ao}. Additionally, all parameters, exhibit some signs that parameters for the individual may regress towards a personal mean (see Figure 2). And neither model exhibits any convincing evidence that the levels of fitness changes in the trial explains any additional variance in the parameters. But we cannot conclude whether this is due to a low level of exercise remodeling in participants, or whether the models are not able to detect these effects on average. Case analysis shows that parameter for both models can change in a manner expected to be benefits after exercise. The models also seem to be able to track changes in parameters similarly to other conventional techniques given variations in the data within and between individuals, but to varying degrees of correlation.

For which waveform is most useful in the context of computing changes, correlations between model changes and conventional change estimates are higher for the carotid pressure waveform, suggesting that carotid waveforms may be more useful for computing changes (Tables 4 and B.14). The changes are on average larger in absolute magnitude for the arterial parameters using the carotid waveform, but the opposite for E_{max}, where the finger pressure waveform estimates higher changes (3 and B.13). We would initially expect this as the waveform is closer to the arterial waveform in shape, but this study allowed us to investigate if the estimated chnages using the different waveforms were equally informative or useful. In summary, the changes computed for estimates based on the carotid waveform are more informative than the finger pressure derived estimates, when compared to conventional estimation methods.

5. Conclusion

The explanatory analysis shows that the cardiovascular model parameter changes correlate at least moderately well to changes computed from more conventional estimation techniques. This applies for arterial parameters using the carotid pressure waveform. This result suggests that the estimation method and model are able to at least partially capture changes in the data from week to week. The estimates of $E_{\max}$ are not often clearly correlated with conventional estimates, and it is therefore harder to argue that they are sensitive to the changes captured by the hemodynamics. For participants included in the case study, the arterial parameters for over half of participants experienced changes in the direction expected from an increased amount of exercise. However, by analyzing the study population using regression models we found no clear effect of cardiorespiratory fitness influence on the model parameters representing arterial compliance, resistance and maximal left-ventricular elastance. The model based mean absolute changes over the study period were not considerably larger or smaller than estimated changes from before to after a CPET test within a span of 24 hours. To be able to learn more about parameter changes we recommend focusing on carotid or more central waveforms, as parameters based on these correlate better with conventional estimates than finger pressure based estimates, despite their relative ease of collection. Additionally, aside from better correlation of $E_{\max}$ estimates between estimation methods, no results indicate that there is a considerable benefit to using a closed-loop model in terms of tracking parameter changes even though it describes more details of the cardiovascular system. The open-loop model produces estimates for maximal ventricular elastance that yield a higher degree of explained variance in the regression analysis, and thereby detects more explanatory factors for the parameter. Regression models suggest that adding information about $VO_{2,\max}$ can not explain more of the variability in parameter estimates in a majority of cases. This suggests that the remodelling effect is either too small, or the model and parametrization procedure is unable to track the changes reliably. Then the majority of the explanation of the computed parameter changes lies in week-to-week or day-to-day changes, as changes in SV is found to be better at explaining the parameter variability, but uncertainty in the model optimization can not be ruled out as an explanatory factor.

6. Acknowledgements

We Thank Emma M.L. Ingeström for her contribution to the study design, and for her efforts to design the clinical trial. We would also like to thank Kjell-Arne Øyen and Hans Olav Nilsen for the data collection.

7. Funding

The study is funded by the Norwegian University of Science and Technology (NTNU) through the Digital Transformation Initiative.

Availability of data and materials

The datasets generated and/or analysed during the current study are not publicly available to protect participant confidentiality.

Ethics approval and consent to participate

The study from which the data obtained was approved by Regional Committee on Medical and Health Research Ethics of Norway (Identifier: 2019/1084) and preregistered on clinicaltrials.org (Identifier: NCT 04151537). Written informed consent was obtained from all participants.

Competing interests

The authors have no competing interests to declare.

Consent for publication

Not Applicable.

Authors' contributions

N.B. wrote the main manuscript text. J.S., and U.W. contributed to and edited the main manuscript. N.B. performed all analysis and created all figures with advice from all other authors. N.B. and J.S. cooperated on writing the code used in the analysis. L.H. supervised the work. All authors reviewed the manuscript.

References

[1] M. H. Forouzanfar, P. Liu, G. A. Roth, M. Ng, S. Biryukov, L. Marczak, L. Alexander, K. Estep, K. Hassen Abate, T. F. Akinyemiju, R. Ali, N. Alvis-Guzman, P. Azzopardi, A. Banerjee, T. Bärnighausen, A. Basu, T. Bekele, D. A. Bennett, S. Biadgilign, F. Catalá-López, V. L. Feigin, J. C. Fernandes, F. Fischer, A. A. Gebru, P. Gona, R. Gupta, G. J. Hankey, J. B. Jonas, S. E. Judd, Y.-H. Khang, A. Khosravi, Y. J. Kim, R. W. Kimokoti, Y. Kokubo, D. Kolte, A. Lopez, P. A. Lotufo, R. Malekzadeh, Y. A. Melaku, G. A. Mensah, A. Misganaw, A. H. Mokdad, A. E. Moran, H. Nawaz, B. Neal, F. N. Ngalesoni, T. Ohkubo, F. Pourmalek, A. Rafay, R. K. Rai, D. Rojas-Rueda, U. K. Sampson, I. S. Santos, M. Sawhney, A. E. Schutte, S. G. Sepanlou, G. T. Shifa, I. Shiue, B. A. Tedla, A. G. Thrift, M. Tonelli, T. Truelsen, N. Tsilimparis,

K. N. Ukwaja, O. A. Uthman, T. Vasankari, N. Venketasubramanian, V. V. Vlassov, T. Vos, R. Westerman, L. L. Yan, Y. Yano, N. Yonemoto, M. E. S. Zaki, and C. J. L. Murray, "Global Burden of Hypertension and Systolic Blood Pressure of at Least 110 to 115 mm Hg, 1990-2015Global Burden of Hypertension and Systolic Blood Pressure of at Least 110 to 115 mm Hg, 1990-2015Global Burden of Hypertension and Systolic Blood Pressure of at Least 110 to 115 mm Hg, 1990-2015," JAMA, vol. 317, pp. 165–182, 01 2017.

[2] B. E. Smith and V. M. Madigan, "Understanding the haemodynamics of hypertension," Current Hypertension Reports, vol. 20, p. 29, Apr. 2018.

[3] T. Conover, A. M. Hlavacek, F. Migliavacca, E. Kung, A. Dorfman, R. S. Figliola, T.-Y. Hsia, A. Taylor, S. Khambadkone, S. Schievano, M. de Leval, T.-Y. Hsia, E. Bove, A. Dorfman, G. H. Baker, A. Hlavacek, F. Migliavacca, G. PennatiI, G. Dubini, A. Marsden, I. Vignon-Clementel, R. Figliola, and J. McGregor, "An interactive simulation tool for patient-specific clinical decision support in single-ventricle physiology," The Journal of Thoracic and Cardiovascular Surgery, vol. 155, no. 2, pp. 712–721, 2018.

[4] R. Meiburg, W. Huberts, M. C. M. Rutten, and F. N. van de Vosse, "Uncertainty in model-based treatment decision support: Applied to aortic valve stenosis," International Journal for Numerical Methods in Biomedical Engineering, vol. 36, no. 10, p. e3388, 2020.

[5] H. Ho, H. B. Yu, A. Bartlett, and P. Hunter, "An in silico pipeline for subject-specific hemodynamics analysis in liver surgery planning," Computer Methods in Biomechanics and Biomedical Engineering, vol. 23, no. 4, pp. 138–142, 2020. PMID: 31928213.

[6] W. Huberts, S. G. Heinen, N. Zonnebeld, D. A. van Den Heuvel, J.-P. P. de Vries, J. H. Tordoir, D. R. Hose, T. Delhaas, and F. N. van de Vosse, "What is needed to make cardiovascular models suitable for clinical decision support? a viewpoint paper," Journal of Computational Science, vol. 24, pp. 68–84, 2018.

[7] C. Audebert, G. Peeters, P. Segers, W. Laleman, D. Monbaliu, H. Korf, J. Trebicka, I. E. Vignon-Clementel, and C. Debbaut, "Closed-loop lumped parameter modeling of hemodynamics during cirrhogenesis in rats," IEEE Transactions on Biomedical Engineering, vol. 65, no. 10, pp. 2311–2322, 2018.

[8] J. W. Gerringer, J. C. Wagner, D. Vélez-Rendón, and D. Valdez-Jasso, "Lumped-parameter models of the pulmonary vasculature during the progression of pulmonary arterial hypertension.," Physiological reports, vol. 6, Feb 2018.

[9] B. Williams, G. Mancia, W. Spiering, E. Agabiti Rosei, M. Azizi, M. Burnier, D. L. Clement, A. Coca, G. de Simone, A. Dominiczak, T. Kahan, F. Mahfoud, J. Redon, L. Ruilope, A. Zanchetti, M. Kerins, S. E. Kjeldsen, R. Kreutz, S. Laurent, G. Y. H. Lip, R. McManus, K. Narkiewicz, F. Ruschitzka, R. E. Schmieder, E. Shlyakhto, C. Tsioufis, V. Aboyans, and I. Desormais, "2018 esc/esh guidelines for the management of arterial hypertension.," European heart journal, vol. 39, pp. 3021–3104, Sep 2018.

[10] R. H. Fagard and V. A. Cornelissen, "Effect of exercise on blood pressure control in hypertensive patients," European Journal of Preventive Cardiology, vol. 14, no. 1, p. 12 – 17, 2007. Cited by: 257; All Open Access, Bronze Open Access.

[11] H. E. Molmen-Hansen, T. Stolen, A. E. Tjonna, I. L. Aamot, I. S. Ekeberg, G. A. Tyldum, U. Wisloff, C. B. Ingul, and A. Stoylen, "Aerobic interval training reduces blood pressure and improves myocardial function in hypertensive patients.," European journal of preventive cardiology, vol. 19, pp. 151–60, Apr 2012.

[12] A. W. Ashor, J. Lara, M. Siervo, C. Celis-Morales, and J. C. Mathers, "Effects of exercise modalities on arterial stiffness and wave reflection: a systematic review and meta-analysis of randomized controlled trials.," PloS one, vol. 9, p. e110034, 2014.

[13] D. Montero, E. Roche, and A. Martinez-Rodriguez, "The impact of aerobic exercise training on arterial stiffness in pre- and hypertensive subjects: A systematic review and meta-analysis," International Journal of Cardiology, vol. 173, no. 3, pp. 361 – 368, 2014.

[14] A. Oláh, A. Kovács, Árpád Lux, M. Tokodi, S. Braun, B. K. Lakatos, C. Mátyás, D. Kellermayer, M. Ruppert, A. A. Sayour, B. A. Barta, B. Merkely, and T. Radovits, "Characterization of the dynamic changes in left ventricular morphology and function induced by exercise training and detraining," International Journal of Cardiology, vol. 277, pp. 178–185, 2019.

[15] J. Nauman, X. Sui, C. J. Lavie, C. P. Wen, J. A. Laukkanen, S. N. Blair, P. Dunn, R. Arena, and U. Wisløff, "Personal activity intelligence and mortality - data from the aerobics center longitudinal study.," Progress in cardiovascular diseases, vol. 64, pp. 121–126, Jan-Feb 2021.

[16] B. M. Nes, C. R. Gutvik, C. J. Lavie, J. Nauman, and U. Wisløff, "Personalized activity intelligence (pai) for prevention of cardiovascular disease and promotion of physical activity.," The American journal of medicine, vol. 130, pp. 328–336, Mar 2017.

[17] N. L. Bjørdalsbakke, J. Sturdy, E. M. L. Ingeström, and L. R. Hellevik, "Monitoring variability in parameter estimates for lumped parameter models of the systemic circulation using longitudinal hemodynamic measurements," BioMedical Engineering OnLine, vol. 22, p. 34, Apr. 2023.

[18] G. W. H. Organization, "Who guidelines on physical activity and sedentary behaviour," 2020.

[19] K.-A. Øyen, "The effect of personal activity intelligence (pai) on ambulatory blood pressure in adults with elevated blood pressure: a 12-week pilot randomized controlled trial," master's thesis, Norwegian University of Science and Technology, 2020.

[20] N. L. Bjørdalsbakke, J. T. Sturdy, D. R. Hose, and L. R. Hellevik, "Parameter estimation for closed-loop lumped parameter models of the systemic circulation using synthetic data," Mathematical Biosciences, vol. 343, p. 108731, 2022.

[21] M. U. P. Brandão Rondon, M. J. N. Alves, A. M. F. Braga, O. T. U. Teixeira, A. C. P. Barretto, E. M. Krieger, and C. E. Negrão, "Postexercise blood pressure reduction in elderly hypertensive patients," Journal of the American College of Cardiology, vol. 39, no. 4, pp. 676–682, 2002.

[22] B. W. Smith, J. Chase, R. I. Nokes, G. M. Shaw, and G. Wake, "Minimal haemodynamic system model including ventricular interaction and valve dynamics," Medical Engineering & Physics, vol. 26, no. 2, pp. 131 – 139, 2004.

[23] P. Segers, N. Stergiopulos, P. Verdonck, and R. Verhoeven, "Assessment of distributed arterial network models," Medical and Biological Engineering and Computing, vol. 35, pp. 729–736, Nov. 1997.

[24] P. H. M. Bovendeerd, P. Borsje, T. Arts, and F. N. van De Vosse, "Dependence of intramyocardial pressure and coronary flow on ventricular loading and contractility: a model study.," Annals of biomedical engineering, vol. 34, pp. 1833–45, Dec 2006.

[25] N. Stergiopulos, J. J. Meister, and N. Westerhof, "Determinants of stroke volume and systolic and diastolic aortic pressure.," The American journal of physiology, vol. 270, pp. H2050–9, Jun 1996.

[26] P. Virtanen, R. Gommers, T. E. Oliphant, M. Haberland, T. Reddy, D. Cournapeau, E. Burovski, P. Peterson, W. Weckesser, J. Bright, S. J. van der Walt, M. Brett, J. Wilson, K. Jarrod Millman, N. Mayorov, A. R. J. Nelson, E. Jones, R. Kern, E. Larson, C. Carey, l. Polat, Y. Feng, E. W. Moore, J. Vand erPlas, D. Laxalde, J. Perktold, R. Cimrman, I. Henriksen, E. A. Quintero, C. R. Harris, A. M. Archibald, A. H. Ribeiro, F. Pedregosa, P. van Mulbregt, and S. . . Contributors, "Scipy 1.0: Fundamental algorithms for scientific computing in python," Nature Methods, 2020.

[27] R. D. Mosteller, "Simplified calculation of body-surface area.," The New England journal of medicine, vol. 317, p. 1098, Oct 1987.

[28] N. Westerhof, N. Stergiopulos, M. I. Noble, and B. E. Westerhof, Snapshots of Hemodynamics. Springer International Publising, Springer Nature, third ed., 2010.

[29] H. Senzaki, C.-H. Chen, and D. A. Kass, "Single-beat estimation of end-systolic pressure-volume relation in humans," Circulation, vol. 94, no. 10, pp. 2497–2506, 1996.
[30] K. Sunagawa, A. Yamada, Y. Senda, Y. Kikuchi, M. Nakamura, T. Shibahara, and Y. Nose, "Estimation of the hydromotive source pressure from ejecting beats of the left ventricle," IEEE Transactions on Biomedical Engineering, vol. BME-27, no. 6, pp. 299–305, 1980.
[31] S. Seabold and J. Perktold, "statsmodels: Econometric and statistical modeling with python," in 9th Python in Science Conference, 2010.
[32] R. Ross, B. H. Goodpaster, L. G. Koch, M. A. Sarzynski, W. M. Kohrt, N. M. Johannsen, J. S. Skinner, A. Castro, B. A. Irving, R. C. Noland, L. M. Sparks, G. Spielmann, A. G. Day, W. Pitsch, W. G. Hopkins, and C. Bouchard, "Precision exercise medicine: understanding exercise response variability," British Journal of Sports Medicine, vol. 53, no. 18, pp. 1141–1153, 2019.
[33] J. Cléroux, N. Kouamé, A. Nadeau, D. Coulombe, and Y. Lacourcière, "Aftereffects of exercise on regional and systemic hemodynamics in hypertension.," Hypertension (Dallas, Tex. : 1979), vol. 19, pp. 183–91, Feb 1992.
[34] V. Manoliu and C. M. Stanescu, "Model for left ventricular contractility related to time-varying elastance based on echocardiographic measurements," in 2011 7TH INTERNATIONAL SYMPOSIUM ON ADVANCED TOPICS IN ELECTRICAL ENGINEERING (ATEE), pp. 1–4, 2011.
[35] G. E. Garavaglia, F. H. Messerli, B. D. Nunez, R. E. Schmieder, and E. Grossman, "Myocardial contractility and left ventricular function in obese patients with essential hypertension," The American Journal of Cardiology, vol. 62, no. 9, pp. 594–597, 1988.
[36] M. M. Fernandes-Silva, A. M. Shah, B. Claggett, S. Cheng, H. Tanaka, O. M. Silvestre, W. Nadruz, B. A. Borlaug, and S. D. Solomon, "Adiposity, body composition and ventricular-arterial stiffness in the elderly: the atherosclerosis risk in communities study.," European journal of heart failure, vol. 20, pp. 1191–1201, Aug 2018.
[37] L. Itu, P. Sharma, B. Georgescu, A. Kamen, C. Suciu, and D. Comaniciu, "Model based non-invasive estimation of pv loop from echocardiography.," Annual International Conference of the IEEE Engineering in Medicine and Biology Society. IEEE Engineering in Medicine and Biology Society. Annual International Conference, vol. 2014, pp. 6774–7, 2014.

Appendices

Appendix A. Participant Characteristics

Tables A.11 and A.12 give additional statistics about the participants in the different subgroups based on different blood pressure waveforms.

Appendix B. Closed-Loop Model Results

The appended tables show results for the closed-loop cardiovascular model.

Appendix C. Pairplots

Figures C.4 and C.3 show the pairplots for scatterplots between different variables applied in the regression analysis as well as the participants included in the case study.

	n = 14	
Height	174.1±8.9	cm
Weight	86.3±15.5	kg
BSA	2.0±0.2	m^2
BMI	28.4±4.1	kg/m^2
Age	56.5±3.7	years
Sex M/F	6/8	-
SBP	136.0±7.4	mmHg
DBP	84.8±6.0	mmHg
$VO2_{max}$	36.4±6.8	mL/(kg min)
24h ABPM awake SBP	137.1±10.5	mmHg
24h ABPM awake DBP	82.9±7.0	mmHg
SV (4D)	88.7±21.5	mL
SV LVOT	85.7±20.1	mL

Table A.11: Baseline characteristics of the study population included with carotid pressure waveforms. SBP and DBP signifies systolic and diastolic office blood pressure measurement. BSA: body surface area, BMI: body mass index, ABPM: ambulatory blood pressure monitoring, SV: stroke volume, LVOT: left-ventricular outflow tract. 4D refers to 3D measurement averaged over time.

	n = 9	
Height	171.2±9.8	cm
Weight	79.2±11.6	kg
BSA	1.9±0.2	m^2
BMI	27.0±3.4	kg/m^2
Age	57.3±3.3	years
Sex M/F	3/6	-
SBP	138.6±9.0	mmHg
DBP	85.3±5.5	mmHg
$VO2_{max}$	34.8±8.3	mL/(kg min)
24h ABPM awake SBP	133.7±7.3	mmHg
24h ABPM awake DBP	81.8±5.8	mmHg
SV (4D)	73.3±11.2	mL
SV LVOT	75.6±15.8	mL

Table A.12: Baseline characteristics of the study population included with finger pressure waveforms. SBP and DBP signifies systolic and diastolic office blood pressure measurement. BSA: body surface area, BMI: body mass index, ABPM: ambulatory blood pressure monitoring, SV: stroke volume, LVOT: left-ventricular outflow tract. 4D refers to 3D measurement averaged over time.

Parameter	Wave-form	Estimation method	Maximal abs. change	Minimal abs. change	Maximal change	Minimal change	Mean change	Mean abs. change	Units
R_{sys}	C	Model	0.211	0.001	0.211	-0.174	-0.009	0.081	$\frac{\text{mmHg} \cdot \text{s}}{\text{mL}}$
C_{ao}	C	Model	0.660	0.004	0.473	-0.660	0.037	0.220	$\frac{\text{mL}}{\text{mmHg}}$
E_{max}	C	Model	0.465	0.007	0.362	-0.465	-0.027	0.133	$\frac{\text{mmHg}}{\text{mL}}$
R_{sys}	C	Conv.	0.213	0.000	0.213	-0.203	-0.011	0.091	$\frac{\text{mmHg} \cdot \text{s}}{\text{mL}}$
C_{ao}	C	Conv.	0.324	0.001	0.265	-0.324	0.016	0.122	$\frac{\text{mL}}{\text{mmHg}}$
E_{max}	C	Conv.	0.793	0.004	0.504	-0.793	-0.074	0.188	$\frac{\text{mmHg}}{\text{mL}}$
R_{sys}	F	Model	0.144	0.003	0.144	-0.141	-0.010	0.050	$\frac{\text{mmHg} \cdot \text{s}}{\text{mL}}$
C_{ao}	F	Model	0.625	0.001	0.624	-0.398	0.077	0.207	$\frac{\text{mL}}{\text{mmHg}}$
E_{max}	F	Model	0.631	0.006	0.628	-0.631	0.027	0.234	$\frac{\text{mmHg}}{\text{mL}}$
R_{sys}	F	Conv.	0.163	0.002	0.157	-0.163	-0.019	0.055	$\frac{\text{mmHg} \cdot \text{s}}{\text{mL}}$
C_{ao}	F	Conv.	0.243	0.001	0.243	-0.113	0.065	0.098	$\frac{\text{mL}}{\text{mmHg}}$
E_{max}	F	Conv.	0.793	0.019	0.161	-0.793	-0.175	0.207	$\frac{\text{mmHg}}{\text{mL}}$

Table B.13: Maximal, minimal, average and average absolute changes for total peripheral resistance (R_{sys}), systemic arterial compliance (C_{ao}), and maximal left-ventricular elastance (E_{max}). Results are given for parameter changes produced by closed-loop model optimization and by computation using conventional equations, based on both carotid (C) and finger (F) pressure waveforms. Maximal and minimal changes are given unsigned, and can be any changes between the first, second and third measurement days. The carotid measurements describe 14 participants with carotid pressure measurements, while the finger pressure includes 9 participants with synchronized flow and pressure.

Parameter	Wave-form	Temporal change (meas. day)	r	p value	CI95%
R_{sys}	C	1-2	0.994	$< 10^{-3}$	[0.98, 1.00]
R_{sys}	C	1-3	0.995	$< 10^{-3}$	[0.98, 1.00]
R_{sys}	C	2-3	0.990	$< 10^{-3}$	[0.97, 1.00]
R_{sys}	C	All	0.993	$< 10^{-3}$	[0.99, 1.00]
C_{ao}	C	1-2	0.594	0.025	[0.09, 0.86]
C_{ao}	C	1-3	0.816	$< 10^{-3}$	[0.50, 0.94]
C_{ao}	C	2-3	0.594	0.025	[0.09, 0.85]
C_{ao}	C	All	0.674	$< 10^{-3}$	[0.47, 0.81]
E_{max}	C	1-2	-0.286	0.343	[-0.72, 0.31]
E_{max}	C	1-3	-0.631	0.021	[-0.88, -0.12]
E_{max}	C	2-3	-0.222	0.446	[-0.67, 0.35]
E_{max}	C	All	-0.391	0.013	[-0.63, -0.09]
R_{sys}	F	1-2	0.978	$< 10^{-3}$	[0.90, 1.00]
R_{sys}	F	1-3	0.991	$< 10^{-3}$	[0.95, 1.00]
R_{sys}	F	2-3	0.995	$< 10^{-3}$	[0.98, 1.00]
R_{sys}	F	All	0.990	$< 10^{-3}$	[0.98, 1.00]
C_{ao}	F	1-2	-0.124	0.750	[-0.73, 0.59]
C_{ao}	F	1-3	0.320	0.402	[-0.44, 0.81]
C_{ao}	F	2-3	0.525	0.147	[-0.21, 0.88]
C_{ao}	F	All	0.215	0.281	[-0.18, 0.55]
E_{max}	F	1-2	-0.192	0.650	[-0.59, 0.79]
E_{max}	F	1-3	-0.321	0.438	[-0.84, 0.50]
E_{max}	F	2-3	-0.418	0.263	[-0.85, 0.34]
E_{max}	F	All	-0.327	0.110	[-0.64, 0.08]

Table B.14: Correlation statistics for parameter changes from total peripheral resistance (R_{sys}), systemic arterial compliance (C_{ao}), and maximal left-ventricular elastance (E_{max}). Results are given for correlations between parameter changes produced by closed-loop model optimization and by computation using conventional techniques, based on both carotid (C) and finger (F) pressure waveforms.

Parameter	Estimation change	Temporal change	Mean abs. change	Mean change
R_{sys}	Model	CPET week 0	0.046(0.040)	0.018(0.063)
R_{sys}	Model	CPET week 12	0.059(0.020)	0.026(0.063)
R_{sys}	Model	Pre CPET week 0-12	0.047(0.063)	-0.036(0.070)
R_{sys}	Conv.	CPET week 0	0.052(0.043)	0.016(0.072)
R_{sys}	Conv.	CPET week 12	0.064(0.022)	0.035(0.065)
R_{sys}	Conv.	Pre CPET week 0-12	0.055(0.066)	-0.053(0.067)
C_{ao}	Model	CPET week 0	0.121(0.167)	0.114(0.173)
C_{ao}	Model	CPET week 12	0.183(0.356)	-0.179(0.359)
C_{ao}	Model	Pre CPET week 0-12	0.312(0.348)	0.312(0.348)
C_{ao}	Conv.	CPET week 0	0.072(0.071)	0.068(0.076)
C_{ao}	Conv.	CPET week 12	0.031(0.024)	-0.003(0.044)
C_{ao}	Conv.	Pre CPET week 0-12	0.127(0.069)	0.127(0.069)
E_{max}	Model	CPET week 0	0.126(0.071)	0.126(0.071)
E_{max}	Model	CPET week 12	0.177(0.116)	-0.017(0.234)
E_{max}	Model	Pre CPET week 0-12	0.113(0.078)	0.113(0.078)
E_{max}	Conv.	CPET week 0	0.082(0.090)	-0.082(-0.090)
E_{max}	Conv.	CPET week 12	0.070(0.040)	0.070(0.040)
E_{max}	Conv.	Pre CPET week 0-12	0.281(0.078)	-0.281(0.078)

Table B.15: Average and average absolute parameter changes over different periods throughout the study period, describing the parameter change from measurements made before a CPET and the day after. Standard deviations are given in parentheses. Pre CPET denotes parameter changes calculated between the first and final measurement day based on measurements made prior to the CPET. Results are given for parameter changes produced by closed-loop model optimization and by computation using conventional techniques, based on the finger pressure waveforms.

DV:	$R_{\text{sys},3}$	$C_{\text{ao},3}$	$E_{\text{max},3}$	$\Delta_{1,3}R_{\text{sys}}$	$\Delta_{1,3}C_{\text{ao}}$	$\Delta_{1,3}E_{\text{max}}$
Intercept	0.590*	0.967*	0.988*	-0.013	0.056	-0.041
$R_{\text{sys,avg}}$-$R_{\text{sys,pop}}$	0.102*					
$C_{\text{ao,avg}}$-$C_{\text{ao,pop}}$		0.112*				
$E_{\text{max,avg}}$-$E_{\text{max,pop}}$			0.164*			
$R_{\text{sys,1}}$-$R_{\text{sys,pop}}$				-0.061*		
$C_{\text{ao,1}}$-$C_{\text{ao,pop}}$					-0.149*	
$E_{\text{max,1}}$-$E_{\text{max,pop}}$						-0.063
Adj. r^2	0.637	0.231	0.644	0.265	0.319	0.076
N	14	14	14	14	14	14
F-statistic	23.81	4.911	24.47	5.682	7.095	2.067
F-test p-value	0.000*	0.047*	0.000*	0.035*	0.021*	0.176

Table B.16: Ordinary linear regression models based on the difference between the individual average parameter values over the two first measurement days (subscript: avg) and the population average (subscript: pop). The model parameters are optimized for the closed-loop model using the carotid pressure waveform. Indices, 1-3 indicate measurement day. DV: dependent variable.

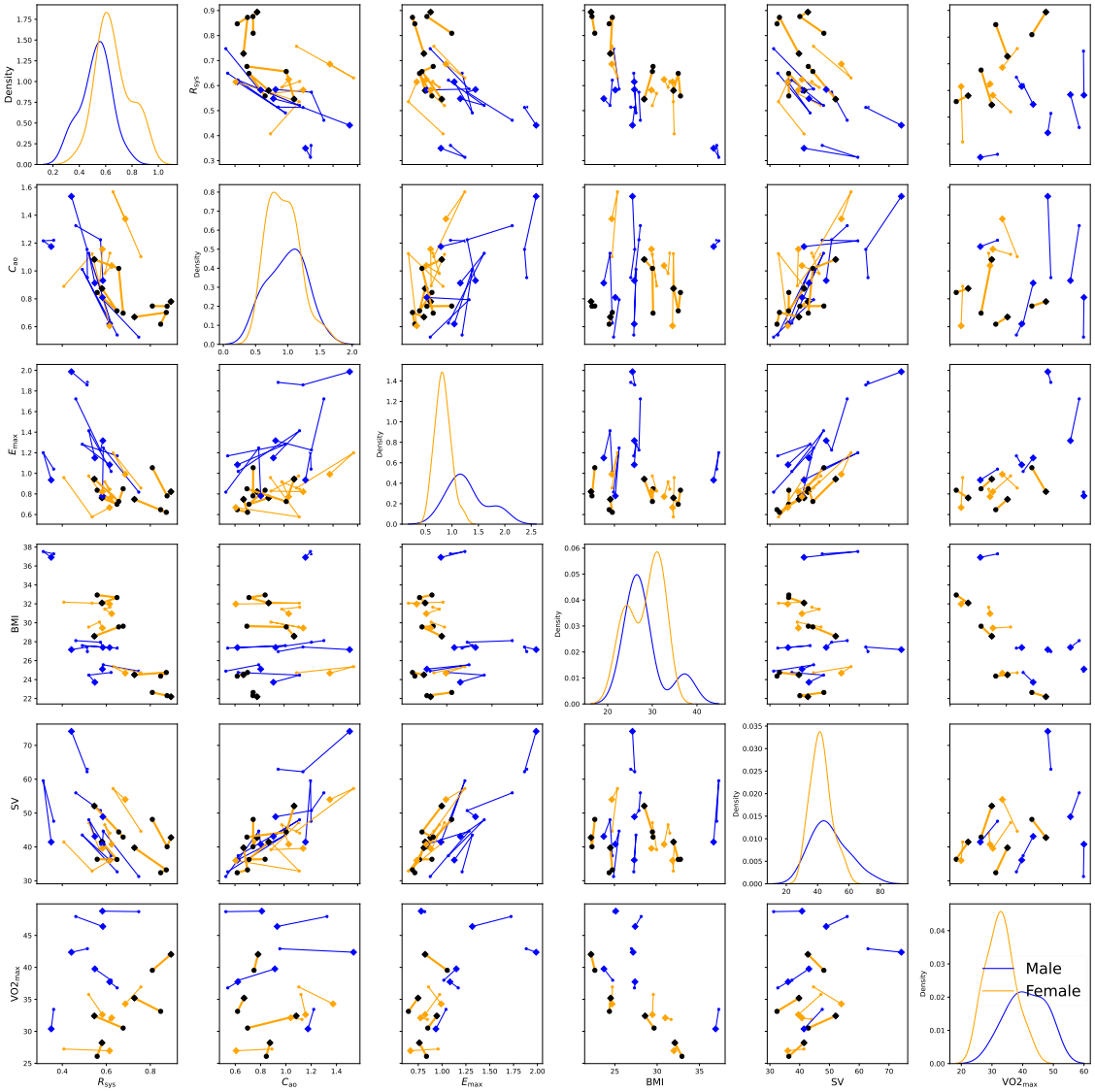

Figure C.3: Pairplots of variables used in the regression analysis. The parameter values are optimized for the open-loop model. The participants with $VO2_{max}$ changes in the top quartile are marked by black markers. The final measurement day is marked by a diamond. The colour encoding indicates sex.

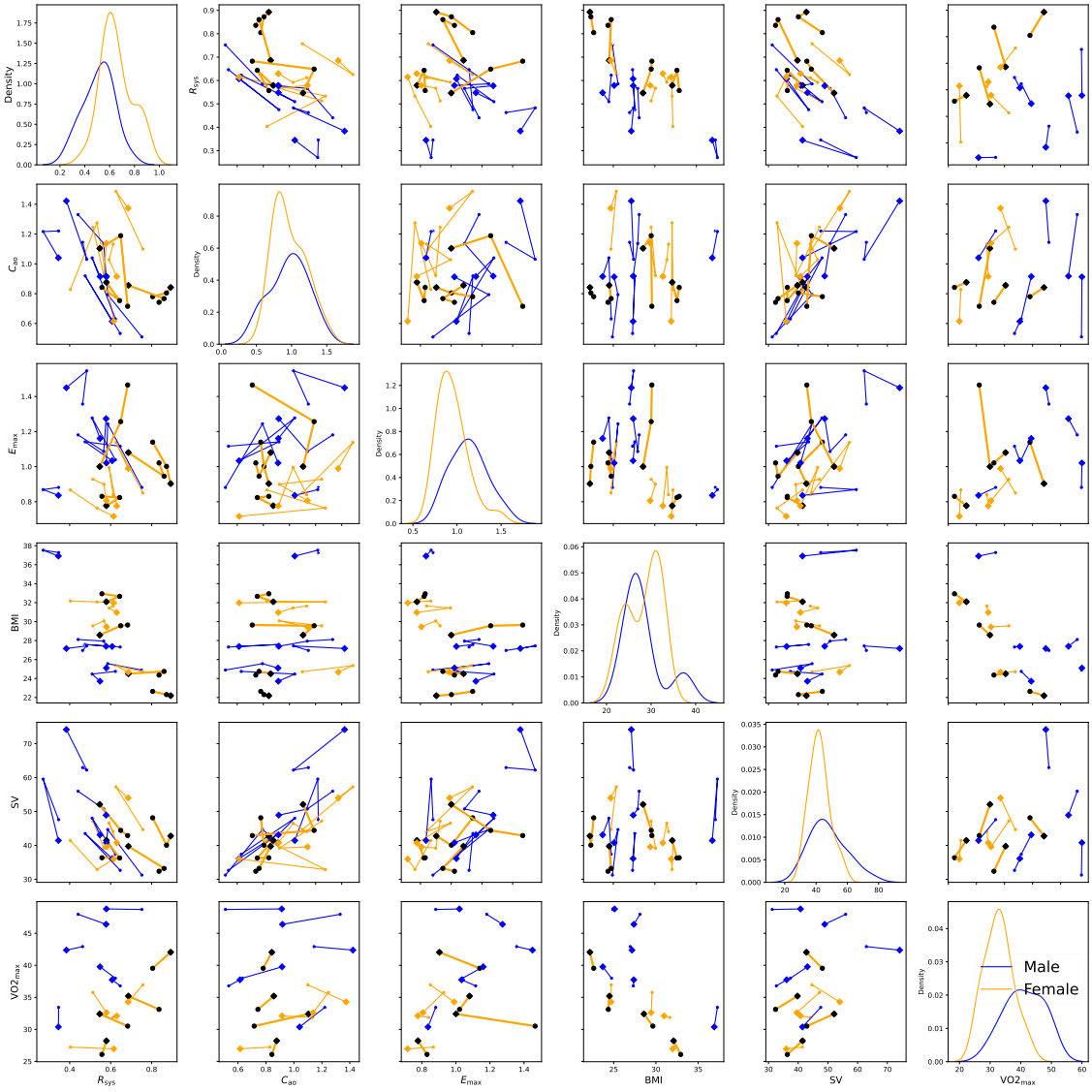

Figure C.4: Pairplots of variables used in the regression analysis. The parameter values are optimized for the closed-loop model. The participants with $VO2_{max}$ changes in the top quartile are marked by black markers. The final measurement day is marked by a diamond. The colour encoding indicates sex.